VARIATION IN THE PREY FIELD OF NORTH ATLANTIC RIGHT WHALES (*EUBALAENA GLACIALIS*) IN ROSEWAY BASIN

by

Kimberley Teresa Ann Davies

Submitted in partial fulfilment of the requirements
for the degree of Doctor of Philosophy

at

Dalhousie University
Halifax, Nova Scotia
August 2012

DALHOUSIE UNIVERSITY

DEPARTMENT OF OCEANOGRAPHY

The undersigned hereby certify that they have read and recommend to the Faculty of Graduate Studies for acceptance a thesis entitled "VARIATION IN THE PREY FIELD OF NORTH ATLANTIC RIGHT WHALES (*EUBALAENA GLACIALIS*) IN ROSEWAY BASIN" by Kimberley Teresa Ann Davies in partial fulfilment of the requirements for the degree of Doctor of Philosophy.

Dated: August 8, 2012

External Examiner: _____

Research Co-Supervisors: _____

_____

Examining Committee: _____

_____

_____

_____

Departmental Representative: _____

DALHOUSIE UNIVERSITY

DATE: August 8, 2012

AUTHOR: Kimberley Teresa Ann Davies

TITLE: VARIATION IN THE PREY FIELD OF NORTH ATLANTIC RIGHT WHALES (*EUBALAENA GLACIALIS*) IN ROSEWAY BASIN

DEPARTMENT OR SCHOOL: Department of Oceanography

DEGREE: PhD CONVOCATION: October YEAR: 2012

_____

Signature of Author

To my mother, father and brother

Table of Contents

.

List of Tables

List of Figures

Abstract

'Critical Habitat' is the habitat required to close the life history of an endangered species and is a fundamental requirement for species recovery for two reasons; the role of habitat in population limitation and viability must be determined, and the habitat must be protected. The North Atlantic right whale is an endangered species that annually migrates to the Grand Manan Basin and Roseway Basin Critical Habitats to feed on diapausing calanoid copepods that are typically aggregated at depths of 100 to 150 m. In this thesis I quantify spatial and temporal variation in the copepod prey field and occupancy of right whales in Roseway Basin, and use this information to identify the location and extent of right whale Critical Habitat. To accomplish this, I measured copepod abundance and energy density (kJ m^{-3}) using optical, acoustic and net collection methods during 2007 to 2009. Oceanographic processes that affect variation in the copepod prey field include slope water intrusions, water mass density, gyre-like circulation and frontal features. Aggregations of diapausing copepods are maintained on the southern slope of Roseway Basin by cross-isobath tidal advection, and are advected along-isobath by the residual flow. Tidal advection at a front, coupled with along-isobath advection and shear in the horizontal currents serve to accumulate copepods along the slope where aggregations are maintained for at least 7 days. The abundance, stage-structure, species composition and aggregation locations of copepods, as well as the hydrography and circulation, were variable among the three years of the study. A 20 year time series of right whales, copepods and hydrography revealed that interannual whale occupancy in the Critical Habitats is variable and can be explained by prey field variation only in Roseway Basin. Factors other than the local prey field affect the number of whales that occupy Grand Manan Basin. Variation in the right whale prey field could not be explained by temperature and phytoplankton-dependent growth in the Scotia - Fundy -Gulf of Maine region. The results of this thesis assisted in establishing the Roseway Basin right whale Critical Habitat in 2008, and the cross-disciplinary nature of the study also provides new insights into the relationships between biology and physics in Scotian Shelf - Gulf of Maine basins.

List of Abbreviations and Symbols Used

Abbreviation	Definition	Units
α	Frequency-specific absorption coefficient of water	m^{-1}
γ	Lipid/dry weight ratio	
λ	Wavelength	m
σ_t	Water mass density (P=0, S, T)	kg m^{-3}
ρ	Average water column density	kg m^{-3}
$d\rho/dx$	Cross-isobath change in density	kg m^{-2}
®	Registered Trademark	
A	Whale energy assimilation efficiency	
BML	Bottom mixed layer	m
C	Factory estimated calibration coefficient	
C3, C4, C5	Copepodid stages-C3, C4 and C5	
Chl a	Chlorophyll a	
[*Calanus*]	Water column integrated *Calanus finmarchicus* concentration	m^{-3}
df	Degrees of Freedom statistic	
dtide	Tidal displacement	m
d_U	Cross-isobath current displacement	m
dv	Along-isobath current displacement	m
DW	Dry weight	g
E	Total copepod energy available	J
E	Echo intensity	
EC_{CAL}	Gross energy content per individual copepod	J
EC_{DW}	Dry-weight specific gross energy content	kJ g^{-1}
EC_{METHOD}	Energy content measurement method	
EC_{OSV}	Individual energy content inferred from oil sac volume	J
E_r	Real time reference level for the echo intensity	
ESD	Equivalent Spherical Diameter	µm
f	Coriolis coefficient	s^{-1}
g	Acceleration due to gravity	m^2 s^{-1}
G_0	Emerging adult generation of the year	
G1	First of the year generation of copepods	
G2	Second of the year generation of copepods	
k	von Karman's constant	
K_c	Beam-specific constant that converts *E* to dB units	
L_{DBM}	$10\log_{10}$(transmit pulse length)	m
NPP	Net phytoplankton productivity	gC m^{-2} yr^{-1}
OSA	Oil sac area	mm^2
OSL	Oil sac length	mm
OSV	Oil sac volume	mm^3
P	P-value statistic	

Abbreviation	Definition	Units
P(whale)	Relative probability of observing a right whale	
P_{DBW}	$20\log_{10}$(transmit power)	
PrL	Copepodite prosome length	mm
PrW	Copepodite prosome width	mm
R	Slant range	m
R	Rouse number	
r^2	Coefficient of determination	
R_b	Whale basal metabolic demans	J d^{-1}
resid	Residual current velocity	m s^{-1}
R_f	Whale foraging energy demand	J d^{-1}
R_m	Whale migration energy demand	J d^{-1}
R_s	Whale fasting storage demand	J d^{-1}
R_{TE}	Whale total daily energetic demand over the year	J d^{-1}
S	Salinity	
$S(z,t)$	Relative zooplankton concentration (log-space)	dB
$s(z,t)$	Relative zooplankton concentration (linear space)	m^{-3}
s_{rel}	Relative zooplankton concentration scaling factor	m^{-3}
t	Student's t-statistic	
t	Time	sec
T	Temperature	^oC
T_f	Time spent foraging	hours
TS	Frequency-specific target strength	
T-S	Temperature - salinity	
T_x	Transducer temperature	^oC
U	Cross-isobath current velocity	m s^{-1}
u*	Velocity scale of the eddies in the bottom boundary layer	
V	Along-isobath current velocity	m s^{-1}
V_{wc}	Water column integrated volume	m^{-3}
$\Delta v/\Delta z$	Change in along-isobath current velocity with depth	s^{-1}
W	Vertical current velocity	m s^{-1}
z	Depth	m
ADCP	Acoustic Doppler Current Profiler	
ANCOVA	Analysis of covariance	
ATBA	Area to be Avoided	
ATMT	Asymmetric tidal mixing transport	
AZMP	Atlantic Zone Monitoring Program	
BF	Batfish	
BIONESS	Bedford Institute of Oceanography Net and Environmental Sampling System	
BT	Bottle	
BW	Basin Water	
CF5	Stage-C5 *Calanus finmarchicus* copepodids	
CH4	Stage-C4 *Calanus hyperboreus* copepodids	

Abbreviation	Definition	Units
CIL	Cold Intermediate Layer	
CPR	Continuous Plankton Recorder	
CSAS	Canadian Science Advisory Secretariat	
CTD	Conductivity, Temperature, Depth instrument	
CV	Coefficient of variation	
DS	Digital Bin Class	
G.O.	General Oceanics	
GoM	Gulf of Maine	
GoSL	Gulf of St. Lawrence	
GPS	Global positioning system	
iBW	Intermediate Basin Water	
IDF	Ideal free distribution	
mBW	Modified Basin Water	
MEDS	Marine Environmental Data Service	
NAFO	Northwest Atlantic Fisheries Organization	
NARWC	North Atlantic right whale Consortium	
NECH	Northeast Channel	
NGO	Non-governmental organization	
NSCC	Nova Scotia Coastal Current	
OPC	Optical Plankton Counter	
SARA	Species at Risk Act	
SD	Standard deviation	
SLEW	Gulf of St. Lawrence Surface Water	
SPUE	Sightings per unit effort	
SS	Scotian Shelf	
SUBS	Streamlined Underwater Buoyancy System	
TUBSS	Towed underwater biological sampling system	

Acknowledgements

Thank you to my thesis advisor, Christopher Taggart, for his steadfast positive guidance and high moral character. Thank you to my co-advisor, Kent Smedbol, for encouraging creative freedom outside my contractual obligations. I acknowledge my thesis committee members, Ian McLaren, Brian Petrie, Tetjana Ross, and Keith Thompson, for each providing unique expertise and perspectives to a multidisciplinary thesis.

Thank you to those involved in my field work; the officers and crew of the R/V Dominion Victory, Patricia Avendano, Darlene Brownell, Matthew Hatcher, Walter Judge, Candace Smith, Doug Schillinger, David Taylor and Angelia Vanderlaan. As well, thank you to the technicians Joel Slade, Miriam Morgan, and Amy Ryan, who assisted in much of the lab work. Thank you to Yvan Simard, Catherine Johnson, Moira Brown, and Erica Head for consultations and reviewing various portions of my work. I thank everyone in the Taggart lab, past and present: Anna Neuheimer, Angelia Vanderlaan, David Taylor, Matthew Hatcher, Julie Sperl, Janelle Hrycik, Franziska Broell, Tara Tapics, Sean Brillant and Diego Ibarra. A special thank you to those students and post-docs outside the lab who have been the best of friends: Jeff Barrell, Remi Daigle, Michelle Lloyd, Megan Saunders, Leah Sauchyn, Ramon Filguera, Dan Reed and Will Burt.

Thank you to my family, Ann, Barry, Chris and Lindsay Davies and Jen Freeman, for all the love and support given since I was a seed. Finally, thank you to Jonny Badger for being so positive and supportive during the crescendo and finale of this work, and to our little one for setting a hard deadline for completion.

Funding for this research was provided by the Department of Fisheries and Oceans Canada, Species at Risk Habitat Stewardship Program, National Science and Engineering Research Council of Canada, Canadian Wildlife Federation, and World Wildlife Fund.

Chapter 1

Introduction

At the broadest scale I research the oldest question in ecology: what causes the abundance and distribution of populations to vary? The ultimate goal of this research is to accurately predict population change into the future. This question is still posed because explaining population variation requires measuring driving factors at the individual (e.g., physiology), population (e.g., fecundity) and ecosystem (e.g., climate) levels. These factors vary in space and time among populations, species, and ecosystems, so prediction can quickly become intractable. Hence ecologists are still in the 'explaining variance' phase of the scientific process, and that is why the oldest question in ecology remains a valid one.

Learning how a population is related to its physical and biological habitat is a broad and central aim in population ecology and conservation ecology. Researchers generally want to describe and quantify the relationships between habitat and parameters such as size, rate of change, and general health. Habitats that could be central to maintaining the health and reproductive potential of a population include those used for breeding, feeding, food supply, nursing, and migration. The diversity of habitat types that a population uses will depend on its dispersal ability (e.g., grasses vs. oceanic fish) and demographic specialization (e.g., young forage on different foods or in different niches than adults). Assessing variation in habitat use is therefore particularly important in studies of highly migratory species.

Measuring population variation is particularly difficult in the large diffusive and advective ocean, and the 3D structure adds further complexity to studying a species' ecology. For example, many higher trophic organisms such as fish and whales depend upon plankton that are nearly passive particles and are strongly affected by ocean currents. Thus quantifying the distributions of a population and its habitat in the ocean requires explicit consideration of space and time variation in the fluid environment. This

is the major goal behind many questions in biological oceanography and is the main focus of this thesis.

1.1 Critical Habitat

The accuracy needed to explain population variation often depends on the consequences of being wrong. Species extinction is the most extreme consequence of being wrong, hence population studies of endangered species are given high priority by ecologists, governments and the general public. Recovery strategies for these species typically seek to stabilize, sustain or increase population size (e.g., Rosenfeld and Hatfield 2005).

Defining and identifying the habitat that is critical to the life history of a species ('Critical Habitat') is fundamental to the recovery of endangered species because the role of habitat in population limitation and viability needs to be determined, and anthropogenic threats need to be mitigated when and where such species are most likely to be found. Legal designation and protection of these areas then depends on well-defined basic life histories, as well as measures of the quantity and distribution of different habitats and of the species reliance on them. Inaccurate or incomplete information concerning a species' ecology can lead to ineffectual management that fails to protect against species extinction.

Endangered animals devote much time aggregated in foraging habitats, where there are predictable, nutritionally valuable, and spatially and temporally constrained food sources (Darimont *et al.* 2008). Metrics on which Critical Habitat could be based in foraging habitats include the quantity and spatial configuration of prey, temporal (e.g., seasonal) variation in the prey field, basic life histories of the prey, and geophysical features that promote predictable prey aggregations. Persistent physical oceanographic features are especially important to use as habitat metrics in the ocean, where geological or bathymetric features can be irrelevant or absent within a forager's niche. For example, physical oceanographic processes that promote accumulation of plankton should be studied in areas where endangered species forage on such aggregations.

Canada has recognized about 50 marine mammal and fish populations listed as 'Endangered' or 'Threatened'; however, only three at-risk marine species have Critical Habitat explicitly defined and protected in their Species at Risk recovery strategies:

Pacific resident killer whales (Fisheries and Oceans Canada 2008), Northern Bottlenose whales of the Scotian Shelf population (Fisheries and Oceans Canada 2010) and North Atlantic right whales (Brown *et al.* 2009). Foraging habitat designations of all three species were based on whale sightings data and geophysical features that could accumulate aggregations of prey (salmon, squid or copepods, respectively). North Atlantic right whales are the only species whose Critical Habitat designation includes spatially explicit prey field measurements and associated oceanographic features; information that was provided in part by the research presented in this thesis. This shows that Canada has found defining Critical Habitat for marine species to be a stumbling block, and the most common reason for this is lack of information on habitats in the marine ecosystem.

Fisheries and Oceans Canada was successfully sued twice in the last year by a conglomerate of nine non-governmental organizations (NGOs) for failing to adequately protect Pacific resident killer whale Critical Habitat after it was defined (David Suzuki Foundation 2010). A variety of arguments were presented, including some concerning the ecology of their main prey species, Pacific salmon (e.g., failure to adequately protect the food source) and on the interactions between killer whales and their prey (e.g., resource availability and use) (Federal Court Docket 2010). It should be noted that in this case, as in many, socioeconomic and conservation goals were in direct conflict. It is not enough to correctly identify Critical Habitat using 'proxies' such as a species' distribution, although still a useful tool as a first approximation. To truly protect Critical Habitat, management strategies need to be based on the intricacies of how a species is affected by its niche. Examples of research required for foraging habitat include investigation of: spatially explicit data on prey distribution and abundance, underlying mechanisms that facilitate predator-prey interactions, and nutritional requirements of the forager. My thesis directly addresses these research areas for right whales.

1.2 North Atlantic right whales

North Atlantic right whales are a critically endangered species that migrates along the eastern seaboard of North America. A hunting ban on these animals has been in place since the 1930s, but the species has shown little sign of recovery until recently; the best

population estimate currently stands at ~500 individuals (NARWC 2009). Caswell *et al.* (1999) estimated extinction probabilities centered on the year 2200 based on the then contemporary population dynamics. Several hypotheses have been advanced to explain the prolonged lack of recovery, including intrinsically low reproductive rate (Knowlton *et al.* 1994), genetic variability (Waldick *et al.* 2002), prey field dynamics (Baumgartner et al. 2003a, Michaud and Taggart 2007) and anthropogenic affects (Vanderlaan and Taggart 2009). Mortality from vessel strikes and fishing gear entanglements account for one half of all reported deaths (Moore *et al.* 2007), and these deaths occur because migratory routes and resident areas of the whales intersect major fishing grounds and shipping lanes along the eastern seaboard (Vanderlaan *et al.* 2008).

Critical Habitat needed to be defined, identified and protected for right whales for two reasons. The most important reason was to define the areas where whales are most likely to aggregate so that it could be protected for use by right whales. Analyses based on whale sightings and spatially explicit prey field data have led to the designation of two critical feeding habitats in the Scotia-Fundy region: Grand Manan Basin in the Bay of Fundy and Roseway Basin on the southwest Scotian Shelf (Figure 1.1). Up to 2/3 of the entire species use these feeding grounds in late-summer to feed at depths >100 m on their preferred prey, diapausing Calanoid copepods (Kraus *et al.* 2005, Baumgartner *et al.* 2003a). Both regions formerly intersected major shipping lanes and are currently subject to fishing pressure. Modeling studies of the risk of right whale death in these habitats showed that vessel re-routing reduced the relative risk of a lethal collision by 62 % in Grand Manan Basin and 82 % in Roseway Basin with minimal cost to mariners (Vanderlaan and Taggart 2009). These investigations led to the mandatory (Grand Manan) and voluntary (Roseway) re-routing of ships around the now-Critical Habitats in 2005 and 2008, respectively. Efforts are currently underway to minimize the risk of whale death by fishing gear entanglement within the Critical Habitat zones (Vanderlaan and Taggart 2010).

The second reason to study these important feeding habitats is to determine how habitat limits right whale populations. Determining how many right whales the Critical Habitats can support can provide insights into distributional variability of right whales among Critical Habitats, and possibly help explain the lack of recovery of the species.

This will also help reach conservation goals by estimating the amount of habitat necessary to attain a target number of animals to meet recovery goals. Vanderlaan (2009) estimated that on average 17 whales (range 0 - 117) are sighted in the Roseway Basin habitat annually and these remain in the habitat for an average of 136.4 (±70.9) days in any given year. Survey data also show that Roseway was abandoned by right whales for several years in the mid-nineties, and during that time the average calving interval of whales in the Bay of Fundy increased from 3 to 6 years (Brown *et al.* 2001). There is some evidence suggesting that when whales abandon Roseway they are found instead in Grand Manan Basin and vice versa, thus putting greater pressure on one Critical Habitat when the other is less lucrative. The high variance in annual occupancy, residence times and calving leads naturally to the hypothesis that available food energy is also variable and causes variation in the number of whales the habitat can support. However, these hypotheses have not been related to measures of prey abundance and energy in the Critical Habitats during that time.

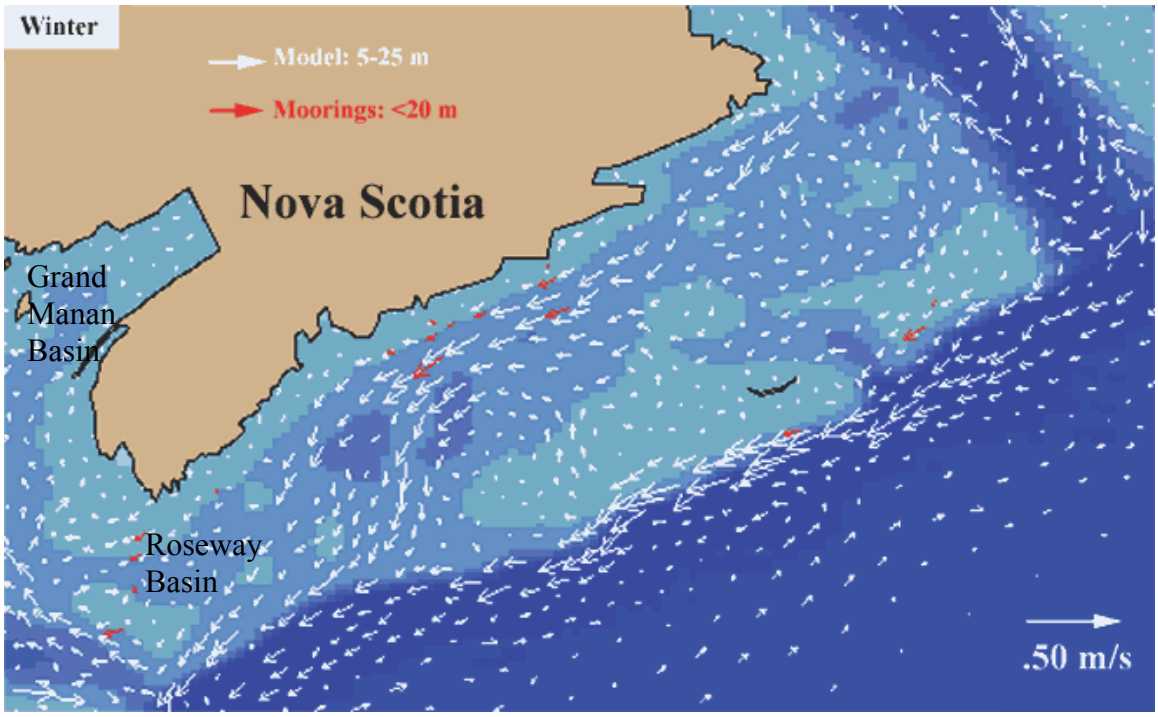

Figure 1.1 The Scotian Shelf and Bay of Fundy, showing the major Basins and circulation pattern (arrows). Figure source: Fisheries and Oceans Canada Ocean and Ecosystem Science: http://www2.mar.dfo-mpo.gc.ca/science/ocean/coastal hydrodynamics / circulation_modelling/table_2/5c.html

Effort to elucidate the relationships between right whales and their prey was initially focused in Grand Manan Basin because it is occupied consistently by right whales, while Roseway Basin is considered a more ephemeral habitat because of high interannual variation in right whale sightings there. This research confirmed that within Grand Manan Basin, right whales feed on deep, diapausing layers of the copepod *Calanus finmarchicus* stage-C5 (Woodley and Gaskin 1996, Baumgartner *et al*. 2003a; 2003b, Baumgartner and Mate 2003). The spatial and temporal extent of the deep copepod layer measured by Michaud and Taggart (2007; 2011) was used to identify the boundaries of the current Critical Habitat identified in the Species at Risk Act (SARA) Recovery Strategy for right whales (Brown *et al*. 2009). Critical Habitat for right whales was then defined as any area that "possesses the environmental, oceanographic and bathymetric conditions that aggregate concentrations of right whale prey, especially stage-C5 *Calanus finmarchicus* copepodids, at interannually predictably locations" (Brown *et al*. 2009). The spatial distribution and extent of the prey field in Roseway Basin had yet to be measured, therefore Critical Habitat was not identified based on habitat attributes as was done for Grand Manan Basin (Michaud and Taggart 2011). However, at the time of its publishing, the Recovery Strategy for North Atlantic right whales included Roseway Basin as a Critical Habitat area, based partly on the preliminary data collected for this thesis (Brown *et al*. 2009). The Strategy contained provisional Critical Habitat boundaries for Roseway Basin that encompassed the historical right whale sightings distribution in that area (Vanderlaan *et al*. 2008) with the stipulation that the Critical Habitat boundaries defined in that Strategy may be later refined based on the final outcome of this thesis (Brown *et al*. 2009).

1.3 Calanoid copepods on the Scotian Shelf

Calanus spp. are among the most abundant mesozooplankton in the North Atlantic and particularly on the Scotian Shelf where they are the primary food of many marine animals, ranging from euphausiids and juvenile silver hake to whales (Båmstedt 1986, Sameoto and Herman 1990, Albers *et al.* 1996, Baumgartner and Mate 2003). Much information is available concerning their life history and advective dynamics. The life cycle of *C. finmarchicus* on the Scotian Shelf is seasonal, with two generations (G1

augmented by a smaller G2) produced between March and May, and most of them descending into deep Basins by July – September (McLaren *et al.* 2001). The G1 generation in March is produced from individuals that had overwintered in the deep Basins of the Shelf, or from the overwintering population over the continental slope as its slope water mass intrudes onto the Shelf in late winter. They proceed through temperature and food-dependent growth from eggs through several stages in near-surface waters while feeding on the spring bloom of phytoplankton. During this time they are subject to advection by surface circulation that moves generally northeast-southwest along the Shelf and slope (Figure 1.1). A small portion of G1 molt to adult and reproduce to form a G2 generation, but most G1 halt molting at stage-C5, enter diapause and descend to depths by July (McLaren *et al.* 2001). The G2 generation does the same later in the season, and by September, both generations have mostly descended to depth. *Calanus hyperboreus* and *Calanus glacialis* are two Arctic species present on the Scotian Shelf; they are brought in from the Labrador Sea through the Gulf of St Lawrence. In the Arctic, they have longer life cycles than *C. finmarchicus; C. glacialis* has a life cycle of 1 - 3 years while *C. hyperboreus* has a life cycle of up to 5 years with multiple diapausing phases. These two species do not reproduce in significant numbers in the Scotia-Fundy region but do accumulate in Basins at stage C4 and C5 as they are advected from the NE Shelf (Sameoto and Herman 1990).

The late-stage diapausing copepodids are a high-quality food source because they contain accumulated energy-rich storage lipids as an adaptation to seasonal periods of food shortage (Lee 1974, Hirche 1996, Lee *et al.* 2006). The copepods accumulate the lipids by feeding on phytoplankton near the surface during spring and summer. The lipid energy is stored primarily as wax ester in large oil sacs that generally comprise >50% of the body cavity (McLaren *et al.* 1989, Hirche 1997, Pepin and Head 2009). Throughout autumn the C4s and C5s enter diapause and rest over the autumn and early winter in Shelf Basins at depths >100 m, or over the continental slope at depths > 1000 m, surviving solely on their lipid reserves. In late-summer, when the copepods are highest in energy and concentrated near the bottom of deep Basins of the Scotia-Fundy region, right whales take advantage of the high energy, highly concentrated food source.

It is well known that variation in the distribution of Scotian Shelf zooplankton assemblages is determined primarily by advective processes (Tremblay and Roff 1983). There are gradients in the species makeup in the northeast-southwest (along-shelf) direction and the inshore-offshore (cross-shelf) direction that are caused by advection and mixing between cold, fresh water from the inshore arm of the Nova Scotia Coastal Current (NSCC) and warmer, saltier continental slope-influenced water, both of which travel in a NE - SW direction along the Shelf and mix together as slope water seasonally intrudes onto the Shelf. Zooplankton assemblage gradients in a cross-shelf direction at the surface are best explained by different species associated with either of these water masses, hence there are strong hydrographic associations within and among these assemblages (Tremblay and Roff 1983). For example, Arctic species like *C. hyperboreus* and *C. glacialis* tend to inhabit the inshore waters where the NSCC dominates, while off-Shelf species like *C. finmarchicus* tend to inhabit the slope-influenced waters (Tremblay and Roff 1983). These community gradients are obliterated during times when and where there is more mixing between the Shelf and slope water masses (Tremblay and Roff 1983). Along-shelf gradients in *Calanus* spp. composition result from the cold water containing larger Arctic *Calanus* spp. dominating on the eastern Shelf near the Gulf of St. Lawrence outflow, and warmer water *Calanus finmarchicus*, a slope-water associated species, dominating on the western Scotian Shelf (Head *et al.* 1999). Significant interannual variation in springtime production of Scotian Shelf zooplankton has been attributed partially to variation in the volume flux of these different water masses. In summer, the animals enter diapause and migrate to the deep Basins on the Shelf, which are filled with relatively warm, salty slope water. The diapausing copepods normally seek colder, higher density water at depth, and hence the hydrographic associations change between the surface populations and the diapausing populations.

Much of the work on *Calanus* spp. variation on the Shelf has focused on dynamics at the near-surface, but the vertical dimension is also important because there are times when slope water intrudes onto the Shelf only at greater depth (Petrie and Drinkwater 1993). There is strong evidence that slope water intrusions onto the Shelf at the surface in spring bring adult (G_o) early stage (G_1) *C. finmarchicus* onto the Shelf, which later in the season populate the deep Basins as they mature to diapause stage (Head

et al. 1999, Herman *et al.* 1991, McLaren *et al.* 2000). In addition, the dominant mode of inter-decadal hydrographic variability is winter deep water slope intrusions that have a time lag in surface expression of weeks to months (Petrie and Drinkwater 1993), meaning that *C. finmarchicus* overwintering in the deep slope water could also supplement the Shelf Basins before the spring emergence from diapause. Further, the only coupled biological-physical model that estimates *C. finmarchicus* abundance variation with respect to both advection and copepod production on the Scotian Shelf shows that summer-autumn deep slope intrusions are a source of 28% of the net production of *C. finmarchicus*, where copepods mature off-Shelf in a slope water gyre and are advected onto the Shelf through deep channels in slope water (Zakardjian *et al.* 2003).

1.4 Objectives

The goal of my thesis is to quantify spatial and temporal variation in the copepod prey field of North Atlantic right whales in Roseway Basin on the western Scotian Shelf, and to use this information to identify the location and extent of right whale Critical Habitat in that area. To accomplish this goal, I first measure the lipid-energy content of *Calanus* spp. diapausing in Roseway Basin (Chapter 2), then characterize spatial variation of the prey field energy density at a habitat scale using optical and net collections from field surveys conducted in 2008 (Chapter 3). These data form the basis for Roseway Basin's designation as right whale Critical Habitat and will permit testing of the definition of Critical Habitat that was developed based primarily on data from Grand Manan Basin. Critical Habitat carrying capacity is assessed by estimating the amount of food energy available to the whales in the Basin and comparing the results to similar measurements made in Grand Manan Basin by Michaud (2005) (Chapter 3). Co-located Conductivity, Temperature, Depth instrument (CTD) data will be used to examine prey and water mass associations and explore the mechanisms of prey retention and advection within the habitat (Chapter 3).

SARA-compliant Critical Habitat boundaries are by operational necessity geographically fixed (i.e., lines on a map) because conservation management of dynamic habitats can be expensive and difficult to achieve logistically in off-shore areas. If static boundaries are to encompass a dynamic habitat such as a zooplankton aggregation, the

boundaries should contain the entire potential spatial extent within which the habitat moves. My second goal is therefore to quantify variation in the right whale prey field at a habitat boundary where whales are known to aggregate, and resolve details of prey movement at scales that are relevant to a foraging right whale (Chapter 4). Using a Eulerian and, where possible, a Lagrangian approach with moored Acoustic Doppler Current Profilers (ADCPs) equipped with CTDs, physical processes that cause variation in the prey field at the scale of a foraging whale are identified. These include tides, residual mean flow, frontal accumulation, mixing and water mass variation. This information will be used to define the habitat boundaries based on their widest possible extent.

I use these contemporary analyses to calibrate time series (1987-2009) of prey and hydrographic data that are spatially limited in each of the late-summer Critical Habitats (Chapters 5 and 6). My analyses provide insights into whether or not interannual variability in the number of right whales that return to the Scotia-Fundy region can be explained by variation in the prey fields of Grand Manan and Roseway Basins. The underlying physical mechanisms that cause variation in the right whale prey field in the Scotia-Fundy habitats are investigated to assess the effect of water mass advection on the prey fields and to determine the degree of prey field connectivity between the two major late-summer Critical Habitats. My findings are synthesized in the final chapter (Chapter 7).

Consequently, this thesis is divided into seven chapters (including this introduction); Chapters 2 to 6 address the above objectives. These chapters have been designed as 'stand-alone' manuscripts for submission for primary publication. The reader is forewarned that parts within this introduction, and the subsequent chapters, contain some repetition. The data used in Chapter 2 were originally developed as an Honors Thesis[1] by a student who worked on a portion of my Ph.D. research data, and is now published in the Journal of Plankton Research[2]. During the development of the

[1] Ryan, Amy. 2011. Variation in the gross energy content of two *Calanus* species: food for right whales in the Roseway Basin feeding habitat. Honors thesis, Dalhousie University

[2] Davies, K.T.A., Ryan, A. and Taggart, C.T. 2012 Measured and inferred gross energy content in diapausing *Calanus* spp. in a Scotian Shelf basin. Journal of Plankton Research34(7): 614 – 625

thesis into a manuscript, I took the role as lead author by performing new statistical analyses, incorporating new ideas, and leading a complete re-write of the original paper. As a result, the new version is a stand-alone piece of work and bears no resemblance to the original work, hence it is appropriately included in this thesis. Chapter 4 has been submitted to Marine Ecology Progress Series[3], with myself as lead author. I was the primary person responsible for all data processing and analysis, writing and development of this manuscript.

[3] Davies, K.T.A., Ross, T. and Taggart, C.T. Tidal and residual current influence on copepod aggregations along a shelf-basin margin. *Submitted on -2-Mar-2012 to Marine Ecology-Progress Series. Manuscript ID 10318*

Chapter 2

Measured and Inferred Gross Energy Content in Diapausing *Calanus* spp. in Roseway Basin

2.1 Introduction

2.1.1 Ecological role of lipid energy stored in Scotian Shelf copepods

Calanus spp. are among the most widely dispersed and abundant mesozooplankton in the North Atlantic and particularly on the Scotian Shelf where they are the primary food of many marine animals, ranging from euphausiids and juvenile silver hake to North Atlantic right whales (Båmstedt 1986, Sameoto and Herman 1990, Albers *et al.* 1996, Baumgartner and Mate 2003). The late-stage diapausing copepodites, typically C4 and C5, are high-quality food because they contain accumulated energy-rich storage lipids as an adaptation to seasonal periods of food shortage (Lee 1974, Hirche 1996, Lee *et al.* 2006). The copepods accumulate the lipids by feeding on phytoplankton near the surface during spring and summer. The lipid energy is stored primarily as wax ester in large oil sacs that generally comprise >50% of the body cavity (McLaren *et al.* 1989, Hirche 1997; Pepin and Head 2009). Throughout summer the C4s and C5s enter diapause and rest over the winter in Shelf Basins at depths >100 m, surviving solely on their lipid reserves.

Estimates of copepod energy content are useful for a variety of ecological applications that include models of aquatic ecosystem function, energy flow, carrying capacity, and physiology etc. A useful application of energy estimation in the field of marine trophic ecology is its use in calculating the energy density (kJ m^{-3}) of local habitat-scale copepod populations. Energetic estimates are typically inferred from simple abundance measurements (e.g., Beardsley *et al.* 1996, Baumgartner and Mate 2003, Zhou *et al.* 2009), while others have estimated oil sac volume as a proxy for energy content (Reiss *et al.* 1999, Pepin and Head 2009). Less often, population level energy density is measured from both individual energy content and abundance (Michaud and Taggart 2007, 2011). There is a clear advantage to incorporating direct estimates of energy content into such studies, but to do so reliably requires that various factors be considered.

These revolve around questions such as: 1) how to approximate copepod energy in systems containing different species with similar ecological roles, 2) how to best infer energy content using straightforward techniques, and 3) can reliable estimates be derived from chemically preserved specimens? The answers to these questions will help introduce the use of energy content into a broader spectrum of research programs and by providing estimates that can be drawn from the extant literature as well as archived material.

2.1.2 Environmental influences on *Calanus* spp. energy content

Diapausing copepods, dominated in late-summer by *Calanus finmarchicus* stage-five copepodites (hereafter CF5) and *Calanus hyperboreus* stage-four copepodites (hereafter CH4), reside together in deep Basins on the western and central Scotian Shelf (Sameoto and Herman 1990, Herman *et al.* 1991, Sameoto and Herman 1992, Head *et al.* 1999). *C. hyperboreus* is a colder-water species transported from the Labrador Sea through the Gulf of St. Lawrence and along the Scotian Shelf via the Nova Scotia Coastal Current, whereas *C. finmarchicus* is transported to the Shelf from the Gulf of St. Lawrence, from Scotian Shelf Basins, and from the continental slope waters. The co-occurrence of the two species in central and western Shelf Basins is due to water mass exchange and mixing on the continental Shelf.

Presumably as adaptation to long periods of food shortage, especially in high-latitude regions, *C. hyperboreus* have a larger body size and accumulate a greater proportion of longer chain, higher energy, wax esters than do *C. finmarchicus* (Falk-Petersen *et al.* 2009, Albers *et al.* 1996). These two properties make the former species energetically more valuable to predators in high latitude food webs. This inter-species variation necessitates that the energy content and size distribution of each species be measured separately and considered separately in ecological applications. Both species, however, vary greatly in body size, energy content and life span in response to their highly variable environments (Falk-Petersen *et al.* 2009), and so their relative energetic values across latitudes may vary.

2.1.3 Energy content of *Calanus* spp. inferred from oil sac volume

Oil sac volume (OSV) is a metric widely used to estimate relative changes in copepod energy content (Plourde and Runge 1993, Reiss *et al.* 1999, Pasternak *et al.* 2001, Hasset 2006, Pepin and Head 2009) because it is easily estimated using morphometric dimensions obtained by microscopy and imaging. Collection of direct energy content measurements requires specialized training and equipment, and provides a higher degree of precision. In part, for these reasons, much research effort has been expended to develop empirical relations between the OSV and energy content in marine zooplankton, particularly *C. finmarchicus* (e.g., Arts and Evans 1991, Miller *et al.* 1998). The above research addresses issues such as the geometrical shape equations used to approximate the oil sac volume in relation to the orientation of the animal when measured, and the various techniques used to directly estimate energy content. OSV-inferred wax ester content is well correlated with direct chromatographic measurements of wax ester but there is evidence that the former overestimates the latter (Miller *et al.* 1998, Vogedes *et al.* 2010), and alternatives such as the oil sac area being used as a proxy for energy content have been proposed (Vogedes *et al.* 2010).

2.1.4 The effect of preservation on energy content estimation

Sample freezing (typically flash-freezing in liquid nitrogen) is the standard preservation method used for energy content analysis of zooplankton (e.g., Omori 1978, Miller *et al.* 1998, Miller *et al.* 2000, Michaud and Taggart 2007). Most zooplankton samples collected for reasons other than energy content analysis are usually preserved in 4 to 10% formalin. Formalin collections represent massive, readily available, historical catalogues of biological material that are a potentially valuable source of information when energy content estimation becomes desirable or necessary at some later date. Formalin-preserved samples are not normally used for energetic studies because formalin causes some lipid loss either by oil sac leakage or exchange with the surrounding preservation solution through the anal pore after death (Morris 1972, Steedman 1976, Salonen and Sarvala 1985). There is also some evidence that hydrolysis of the lipid and degradation of the polyunsaturated fatty acids may occur (Morris 1972). However, some researchers addressing energy content analysis have used only those animals that retain visibly intact

oil sacs regardless of preservation technique (e.g., Reiss *et al.* 1999). Thus, it is possible that some lipid loss may be tolerated as long as there are individuals that retain intact oil sacs.

2.1.5 Objectives

The objectives of this study are to measure the energy content of diapausing CF5 and CH4 and determine the effects of species, size, measurement method and preservation on energy content. I do this by measuring gross energy (J) content of diapausing CF5 and CH4 field-samples, collected in Roseway Basin (43^0 N, 65.2^0 W) on the western Scotian Shelf, that were preserved by freezing or in 4% buffered formalin. I also examine empirical relations between and among direct energy content estimates for each species and the inferred energy content estimates using both formalin and frozen-preserved specimens.

2.2 Methods

2.2.1 Samples

Zooplankton samples were collected at several stations in Roseway Basin aboard the R/V Dominion Victory in September 2007. September coincides with the timing of maximum CF5 concentration and energy content at depth (Michaud and Taggart 2007, 2011). My results and conclusions extend only to copepodites that have recently entered diapause and have full oil sacs; i.e., they are at or near their annual maximum in energy content as occurs elsewhere (Comita et al. 1966, Scott et al. 2000), and thus represent a high quality food source. A Bedford Institute of Oceanography Net and Environmental Sampling System (BIONESS; Sameoto et al. 1980) towed at a nominal 1 $m \cdot s^{-1}$ and equipped with seven 333-μm mesh nets was used to collect the samples. Only those nets (n=9) that opened and closed at depths greater than 108 m (range 108–150 m) were used in my analysis. Upon net retrieval, two 5 ml sub-samples of concentrated zooplankton from each net were frozen in liquid nitrogen and later transferred to a -70 °C freezer. The remainder of each sample was preserved in 4% buffered formalin for taxonomic and abundance analysis. Samples were preserved for 1 to 2 years before undergoing energy content analysis.

2.2.2 Energy content measured by calorimetry

All zooplankton were identified and counted following Michaud and Taggart (2007). The average proportion of mesozooplankton within each net attributed to CF5s and CH4s was estimated, and energetic analyses were performed on each species. Detailed abundance data by species is provided for 2007 in Chapter 5.

Gross energy content was estimated using a Parr® 1266 semi-micro oxygen-bomb calorimeter following Michaud and Taggart (2007). Individuals were selected from all net collections as needed under the assumption that horizontal spatial variation among variables at scales <10 km within the Basin was negligible. Only animals with visually intact oil sacs were selected for analysis. Copepodite prosome length (PrL, mm) and width (PrW, mm) was measured using a dissecting microscope and an ocular micrometer. PrL and PrW were converted to equivalent spherical diameter (ESD) using the prolate spheroid volume approximation. Copepods were then sorted among six geometric mean ESD size classes (Table 2.1) selected to correspond to a range of digital size classes measured using an Optical Plankton Counter (OPC). I did this for eventual estimation of size-specific energy terms using OPC abundance-at-size data (Chapter 3); previously an average-energy term has been applied across all OPC size classes (e.g., Michaud and Taggart 2011).

Three replicates from each of the frozen-preserved, and two replicates from the formalin-preserved samples, were analyzed in this manner. Calorimeter sensitivity did not allow for the analysis of individual copepods; hence each replicate consisted of 20 individuals within each size class (35 bulk samples). Each bulk sample was wet-weighed using a Mettler® AJ 100 balance (±0.0001 g) and freeze-dried for eight hours. Samples were then dry-weighed, pressed into 3 mm-diameter pellets, and combusted in random order using one of two calibrated Parr® 1107 oxygen micro-bombs. Details on calibration, corrections for nitric and sulphuric acid formation and conversion factors are provided by Michaud and Taggart (2007). Energy content estimates are presented as dry-weight specific gross energy content (EC_{DW}, kJ g^{-1}) and gross energy content per individual copepod (EC_{CAL}, J); that is the product of EC_{DW} and the pellet dry weight divided by the number (20) of copepods in the bulk sample. Ten individuals from each

species, size class and preservation technique were sorted from the original collections as above, freeze dried and individually weighed using a Sartorius® balance (±0.00001 g).

2.2.3 Inferred energy content

One replicate from each size class within each preservation technique (frozen and formalin-preserved) destined for calorimetry was first photographed using a Nikon® Coolpix 995 digital camera for micrometer-calibrated image analysis. PrL, PrW, prosome length and oil sac length and width were measured using ImageJ (version 1.41) freeware. Oil sac volume (OSV, mm^3) was estimated using the cylindrical approximation (Miller *et al.* 1998). Lipid content (g) was estimated from OSV using a lipid density of 0.9 g ml^{-1} (Miller *et al.* 1998, Visser and Jonasdottir 1999). Individual energy content (EC_{OSV}, J) was inferred from lipid content assuming a lipid-energy content of 39.5 kJ g^{-1} (Lamprecht 1999). Prosome volume was calculated from PrL and PrW assuming a prolate spheroid and OSV was expressed as a proportion of prosome volume. Comparisons of prosome and oil sac shape were made among species and preservation techniques.

2.2.4 Preservation Effects

I quantified the effects of preservation on individual dry weight, pellet dry weight, EC_{DW}, EC_{CAL}, and EC_{OSV} by comparing all variables between the frozen- and formalin-preserved samples within and between species.

2.2.5 Statistical Analyses

Statistical tests were performed separately for each species because their size ranges did not overlap across all size classes. Differences in EC_{DW} or DW (both individual copepod and bulk-sample pellet) among size classes and between preservation techniques were assessed using analysis of covariance (ANCOVA). Differences in EC_{DW} between species, ignoring size, were subsequently determined using Student's t-test. The effects of size, preservation and measurement method (EC_{CAL} and EC_{OSV}) on individual energy content were determined using a General Linear Model that allowed me to (1) accommodate the

Table 2.1 Summary of the *C. finmarchicus* stage-5, CF5 and *C. hyperboreus* stage-4, CH4 sorting methods indicating preservation, size (ESD) ranges with the corresponding Geometric Mean ESD (µm) for each size class, and the number of replicates for each measurement method (EC_{CAL} and EC_{OSV}).

Species	Preservation	Size Range (µm)	Geometric Mean ESD (µm)	Number of Replicates EC_{CAL}*	Number of Replicates EC_{OSV}**
C.finmarchicus (CF5)	Frozen	823-936	880	3	20
		943-1058	1001	3	20
		1064-1182	1123	3	20
		1187-1307	1247	3	20
	Formalin	823-936	880	2	20
		943-1058	1001	2	20
		1064-1182	1123	2	20
		1187-1307	1247	2	20
C. hyperboreus (CH4)	Frozen	1187-1307	1247	3	20
		1312-1434	1373	3	20
		1439-1562	1501	3	20
	Formalin	1187-1307	1247	2	20
		1312-1434	1373	2	20
		1439-1562	1501	2	20

*Each replicate contains a bulk sample of 20; **Each replicate is an individual copepod

unbalanced design (Type III Sum of Squares), and (2) use a mixture of covariates (size) and discrete explanatory variables (preservation and measurement method). EC_{CAL} was expressed as a function of pellet dry weight and size, ignoring species, and analyzed using linear regression. Finally, the proportion of the prosome volume occupied by the oil sac volume was compared between preservation techniques using a t-test on arcsine square-root transformed data. Averages for all relevant metrics are presented as ± one standard deviation (SD).

2.3 Results

2.3.1 Energy content measured by calorimetry

Calanus finmarchicus C5 and *C. hyperboreus* C4 copepodites comprised 64 ±17% and 19 ±9% of the mesozooplankton abundance, respectively, at collection depths >108 m in Roseway Basin. The remaining 17% was comprised of *C. finmarchicus* C4 and adult stages, *C. glacialis*, *Centropages* spp., *Metridia* spp. and *Pseudocalanus* spp.

Size explained the most variation in both dry weight and individual energy content. EC_{DW} did not vary with size within each species and there was no significant interaction between size and preservation (Table 2.2; Figure 2.1a, b). There was no difference in EC_{DW} between species (t = 0.87; P = 0.390; df = 27) and therefore the overall average was estimated at 27.9 ±5.0 kJ g^{-1}. Pellet dry weight increased with size regardless of preservation and again there was no significant interaction between size and preservation (Table 2.3, Figure 2.1c, d). Similarly, the CF5 (Figure 2.1e) and the CH4 (Figure 2.1f) individual energy content estimates both increased as a function of size with no significant interaction with preservation technique (Table 2.4). Estimates of EC_{CAL} among frozen CF5s increased with size from 4.4 ±0.79 J to 10.9 ±2.2 J between the smallest and largest size class. The frozen CH4s contained greater energy content than frozen CF5s, varying between 9.4 ±1.5 J and 12.7 ±2.5 J. Within the single overlapping size class I detected no difference in EC_{CAL} estimated using frozen samples of the two species (t = 0.56; P = 0.108, df = 5). This means that, for all practical applications, EC_{CAL} varies only as function of size and not with species or preservation (r^2=0.75, P < 0.001, Figure 2.2a). EC_{CAL} can also be expressed as a function of dry weight; EC_{CAL} estimates increased with pellet DW across all size classes (r^2 = 0.76; P < 0.001, Figure 2.2b).

2.3.2 Inferred energy content

Energy content estimates did not differ between the EC_{CAL} and EC_{OSV} measurement methods (EC_{METHOD}) for the two species and there were no significant interaction terms between EC_{METHOD} and size (Table 2.4). For the CH5s, there was also no significant EC_{METHOD}*Preservation interaction term. There was, however, a significant EC_{METHOD}*Preservation interaction term for CH4s. The difference between species in the EC_{METHOD}*Preservation interaction term is apparent by comparing Figures 2.1e, f, g and h. There was no effect of preservation on either species when energy content was measured using calorimetry (Figure 2.1e, f). When CH4 energy content was inferred from oil sac volume, the EC_{OSV} estimate (Figure 2.1h) was significantly smaller in the preserved animals than in the frozen animals at all sizes, while there was clearly no difference in EC_{CAL} between the frozen and formalin-preserved CF5s (Figure 2.1g).

2.3.3 Preservation Effects

There was no effect of preservation on EC_{DW} estimates among the CF5 (Table 2.2) samples or on their individual energy content estimates (Table 2.4; frozen 6.04 ±3.09 J; formalin 5.41 ±2.49 J). There was also no effect of preservation on the CH4 estimates of EC_{DW} (Table 2.2). However, individual energy content of CH4s was affected differently by preservation, depending on the measurement method (Table 2.4). There appeared to be no effect of preservation on EC_{CAL} (Figure 2.1f), while EC_{OSV} estimates of formalin-preserved specimens was lower than those of frozen-preserved specimens (Figure 2.1h). Consistent with the lack of preservation effect on EC_{CAL} for either species, I did not find an effect of preservation on either pellet dry weight (Table 2.3, Figure 2.1b,c) or on individual dry weight (CF5 P =0.055; CH4 P =0.295) for either species (Figure 2.1i, j).

The lower EC_{OSV} measured on formalin-preserved specimens of CH4s compared with frozen-preserved specimens may be explained by variation in the oil sac shape. Formalin preservation appeared to result in longer, narrower oil sacs in both species but the effect was more pronounced in CH4s (Figure 2.3a, b). Variation in the oil sac width among CH4 individuals also decreased substantially in formalin. CH4 formalin-preserved oil sacs occupied 5 to 25 % of the prosome volume while frozen-preserved oil sacs

occupied significantly more, ranging between 10 and 45% (t = 6.03; P = <0.001, df = 116, Figure 2.3d, f). Differences were less substantial, though significant, among the CF5s, where frozen-preserved oil sacs occupied 10 to 60% of the body volume while formalin-preserved sacs comprised between 10 and 40% (t = 2.56; P = 0.011, df = 154, Figure 2.3c, e). Taken together, these results imply that when preserved in formalin, the larger CH4 oil sacs appear to change shape compared to the smaller CF5 oil sacs.

Table 2.2 Results of an ANCOVA test for the effects of size (μm), and preservation (Pres), on dry-weight specific energy content (EC_{DW}, kJ g^{-1}) of *C. finmarchicus* stage-5, CF5 and *C. hyperboreus* stage-4, CH4.

Species	Source of variation	Sum of Squares	df	Mean Square	F	*P*-value
Calanus finmarchicus (CF5)	Size	112.03	1	91.77	2.52	0.132
	Pres[1]	4.92	1	13.45	0.37	0.552
	Pres x Size	15.64	1	15.64	0.43	0.522
	Error	582.79	16	36.42		
	Total	715.39	19			
Calanus hyperboreus (CH4)	Size	4.87	1	5.07	0.62	0.448
	Pres[1]	11.58	1	0.05	0.01	0.942
	Pres x Size	0.20	1	0.20	0.02	0.879
	Error	90.01	11	4.334		
	Total	106.66	14			

CF5: r^2=0 .19; CH4: r^2= 0.16. 1. Preservation = frozen or formalin-preserved

Table 2.3 Results of an ANCOVA test for the effects of size (µm), and preservation (Pres), on pellet dry weight (g) of *C. finmarchicus* stage-5, CF5 and *C. hyperboreus* stage-4, CH4.

Species	Source of variation	Sum of Squares (x 10^{-5})	df	Mean Square (x 10^{-5})	F	*P*-value
Calanus finmarchicus (CF5)	Size	3.00	1	2.99	87.62	<0.001
	Pres[1]	0.01	1	0.01	0.85	0.370
	Pres x Size	0.01	1	0.01	0.75	0.399
	Error	0.55	16	0.01		
	Total	3.57	19			
Calanus hyperboreus (CH4)	Size	2.22	1	2.26	49.22	<0.001
	Pres[1]	0.01	1	0.01	1.02	0.333
	Pres x Size	0.01	1	0.01	0.98	0.343
	Error	0.05	11	0.01		
	Total	2.29	14			

CF5: r^2=0 .19; CH4: r^2= 0.16. 1. Preservation = frozen or formalin-preserved

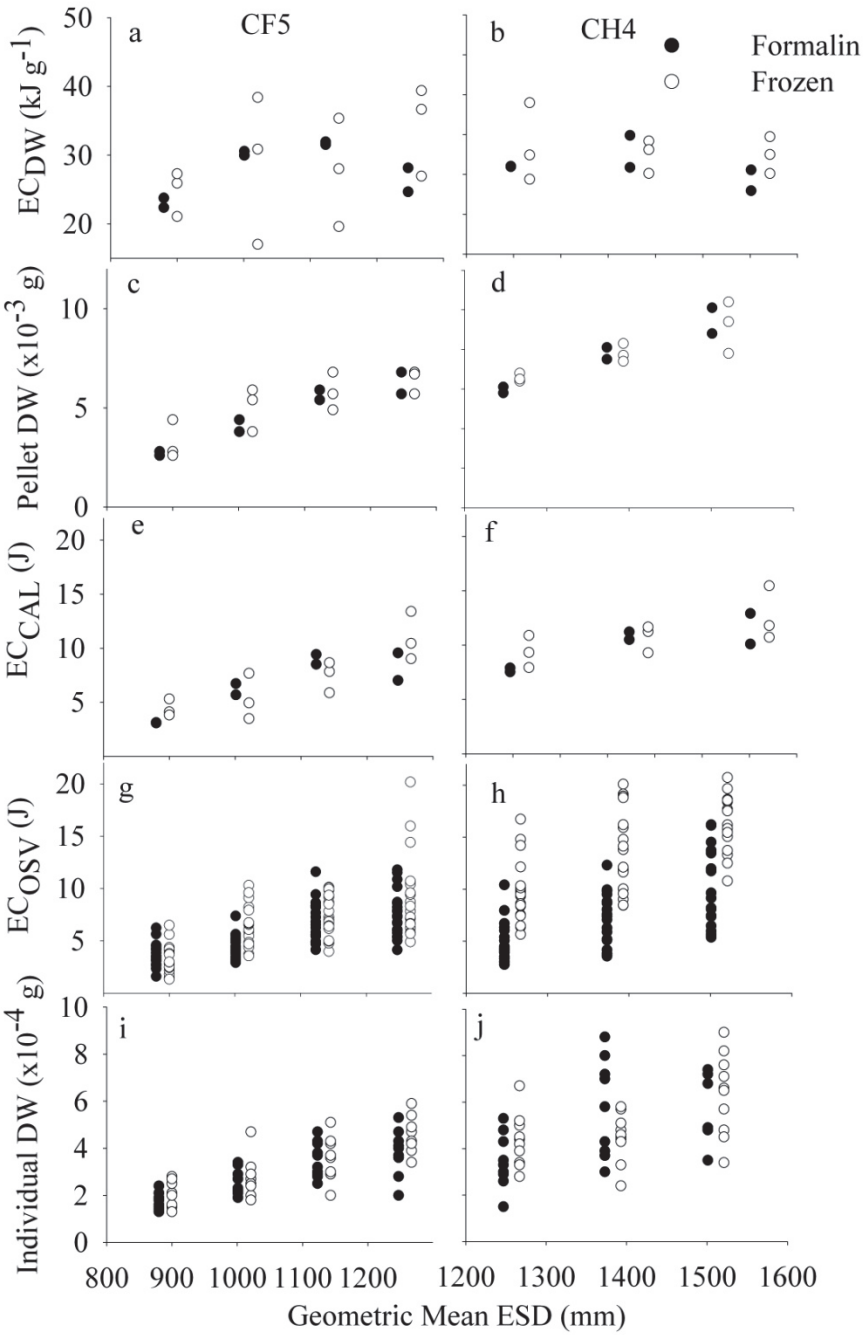

Figure 2.1 Copepod energy content (EC) measured by weight-specific calorific value (EC_{DW}, kJ g^{-1}; a, b), dry weight of the sample pellet used for calorimetry (c,d), individual energy content measured by calorimetry (EC_{CAL}; e, f) or inferred from volumetric oil sac approximations (EC_{OSV}; g, h), wherein each increases with size (geometric mean ESD, µm) in both frozen- (open symbols) and formalin-preserved (closed symbols) *C. finmarchicus* stage-5, CF5 (a, c, e, g, i) and *C. hyperboreus* stage-4, CH4 (b, d, f, h, j). Dry weight measured on individual copepods (i, j) also increased with size. For EC_{DW}, pellet DW and EC_{CAL}, each symbol represents a bulk sample of 20 copepods. Animals in the frozen-preserved ESD category are offset by 20 µm for clarity.

Table 2.4 Results of a General Linear Model test for the effects of size (ESD, µm), preservation (Pres), and energy content measurement method (EC_{METHOD}) on individual energy content (J) of *C. finmarchicus* stage-5, CF5 and *C. hyperboreus* stage-4, CH4.

Species	Source of variation	Type III Sum of Squares	df	Mean Square	F	*P*-value
CF5	Size	649.87	1	294.02	70.44	<0.001
	EC_{METHOD}[1]	11.99	1	1.34	0.32	0.572
	Pres[2]	34.80	1	9.43	2.26	0.135
	EC_{METHOD} x Pres	1.22	1	1.22	0.29	0.589
	EC_{METHOD} x Size	3.19	1	2.41	0.58	0.449
	Size x Pres	13.36	1	13.36	3.20	0.075
	EC_{METHOD} x Pres x Size	0.77	1	0.12	0.10	0.750
	Error	722.12	172	4.17		
	Total	1436.55	179			
CH4	Size	747.13	1	198.36	26.41	<0.001
	EC_{METHOD}[1]	1.63	1	15.74	2.10	0.150
	Pres[2]	925.81	1	0.00	0.00	0.980
	EC_{METHOD} x Pres	76.43	1	76.43	10.18	0.002
	EC_{METHOD} x Size	14.69	1	15.31	2.04	0.156
	Size x Pres	1.91	1	1.91	0.25	0.615
	EC_{METHOD} x Pres x Size	0.10	1	0.10	0.02	0.681
	Error	961.28	127	7.51		
	Total	2729.65	134			

CF5: r^2=0 .48; CH4: r^2= 0.63.

1. EC_{METHOD} = EC_{CAL}, EC_{OSV}; 2. Preservation = frozen or formalin-preserved

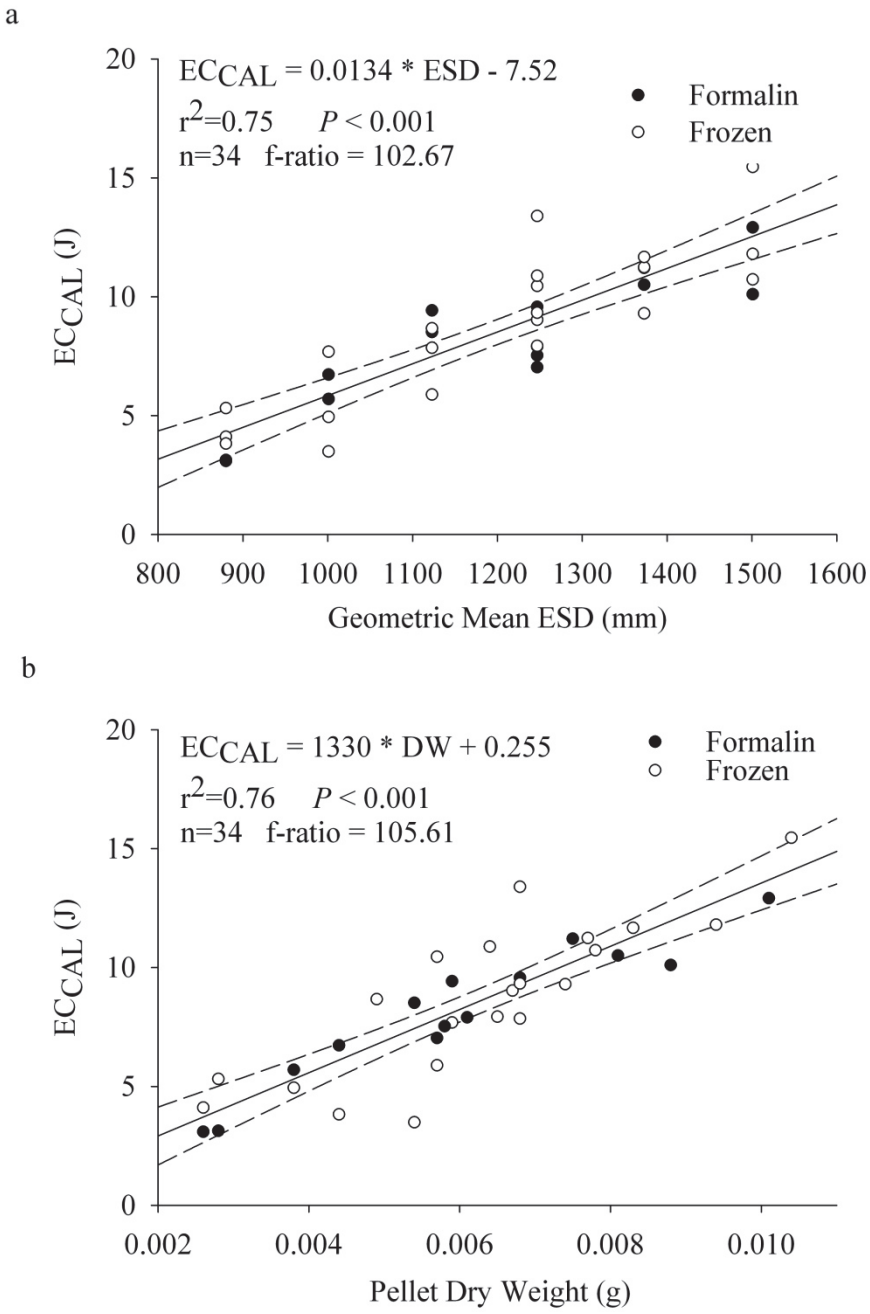

Figure 2.2 Relationship between individual energy content (EC_{CAL}, J) and (a) size or (b) pellet DW for frozen-preserved (open symbols) and formalin-preserved (closed symbols) *C. finmarchicus* stage-5, CF5 and *C. hyperboreus* stage-4, CH4. Both species and preservation techniques were combined in a single regression equation because no statistical differences were found within each explanatory variable. Dashed lines are the 95% confidence intervals for the expected energy content and each symbol represents a bulk sample of 20 copepods.

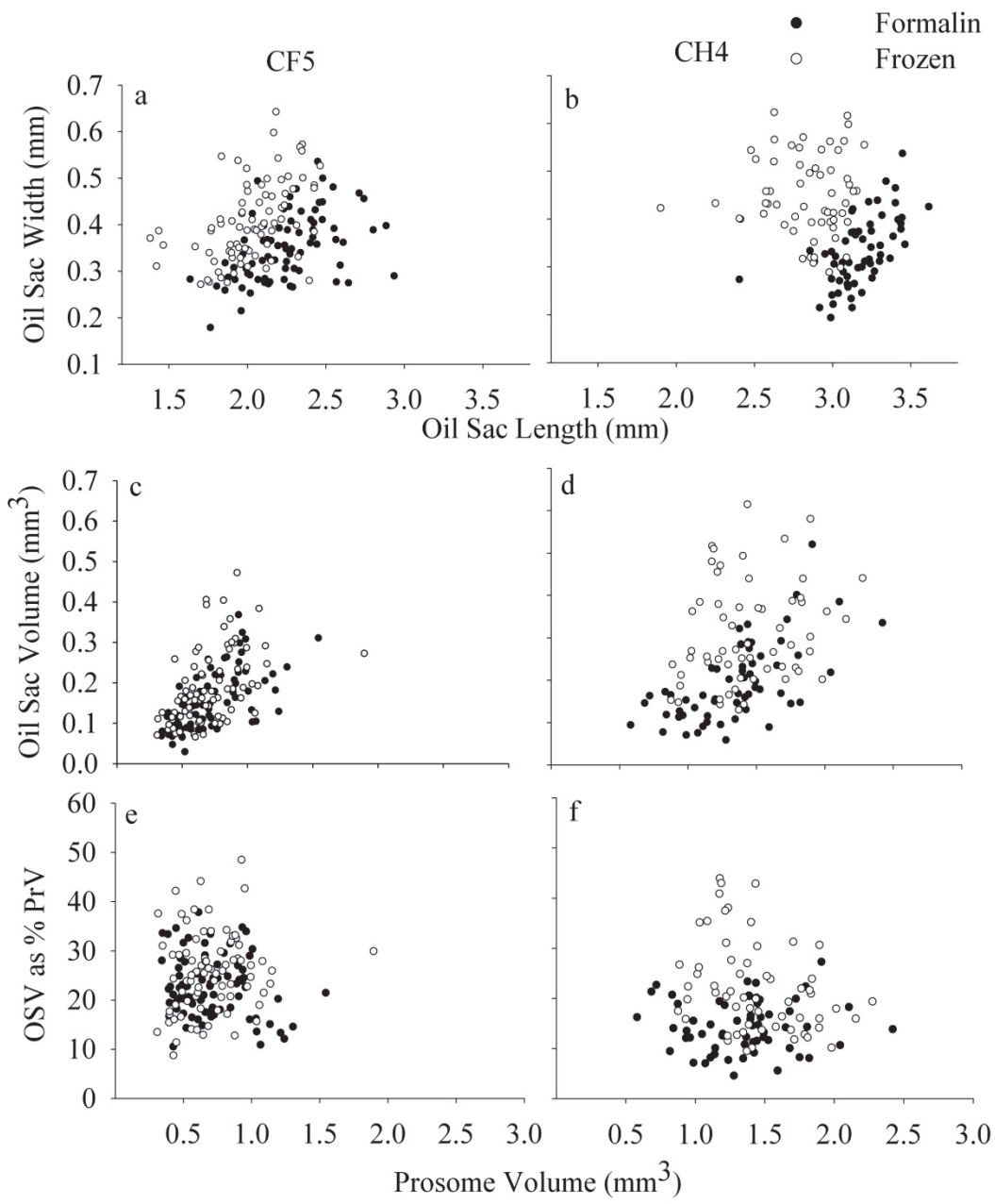

Figure 2.3 Scattergrams of relations between oil sac width (mm) and oil sac length (mm) for frozen- (open symbols) and formalin-preserved (closed symbols) *C. finmarchicus* stage-5, CF5 (a) and *C. hyperboreus* stage-4, CH4 (b) illustrating the variation in the effect of preservation on oil sac shape between the two species. The differential preservation effect is further illustrated with CF5 (c, e) and CH4 (d, f) cylindrical oil sac volume (OSV, mm^3), and cylindrical OSV as a percentage of the prosome volume, in relation to its prosome volume (mm^3).

2.4 Discussion

I directly measured gross energy content in (assumed) diapausing *Calanus* spp. collected on the Scotian Shelf during late-summer and related the measures to morphometric quantities that are easily measured in the laboratory and field. With these measurements I was able to determine three main relationships that provide greater insights into how estimates of energy content can be determined from frozen- or formalin-preserved animals and using a range of metrics. First, I established that size (ESD) explains most of the variation in directly measured individual energy content (EC_{CAL}) and that the variation was not significantly influenced by the formalin preservation technique. Second, I found no difference in EC_{DW} (a measure of energy quality) between the species and stages examined and that diapausing *C. finmarchicus* and *C. hyperboreus* on the Scotian Shelf together have a dry-weight specific energy content of 27.9 ±5.0 kJ g^{-1} (mean ±S.D). Third, I determined that among overlapping size classes (in ESD) there is no difference in EC_{CAL} between the two species and stages. Thus, I conclude these relationships can be used to estimate energy available to *Calanus* spp. predators with relatively simple and readily available sampling devices and simple metrics (e.g., size).

The usefulness of my calibrations rests on the accuracy of the calorimetry measurements. Accuracy can be assessed through comparisons with energy measurements made on *Calanus* spp. elsewhere in the North Atlantic. Estimates of EC_{DW} among large copepods, including CF5s and CH4s, varies between 17 and 30 kJ·g^{-1} at low- to mid-latitudes and increases at higher latitudes (Båmstedt 1986), a range that brackets my average EC_{DW} estimate. Energy content in CF5s measured in nearby Grand Manan Basin was 32.1 ±13.5 kJ·g^{-1} (Michaud and Taggart 2007), an estimate that also brackets my estimate, and more importantly it is an estimate that did not vary across size (also the case in my results) or across the May through Oct season. From this, I can reasonably conclude that my results based on September samples can be assumed to be constant over the same seasonal period. Comita *et al.* (1966) also estimated 31.2 ±0.8 kJ·g^{-1} over the May though Oct period in the Clyde Sea. Thus, my results are commensurate with several independent results above. The small differences in EC_{DW} estimates among studies could be attributed to geographic variability, time of year, depth distribution, or feeding conditions (Pepin and Head 2009), and perhaps measurement

techniques. I can also reasonably conclude that the effect of individual variability in energy content among copepods was minimized in my study relative to other studies (e.g., Bamstedt, 1988) by using diapausing copepods collected at depth during the time of year when oil sacs are near their maximum (Miller *et al.* 2000) and have the lowest variability among individuals (Pepin and Head 2009).

2.4.1 Environmental influences on *Calanus* spp. energy content

Higher trophic level predators in Roseway Basin are feeding on a mix of co-located CF5s and CH4s. I found that individual energy content in frozen CF5s and CH4s varied only because larger animals contained greater energy (EC_{CAL}) than smaller animals and, in contrast to Arctic food webs, not due to variation in energy quality (EC_{DW}) between species. This makes the application of energy terms to abundance-at-size measurements of the two co-located species straightforward in my study area, which is particularly useful when using in situ techniques such as the optical plankton counter (Chapter 3). Oil sacs of Arctic *C. hyperboreus* have slightly greater calorific content than *C. finmarchicus* because wax esters in the former have a greater proportion of long chain 22:1(*n*-11) fatty acids (Albers *et al.* 1996), likely an adaptation to the extreme Arctic environment. My data may imply that the more temperate populations of *C. hyperboreus* do not accumulate such long chain fatty acids, likely because they do not experience the long periods of food shortage typically experienced by Arctic populations. This difference is also evident in an Arctic (Fram Strait, 78^0N) compared with a north-temperate (North Sea, 58^0N) population of *C. finmarchicus* (Kattner 1989).

The presence of the Nova Scotia Coastal Current on the Scotian Shelf means that individual copepods diapausing in the Shelf Basins are more energetically valuable to their predators compared with those diapausing nearby in Grand Manan Basin, Bay of Fundy. I offer two explanations for this. First, the coastal current brings *C. hyperboreus* to the Shelf Basins but only periodically intrudes farther southwest into the Bay of Fundy and Gulf of Maine (Aretxabaleta *et al.* 2008, Aretxabaleta *et al.* 2009), where this high-latitude, cold-water species is typically found at low abundance (8 m^{-3}; CF5:CH4 80:1; Michaud and Taggart 2007). Second, lower temperatures promote greater copepod body weight (Kattner 1989, McLaren *et al.* 1989), and total energy scales positively with body

weight as detailed above. It is not surprising, then, that I found individual CF5 energy content in Grand Manan Basin (Bay of Fundy) was on average less than half (EC_I = EC_{CAL}, 3.31 J, range 1 to 5 J; Michaud and Taggart 2007) that reported here for Roseway Basin at 6.9 J (range 3 to 11). The range of CF5 prosome lengths was not different between the two Basin habitats (2 to 3 mm), however individual CF5s in Roseway Basin weighed twice that per unit length ($DW = -7.13 \times 10^{-4} + 4.40 \times 10^{-4}$ PrL) observed for CF5s in the Grand Manan Basin ($DW = -3.8 \times 10^{-4} + 2.13\ 10^{-4}$ PrL; Michaud 2005). These are relevant ecological findings. For example, species such as the endangered right whales rely on copepod populations in both habitats, and the energetic dependence of right whales on diapausing copepods is critical to several aspects of right whale recovery, such as explaining variation in calving rates (Klanjscek *et al.* 2007, Michaud and Taggart 2010, Miller *et al.* 2011, Chapter 3).

2.4.2 Energy content of *Calanus* spp. inferred from oil sac volume

Gross energy content inferred from oil sac volume (OSV) was not different from energy content measured using calorimetry on frozen samples (EC_{CAL}). Thus, energy content inferred from OSV offers a simple and practical metric for addressing questions related to absolute energy content. Accordingly, copepod oil sac volume estimated in a relative manner (e.g., Plourde and Runge, 1993, Reiss *et al.* 1999, Pasternak *et al.* 2001, Hasset 2006, Pepin and Head 2009) may be convertible to absolute energy content using my analytical protocols. The OSV metric has an additional advantage over calorimetry because it can be estimated in the field using simple body size metrics, and can be estimated on individuals.

Vogedes *et al.* (2010) argue that energy content inferred from OSV over-estimates the chromatographic estimates of wax ester content by a factor of 2. I found no similar discrepancy between energy content estimated from calorimetry and that inferred from OSV. I was able to make a direct comparison between total energy (EC_{CAL}) and oil sac energy (EC_{OSV}) because my measurements used only copepods that had recently entered diapause and hence had full oil sacs; in this state the relationship between CF5 calorific value and wax ester (oil sac) energy measured by chromatography centers on 1:1 (Michaud and Taggart 2007). Vogedes *et al.* (2010) also developed an oil sac cross-

sectional area calibration and concluded that the oil sac area (EC_{OSA}) approximation has greater predictive power for estimating wax ester content than does an OSV approximation. However, using OSA as a proxy for a volumetric quantity such as energy content assumes that the oil sac shape is constant. It is easily demonstrated that a spherical oil sac and a long, thin cylindrical oil sac of equal area, have different volumes and hence estimates of wax ester content will differ. Variation in oil sac shape among copepod species, and under different environmental conditions, may thus limit the predictive power of the OSA calibration. The use of area may be unnecessary in any event because my results are consistent with the conventional use of OSV-inferred energy content. This led me to apply their OSA calibration equation, which Vogedes *et al.* (2010) claim can be used in other studies, to my copepods, and compare the results to my calorimetric measurements. I caution that, when making this comparison, my copepods were fresh-frozen or formalin-preserved, while the copepods in Vogedes *et al.* (2010) were freshly caught animals, which may have an effect.

The oil sac area proxy developed by Vogedes *et al*. (2010) substantially underestimated copepod gross energy content of copepods in my study, particularly in the smaller CF5 (Figure 2.4a,b,c,d). This result is most simply explained by oil sac shape variation between copepods in my study and copepods used by Vogedes *et al.* (2010) collected from a different region of the North Atlantic. OSA/OSV ratios from both studies were within approximately the same range (~2 to ~8) but were highly variable for species in the 2 to 3.5 mm prosome length class (Figure 2.4e). At smaller lengths within my CF5 range, the ratios measured by Vogedes *et al.* were at the upper end of what I measured. This is because CF5 oil sacs measured in my study were larger in area per unit length than theirs (Figure 2.4f). Animals with larger OSA/OSL (my study) have proportionally larger volume than animals with smaller OSA/OSL (Vogedes *et al.* 2010), and hence contain more lipid for a given measured area than a calibration based on the copepods used by Vogedes *et al.* would predict.

My larger CH4 oil sac shape coincided most closely with oil sacs of *C. glacialis* measured by Vogedes *et al.* (Figure 2.4e, f), while CH4 oil sacs they measured were both longer and greater in area than CH4s measured in my study. The coincidence in oil sac shape between my CH4s and their *C. glacialis* is likely the reason why I saw less

deviation between EC_{OSA} and gross energy in CH4s than CF5s. I also found a high degree of individual variability in oil sac shape that increased at smaller prosome lengths. Since the Vogedes *et al.* (2010) calibration was performed on only a few individuals per size class, individual variability within their relationship was almost certainly underestimated. I conclude that oil sac area does not accurately predict energy content in the copepods used in my study because the animals used to develop the calibration had oil sacs that differed in shape from those of my copepods.

2.4.3 The effect of preservation on energy content estimation

Archived samples of CF5s preserved in formalin can potentially be used to answer questions concerning energetics. Direct and inferred estimates of energy content among lipid-replete CF5s preserved in formalin for up to two years did not differ from estimates derived from those preserved by freezing; the latter being the standard preservation method used in most energetic studies. I caution that oil sac integrity is not maintained by all individuals preserved in formalin. Oil (lipid) droplets were prevalent in the preservation solution in my sample collections and there were many individuals with obviously ruptured oil sacs. However, my analysis shows that using only those newly-diapausing and preserved CF5 individuals with full and intact oil sacs can provide reliable, unbiased estimates of gross energy content. Degradation of the polyunsaturated fatty acids has been hypothesized to occur in formalin (Morris 1972). My results indicate that either degradation did not occur during sample storage over one to two years, or that degradation, presumably to shorter fatty acid chains, does not measurably decrease the energy quality, because EC_{DW} did not vary between the two preservation techniques.

In contrast to the CF5s, the CH4s appear to be more susceptible to oil sac shape change in formalin, and this may preclude the use of the simpler method of inferring energy from OSV. Preservation had no effect on either EC_{CAL} or dry weight (direct measures), but did influence inferred energy content in CH4. This preservation effect on inferred energy content could be due to the geometric shape approximation applied. To demonstrate this, I applied a correction factor that converted cylindrical OSV measured from the lateral aspect to the average between OSV measured from a lateral and a dorsal aspect, a metric provided by Miller *et al.* (2000; their Figure 2) for use with CF5s,

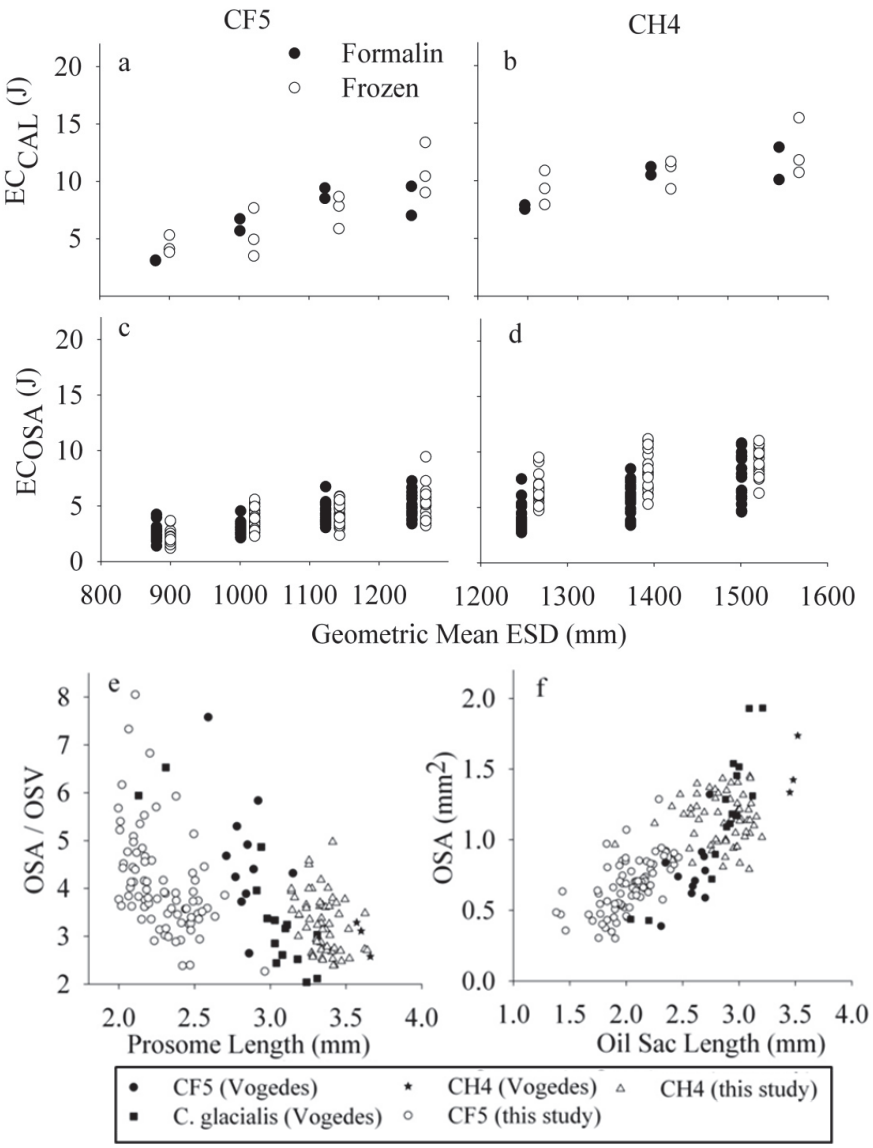

Figure 2.4 Comparison between copepod energy content (EC) measured by calorific value (EC_{CAL}; a, b) and energy content inferred from areal oil sac approximations using the calibration equation in Vogedes *et al.* 2010 (EC_{OSA}; c, d), in both frozen- (open symbols) and formalin-preserved (closed symbols) *C. finmarchicus* stage-5, CF5 (a, c) and *C. hyperboreus* stage-C4, CH4 (b, d). Animals in the frozen-preserved ESD category are offset by 20 µm in a,b,c,d for clarity. Energy content variation between my study and Vogedes *et al.* 2010 is interpreted by comparing oil sac shape between copepods in this study and copepods used to develop the oil sac area proxy in Vogedes *et al*. (2010); e) OSA/OSV ratios for *C. finmarchicus* stage-5, CF5 and *C. hyperboreus* stage-C4, CH4 (my study, open symbols) and CF5, *C. glacialis* and CH4 (Vogedes study, closed symbols). f) Oil sac area (OSA) increased linearly with oil sac length (OSL) in both studies, but my CF5 were smaller and had greater OSA/OSL ratios.

because the oil sacs of larger individuals become oblate rather than circular in the transverse section, and I assumed that the larger CH4s underwent the same shape change. When applied, this correction decreased the difference in CH4 cylindrical EC_{OSV} between preservation techniques by 7 %. I then assumed that a frozen CH4 oil sac reflects that of a fresh oblate spheroid oil sac, and that formalin moulds it into a longer, more cylindrical form, consistent with the morphometric changes I measured. Under this assumption the difference between formalin-preserved and frozen animals declined by as much as 11 %. It is possible, then, that the 'effect' of formalin on EC_{OSV} was an artefact of the geometric approximation, and different approximations should be developed to correct this.

There are two caveats when using formalin-preserved CF5 specimens: 1) only those specimens with intact oil sacs should be chosen for analysis, and 2) time and handling likely affect oil sac integrity. Vigorous shaking may easily damage delicate oil sacs. The rate of passive lipid loss is probably highest in the first few weeks and declines thereafter. Dry weight loss was 37 % (Giguere *et al.* 1989) and 20 % (Omori 1978) in copepods preserved for one week, while after one year a similar 30 to 35 % loss was measured (Bottger and Schnack, 1986).

In summary, size was the most important factor causing variation in energy content of copepods diapausing in Roseway Basin; energy did not vary among species. In Chapter 3, I will use these estimates to examine the energy available to right whales in the Roseway Basin habitat. Oil sac volume is a good approximation of total energy in copepods that are at their annual maximum in lipid content, and formalin-preserved samples can be used to answer questions concerning energetics if animals with full oil sacs are chosen for analysis.

Chapter 3

Spatial Variation in the Right Whale Prey Field in the Roseway Basin: Implications for Critical Habitat

3.1 Introduction

3.1.1 Critical Habitat of endangered marine species in Canada

Under the Canadian federal Species at Risk Act (SARA, est. 2002), the habitat required to close the life history of endangered or threatened species must be formally identified so that it can be protected to promote species recovery. If information is inadequate to describe Critical Habitat, then research must be scheduled for the purpose of describing and identifying it in the future. Definition, identification and protection of Critical Habitat are primary objectives of SARA because the entire range occupied by all endangered species cannot feasibly be protected after human social and economic factors are taken into consideration (Vanderzwaag and Hutchings 2005). This is particularly true for highly migratory species that include endangered marine fish and mammals. However, Canada has about 50 marine mammal and fish populations listed as 'Endangered' or 'Threatened', and identifying and describing Critical Habitat for these species has been difficult and less than timely. The most common reason for this is a lack of habitat data in the ocean. As a consequence, since SARA was implemented in 2003, Critical Habitat has not been fully defined based on habitat attributes for protection of a marine species in Canada. Deficiencies in both the knowledge and protection of marine Critical Habitat have not gone unnoticed. For example, in 2012 the federal government lost a court appeal against a coalition of nine environmental agencies who argued that Fisheries and Oceans Canada had failed to legally protect Critical Habitat for resident killer whales in British Columbia.

3.1.2 Critical Habitat for North Atlantic right whales

North Atlantic right whales are a critically endangered species that migrate to Canadian waters to feed in summer (June-October). Based on right whale sightings, Grand Manan Basin in the Bay of Fundy and Roseway Basin on the Scotian Shelf were identified as primary areas of right whale aggregation. The pioneering prey field work by Murison and Gaskin (1989) identified Grand Manan Basin as a likely feeding habitat. These two areas were initially designated (but not legislated) as Right Whale Conservation Areas in 1993, and subsequent research concerning the relationship between right whales and their prey was undertaken. Effort was initially focused on Grand Manan Basin due to consistent annual occupancy by right whales, whereas Roseway Basin was considered a more ephemeral habitat due high variation in right whale occupancy there (Kraus and Rolland 2007). Research confirmed that within Grand Manan Basin, right whales feed on deep, diapausing layers of the copepod *Calanus finmarchicus* stage-C5 (Woodley and Gaskin 1996, Baumgartner *et al*. 2003a; 2003b, Baumgartner and Mate 2003) and the spatial and temporal extent of the deep copepod layer measured by Michaud and Taggart (2007; 2011) was used to identify the boundaries of the current Critical Habitat in the SARA Recovery Strategy for right whales (Brown *et al*. 2009). Critical Habitat was then defined as any area that "possesses the environmental, oceanographic and bathymetric conditions that aggregate concentrations of right whale prey, especially stage-C5 *Calanus finmarchicus* copepodites, at interannually predictably locations" (Brown *et al*. 2009).

3.1.3 Identifying Critical Habitat in Roseway Basin

Roseway Basin has also been identified as an area where right whales aggregate (e.g., Baumgartner and Mate 2003; 2005, Kraus and Rolland 2007, Vanderlaan *et al*. 2008) and where diapausing C5s are abundant at depth (Baumgartner *et al*. 2003a). However, the spatial distribution of the prey field in Roseway Basin had yet to be measured, precluding definition of Critical Habitat in that habitat. When it was published, the Recovery Strategy for North Atlantic right whales included Roseway Basin as a Critical Habitat area, based partly on the preliminary data collected for this thesis (Brown *et al*. 2009). The Strategy contained provisional Critical Habitat boundaries for Roseway Basin that

encompassed the historical right whale distribution (Vanderlaan *et al*. 2008) with the stipulation that the Critical Habitat boundaries defined in that Strategy may be later refined based on the final outcome of this thesis (Brown *et al*. 2009).

3.1.4 Oceanographic processes that aggregate right whale prey in deep basins

Variation in right whale prey abundance within a basin can be caused by at least three different processes; variation in the sources of prey to the basin, retention mechanisms within the basin that maintain the prey resource over time, and aggregation processes within the basin that create high concentration prey patches. Several hypotheses have been put forth to explain diapausing copepod sources and mechanisms of accumulation and retention in deep basins in the Scotia-Fundy region.

3.1.4.1 Sources of diapausing copepods to the Basins

It is well established that the Scotian Shelf has two major water masses that are sources of plankton to the deep Shelf basins. The first is a cold, fresh water mass from the Gulf of St. Lawrence (GoSL), containing cold-adapted *Calanus* spp. such as *C. glacialis* and *C. hyperboreus*, that is transported along the inner Shelf by the Nova Scotia Coastal Current. The second water mass is warm, salty continental slope water that contains high concentrations of *C. finmarchicus,* a sub-Arctic and boreal species (e.g., Tremblay and Roff 1983, Sameoto and Herman 1990, Herman *et al*. 1991, Head *et al*. 1999, McLaren *et al*. 2000, Zakardjian *et al*. 2003). The outer arm of the Nova Scotia Coastal Current flows southwest along the continental slope and mixes with slope water before intruding on-shelf into the central and western Shelf basins. As a consequence, basins on the eastern Scotian Shelf (e.g., Louisbourg Basin) are dominated by Arctic copepod species, whereas basins on the central and western Scotian Shelf are dominated by *C. finmarchicus*. It is hypothesized that the addition of slope water to the central and western Scotian Shelf plays a pivotal role in the population dynamics of *C. finmarchicus* on the Shelf (Head *et al*. 1999, Zakardjian *et al*. 2003), and that interannual variation in slope water intrusions to Roseway Basin may explain variation in *C. finmarchicus* and right whale abundance in that habitat (Patrician and Kenney 2010). *Calanus*

finmarchicus can be supplied to Grand Manan Basin from the Scotian Shelf, Gulf of Maine and Northeast Channel (Michaud 2005).

3.1.4.2 Retention of diapausing copepods within the Basins

Retention of diapausing copepods in deep basins is thought to occur primarily because of weak current velocities and gyre-like circulation below the sill depth. Copepods advected continuously into the surface waters of basins in late-summer sink when they enter diapause and become trapped below the sill, where they are retained and accumulate over time. This hypothesis was put forth to explain the distribution and maintenance of diapausing copepod aggregations at depth in Emerald and Lahave Basins, which are located east of Roseway Basin on the Shelf (Herman *et al*. 1991). The timing of maximum annual *C. finmarchicus* C5 abundance in Grand Manan Basin coincides with the maximum particle retentiveness of a seasonal gyre in the Basin that is maintained by tidal rectification and baroclinicity (Aretxabaleta *et al*. 2008). Gyre-like circulation in Roseway Basin has been inferred from a baroclinic circulation model (Hannah *et al*. 2001), but no in-situ work had been undertaken to confirm its existence.

Right whales may take advantage of a gyre-like circulation mechanism to maximize their foraging efficiency, with the deepest regions providing the best foraging grounds for the whales. The center of the seasonal gyre in Grand Manan Basin (Aretxabaleta *et al*. 2008) is co-located with the center of the right whale distribution located at the geographic center of the Basin (Vanderlaan *et al*. 2008), which lends credence to the above hypothesis in that habitat. However, the center of the right whale sightings distribution in Roseway Basin is not located over the deepest part of the Basin, but rather along the southern boundary of the Basin (Figure 3.1), suggesting that the deepest part of Roseway is unlikely to be the ideal foraging area. If a gyre-like circulation exists in Roseway Basin, its center may not be in the Basin center, and the processes that generate it may not be the same as in Grand Manan Basin, both of which could affect how the right whales use the process to their advantage, and how Critical Habitat might be defined.

3.1.4.3 Aggregation of high-density prey patches within the Basins

Right whales require highly concentrated patches of prey within a feeding habitat to maximize their energy intake and minimize the time spent foraging. The animals do not have behavioral mechanisms to accomplish this, so they rely on the environment to aggregate their prey (Baumgartner *et al.* 2007). Gyre-like circulation can assist in aggregating prey at the Basin-scale, but whales require smaller-scale aggregation processes as well. An association between the spatial variation in right whale occurrence and the presence of surface temperature fronts in Roseway Basin was identified as one possible process (Baumgartner *et al*. 2003a). The authors hypothesized that these fronts extend through the water column and, like gyres, promote aggregations through the interaction between plankton buoyancy and current velocities at the front (e.g., Franks 1992). Frontal aggregations of copepods at tidal mixing fronts on the margins of Grand Manan Basin (Michaud and Taggart 2011) and Georges Bank (Wishner *et al.* 2006) have also been proposed. Neither the mechanisms by which frontal accumulation occurs, nor the degree to which right whales rely on such mechanisms, have been investigated in the Shelf basins.

3.1.5 Objectives

The primary objective of this chapter is to measure the concentration, energy density, spatial distribution and extent of the prey field in Roseway Basin with the goal of identifying right whale Critical Habitat in this area, as was achieved for Grand Manan Basin (Michaud and Taggart 2011). To meet this objective, I measured the spatial distribution of the right whale prey field using optical plankton counter data and express it in terms of prey concentration (m^{-3}) and also energy density (kJ m^{-3}), following Michaud and Taggart (2011). Using the results, I then discuss the definition of Critical Habitat for Roseway Basin, evaluate the provisional Critical Habitat boundaries, and make conservation recommendations for the future of the habitat. I further use the data to estimate the carrying capacity for right whales in Roseway Basin in 2008.

My second objective is to examine the oceanographic and bathymetric conditions responsible for the accumulation and retention of diapausing copepod aggregations in the Basin. Specifically, I aim to identify whether or not slope water intrusions, gyre-like

circulation and fronts occur in the Basin, and examine the distribution of right whale prey with respect to these features. I address this objective by examining co-located copepod and hydrographic data between the surface and 160 m depth at high resolution across the entire Basin, with a focus on the deep Basin. In the Discussion, I summarize all the insights gleaned from the data concerning the following questions: Are slope water intrusions an important source of diapausing copepods to the Basin? Are the deepest parts of the Basin associated with a closed circulation that passively aggregates and retains diapausing C5s? Do ocean fronts (both tidal fronts and water mass fronts) lead to aggregated plankton in the Basin?

3.2 Methods

3.2.1 BIONESS data collection

An oceanographic survey was conducted in Roseway Basin during 04-13 September 2008 from the R/V *Dominion Victory*. Zooplankton samples were collected at four stations using a Bedford Institute of Oceanography Net and Environmental Sampling System (BIONESS; Sameoto *et al*. 1980) towed at ~1m s^{-1} and equipped with five to seven 333 μm-mesh nets (1 m^2 opening; 1.5 m length). Sampling stations were situated along the southern slope of the Basin in the center of the historical right whale sightings distribution and in the vicinity of other instruments deployed, for calibration purposes (Figure 3.1). At stations B01, B03 and B04, BIONESS Net-1 collected a sample from the surface to ~10 m above bottom while subsequent nets sequentially opened and closed to sample discrete strata between near bottom and the surface. At station-B02, the BIONESS tow was completed with all nets opening and closing between 130 – 160 m depth to capture small-scale spatial variation in the prey field at depth. Once recovered, each net sample was filtered through a 330 μm sieve and preserved in 4% buffered formalin.

The BIONESS was fitted with either a Seabird–19 CTD (real-time datastream to ship) or Seabird-37 microCAT CTD (internally recording), two General Oceanics (G.O.) flowmeters to estimate filtered volume, and an Optical Plankton Counter (OPC, Focal Technologies; Herman 1988, 1992). The OPC consisted of a 2 x 25 cm sampling tunnel, located between two pressure cases containing the electronics. I frequently lost

communication with BIONESS due to problems with the conducting cable, and flowmeter data were lost. When flowmeter data were lost, flow speed through each net was estimated from the BIONESS tow speed, which was calculated from ship speed over ground recorded by GPS and the change in instrument depth recorded by the CTD. I assumed that the relative speed over ground of the ship and the instrument are the same, a valid assumption because BIONESS is exceedingly heavy and there is no catenary in the tow cable when BIONESS is towed. Whenever possible, vertical CTD casts were collected using a Seabird-25 CTD. BIONESS data were also collected in the Basin in 2009, and those data are used here only for calibration purposes. The 2009 data were collected at three stations in the same vicinity as in 2008. Flowmeter data were available in 2009.

3.2.2 Zooplankton taxonomic, size frequency and energy content analyses

All large and rare organisms (macrozooplankton; nominally >2 cm) were sorted from the formalin-preserved BIONESS net collections, identified to family, and counted. The remainder of each sample (mesozooplankton; nominally 333 μm to 1 cm) was partitioned using a Folsom splitter until replicate sub-samples of 150 to 200 copepods were obtained. All zooplankton in each sub-sample were counted and identified: copepodids to genus, species and stage and the others to the highest taxonomic resolution possible. Sequential replicate sub-samples were examined until the coefficient of variation (CV) for both the dominant copepod species and stage and the total number of copepods either decreased to ~10% or less, or stabilized, or until a maximum of six sub-samples had been examined. Generally three to four replicates were required and the average CV for the total number of copepods and C5s consistently ranged between 10 and 11%. Random subsamples of 20 to 100 dead individuals of *Calanus finmarchicus* C5s (hereafter CF5) and *Calanus hyperboreus* C4s (hereafter CH4) were taken from each net, photographed under a dissecting scope, and their length and width measured using Image-J (v. 141) digital imaging freeware.

Gross energy (caloric) content of CF5s and CH4s collected in Roseway Basin in 2007 were measured using a Parr® 1266 semi-micro oxygen-bomb calorimeter (Chapter 2). The 2008 frozen samples were lost, so the 2007 energy content estimates are used

here. CF5s and CH4s were first sorted into size classes chosen to correspond with OPC digital bin classes that encompassed the observed size frequency distribution measured using the biological samples. This enabled me to apply size-specific energy terms to the copepod abundance-at-size distributions measured by the OPC. The four CF5 bin classes (*Equivalent Spherical Diameter* (*ESD) range (μm)*) were: 8 (*823-936*), 9 (*943-1058*), 10 (*1064-1182*), and 11 (*1187-1307*). The three CH4 digital bin classes (*ESD range*) were: 11 (*1187-1307*), 12 (*1312–1434*) and 13 (*1439-1562*). Since I found no significant differences in energy content between CF5 and CH4 in the overlapping bin class 11 (Chapter 2) I combined the data for both species in bin class 11 and used the average energy content of all data in that bin class (Table 3.1).

3.2.3 TUBSS-OPC data collection

Zooplankton abundance-at-size estimates, particularly for the CF5 and CH4 combined size distribution, were obtained using an Optical Plankton Counter attached to a V-fin along with a digital flowmeter and a Seabird-37 microCAT CTD. This Towed Underwater Biological Sampling System (TUBSS, Taggart *et al*. 1996, Sprules *et al*. 1998) was deployed in an undulating fashion between 50 m depth and ~10 m above bottom using a vertical speed of ~1 ms^{-1} and ship speed ~3 nm h^{-1} along a series of transects that were pre-determined to encompass the historical right whale distribution (Table 2.2, Figure 3.1). Seven cross-Basin transects (transect-1 to -7) each ~15-30 km in length ran roughly north-west to south-east in a zig-zag pattern. Transect-8 was ~35 km in length and crossed transect-4 and 5. Two along-Basin transects (transect 9-10) intersected the sampling of the other seven. Each transect was transited a single time during the survey. In addition, the southeast half of transect 4 was transited 11 times in 24-hours between 19:15 h (ADST) on 11-Sept and 18:45 h on 12-Sept to capture tidal variation in zooplankton concentration and temperature across the southern margin. Note that the long axis of the tidal ellipse is oriented cross-slope, so the direction of sampling allowed me to measure prey field movement along the tidal axis. Salinity and density data were not recorded during the 24 h transect due to equipment failure.

The OPC recorded plankton abundance-at-size data at 1-sec intervals. Problems with a non-functional CTD hardwired to the TUBSS platform prevented recording of

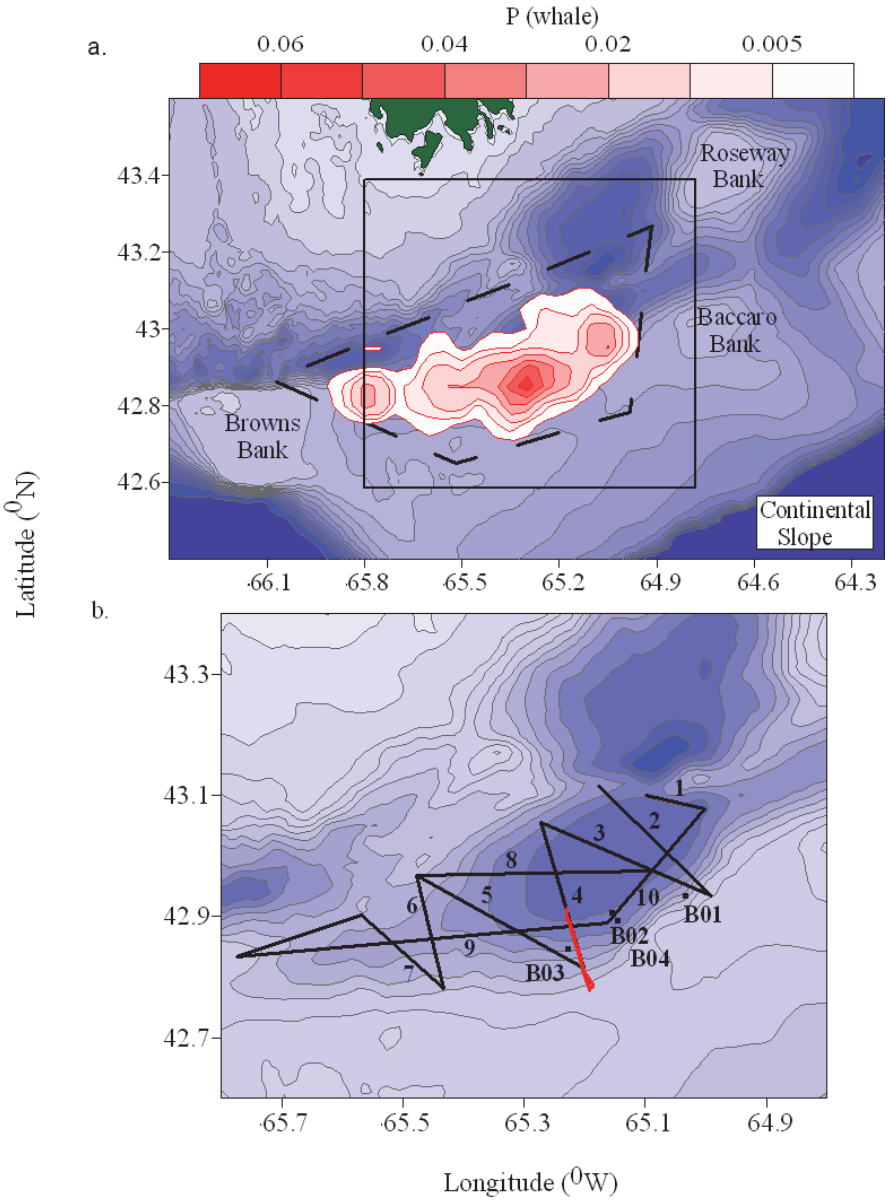

Figure 3.1 Bathymetric chart of the Roseway Basin survey design, showing (a) the distribution of the relative probability of observing a right whale in Roseway Basin (adapted from Vanderlaan *et al*. 2008), where the dashed line represents the boundaries of the provisional Critical Habitat and the solid rectangle represents the boundaries of (b), that shows the zooplankton prey field survey executed in 2008. Each Bedford Institute of Oceanography Net and Environmental Sampling System (BIONESS) tow location is identified by B0x labels and solid lines denote the Towed Underwater Biological Sampling System (TUBSS) transect survey tracks, each of which is identified by numbers 1 - 10. Isobaths are spaced at 10 m. The 24-hour transect line is depicted by a red line in (b).

Table 3.1 Average energy content (J ind^{-1}) and standard error of combined *C. finmarchicus*, CF5, and *C. hyperboreus*, CH4, by bin class (prosome size).

Bin Class	Average Energy Content (J ind^{-1})	Standard Error
8	3.89	0.41
9	5.71	0.72
10	8.07	0.60
11	9.31	0.60
12	10.78	0.42
13	12.20	0.95

Table 3.2 Summary characteristics of each TUBSS transect in Roseway Basin during 04 to 13 September 2008. Provided are transect start and end dates and times (ADT), latitudes (^{0}N) and longitudes (^{0}W), along with nominal headings, length and maximum depths of sampling.

Transect No.	Start Date (mm/dd)	Start Time (hh/mm)	End Date (mm/dd)	End Time (hh/mm)	Start Lat	Start Lon	End Lat	End Lon	Heading	Length (km)	Max depth sampled (m)
1	09/06	01:31	09/06	03:10	43.077	-65.002	43.100	-65.097	NW	8.27	161
2	09/11	12:39	09/11	17:01	42.922	-64.977	43.112	-65.174	NW	27.00	163
3	09/11	07:44	09/11	12:03	43.074	-65.278	42.930	-64.982	SE	29.90	160
4	09/09	17:17	09/09	21:06	42.814	-65.201	43.038	-65.268	NW	26.17	161
5a	09/13	20:11	09/13	17:37	42.967	-65.480	42.875	-65.315	SE	17.00	144
5b	09/09	15:22	09/09	17:17	42.875	-65.318	42.814	-65.201	SE	12.08	143
6	09/08	22:10	09/09	01:50	42.960	-65.477	42.780	-65.433	SE	21.09	132
7	09/09	01:50	09/09	04:47	42.780	-65.433	42.903	-65.568	NW	17.89	128
8	09/13	20:11	09/14	00:45	42.967	-65.480	42.976	-65.089	E	31.88	161
9	09/05	21:00	09/06	01:30	42.898	-65.164	43.076	-65.002	NE	28.25	156
10a	09/09	07:43	09/09	15:21	42.832	-65.775	42.875	-65.320	E	24.16	143
10b	09/13	15:30	09/13	17:39	42.889	-65.154	42.876	-65.316	W	23.99	153

pitch and flowmeter data. To obtain CTD data I attached an internally recording microCAT CTD to the platform, which recorded data at 20-sec or 6-sec intervals that were uploaded after each tow. GPS data were recorded onboard at 60-sec intervals. In lieu of flowmeter data, tow speed was estimated in the manner described for BIONESS. Volume filtered was determined using the product of tow speed, elapsed time and cross-sectional area of the OPC sampling tunnel. The data-streams were integrated prior to data analysis.

Tow speed estimated from the ship GPS was systematically higher when TUBSS was descending, leading to lower depth-specific zooplankton particle concentrations relative to the subsequent ascent. A likely explanation is that on a descent the instrument cable is reeled out freely, reducing instrument drag compared to an ascent when tension on the cable is far higher. If this is true, I expect flowmeter speed and tow speed estimated from ship GPS to be similar on the ascent when drag from TUBSS is high. When drag is low, tow speed estimated from ship GPS should be high relative to the flowmeter speed. To address this problem, I used a limited dataset from 2009 that was collected with TUBSS in the same area aboard the same ship, and for which I had both tow speed from ship GPS and flowmeter data. I compared the 2009 GPS tow speed to the 2009 flowmeter speed averaged over the ascent or descent. As I expected, the two speeds were very similar on the ascent (flowmeter speed = 1.01•tow speed). On the other hand, ship speed was ~10% higher than flowmeter speed on the descent (flowmeter = 0.91•tow speed – 0.02, Figure 3.2). The differences between the ascent and descent were tested using ANCOVA, with flowmeter speed as the dependent variable, tow speed as the covariate, and ascent/descent as a fixed factor. The effect of the covariate was significant ($P<0.001$) and there was no difference in flowmeter speed between the ascent and descent ($P=0.125$). The interaction term was marginally significant ($P=0.033$), indicating that the relationship between flowmeter speed and GPS tow speed was not the same (although it appears very similar) between the ascent and descent. The empirically derived equation relating flow speed and tow speed on the descent in 2009 was used to correct the descent speed in 2008. No correction was made to the ascending tow.

3.2.4 TUBSS-OPC data analysis

The majority of TUBSS-OPC data analyses follow Michaud (2005). Plankton particles measured using the OPC were classified into 4096 digital bin classes (DS_{opc}) that are proportional to the projected particle area. The particle equivalent spherical diameters (ESD_{opc}, μm) were then calculated from DS_{opc} using the following empirical equation (Taggart *et al*. 1996):

$$\mathrm{ESD_{opc}} = 10^{(0.575\log(\mathrm{DSopc}) + 1.870)} \qquad (3.1)$$

To simplify the analysis, the number of digital bin classes was reduced to 64 by using the closest integer value of the square root of each DS_{opc}. Each ESD_{opc} measurement was placed into one of the 64 bin classes, denoted by S_{opc}. The number of particles in each S_{opc} bin class was summed over a 1 s time interval (between two consecutive recorded times). Plankton concentration was estimated for each 1 sec time interval by summing the particles over the S_{opc} bin classes that corresponded to a specific size distribution (next section), then dividing by the filtered volume. The TUBSS-OPC plankton concentration (m^{-3}) series was calibrated with the BIONESS-net concentration using an empirical calibration equation (next section).

The OPC series of plankton concentration was smoothed with a centered, uniformly weighted moving average with window size of 5 s and again with a window size of 7 s. Water column sectional-profiles of the plankton concentration and hydrographic data were contoured using Surfer (Version 8, Golden Software Inc.) with gridding based on inverse distance to a power of two. This means that data points are given less weight the farther they are from the grid node, where weight is proportional to distance from the $(\text{grid node})^{-2}$. The search ellipse radii for concentration data were 5 m in the vertical and 1.5 km in the horizontal. This means that data in a 5 m x 1.5 km ellipse around each grid node were included in the interpolation for a node. For hydrographic properties, the search ellipse radii were 10 m in the vertical and 3 km in the horizontal. A greater search ellipse radius was necessary for the hydrographic data because they were collected at lower resolution than the concentration data. The number of search sectors was 4 with a maximum of 16 data values per sector and no more than 3 empty sectors. Grid nodes were blanked when there were fewer than 8 values.

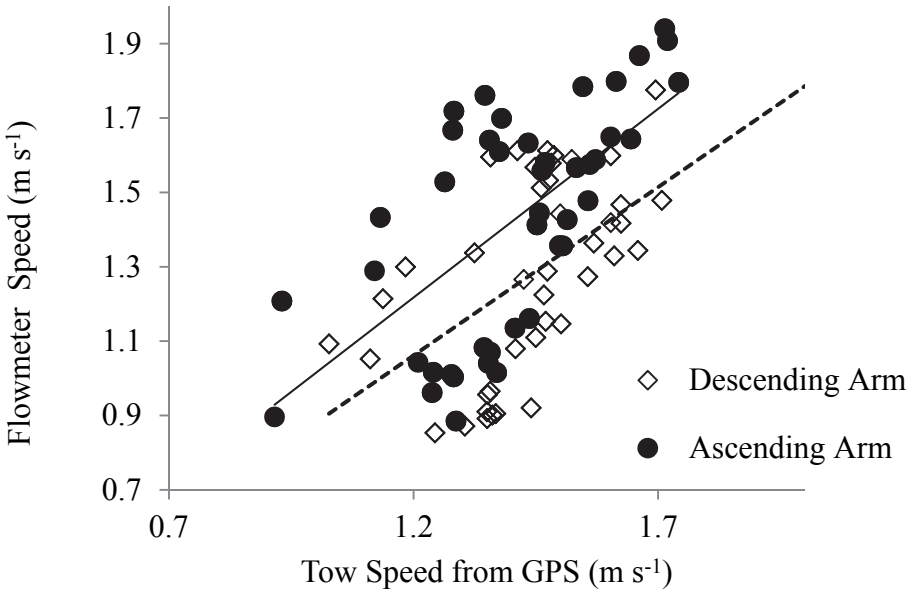

Figure 3.2 Relationship between the speed of TUBSS calculated from the flowmeter, and the tow speed estimated from the ship's GPS in 2009, averaged over the ascending (circles) and descending (diamond) arms of the TUBSS tow-yo. Linear models relating the flowmeter to tow speed are provided for each arm.

Planar (horizontal) distributions of the prey field and water mass structure at depth were determined from the transect data. Estimates of plankton concentration, temperature, salinity and density at each grid node (~5 m vertical resolution) were first integrated over the 100 – 120 m, 120 – 140 m, and 140 - 160 m depth strata as follows:

$$X = \sum \frac{x_i + x_j}{2} * (z_j - z_i) \quad (3.2)$$

where X is the integrated value of the variable x in question at depths (z) i and j of a sub-stratum. The integrated estimates were then expressed volumetrically (e.g., kJ m^{-3}) by dividing the X estimates by the thickness of the stratum (20 m). Subsets of the data were 'advected' from their different times and geographic locations to a common time (high tide) using a numerical circulation model (WebDrogue Drift Prediction Model Ver. 0.66), but the effect was not noticeable because the tidal excursion was very small (3 km) with respect to the total size of the prey field (45 x 25 km) and the scale of data interpolation (1.5 - 3 km horizontally). The planar data were gridded using inverse distance to a power 2 and using search ellipse radii of 0.06 ^{0}N and 0.06 ^{0}W as search parameters.

3.2.5 Calibration of TUBSS-OPC using BIONESS-OPC

Regression analysis comparing the BIONESS-net and BIONESS-OPC plankton concentrations collected in 2008 - 2009 was used to calibrate the TUBSS OPC in 2008. The calibration was based on data from 19 net samples collected at 4 stations in 2008, and from 14 net samples at 3 stations in 2009. First, random samples of CH4s and CF5s (n = 54 to 274) were sorted from deep (> 75 m) net collections, photographed from the lateral view and their prosome lengths and widths measured digitally. Next, CH4 and CF5 prosome volumes were estimated from length and width using a geometric shape approximation for an oblate spheroid, and the ESD of CH4s and CF5s from the net collections (ESD_{net}) was estimated from prosome volume. Because the abundance-at-size distribution measured by the OPC reflects a combination of overlapping CH4 and CF5 size distributions without differentiating by species, I then combined the two species' ESD_{net} distributions, scaling the contribution of each species to all size classes using the average relative concentration over all deep nets. The animals were then classified into DS_{net} using the inverse of Eq. 3.1 and converted into 64 S_{net} size classes equivalent to S_{opc} above. The S_{net} distributions were normal (2009) or slightly right-skewed (2008) and

varied over the same size range in both years, corresponding to S_{net} bin classes 7 to 14 that have geometric mean ESD between 761 and 1630 μm (Figure 3.3a, b). The combined distribution was slightly right-skewed (though still fairly normal) in 2008 because the larger CH4 was present in high abundance relative to CF5 (CF5:CH4 in 2008; 80:20 %, Figure 3.3a). The distribution was normal in 2009 because it was dominated by CF5 (CF5:CH4 in 2009; 95:5 %, Figure 3.3b). The combined S_{net} distribution provided the size frequency estimates for CH4s and CF5s to be selected from the wider S_{opc} size frequency distribution (Figure 3.4). The S_{opc} distribution was shifted to larger size classes (9 to 16) relative to the S_{net} in both years.

The S_{opc} bin classes were integrated over every possible range of size and span in a manner similar to Baumgartner (2003) and Michaud (2005), starting with the combined size distribution of CF5s and CH4s collected in the nets. Analysis of each possible combination is referred to as a 'trial'. For each trial, the integrated data were summed over the BIONESS-net deployment period and divided by the total volume sampled by the OPC over the same period. The derived S_{opc} concentration estimates were then compared with the BIONESS net-specific CH4 and CF5 combined concentration using linear regression of the log normalized data. I chose the span and range that both provided the best estimate of the BIONESS-net derived concentration (highest r^2) and most closely reflected the observed size distribution measured using the net collection (S_{net}). Data from both years were included in the same regression, because the size distributions were similar between years. The optimal size range for integration was between S_{opc} classes 9 to 16 (mean ESD: 1001 – 1891 μm) (Figure 3.5a). This equation was then used to calibrate the TUBSS-OPC distribution of abundance at size.

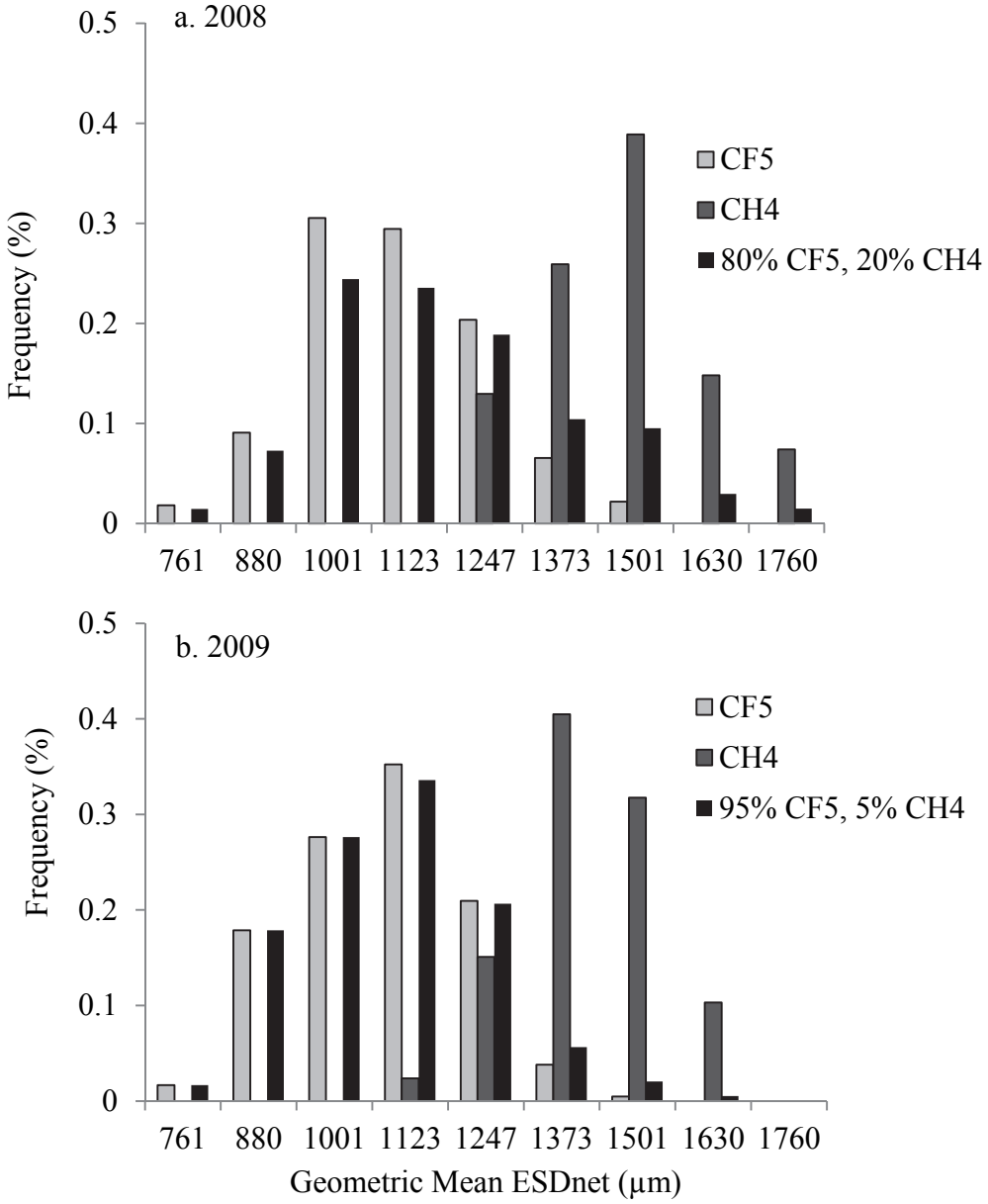

Figure 3.3 ESD_{net} (µm) size frequency distributions of net-collected *C. finmarchicus* C5 (CF5, light grey bars) and *C. hyperboreus* C4 (CH4, dark grey bars) from the deep (> 75 m) depth strata in September (a) 2008 and (b) 2009 where the sizes were determined from digital images of the copepods. The black bars represent the combined size distribution of both species, scaled by their relative proportional concentrations in the nets. The combined distribution is the size frequency distribution measured by the OPC.

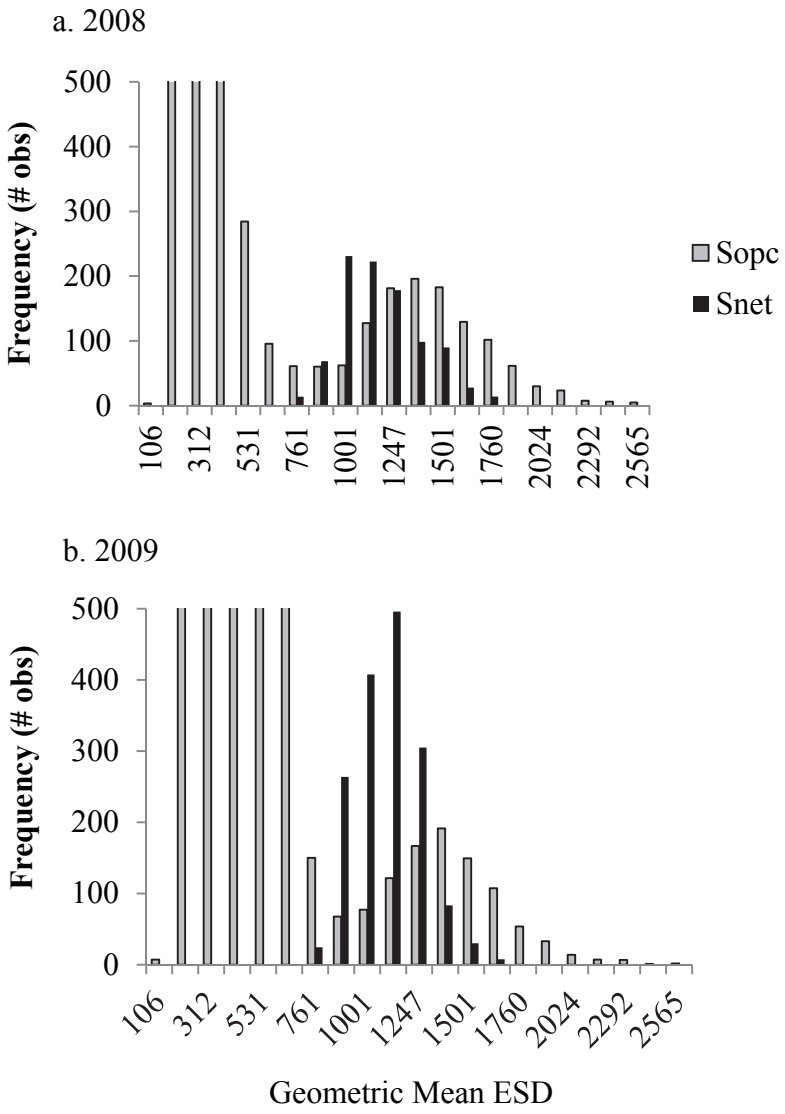

Figure 3.4 BIONESS-OPC derived (grey) and BIONESS-net dervied (black) concentration-at-size distributions collected simultaneously at (a) station B02 with net 5 (2008) or (b) station-B02 with net 2 (2009). Biological samples fell within S_{net} bin classes 7 to 14 (mean ESD: 761 – 1630 μm) and the BIONESS-OPC distributions were shifted relative to S_{net} toward larger size classes, ranging from 9 to 16 (mean ESD: 1001 – 1891 μm). The first six bins are cut off at 500 observations to enhance the ability to see the relevant size range. The first six bins contain small particles such as marine snow that are not relevant to my study.

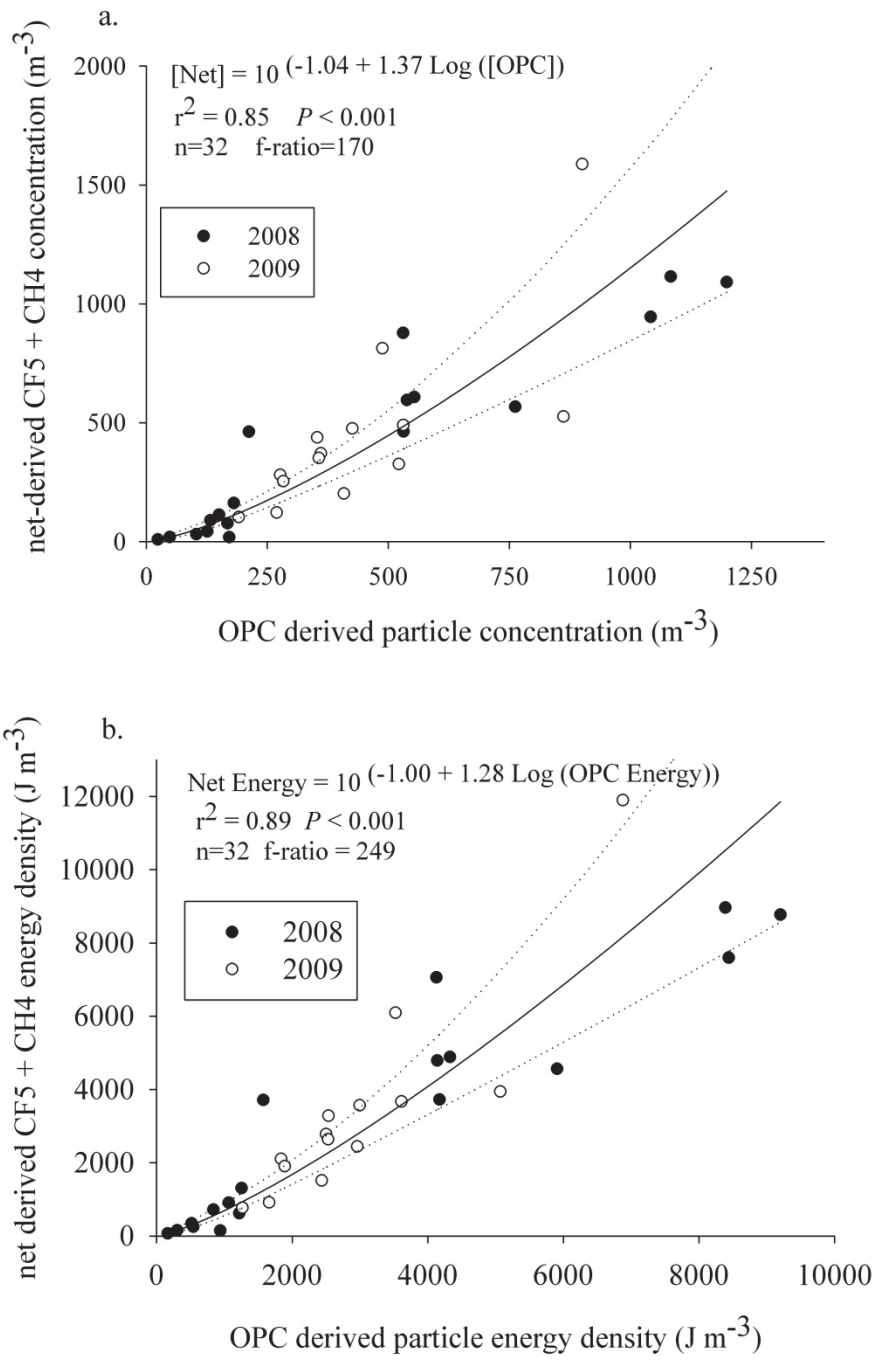

Figure 3.5 Regression-based calibrations of the BIONESS-OPC and corresponding BIONESS-net derived *C. finmarchicus,* CF5 and *C. hyperboreus* CH4 (a) concentrations and (b) energy density, where dotted lines denote the 95 % confidence intervals around the predictions. OPC-derived concentration was estimated as the sum of plankton between S_{opc} size classes 9 to 16 (mean ESD: 1001 μm to 1891 μm) divided by the total OPC volume sampled over the net-sampling period.

3.2.6 Energy Density of the C5 prey field

I had previously measured energy terms for S_{net} classes 8 to 13 (Chapter 2). The copepods were concentrated in S_{net} classes 7 to 14, so I assumed energy content of copepods in class 7 equaled energy content in class 8 and energy content of copepods in class 14 equaled energy content in class 13. If false, this assumption will have little impact since very few of the copepods fell into size classes 7 (mean ESD = 761 μm) or 14 (mean ESD = 1630 μm) in either year. The S_{opc} classes were shifted upward by 2 size classes relative to S_{net} classes, so when I applied the energy terms to the OPC-abundance-at-size distribution, I multiplied energy content from S_{net} class 7 with abundance from S_{opc} class 9, etc. I then integrated the total energy (J) over S_{opc} classes 9 to 16, and the integrated data were summed over the BIONESS-net deployment period and divided by the total volume sampled by the OPC over the same period, to obtain net-specific BIONESS-OPC energy density (kJ m^{-3}). For each corresponding net, the total CH4 + CF5 concentration was divided proportionally into the size classes illustrated in Figure 3.3, and energy content was multiplied by the C4+C5 concentration in each S_{net} class then summed over all S_{net} classes to obtain BIONESS-net derived energy density (kJ m^{-3}). The calibration between OPC- and net-derived energy density was then developed in the same way as concentration (Figure 3.5b) and was used to calibrate TUBSS-OPC energy density. All analyses thereafter were the same for energy density as above for concentration.

3.3 Results

The results are presented by increasing horizontal spatial scale; I begin by describing the general vertical profiles and the small (10 – 100 m) horizontal spatial scales collected with BIONESS, then move to tidal and finally basin-scale variation, both of which were measured using TUBSS. At each scale, I first describe the prey field data, then the hydrographic data and then the associations between the two.

3.3.1 Small-scale spatial variation

The dominant copepod species and stages collected in Roseway Basin in 2008 were *Calanus finmarchicus* stage-C5 (CF5) and *Calanus hyperboreus* stage-C4 (CH4, Table

3.3). Other species and stages represented less than 10 % of the samples by abundance. Both dominant species were concentrated in the deep nets relative to the depth integrated tows. BIONESS-OPC derived estimates of diapausing *Calanus* spp. (CF5 + CH4) concentration were generally low at shallow depths and increased rapidly to 500 - 1000 m^{-3} below 100 m (Figure 3.6, left panels). The deep layer concentration was measured at three stations along the southern slope of the Basin. An especially high concentration patch was measured within 10 m of the seafloor at station-B03, where concentrations exceeded 5000 m^{-3}. The horizontal scale of deep layer patchiness was investigated during a spatial series recorded at depth (station-B02, Figure 3.7). Over the ~1 km transect, copepod concentration showed low frequency (250 m) and high frequency (4 m) variation. At the low frequency, concentrations increased from ~1000 m^{-3} to ~4000 m^{-3}. At the high frequency, concentrations varied by 1000 m^{-3} over 4 m scales, as illustrated in the spectrum Figure 3.7f.

The temperature profiles were similar at B01, B03 and B04 (Figure 3.6, middle panels). Temperature was 16 ^{o}C at the surface, declined to 6 ^{o}C at the main thermocline between 30 and 60 m depth, and remained near constant at ~6 ^{o}C below 60 m. Temperature at depth was slightly elevated at stations-B03 and B04. Salinity and density were measured only at station-B01, where salinity was 31 at the surface, increased to ~33 between 40 and 80 m depth, and remained near constant below 80 m. The density profile was similar to salinity, varying between σ_t = 22.5 kg m^{-3} at the surface and 27 kg m^{-3} at depth. The spatial series at depth showed a weak horizontal variation of water mass properties at 100 – 800 m scales along the transect. At 600 m, temperature and salinity both began to increase by 0.2 ^{o}C and 0.015, respectively by 900 m. The largest increase in T-S occurred at 800 m, suggesting a weak front as there was a corresponding change in density. Copepod concentrations peaked at the front edge, then fell rapidly as density decreased at around 900 m. This maximum in copepod concentration is best described using in a T-S diagram, where the concentration reached a maximum at approximately the midpoint between the two water masses (Figure 3.8). On the warm, salty side of the front, concentrations decreased.

Table 3.3 Species assemblage of dominant zooplankton and concentrations (m^{-3}) in 2008 collected with BIONESS at 4 stations (B01 - B04). Values are provided for depth integrated nets (left column) and nets that collected samples in the deep Basin only (right column). No deep net sampleswere collected at station-B03.

Species	B01		B02		B03		B04	
Tow depth interval:	12 - 137 m	88 - 136 m	0 - 144 m	140 - 150 m	0 - 143 m	N/A	0–147 m	139 – 147 m
Calanus finmarchicus C3	3	0	0	0	<1		<1	0
Calanus finmarchicus C4	13	<1	1	4	9		<1	9
Calanus finmarchicus C5	25	78	118	940	636		474	900
Calanus finmarchicus M	1	2	1	0	2		2	2
Calanus finmarchicus F	4	6	2	13	9		3	<1
Calanus hyperboreus	6	21	59	175	149		142	189
Calanus Glacialis	0	1	5	24	50		3	0
Metridia longa	0	3	1	4	13		4	0
Centropages typicus	38	<1	6	0	27		5	7
Pseudocalanus spp.	7	2	0	1	4		<1	2
Total Mesozooplankton	127	133	212	1161	923		633	1109
Macrozooplankton	<1	0	0	0	0		<1	<1

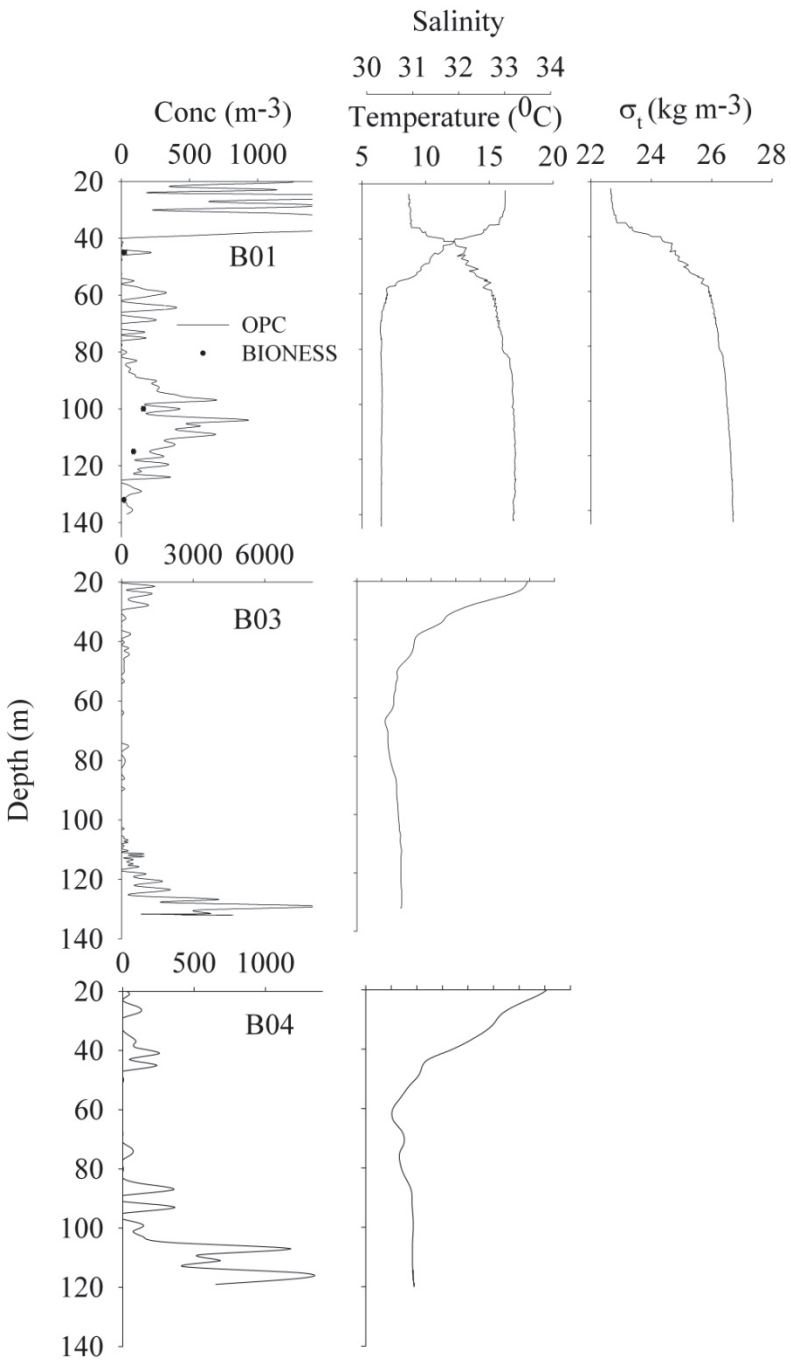

Figure 3.6 Vertical profiles of OPC-derived diapausing *Calanus* spp. concentration (left) and temperature (middle) collected during BIONESS tows B01, B03 and B04 (see Figure 3.1b for geographic location of tows). Salinity and density measurements were collected at station B01 only. Depth-structured net-derived average copepod concentrations (black symbols) are also pictured for B01.

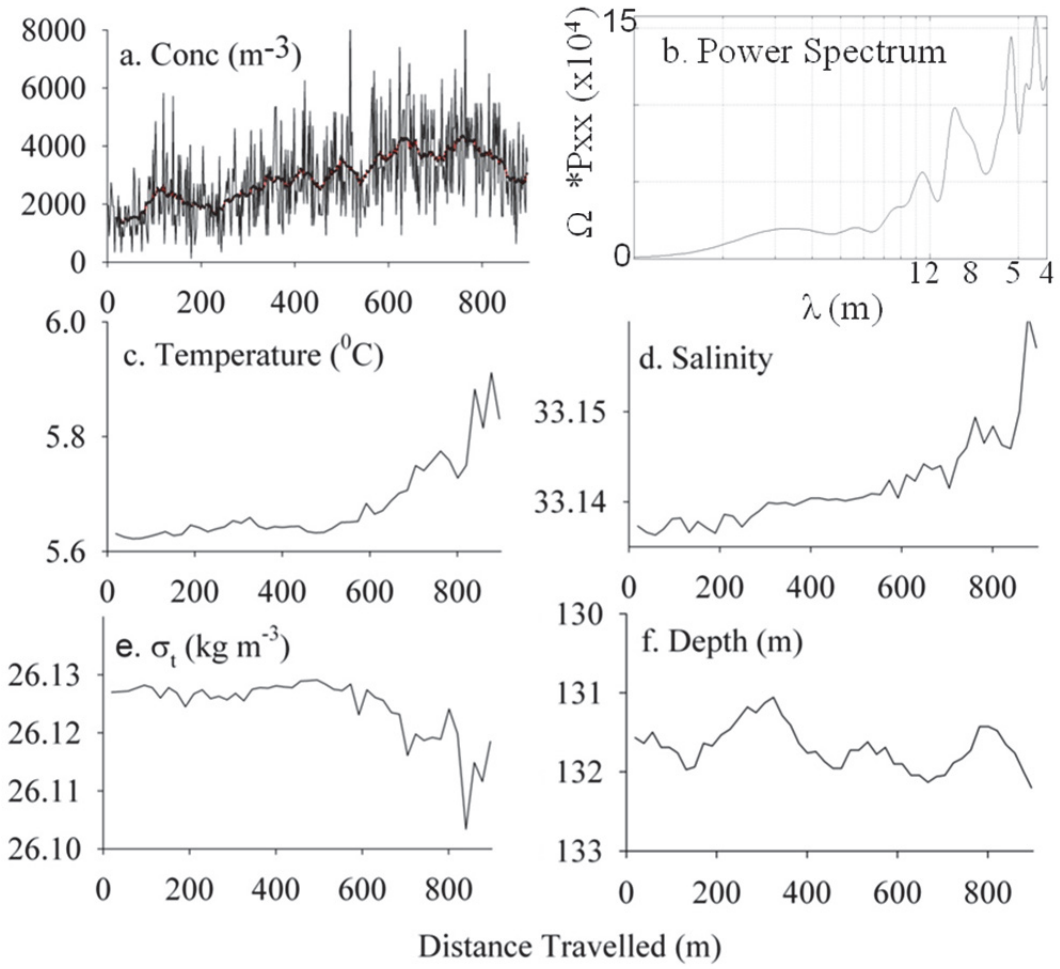

Figure 3.7 High resolution horizontal spatial variation at depth recorded at station-B02 in 2008 showing: (a) BIONESS-OPC derived diapausing copepod concentration with the low pass signal also plotted; (b) power spectrum of the concentration data; c) temperature (^{o}C); d) salinity; e) σ_t (kg m^{-3}); and f) depth (m).

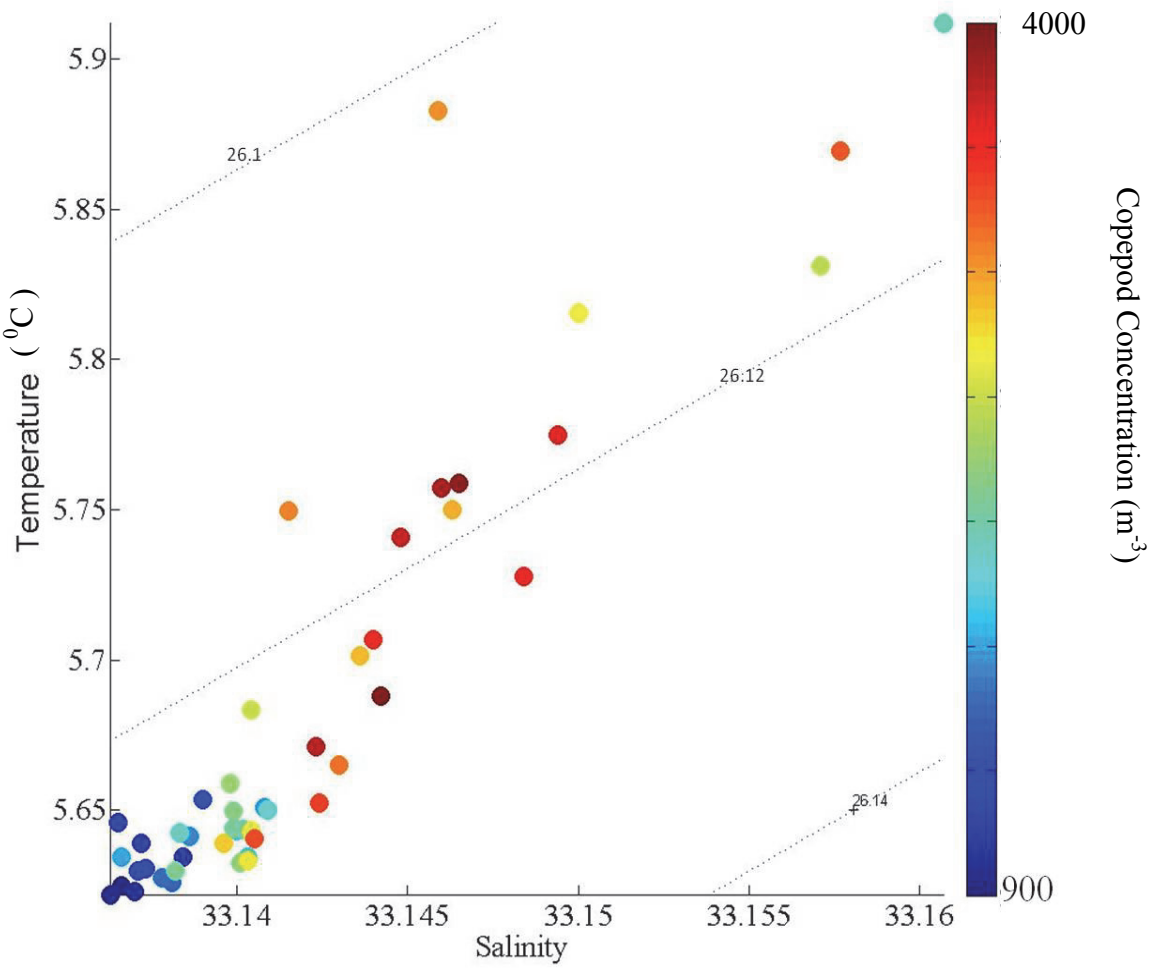

Figure 3.8 Temperature-Salinity diagram showing hydrographic data collected during the sequential series (Figure 3.7 b, c) at ~ 131 m depth. Overlaid on the T-S diagram are the OPC-concentration (m^{-3}) data measured every 20-sec (to match the CTD data resolution) then low-pass filtered as in Figure 3.7a. The OPC concentration estimates are given by the color bar and lines of constant density (σ_t) are provided.

3.3.2 Variation over a tidal cycle

Variation in diapausing copepod concentration and water mass temperature was measured across a 12 km transect that straddled the southern boundary of Roseway (Figures 3.9 and 3.10). The first transit of this transect (panel a) took place during high tide, when the high temperature portion of the water mass was at its most down slope (deepest) position. A 10 m x 4 km sized patch of copepods with concentrations exceeding 1000 m^{-3} was observed between 2 and 6 km along the transect, and between 120 -140 m depth (Figure 3.9a). Concentrations decreased to 100 – 500 m^{-3} upslope of this patch. Between 8 and 12 km, concentrations were also high at shallower depths and were associated with the leading edge of a temperature gradient (Figure 3.10a). On the Basin side of the temperature front, the water temperature was vertically stratified and the copepod patch was concentrated in a region of homogeneous temperature. On the upslope side of the mixing front, water was well mixed showing a strong horizontal gradient in temperature as the water warmed on bank.

On the second and third transits (panels b and c) the position of the front moved upslope with the ebbing tide (Figure 3.10), and the copepod patch decreased in concentration as it spread upslope (Figure 3.9). At low tide (Figure 3.9d) the patch of copepods almost disappeared, leaving only a small patch at 8 km along the transect. The front was positioned on-bank at 14 km, and the water now residing on the slope had a strong thermocline between 80 and 100 m depth that separated the cold water mass in the upper water column from the warmer water mass at depth. On the flood tide, as water moved back down slope, the patch reformed and the front moved back down slope (Figure 3.9e,f; 3.10,e, f). During the second tidal cycle (Figures 3.9 and 3.10, panels g-k) the same patterns were observed: the patch spread upslope and decreased in concentration as the front moved on-bank, and the patch reformed on the down slope phase of the tide.

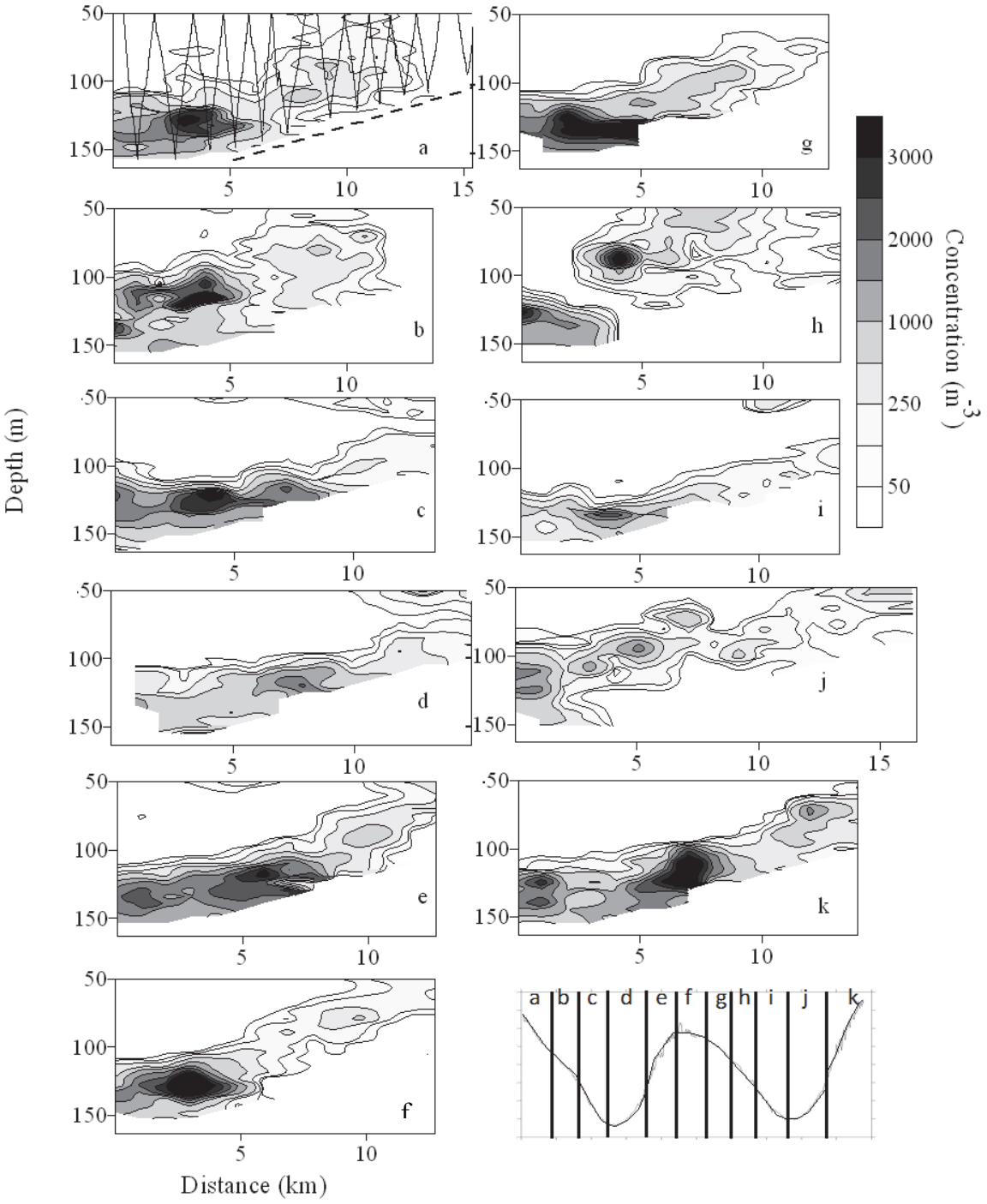

Figure 3.9 Sectional distributions of diapausing copepod concentration (m^{-3}) collected along a ~12km long cross-isobath transect straddling the southern margin of Roseway Basin. The transect was transited 11 times over a 24 hour period during 11-12 September 2008. Each panel (a to k) represents a single transit, and the stage of the tide during each transit is provided in the last panel. The approximate location of the seafloor is depicted by a dotted line in (a) and the TUBSS sampling path is provided in (a) as an example.

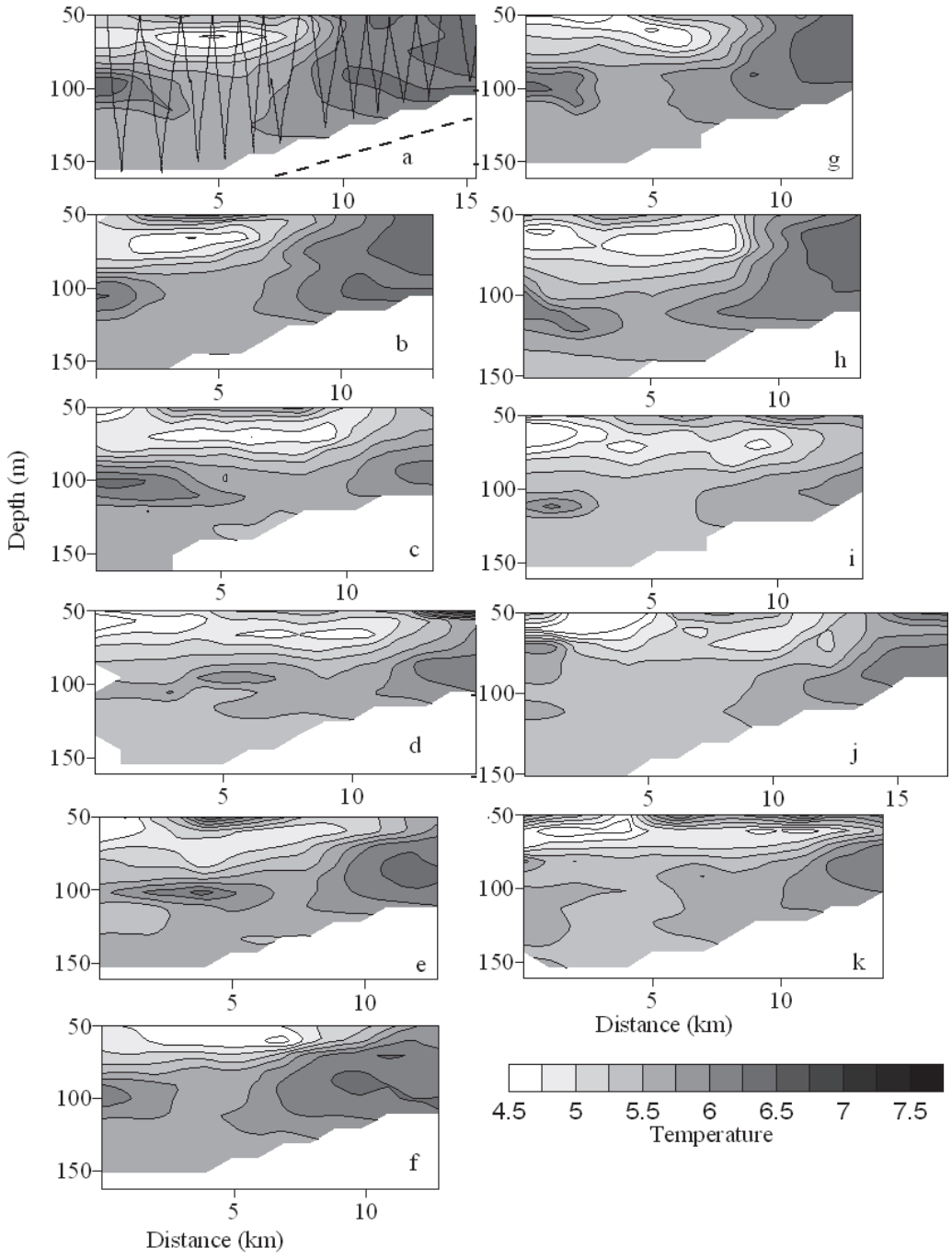

Figure 3.10 Sectional distributions of diapausing temperature (^{o}C) collected along a 12 km long cross-isobath transect straddling the southern margin of Roseway Basin. The transect was transited 11 times over a 24 hour period during 11-12 September 2008. Each panel (a to k) represents a single transit, and the stage of the tide during each transit is provided in Figure 3.9. The approximate location of the seafloor is depicted by a dotted line in (a) and the TUBSS sampling path is provided in (a) as an example.

3.3.3 Variation in copepod concentration and energy density at the Basin scale

The distributions of diapausing copepod concentration and energy density along transect-2 (across-Basin, Figure 3.1b) are presented in Figure 3.11 as representative examples of the results obtained for all transects. Only the distribution of energy density is presented for the other 9 transects (Figures 3.12 and 3.13) as the energy density estimates are what matter most to whales, assuming that the abundance-at-size distribution of copepods was similar throughout the Basin, and thus these distribution patterns should be proportional to the diapausing copepod concentration distribution.

Along transect-2, the concentration of copepods consistently increased with depth (Figure 3.11b) by as much as an order of magnitude, reaching >500 m^{-3} almost exclusively below 100 m with maximum concentrations in excess of 1500 m^{-3} somewhat deeper. The broad scale cross-basin pattern showed a large aggregation of copepods that was evenly distributed across the width of the Basin and tilted upslope on the SE margin to a depth less than 100 m. At a smaller scale, high concentration (>1000 m^{-3}) 'patches' spanning ~1 km in width and 1 to 10 m in height were distributed throughout the aggregation, and were particularly clustered in the deepest part of the Basin. The prey field energy density (Figure 3.11a) along transect-2 shows a pattern very similar to concentration, indicating that my proportionality assumption is sound. Most of the energy was concentrated below 100 m, and reached a maximum >16 kJ m^{-3} in some deep Basin patches.

A large, high energy density aggregation occurred at the eastern-most margin of the Basin, sampled in a cross-Basin direction by transect-1 (Figure 3.12a) and again in an along-Basin direction by transect-10, which was sampled within 2 hours of transect-1 (Figure 3.13e). Energy density in this large patch exceeded 20 kJ m^{-3} and its volume (assuming a cube) was 5 km x 5km x 50 m = 1.25 x 10^9 m^3. Copepods were similarly distributed across transects-2 to 4 as described above (Figure 3.12b-d). Another large, high energy density patch was situated at the 10 - 12 km mark on transect-4. To the west, energy density decreased and was only present along the southern Basin margin in transects-5 to 7 (Figures 3.12e; 3.13a, b). Transects-8 to 10 show this west-east increase in energy density that included a gap of near-zero energy density that is 20 km in length on transect-9 (Figure 3.13d). Along transect 10, which transects the southern slope, the

high energy density patches of copepods had maxima at regular 5 km intervals, corresponding to an hourly time scale, therefore it was not due to tidal advection of the prey field, and instead likely represents real spatial variation in the prey field.

The method of transecting the Basin in many locations in the along- and cross-Basin directions allowed for the integration of energy density and hydrography over various depth ranges along each transect. This provided planar estimates of energy density and hydrography over an area covering ~ 870 – 1400 km^2, depending on the stratum. The planar distributions of energy density revealed that regions of high energy density were found at similar geographic locations among depth strata (Figure 3.14). Consistent with the observed sectional profiles, high energy density patches were restricted to the deep Basin and were virtually absent on the northern and western Basin margins. The lowest energy density occurred in the 100 – 120 m stratum (Figure 3.14a) and increased with depth, exceeding 11 kJ m^{-3} in the 140 – 160 m stratum (Figure 3.14c). In all three strata, the highest energy density patch was situated at the NE margin, and the energy density in the patch at the NE margin increased with depth. A 'tube' of high energy density ran along-Basin in a NE - SW direction in roughly the middle of the Basin. The tube was most prominent in the 120 – 140 m stratum (Figure 3.14b).

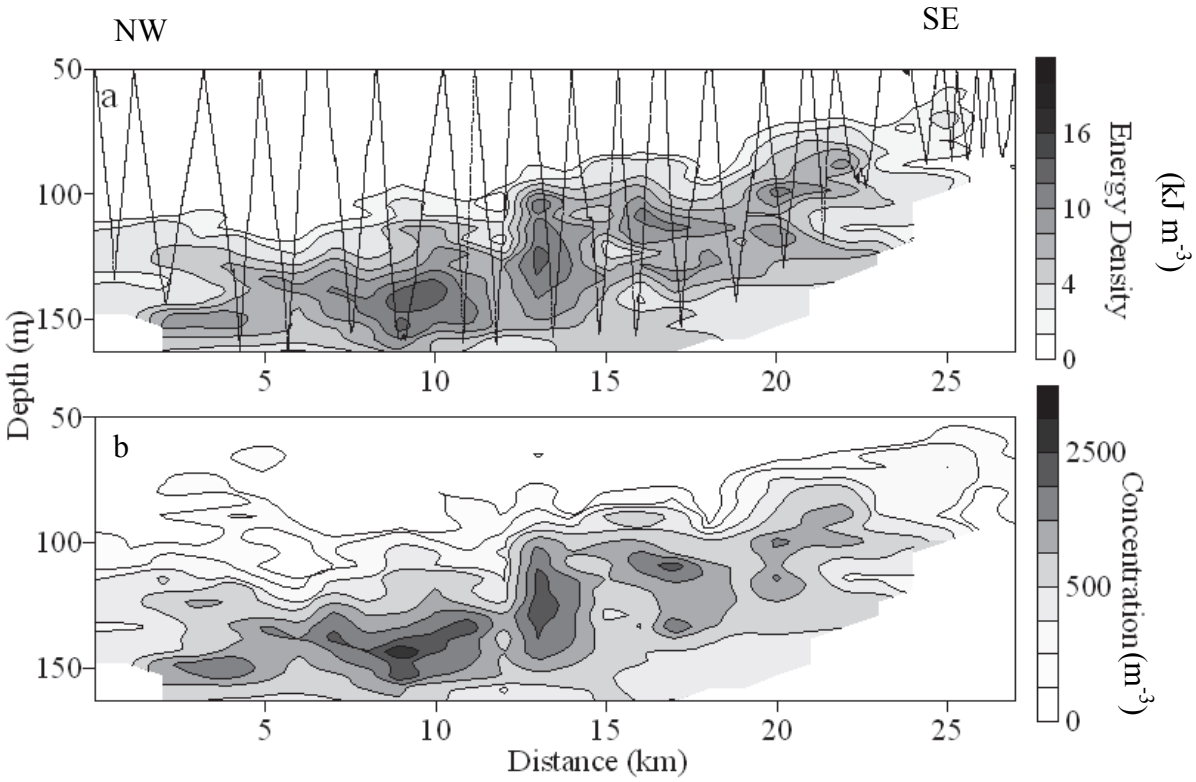

Figure 3.11 Comparison between sectional distributions of diapausing copepod (a) energy density (kJ m^{-3}) and (b) concentration (m^{-3}) collected along transect-2. The TUBSS sampling path is shown with a zig-zagged line in (a), and the transect geographic position is shown in Figure 3.1b. The blank regions at the bottom left and right of each panel represents the seafloor.

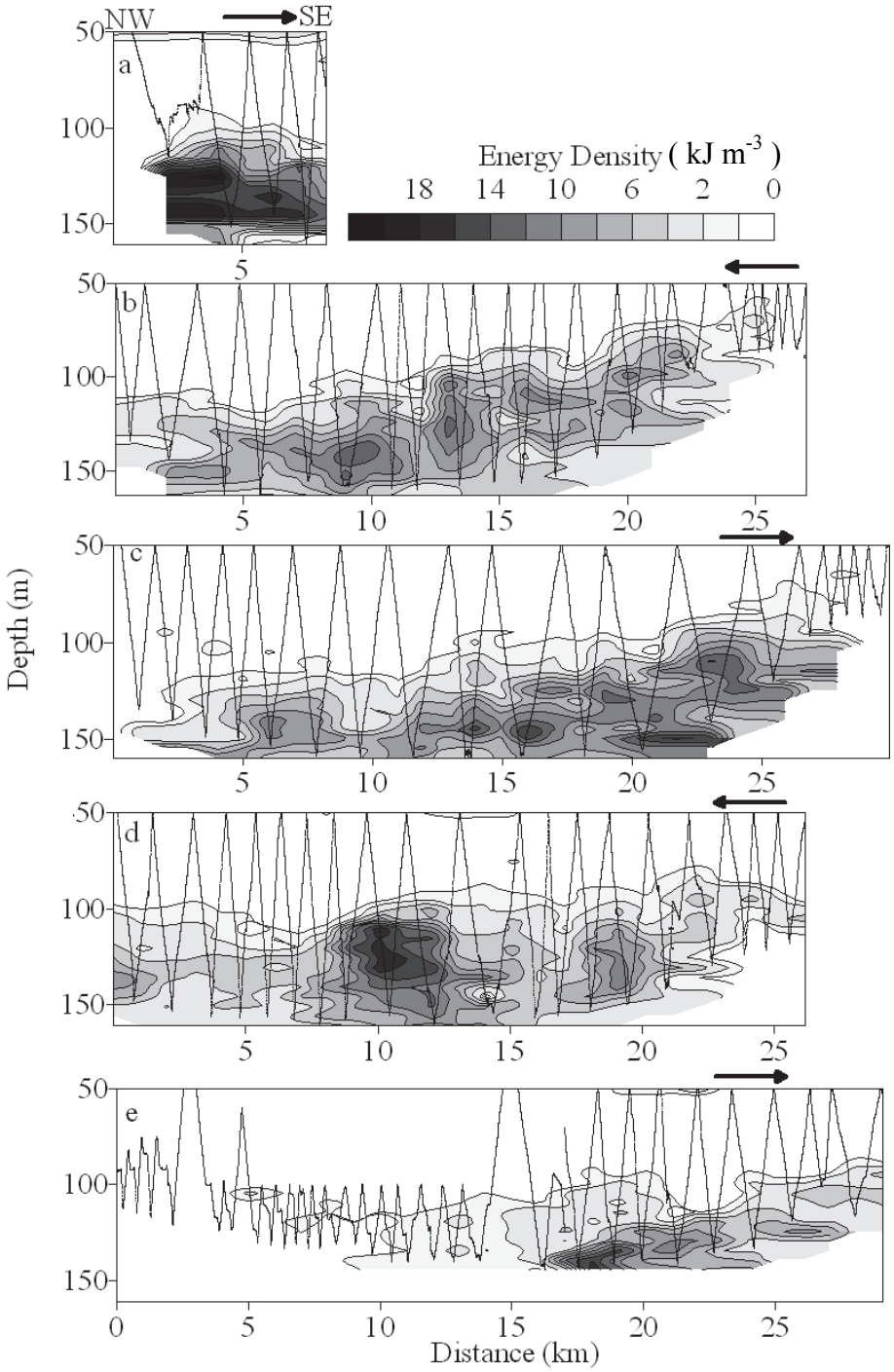

Figure 3.12 Sectional distribution of copepod energy density (kJ m^{-3}), estimated using the TUBSS-mounted OPC in September 2008 in Roseway Basin along the NW to SE transects 1 through 5 (a through e) shown in Figure 3.1. Arrows on each panel denote the direction of the tow and zig-zagged lines show the TUBSS-tow profile. The blank regions at the bottom left and right of each panel represents the seafloor.

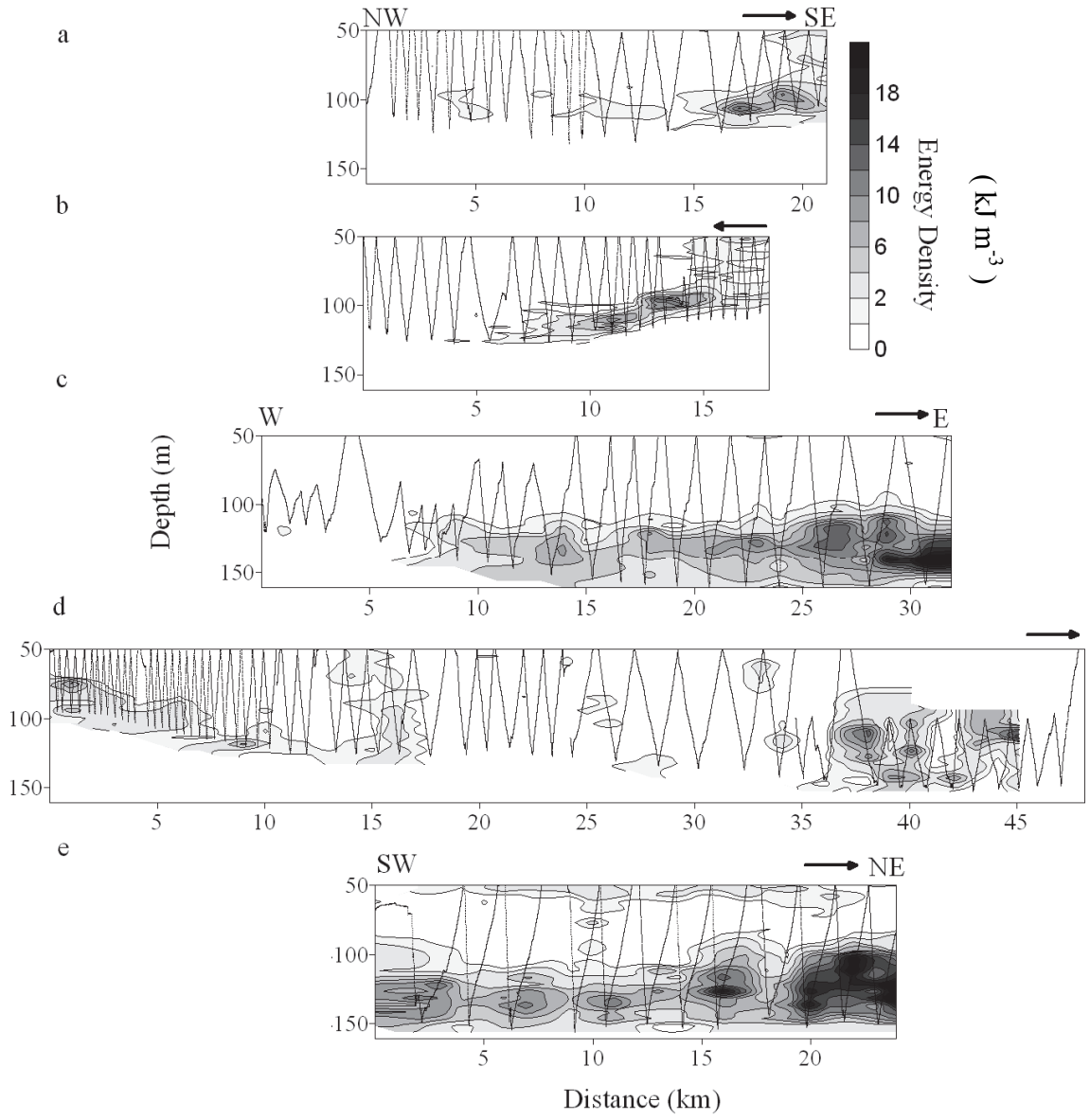

Figure 3.13 Sectional distribution of copepod energy density (kJ m^{-3}), estimated using the TUBSS-mounted OPC in September 2008 in Roseway Basin along the NW to SE transects-6 and -7 (a, b), along the W to E transects-8 and -9 (c, d) and along SW to SE transect-10 (e). Arrows on each panel denote the direction of the tow and zig-zagged lines show the TUBSS-tow profile. The blank regions at the bottom left and right of each panel represents the seafloor.

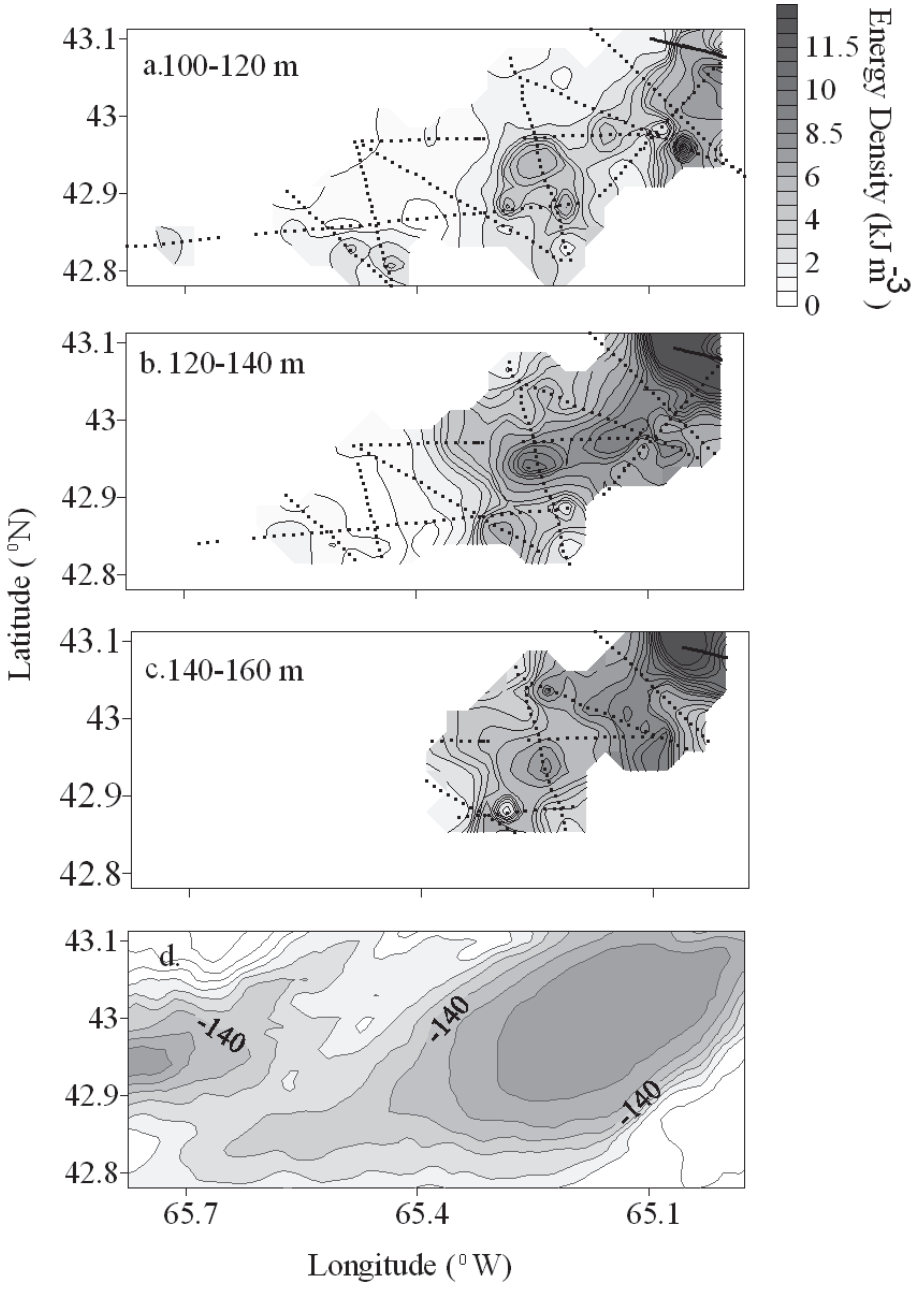

Figure 3.14 Planar distribution of depth integrated average copepod energy density (kJ m^{-3}) in September 2008 in the Roseway Basin over the: a) 100 to 120 m stratum, b) the 120 to 140 m stratum, and c) the 140 to 160 m stratum and d) the bathymetry of the Basin contoured at 10 m intervals with the 140 m contour labeled. The data were derived from each transect in Figures 3.12 and 3.13. Each datum is indicated with black dots in a-c, and blank regions represent insufficient data to make an interpolation (see Section 3.2.4).

3.3.4 Water masses in Roseway Basin

The water masses in the deep (50 – 160 m) region of Roseway Basin represent a 3-end-member system, and the end-members have the same origins as those described for the deep waters of Emerald Basin and the central Scotian Shelf (Gatien 1976, Petrie and Drinkwater 1993, Houghton and Fairbanks 2001). The 3 end-members, depicted with triangles in Figure 3.15, are hereafter referred to as Basin Water (BW, T=3^{o}C, S=32, σ_t=25.5), modified Basin Water (mBW, T=7^{o}C, S=33.3, σ_t=26), and intermediate Basin Water (iBW, T=4.8^{o}C, S=33.1, σ_t=26.3). Basin Water originates in the Gulf of St. Lawrence and is advected along the inner Scotian Shelf by the Nova Scotia Coastal Current (NSCC). Modified Basin Water and intermediate Basin Water also originate in the Gulf of St. Lawrence, but are advected along the continental slope by the outer arm of the NSCC, and as they are advected, they are modified as they mix with warmer, saltier slope waters. iBW is colder, slightly fresher and more dense than mBW because it is modified by slope waters at depth. Water from the Gulf of St Lawrence surface flow was identified as the primary water mass in the shallow (<30 m) waters of Roseway Basin, with T = 16 ^{o}C and S = 30 (e.g, Figure 3.6).

The contribution of each end-member varied with depth in the Basin, and the depth distribution of water masses varied in a cross-Basin direction. On the NW margin of transect-2, BW dominated just below the thermocline at 50 m, and with increasing depth its proportion decreased while the proportion of iBW increased (Figure 3.15). mBW was not present on the NW margin. At mid-Basin along transect-2, BW again dominated just below the thermocline, but it was warmer and more salty, indicating it was mixed with the mBW below it. The influence of BW decreased and mBW increased with increasing depth to ~100 m. Thereafter mBW was replaced by iBW in the deepest part of the Basin. The SE margin, closest to the continental slope, had water that was intermediate in T-S between the NW margin and mid-Basin; this water was a mixture of all three water masses, with greater influence by the two slope-influenced waters than by the BW (Figure 3.15).

End-member contributions in the deep Basin (90 - 160 m) also varied horizontally in both the cross- and along-Basin directions (Figure 3.16). The eastern end of the Basin (transects-1 to 4, and eastern halves of transects-9 and 10) was a mixture of iBW that

predominated on the NW side of the Basin, and mBW that made up the warm core and was found more often along the SE margin. Westward, (transition from blue – yellow in Figure 3.16) iBW was replaced by the BW. The east-west water mass transition between iBW and BW was particularly evident in transects-8 and -9, which given their east-west orientations were able to sample all three water masses.

3.3.5 Water mass variation at the Basin scale

Water mass variation in the deep water across and along Roseway Basin was typical of a Shelf Basin, but also had features that appear unique because of its location at the southwest end of the Shelf and its relatively shallow bottom depth. The most prominent feature was a front that divided the Basin in the NE - SW direction between the cooler, fresher waters, which dominated on the shoreward side, and warmer slope-influenced water that dominated toward the Shelf break. I first discuss the basin-scale temperature structure, for which there was considerable spatial variation, then the more spatially stable salinity and density structure.

In the eastern half of the Basin (transects-1 to 4), which encompassed the deepest area, and will be referred to as the 'deep Basin', was filled with warmer, saltier slope-influenced water that was similar in temperature to water on the SE slope (Figure 3.17a - d). A mBW core, located between 75 m and 125 m depth, extended along the deep Basin between transects-1 to 4. Straddling either side of the warm core were three vertical temperature fronts, one just NW of the Basin center and one on the SE slope. The first separated the cold (4.5 - 5.5 ^{o}C) waters on the NW side of the Basin from warmer slope water in the deep Basin and on the SE slope. This front was evident, for example, at the 7 - 10 km mark on transect-2 (Figure 3.17b). The second front was located at 16 km along the transect, and separated with warm core from cooler water on the SE slope. The third front was located on the SE slope and separated the weakly thermally stratified water from the warmer waters on the bank. This front was evident along transects-1 to 3 (e.g., 25 km mark, transect-2), but was not seen on transect-4 as the bottom slope on the SE margin began to decrease (Figure 3.17b,d). Toward the western end of the Basin where bottom depths shoaled, the cooler, fresher BW on the NW side penetrated further across the Basin, moving the vertical temperature front to the south (transects-5 to 7,

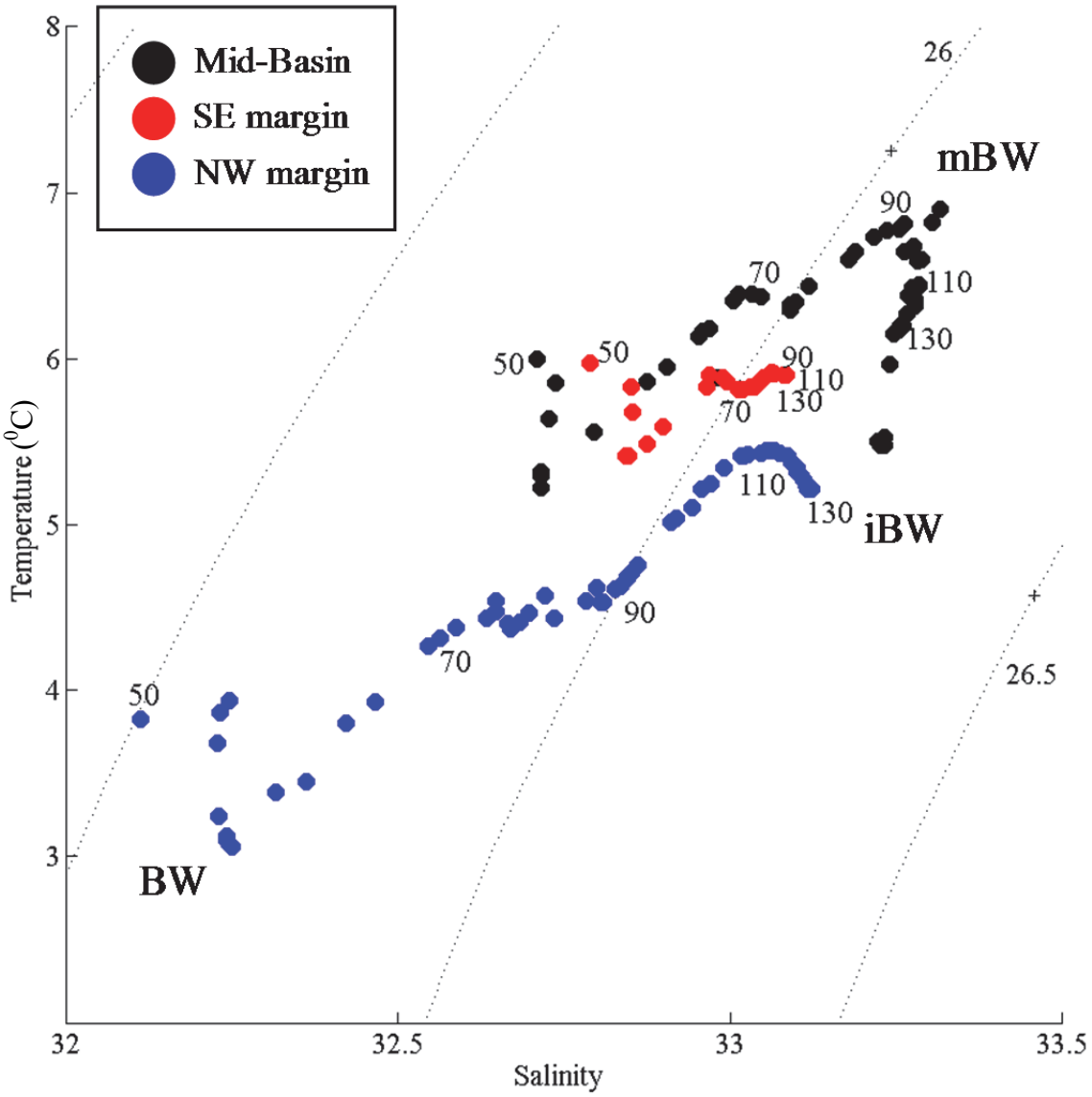

Figure 3.15 Temperature-salinity diagram showing three vertical temperature-salinity profiles collected with the TUBBS-mounted Seabird-37 CTD at > 50 m depth along transect-2 at the NW margin (blue), mid-Basin (black), and SE margin (red) of Roseway Basin. Water mass end-members are shown, where BW = Basin Water, iBW = intermediate Basin Water, and mBW = modified Basin Water. Depths are labeled at 20 m intervals. Dotted lines depict the σ_t isopycnals, which are spaced at 0.5 kg m^{-3} and labeled.

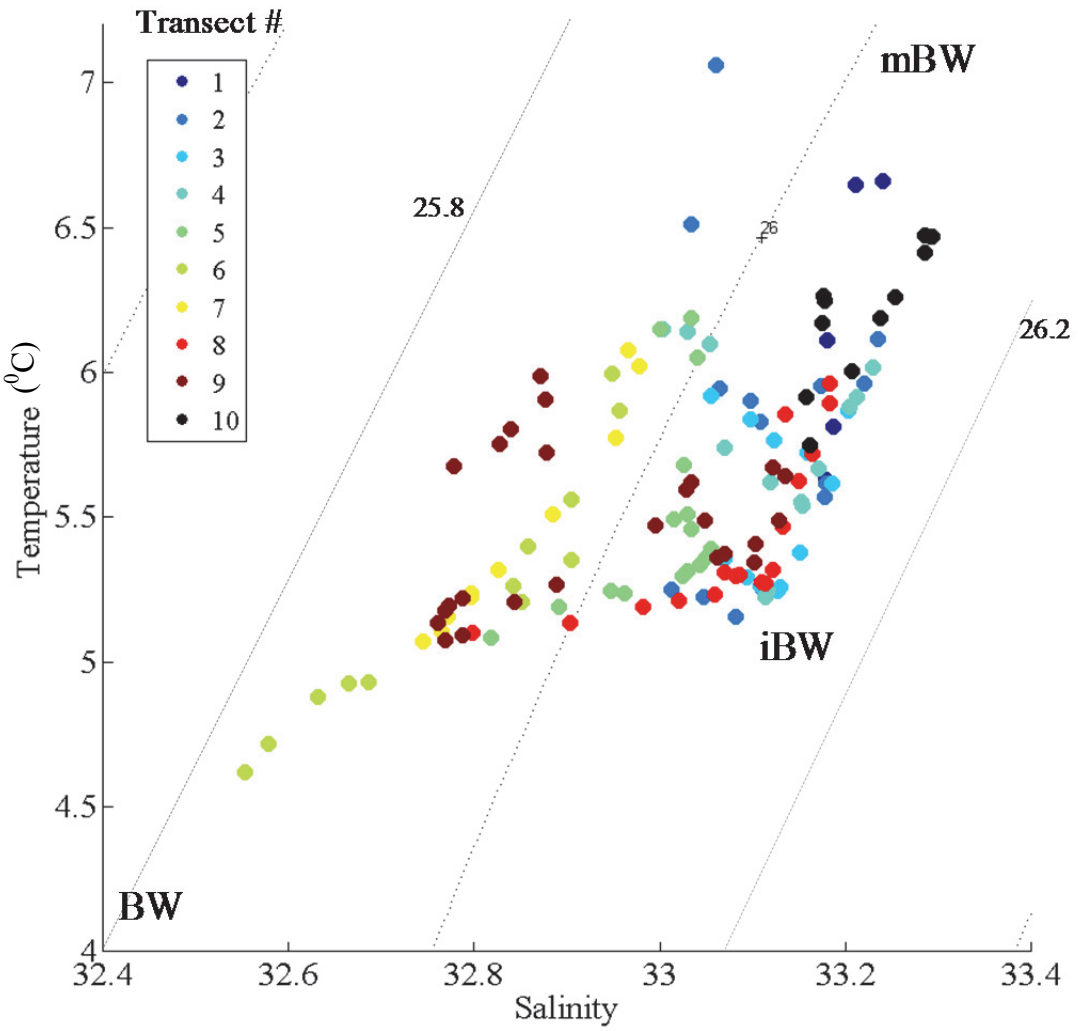

Figure 3.16 Temperature-salinity diagram of the deep water in Roseway Basin where each datum is the average between the 90 - 160 m stratum of each quasi-vertical profile collected with TUBSS along transects 1 to 10. Each transect is represented by a different color. Water mass end-members are shown, where BW = Basin Water, iBW = intermediate Basin Water, and mBW = modified Basin Water. Dotted lines depict the σ_t isopycnals, which are spaced at 0.2 kg m^{-3} and labeled.

Figure 3.17e; 3.18a, b). Transects-9 and 10 along the Basin show clearly the west-east change in water masses from cold at the western end (Figure 3.18d, 15 - 45 km along transect) to warm in the eastern deep Basin (Figure 3.17e). The cooler BW mass was bounded at the western end of the Basin by a vertical warm water front (Figure 3.18d, 10 km mark).

The planar distribution of temperature integrated over the 100 - 120 m (Figure 3.19a), 120 - 140 m (Figure 3.19b) and 140 – 160 m (Figure 3.19c) strata show clearly the temperature front oriented in the middle of the Basin along a NE - SW axis in all strata. Temperature was highest along the SE Basin margin in all strata, and was particularly warm in the NE near the mouth of a channel that separates Baccaro and Roseway Banks and joins the deep water of Roseway Basin to the Shelf break (Figure 3.1a). Temperature along the SE margin was not uniformly warm, but rather contained at least four large warm features (Figure 3.19a). The water was warmest in the 100 - 120 m stratum, and was slightly cooler in the deeper strata (Figure 3.19b, c).

The salinity and density structures in Roseway Basin were less variable than the temperature structure (Figures 3.20 - 3.25). The warm core found in the deep Basin along transects-1 to 4 was also, as expected, the area of highest salinity in the Basin (Figure 3.20a-d). The cold water on the NW side of the Basin was also fresh (<32.5) and caused the halocline to deepen compared to the SE margin, which resulted in a cross-Basin tilting of the halocline and pycnocline at depths above 100 m on transects-1 to 3 (Figures 3.20a-d; 3.21a-d). On the SE slope, where the vertical temperature front was located, the isopycnals tilted their orientation from horizontal to more vertical, indicating a vertically well mixed area likely due to strong tidal currents, as well as evidence of a weak front at that location (Figure 3.21b-e). To the west, (Figures 3.20e; 3.21e; 3.22a, b; 3.23a, b) the warm-salty core, halocline and pycnocline gradually weakened. The deep water became fresher and less dense as the cold-fresh BW extended south across the Basin. The southern slope waters were warm and salty at the western Basin margin and surrounded the tip of the BW at the western end of the Basin. Transects-9 and 10 reflected the west-east gradient of water mass properties (Figure 3.22d; 3.23d).

Spatial gradients in density in the Basin reflect a baroclinic counterclockwise current in the deep Basin. The warm, salty core created a doming of the deep water

isohalines (Figure 3.20a-d) and isopycnals (Figure 3.21a-d) in a NW-SE direction across the Basin. The deep water isohalines and isopycnals tilted downwards at the western end of the Basin consistent with a geostrophic flow toward the south at the western end of the Basin (Figures 3.22d, 3.23d, 20 - 35 km mark). Thus, there appears to be a gyre-like circulation in the Basin that is reflected in the density structure. The planar distribution of density within each depth stratum shows that the highest density water was located in the deep Basin near the NE margin, and a decreasing density gradient radiated outward in all directions (Figure 3.24). This too is consistent with a baroclinic gyre around the Basin, where the NE margin appears to be the location of the gyre center.

A particularly warm, high salinity water mass (i.e., pure mBW) was located along the NE margin of the Basin near the gyre center and could indicate a greater influence of off Shelf waters (Figures 3.19, 3.25). In this area, salinity, like temperature, was highest in the 100 - 120 m depth stratum (Figure 3.25a), and slightly lower in the deeper strata (Figure 3.25b, c). The depth distribution of the mBW mass and its proximity to the shallow (relative to the Basin) channel separating Baccaro and Roseway Banks suggests that this water entered the Basin from the continental slope through this channel. A slope water intrusion through the channel at the NE Basin margin also implies that there was a current flowing southwestward and into the Basin at that margin. Such a current would undergo bathymetric steering, and would likely converge with and augment the baroclinic flow directed toward the NE along the margin, creating a front between mixed water on the Basin slope and the intruding water. Such a front is evident in the planar distributions of all three hydrographic variables at 43^0N latitude (Figures 3.19a, 3.24a, 3.25a), and appears as a sharp salinity discontinuity along transect-10 (Figure 3.22e).

In summary, the hydrography in Roseway Basin is spatially quite variable; the relatively high resolution spatial sampling of the deep Basin revealed the general structure. The middle of the Basin was filled with warmer, saltier water that varied mainly in temperature and had a stable salinity structure, with mBW overlying cooler, fresher iBW. An intrusion at the NE margin of the Basin that converged with the density driven flow of mixed water travelling in the same direction along the SE slope was identified. Along the SE Basin margin, water tended to be mixed, and this created a front on the SE slope between the mixed water and the mBW on the bank. BW dominated at

the northern and western margins above 100 m with iBW at greater depths. A small portion of the southwestern margin remained as mBW, creating a pocket of mBW that surrounded the BW mass at the western Basin margin. As shown in the next section, this structure is important because it is a primary determinant of the distribution of copepods diapausing at depth in Roseway Basin.

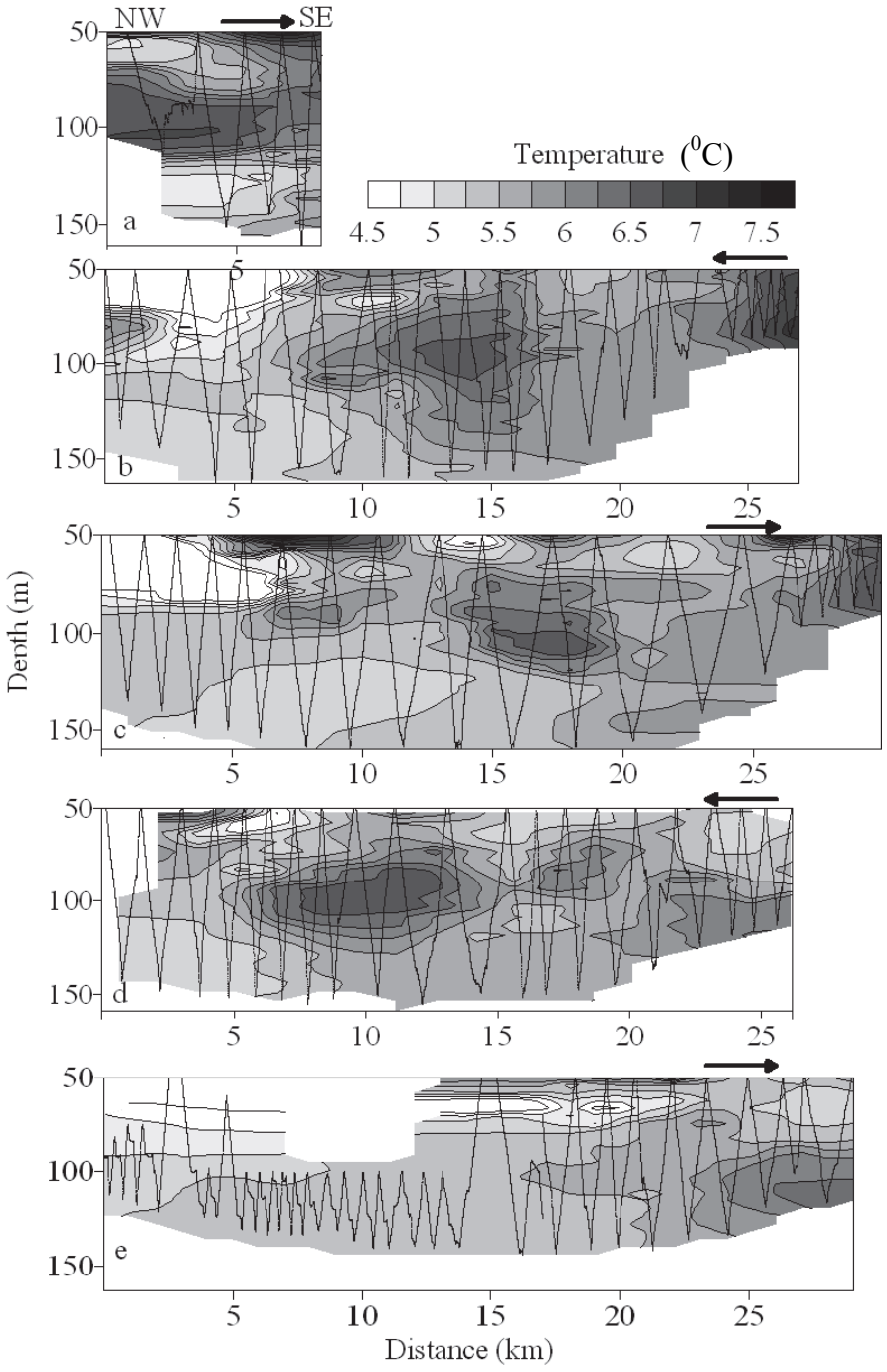

Figure 3.17 Sectional distribution of temperature (^{o}C), estimated using the TUBSS-mounted Seabird-37 CTD in September 2008 in Roseway Basin along the NW to SE transects 1 through 5 (panels a through e). Arrows on each panel denote the direction of the tow and zig-zigged lines show the TUBSS-tow profile. Transect line locations are depicted in Figure 3.1b.

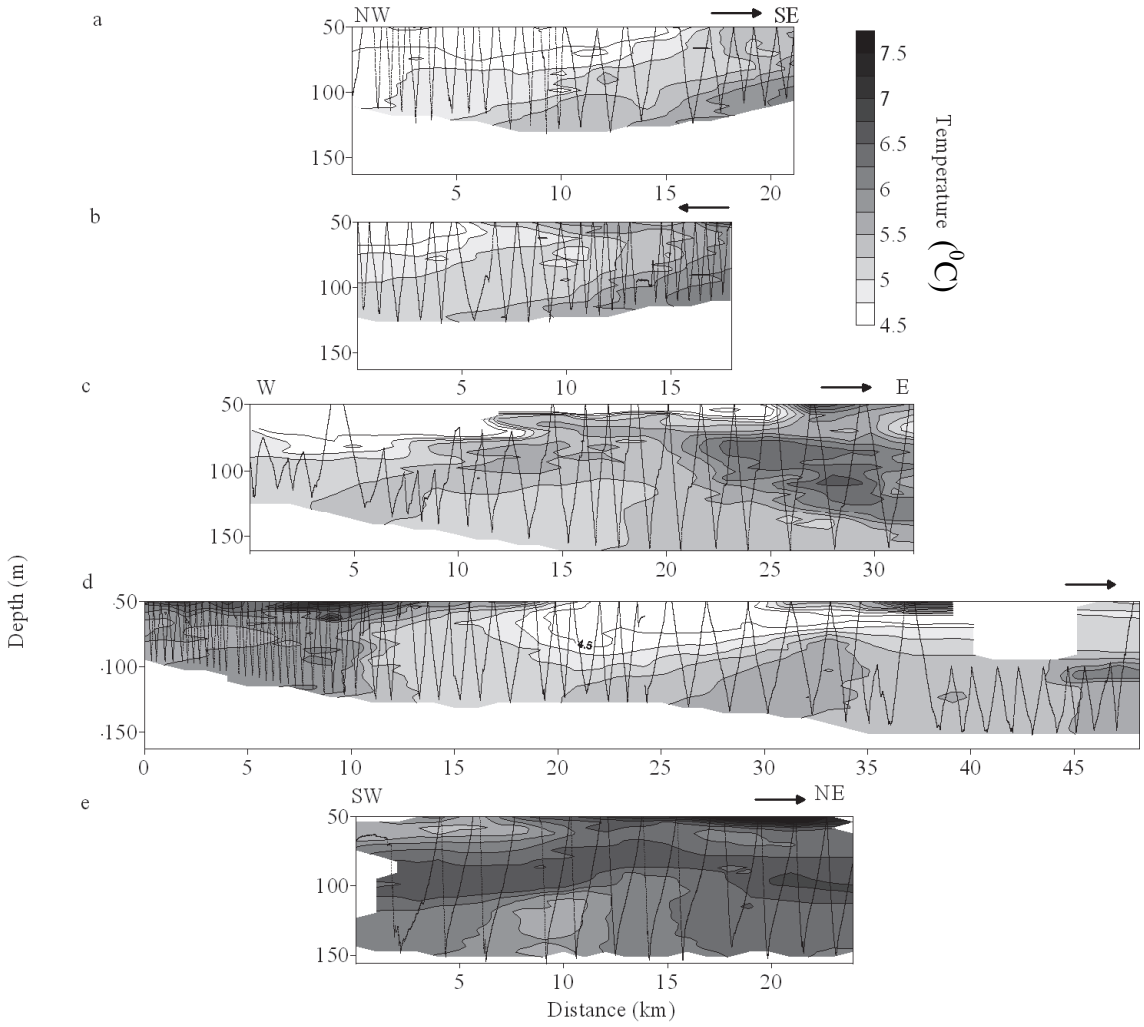

Figure 3.18 Sectional distribution of temperature (°C), estimated using the TUBSS-mounted Seabird-37 CTD in September 2008 in Roseway Basin along the NW to SE transects-6 and -7 (panels a, b), along the W to E transects-8 and -9 (panels c, d) and SW to SE along transect-10 (panel e). Arrows on each panel denote the direction of the tow and zig-zigged lines show the TUBSS-tow profile. Transect line locations are depicted in Figure 3.1b.

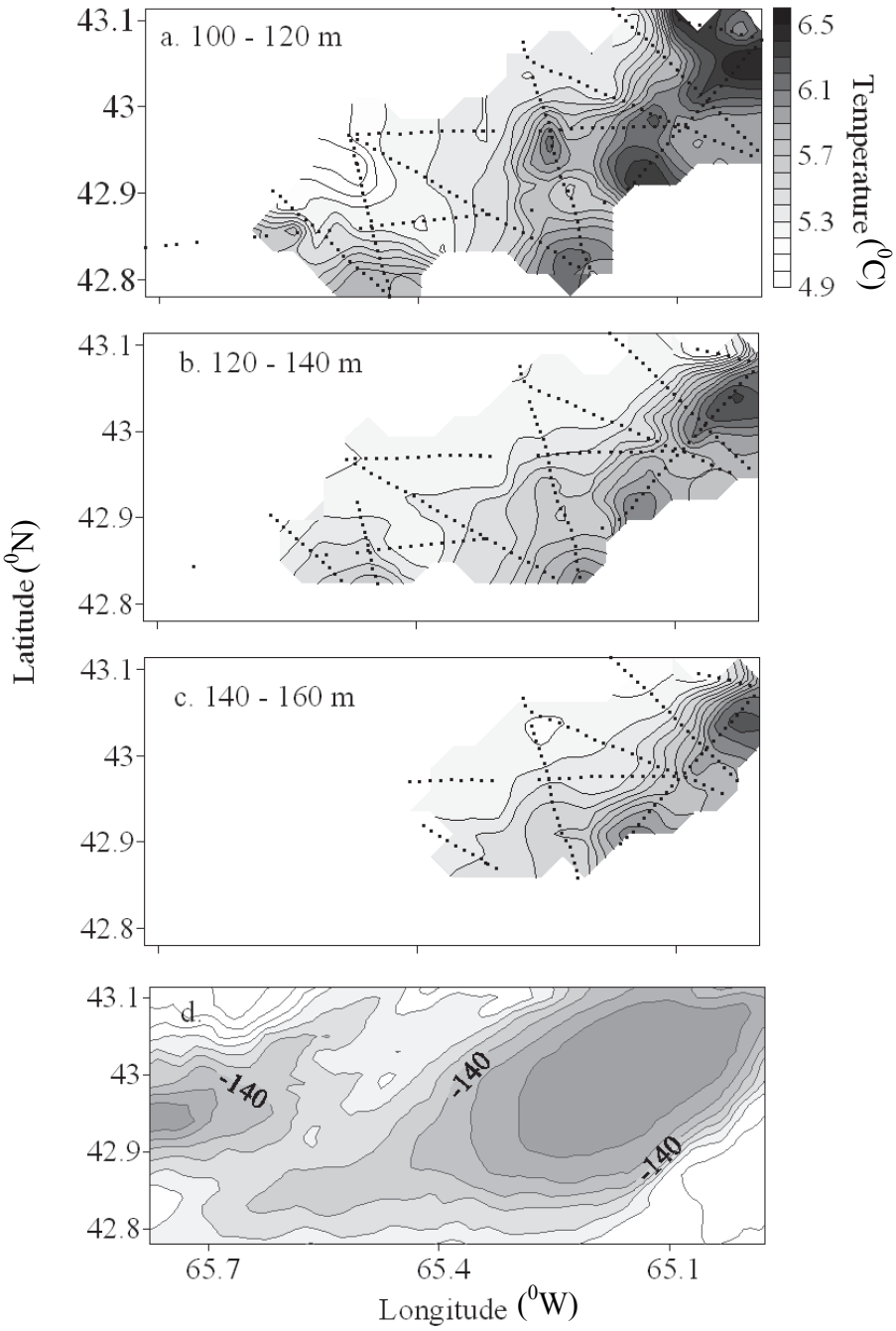

Figure 3.19 Planar distribution of depth averaged water mass temperature (°C) in September 2008 in the Roseway Basin over the: a) 100 to 120 m stratum, b) the 120 to 140 m stratum, and c) the 140 to 160 m stratum. The data were derived from each transect (illustrated in Figures 3.18 and 3.19). Each datum is indicated with black symbols. Where data are depicted without contours, there were insufficient data to make an interpolation (see Section 3.2.4).

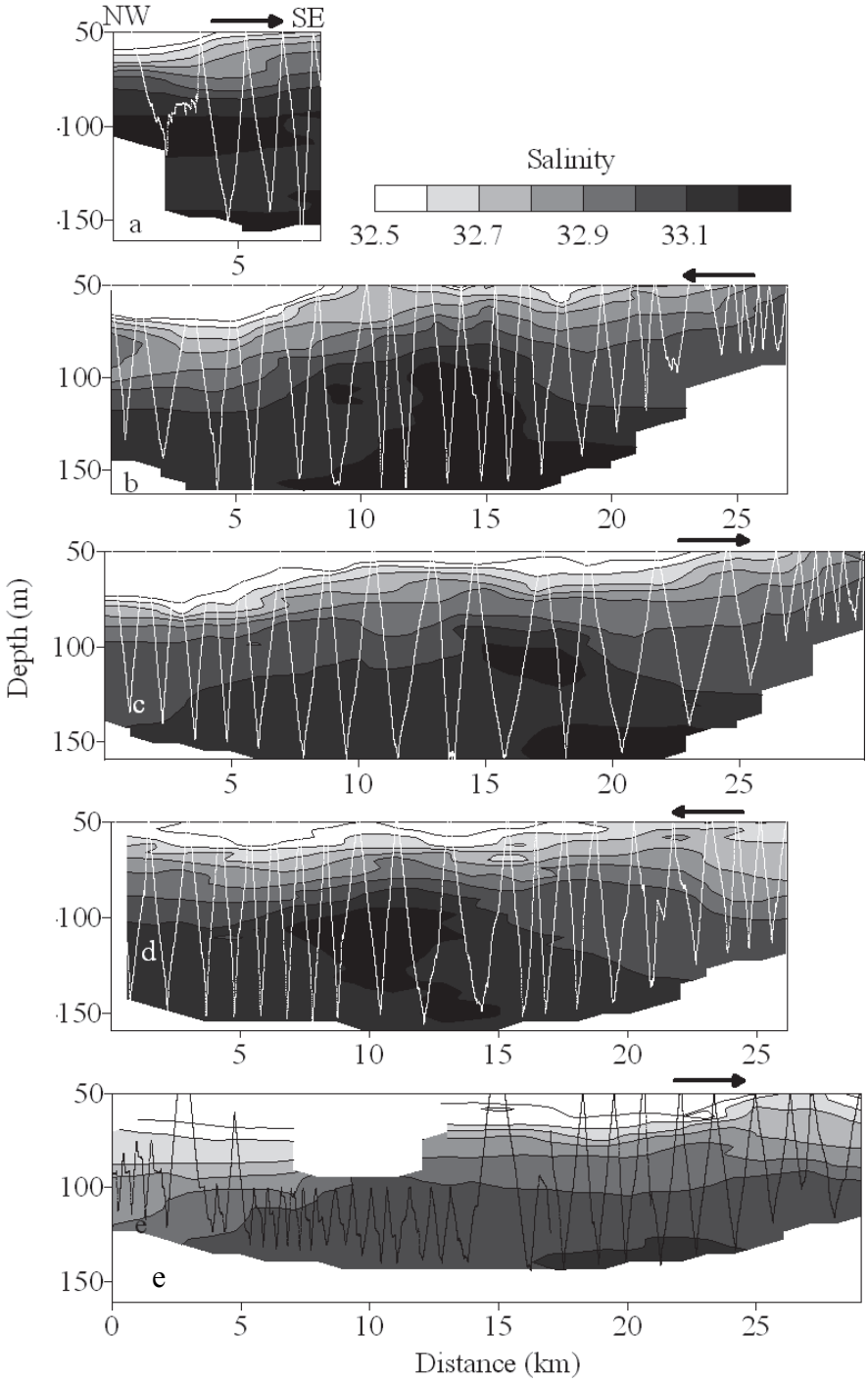

Figure 3.20 Sectional distribution of salinity, estimated using the TUBSS-mounted Seabird-37 CTD in September 2008 in Roseway Basin along the NW to SE transects 1 through 5 (panels a through e). Arrows on each panel denote the direction of the tow and zig-zigged lines show the TUBSS-tow profile. Transect line locations are depicted in Figure 3.1b.

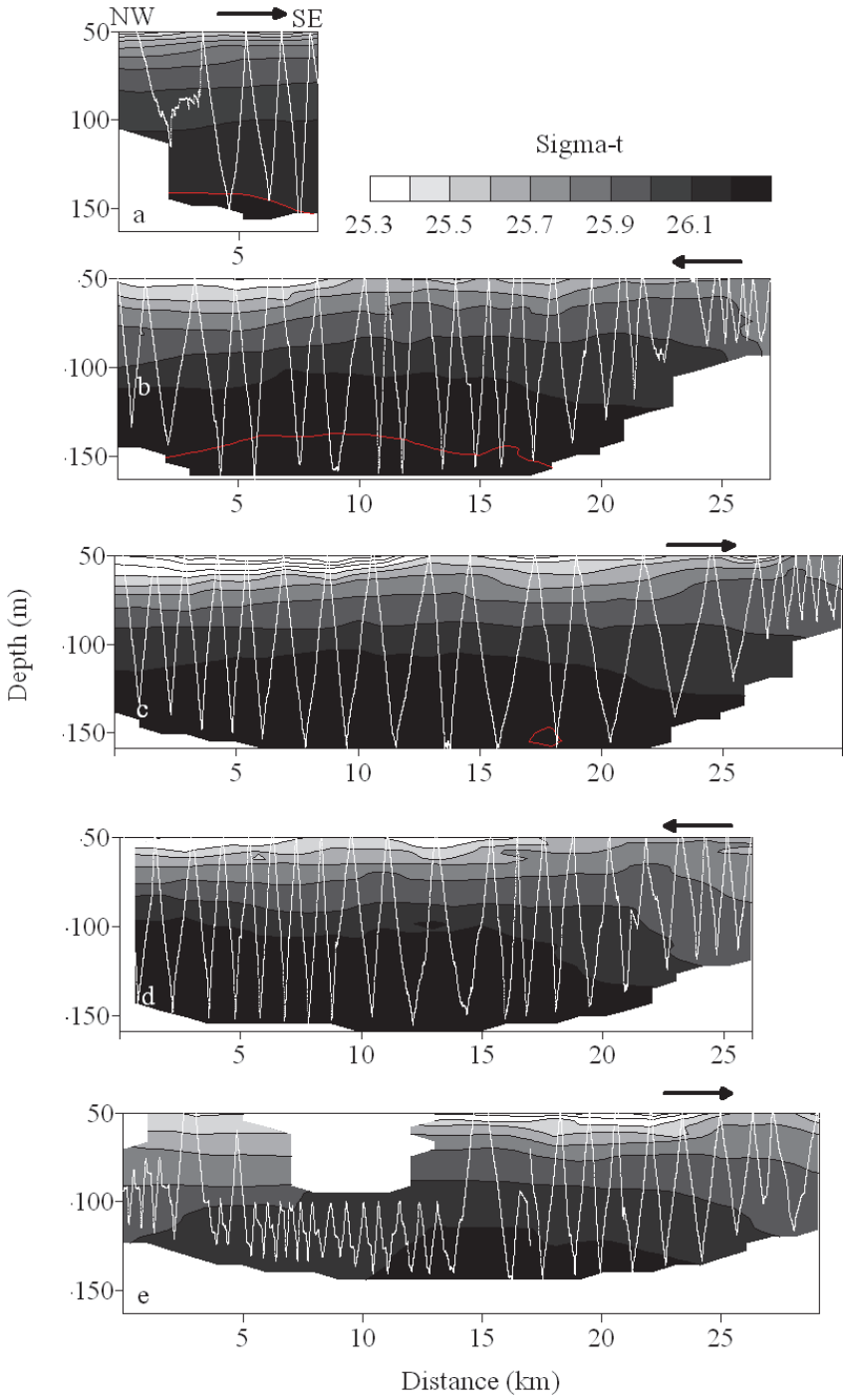

Figure 3.21 Sectional distribution of σ_t (kg m^{-3}), estimated using the TUBSS-mounted Seabird-37 CTD in September 2008 in Roseway Basin along the NW to SE transects 1 through 5 (panels a through e). Arrows on each panel denote the direction of the tow and zig-zigged lines show the TUBSS-tow profile. Transect line locations are depicted in Figure 3.1b. The 26.2 kg m^{-3} isopycnal is depicted with a red line for clarity.

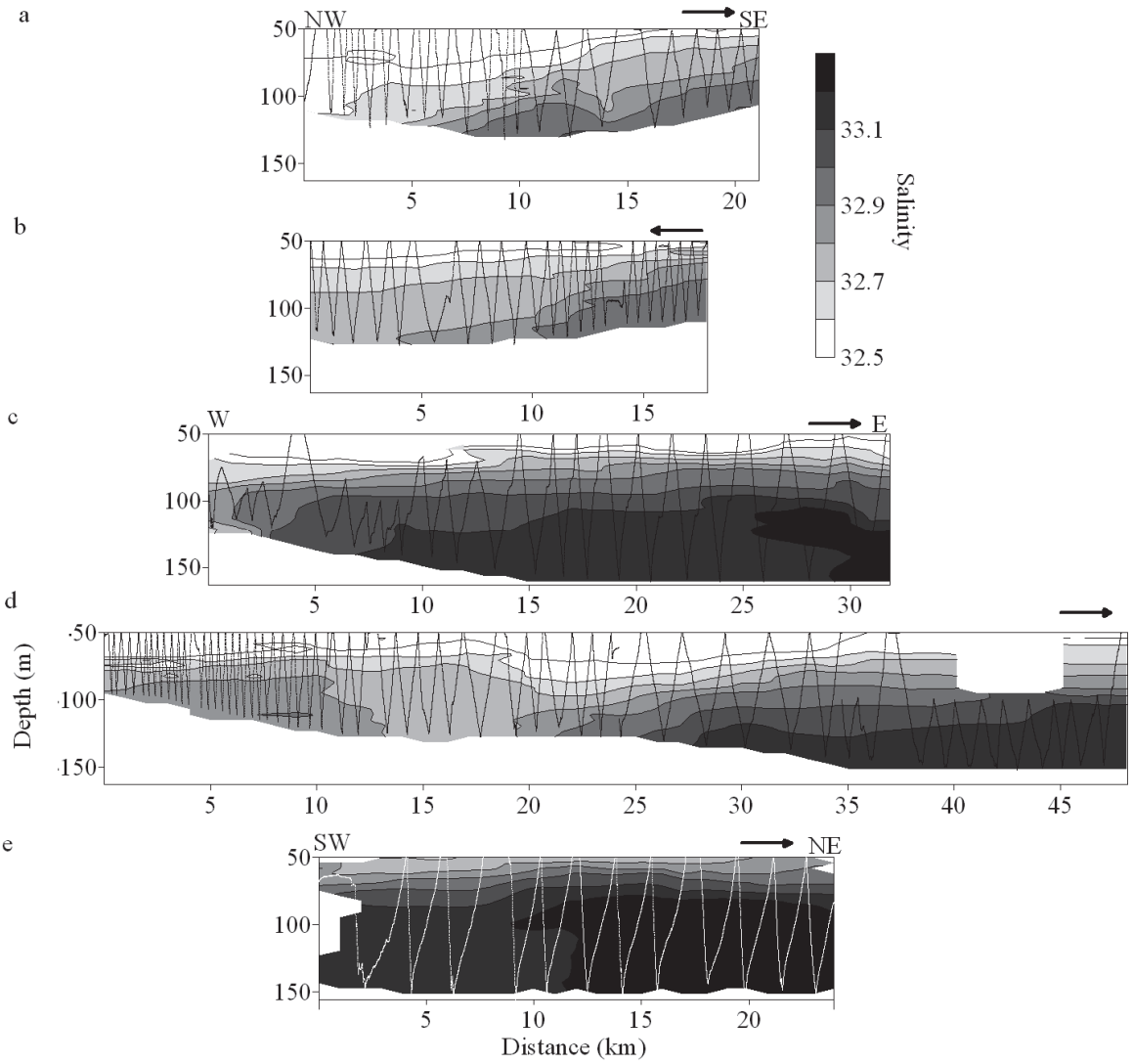

Figure 3.22 Sectional distribution of salinity, estimated using the TUBSS-mounted Seabird-37 CTD in September 2008 in Roseway Basin along the NW to SE transects-6 and -7 (panels a, b), along the W to E transects-8 and -9 (panels c, d) and SW to SE along transect-10 (panel e). Arrows on each panel denote the direction of the tow and zig-zigged lines show the TUBSS-tow profile. Transect line locations are depicted in Figure 3.1b.

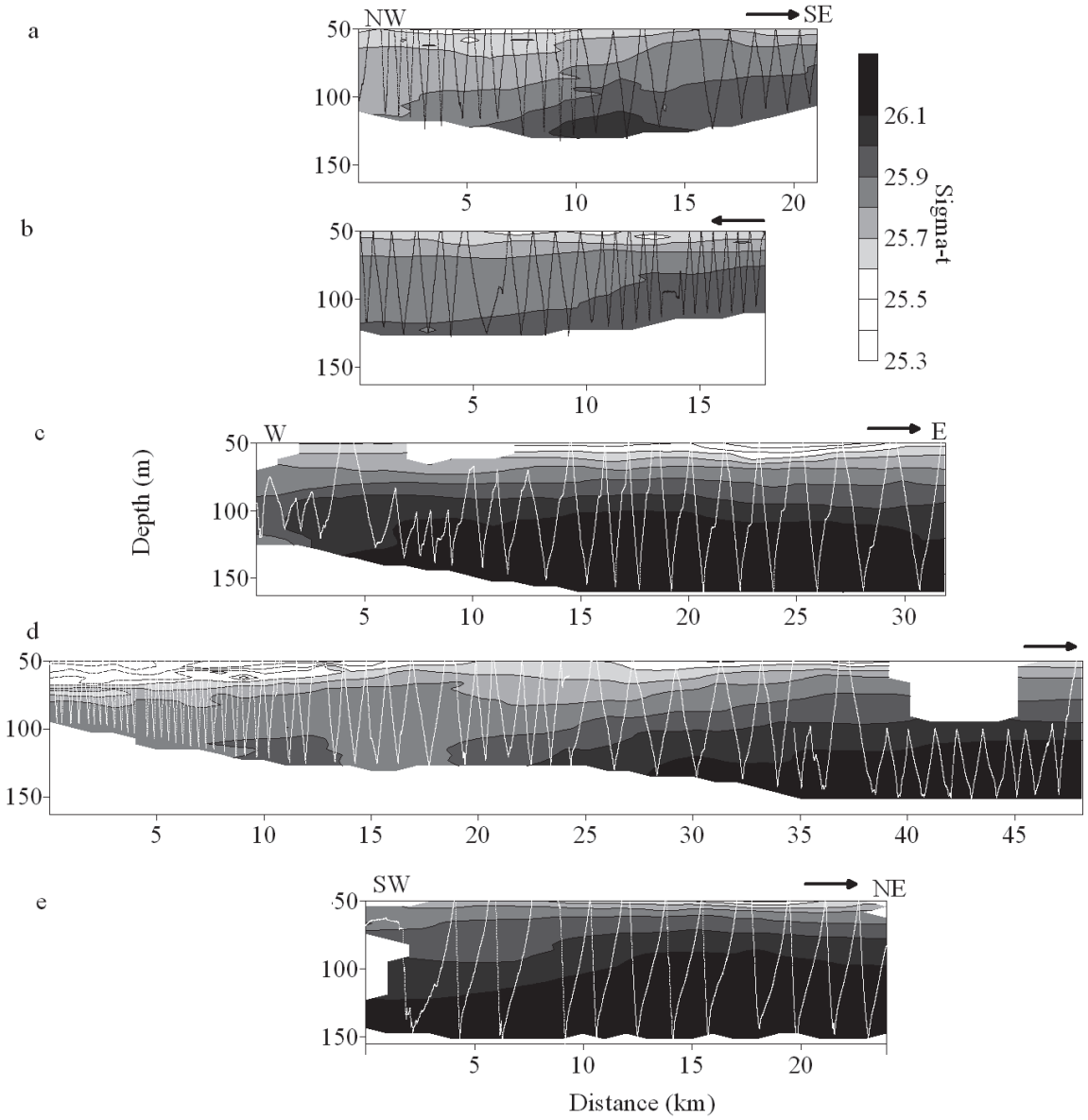

Figure 3.23 Sectional distribution of σ_t (kg m^{-3}), estimated using the TUBSS-mounted Seabird-37 CTD in September 2008 in Roseway Basin along the NW to SE transects-6 and -7 (panels a, b), along the W to E transects-8 and -9 (panels c, d) and SW to SE along transect-10 (panel e). Arrows on each panel denote the direction of the tow and zig-zigged lines show the TUBSS-tow profile. Transect line locations are depicted in Figure 3.1b.

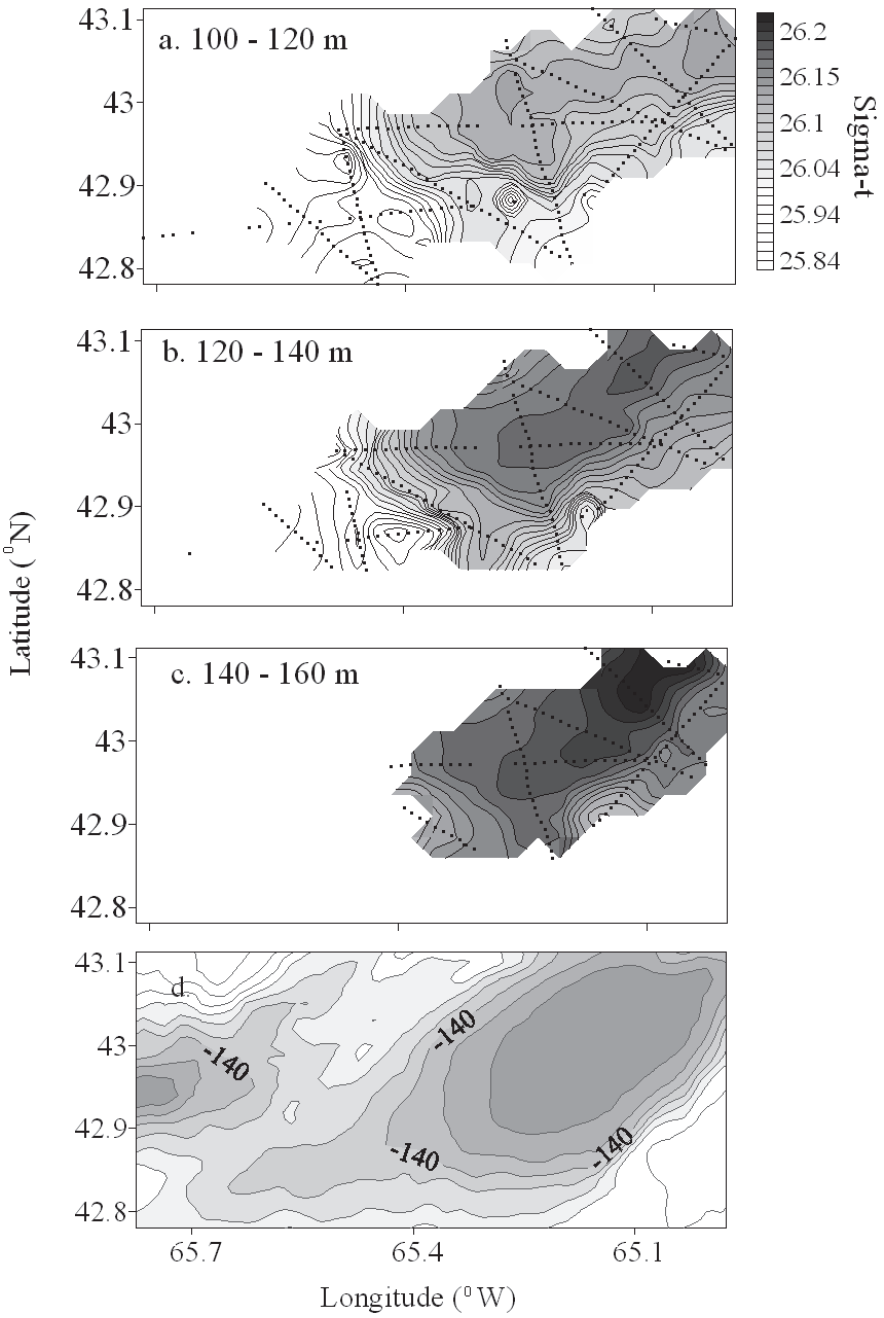

Figure 3.24 Planar distribution of depth averaged water mass σ_t (kg m^{-3}) in September 2008 in the Roseway Basin over the: a) 100 to 120 m stratum, b) the 120 to 140 m stratum, and c) the 140 to 160 m stratum and d) the bathymetry of the Basin contoured at 10 m intervals with the 140 m contour labeled. The data were derived from each transect (see Figures 3.22 and 3.24). Data points are indicated with black dots. Where data points are depicted without contours under them, there was insufficient data to make an interpolation (see Section 3.2.4).

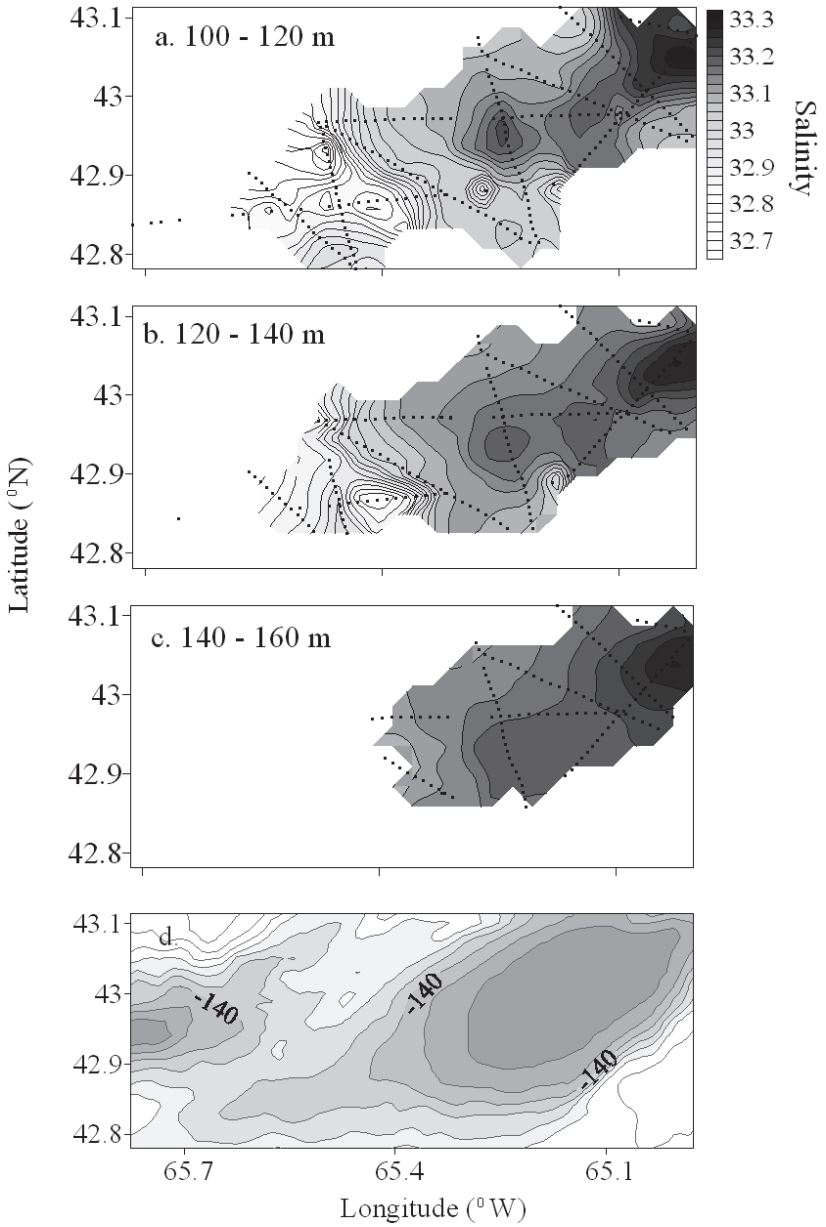

Figure 3.25 Planar distribution of averaged integrated water mass salinity in September 2008 in the Roseway Basin over the: a) 100 to 120 m stratum, b) the 120 to 140 m stratum, and c) the 140 to 160 m stratum and d) the bathymetry of the Basin contoured at 10 m intervals with the 140 m contour labeled. The data were derived from each transect (see Figures 3.21 and 3.23). Data points are indicated with black dots. Where data points are depicted without contours under them, there was insufficient data to make an interpolation (see Section 3.2.4).

3.3.6 Copepod - hydrography associations

The distribution of copepods in Roseway Basin in 2008 reflected the influence of slope water. In all three strata, the highest energy density copepod patch was situated at the NE margin (Figure 3.14) where the intrusion occurred, and a 'tube' of high energy density ran along-Basin in a NE - SW direction in roughly the middle of the Basin, coinciding with the warm-salty mBW core location (Figure 3.19). The tube was most prominent in the 120 – 140 m stratum. There were virtually no copepods present where the influence of BW was high along the northern and western margins, while a large aggregation was encompassed by the slope water masses situated in the deep Basin and on the SE slope (compare Figures 3.14 and 3.19). In addition, the highest energy density patch of copepods co-occurred with slope water intruding into the Basin (Figures 3.14a, 3.19a); this suggests the intrusion is a source of new individual copepods entering the Basin. The along-Basin copepod 'tube' corresponded well with the location of the mBW core that penetrated the middle of the Basin. The tilting of the prey field to shallower depths along the SE margin (Figure 3.12b, c) is a curious phenomenon that appears to be important for right whales given that the highest probability of observing a right whale occurs there (Figure 3.1a), and will be addressed specifically in Chapter 4.

The above results demonstrate that copepods diapausing in Roseway Basin are found primarily in the mBW water mass and not in the BW mass. Explaining whether copepods are found more often in mBW or iBW is difficult because the two slope-influenced water masses are found at similar geographic locations in the Basin, with mBW overlying iBW. To examine prey associations within the slope-influenced water masses, I compared energy density with water mass temperature, salinity and density below 100 m depth at the eastern Basin margin along transect 1 where the intrusion was apparent. I chose this location because slope water most resembles the mBW definition. The energy density data were first smoothed with a 20 s moving average because the hydrographic data were collected at 20 s intervals and could not capture higher frequency variation. I found no clear association between energy density and either of water mass temperature or salinity alone (Figure 3.26a, b) but I did find a clear and strong (r^2=0.82) positive relationship between copepod energy density and water mass density (linear regression: energy density = $194\sigma_t - 5061$, P <0.001, Figure 3.26c). When examining the

T-S diagram of these data with energy density overlaid, energy density is clearly higher in the iBW mass, which is higher in water mass density than the warmer mBW mass (Figure 3.26d). Copepods were rarely found in pure mBW, though they were found in some mBW - iBW mixed water at ~5.9 ^{o}C which may be due to frontal accumulation. Thus, I conclude that copepods diapausing in Roseway Basin are associated with high density iBW. Their presence in higher density water may also explain why they are not found in the BW, which is much lower in density than slope water. This finding has significant implications for interannual variation in copepod abundance in the Basin that I address in Chapters 5 and 6.

I further investigated the relationship between copepod energy density and water mass density by examining the sectional distributions of energy density across each transect as a function of water mass density rather than depth (Figures 3.27 and 3.28). This representation showed that across the entire Basin, copepods were aggregated primarily below the 1026 kg m^{-3} isopycnal. When I examined copepod energy as a function of depth, I observed cross-basin tilting across transects 2 through 4. When energy density was instead plotted as a function of density, the prey field was less tilted across those transects, indicating that the cross-basin isopycnal tilting is partially responsible for the phenomenon (Figures 3.27b-d). Some tilting was still present in Figures 3.27b-d, however the copepods remained primarily below the 1026 kg m^{-3} isopycnal on the southern slope.

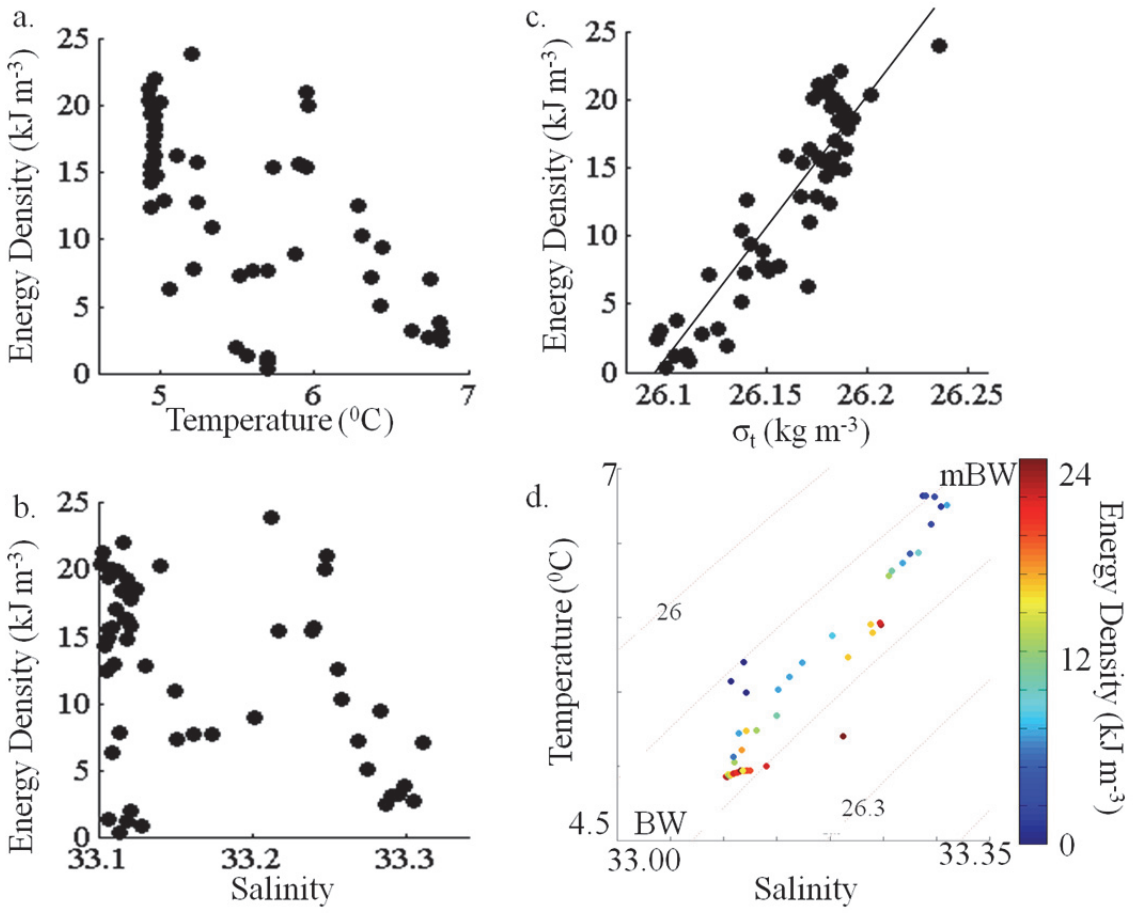

Figure 3.26 Energy density (kJ m^{-3}) of diapausing copepods and water mass (a) temperature (^{O}C) (b) salinity and (c) density (σ_t, kg m^{-3}) below 100 m depth on transect-1. The relationship between energy density and water mass density is depicted on panel c. Panel (d) shows the same data in the form of a Temperature-Salinity diagram overlaid by copepod energy density (color bar). Isopycnals are depicted by dotted lines.

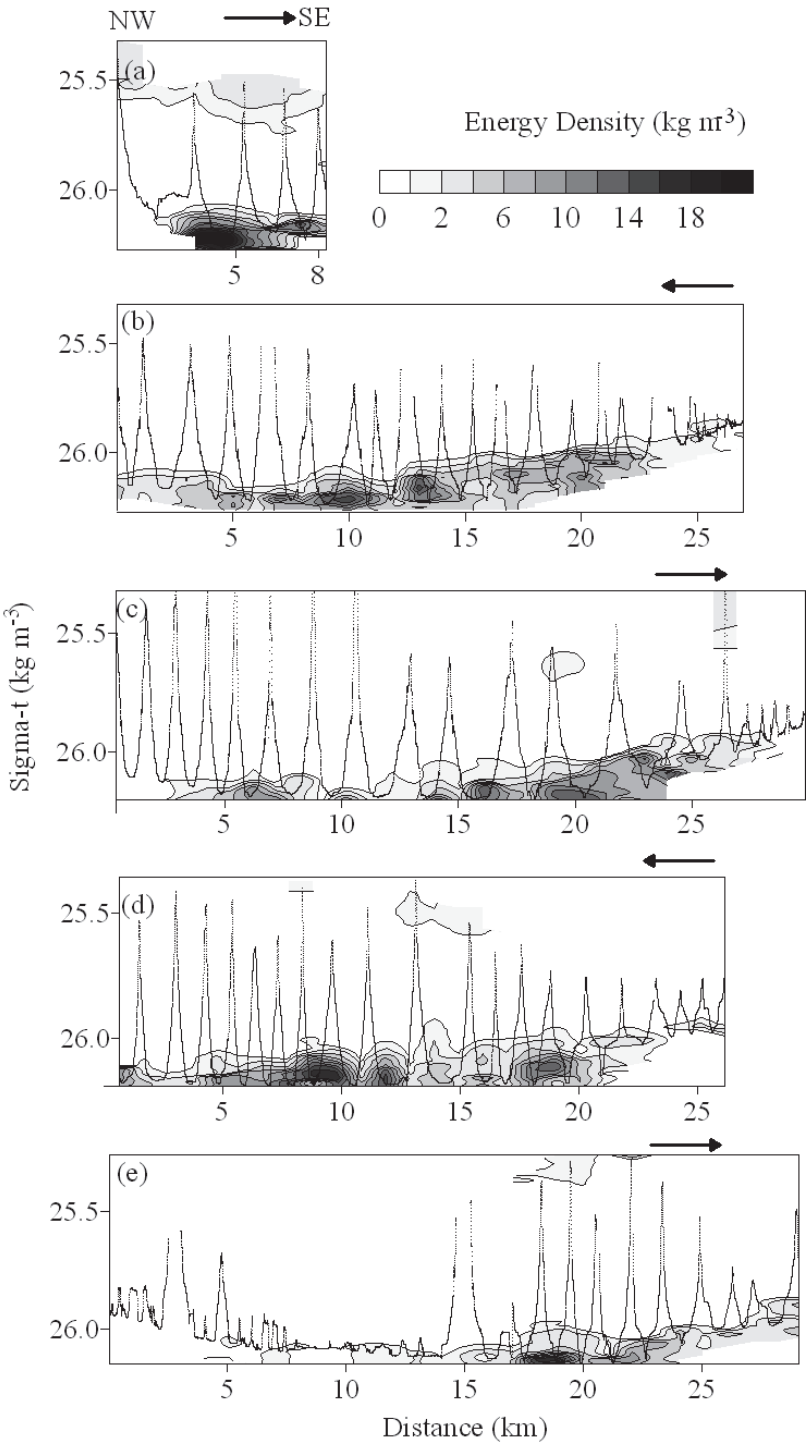

Figure 3.27 Sectional distribution of diapausing copepod energy density (kJ m^{-3}), as a function of distance along the transect (km) and water mass density (kg m^{-3}) below 50 m depth estimated using the TUBSS-mounted OPC in Sept 2008 in Roseway Basin along the transects 1 through 5 (panels a through e). Arrows on each panel denote the direction of the tow and zig-zagged lines show the TUBSS-tow profile. Transect line locations are depicted in Figure 3.1. The blank regions at the bottom left and right of each panel represents the seafloor.

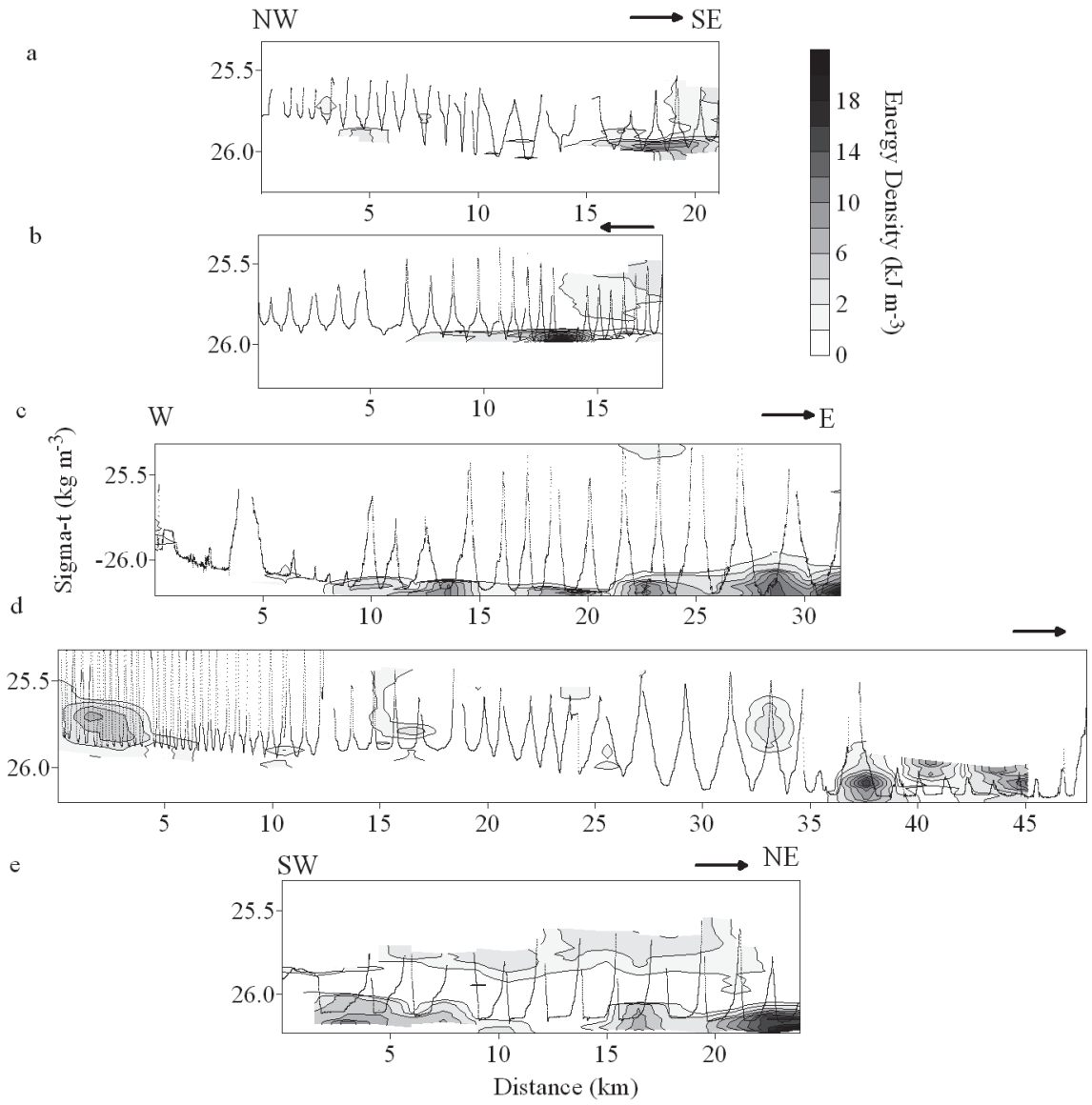

Figure 3.28 Sectional distribution of diapausing copepod energy density (kJ m^{-3}), as a function of distance along the transect (km) and water mass density (kg m^{-3}) below 50 m depth estimated using the TUBSS-mounted OPC in Sept 2008 in Roseway Basin along the transects 6 through 10 (panels a through e). The TUBSS-tow profiles are plotted, and the geographic location of each tow in the Basin is pictured in Figure 3.1b.

3.4 Discussion

3.4.1 Summary of main findings

The most abundant prey species available to right whales in Roseway Basin were the high energy, diapausing stage copepods *C. finmarchicus* stage-C5 and *C. hyperboreus* stage-C4. These copepods were concentrated below 100 m depth in large aggregations that spanned the deep Basin and tilted upslope on the southern Basin margin. Concentrations of these animals at depth varied spatially and over a tidal cycle between 500 and 8000 m^{-3}, while their energy density ranged between near 0 and 23 kJ m^{-3}. Large aggregations exceeding 16 kJ m^{-3} were particularly concentrated near the NE margin of the Basin below 140 m depth. Higher frequency spatial and tidal variation in the prey field showed many smaller patches that were associated with water mass properties. Tidal variation near the southern boundary indicated a patch of prey in the deep Basin that advected upslope as a front moved upslope, and then re-formed on the opposite tidal phase as the front moved down slope. Three water masses were defined in the deep water of Roseway Basin. The right whale prey were found primarily in the warmer, saltier slope-influenced water and were not found in the colder, fresher waters carried from the GoSL by the inner arm of the NSCC. Within the slope-influenced water masses, copepod concentrations showed a strong positive relationship with water mass density, and were found more often in iBW than mBW.

3.4.2 Right whale Critical Habitat in Roseway Basin

During the period of maximum seasonal occupancy of right whales in Roseway Basin, the highest energy density aggregations of right whale prey were situated in the eastern half of the provisional Critical Habitat (Figure 3.29a). This was part of the deepest area of the Basin, and where the influence of the high density iBW was most apparent. The depth and density are two of the most important and easily identifiable oceanographic conditions necessary to promote large aggregations of right whale prey within the Critical Habitat. Other oceanographic conditions less easy to identify, but also very important to the prey field, are the presence of gyre-like circulation that helps retain and re-circulate copepods in the Basin, the presence of ocean fronts at depth, and processes that cause

tilting of the prey field to shallow depths on the southern margin (the latter is addressed in Chapter 4).

I measured the boundaries of the right whale prey field distribution along the northern, southern, and western Basin margins, and determined that they coincided with the 120 m isobath and were well within the provisional Critical Habitat boundaries (Figure 3.29a). Movement of the planktonic prey field is ~ 3 km over a tidal cycle (Webtide v. 0.65, Bedford Institute of Oceanography), and the cross-isobath tidal ellipse advects prey upslope along the southern Basin margin from the 140 m to the 100 m isobath, meaning the provisional boundaries are sufficient to envelope the entire habitat as it moves over tidal and diel scales. This area also coincided with areas of high right whale sighting probability, thereby validating the original use of SPUE as a first-approximation in delineating of right whale habitat (Figure 3.29b). Although I did not find high prey energy density or the oceanographic conditions associated with high energy density in the western half of the provisional Critical Habitat in 2008, in Chapter 5 I show that the western margin has a large copepod population in other years, and I speculate that the western margin may be used more frequently as a feeding habitat than the deep Basin due to the relatively shallow depths of the western margin. Therefore I recommend that the current northern, southern and western Critical Habitat boundaries remain in effect and unchanged in their location.

However, I also identified the channel separating Roseway and Baccaro Banks as a corridor where right whale prey enters the Basin from the continental slope. At this location, where the channel joins Roseway Basin, I identified warm, salty water that contained a very large aggregation of copepods; the largest and highest energy density aggregation in the Basin. My survey design, however, did not extend into the corridor since I was unaware of its importance at the time. Hence the eastern extent of the right whale prey field in Roseway Basin remains undetermined. Both the NE corner of the current Critical Habitat and the proposed corridor joining Roseway Basin to the open ocean have been rarely surveyed for right whales; once per year in 0 – 4 years per 3' grid cell out of a possible 22 years between 1987 - 2008 (Figure 3.29c). Clearly the right whale survey data are inadequate to designate the provisional Critical Habitat boundaries in the corridor. Since the corridor contains the two oceanographic indicators of high

copepod energy density (bottom depth >100 m and presence of slope water), this habitat information warrants designation of this area in the Action Plan for further study of both right whales and their prey field.

The provisional Critical Habitat boundaries were selected to match the voluntary Area to be Avoided (ATBA) boundaries adopted by the International Maritime Organization in 2008 (Vanderlaan and Taggart 2009), and the ATBA was designed to encompass the distribution of right whales between 1987 and 2000 (Vanderlaan *et al*. 2008). This ATBA is currently the most important conservation measure for the Roseway Basin Critical Habitat. Before the ATBA was implemented, vessels transited through the would-be ATBA and to the north of the ATBA (Vanderlaan and Taggart 2009, Figure 3.30a). After the ATBA was implemented, most vessels that had previously transited through the ATBA changed their navigation patterns to re-route, usually south, around the ATBA (Vanderlaan and Taggart 2009, Figure 3.30b). This conservation effort has been very successful for several reasons, but particularly because it reduced the relative risk of lethal vessel strikes to right whales within the ATBA / Critical Habitat by an estimated 82 % (Vanderlaan and Taggart 2009). Therefore it is prudent to consider the above information concerning the corridor with respect to both the legal definition and protection of Critical Habitat, and the current conservation strategy employed to protect right whales within their Critical Habitat (the ATBA). To that end, below I make some recommendations concerning the definition of Critical Habitat, and concerning the extension of the eastern Critical Habitat / ATBA boundary.

(1) Critical Habitat should be defined in Roseway Basin as the area that contains high concentrations and energy density of right whale prey, co-located diapausing *Calanus finmarchicus* stage-C5 and *Calanus hyperboreus* stage-C4. Oceanographic and bathymetric conditions that promote high aggregations of prey include a bathymetric depth >100 m in waters that are influenced by off-Shelf water (particularly iBW), in which the prey are primarily found.

(2) The channel separating Baccaro and Roseway Banks is a corridor for right whale prey entering the Basin from the continental slope. The eastern boundary of the

provisional Critical Habitat area should be extended to include this ecologically important area. Such an extension would not change the shape of the area, and only one of the 4 coordinates that designate the area would need to be changed. To adequately protect this corridor, I recommend the NE extent be extended further to the NE by approximately 35 km (Figure 3.3c, move point 1 to point 1').

(3) The voluntary Area to be Avoided, which re-routes ocean-going vessels around the provisional Critical Habitat, should be extended to prevent whale-vessel collisions in the revised Critical Habitat as well. This conservation measure would come at virtually no cost to mariners because the majority of vessels already voluntarily re-route around the corridor area to avoid the current Critical Habitat while remaining on a straight-line course (Figure 3.30b). Those vessels that have not re-routed around the proposed extension are also those that have crossed the current Critical Habitat (Vanderlaan and Taggart 2009).

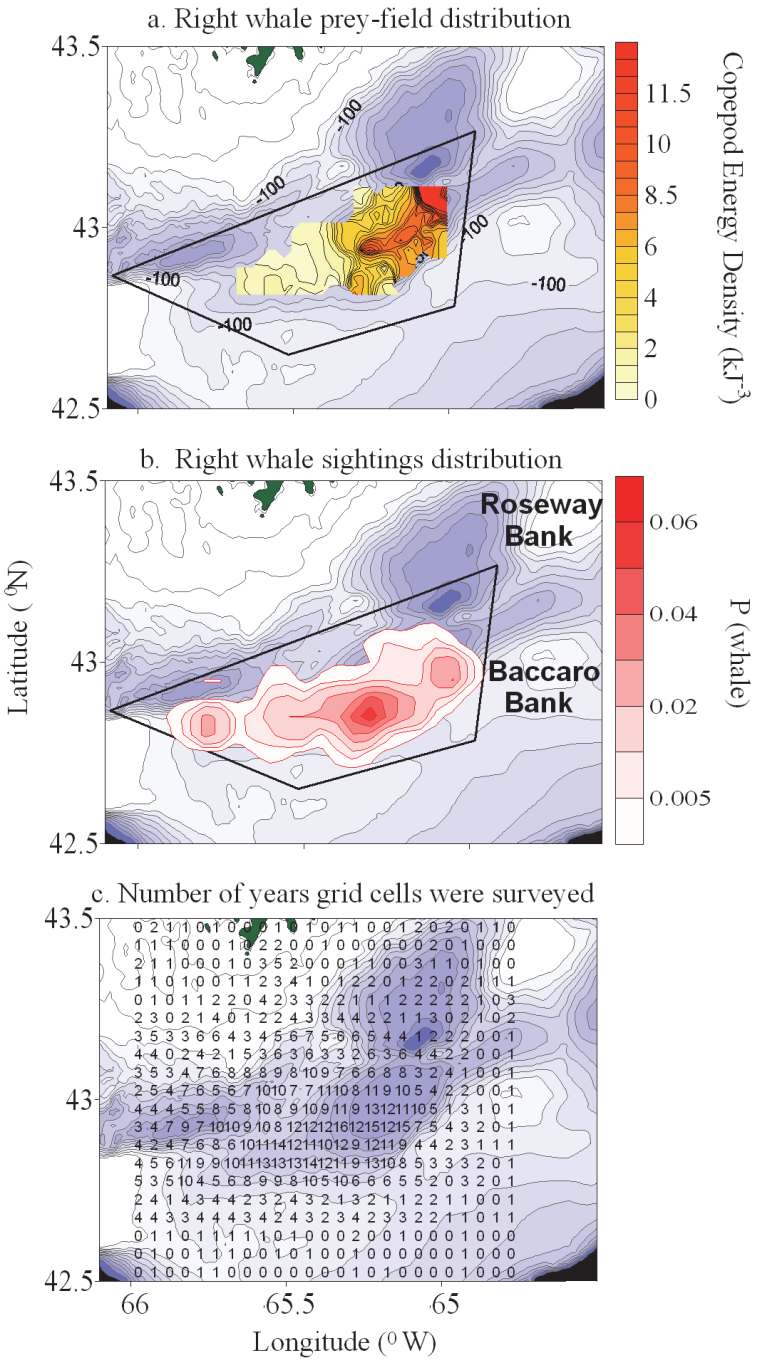

Figure 3.29 Bathymetric chart (10 m intervals) of the distribution of (a) copepod energy density (kJ m^{-3}) in the 140 – 160 m depth stratum in the Roseway Basin Critical Habitat (CH) is compared with (b) the relative probability of observing a right whale in the Roseway Basin Critical Habitat and (c) the number of years each grid cell in the Roseway Basin study area has been surveyed for right whales. The CH boundaries are shown in black in (a) and (b).

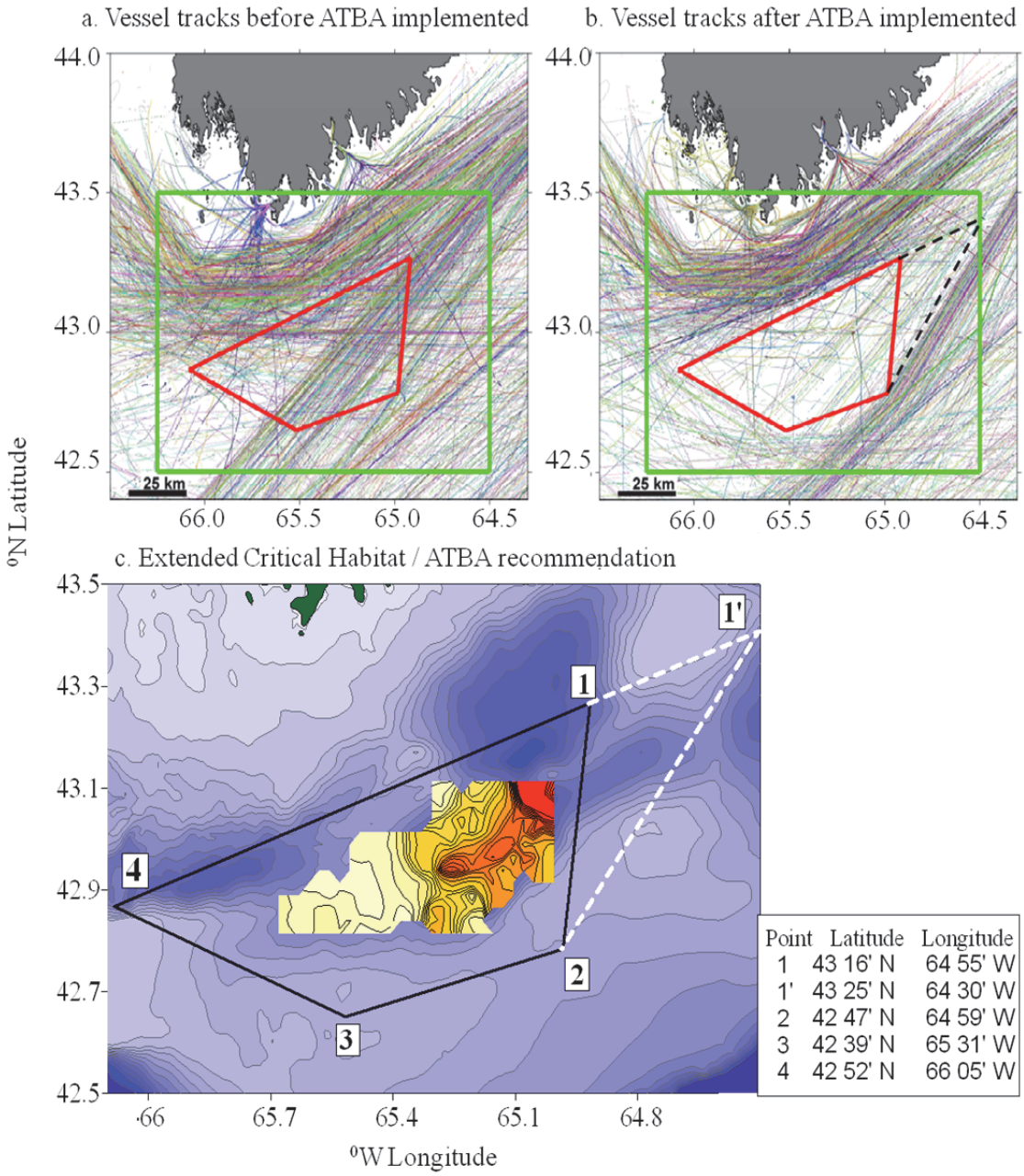

Figure 3.30 Vessel tracks (colored lines) through the Critical Habitat (CH) (a) before the voluntary Area to be Avoided (ATBA) was implemented and (b) after the ATBA was implemented (from Vanderlaan and Taggart 2009), are compared with (c) the distribution of right whale prey energy density (kJ m^{-3}) in the 140 – 160 m depth stratum, and the recommended extension of the CH boundaries in relation to current vessel tracks (b) and right whale prey field (c). The current CH boundaries are in red in (a) and (b) black in (c), and the recommended extension is the dotted line in (b) and (c). The borders of (c) are outlined by a green box in (a) and (b). Geographic positions of the grid corners are provided in (c).

3.4.3 Carrying capacity for right whales in the Critical Habitat in 2008

Here, I use information concerning right whale habitat occupancy in Roseway Basin, a model of right whale energetic demand developed by Michaud (2005), and the energy available in the Roseway Basin habitat in 2008, to estimate the right whale carrying capacity for the Basin.

A formal right whale survey was not undertaken in Roseway Basin in 2008, so I use occupancy statistics estimated over the 1980 – 2005 period by Vanderlaan (2009). The total population abundance of right whales in Roseway Basin was estimated at 107 ±16.7 (average ± SE) over this period, and a median of 17 (range 0 – 117) individuals were sighted in the habitat within any given year. The whales remained in the habitat each year for an average of 136.4 ± 70.9 days. During that time, the animals had a high probability (p) of remaining in that habitat for at least 30 days (p = 0.75), and were less likely to migrate to Grand Manan Basin (p = 0.12) or any other habitat (p = 0.03) to feed (Vanderlaan 2009). The energetic reserves that right whales accumulate in late-summer must sustain their basic metabolism and reproductive costs for the rest of the year, since the animals are believed to fast during their winter migration to southern breeding grounds (Kenney *et al*. 1986). Therefore, I reasonably assume that the food energy accumulated by right whales while occupying Roseway Basin is the only food energy they receive for the year.

Michaud (2005) modeled the total daily energetic demand over the year (R_{TE}, J d^{-1}) needed to support the basal (R_b, J d^{-1}) and feeding (R_f, J d^{-1}) metabolism of right whales feeding for 150 days in the Bay of Fundy, assuming they migrate (R_m, J d^{-1}) for 180 days and fast (R_s, J d^{-1}) for the remaining 30 days. I applied this model for the Roseway Basin habitat, assuming the whales feed for a shorter period of 136 days, migrate for 180 days and fast for 49 days:

$$136R_{TE} = \frac{136R_b + 136R_f + 180R_m + 49R_s}{A} \quad (3.3)$$

where A is an assimilation efficiency of 0.85. R_b was established for a 40 000 kg mammal (in this case, an average sized adult right whale) to be $R_b = 70 \times 40\,000^{0.75}$ kCal d^{-1}, and was converted to J d^{-1} using a conversion factor of 4681.8 J $kCal^{-1}$. For simplicity, each parameter in the model was expressed as multipliers

of R_b. The cost of swimming is $2R_b$, the supplementary cost of foraging is $R_f = \frac{T_f}{24} R_b$ where T_f is the number of hours spent feeding, and the supplementary cost of storage (R_s) is assumed to be equal to the resting cost (R_b) for one month. There are no biological reasons why any parameter should be a multiple of the basal rate, it is only for simplicity since data are not available for each parameter. The final equation describing annual daily energetic demand is:

$$R_{TE} = \frac{R_b + \frac{T_f}{24} R_b + \frac{180}{136} R_b + \frac{49}{136} R_b}{A} \quad (3.4)$$

Various daily foraging times (h d^{-1} spent feeding) were considered by Michaud (2005), and for consistency I present my results for both the minimum and maximum foraging times considered by Michaud (2005); T_f = 4h d^{-1} and 16 h d^{-1}. R_{TE} varied between 3.11 x 10^9 and 3.65 x 10^9 J d^{-1}, depending on T_f.

The carrying capacity (C, whale days) of the sampled area was estimated as the ratio of the energy available (E) to the daily whale energy demand (R_{TE}). The available energy E was estimated from the planar data in Figure 3.14 to be 2.6 x 10^{14} J, sampled over an area of approximately 1200 km^2. The carrying capacity for Roseway Basin in 2008 decreased from 8.4 x 10^4 to 7.1 x 10^4 whale days as feeding time (T_f) increased from 4 to 16 h d^{-1}. I used this model to estimate how many whales the Roseway Basin feeding habitat could support for a year if they fed in the habitat for the full 136 day period. The prey field in Roseway Basin in 2008 could support the basal and feeding demands of a right whale population consisting of 522 to 617 individuals.

Since not more than 117 whales have ever been sighted in Roseway Basin in one year (Vanderlaan 2009), my calculation is an overestimate of the true carrying capacity. In comparison to Roseway, Michaud (2005) estimated that the Grand Manan Basin could support the basal and feeding metabolic costs of 200 right whales for 140 – 159 days. The primary reason why the carrying capacity in Roseway Basin was much higher than Grand Manan is because the energy density in Roseway Basin was double that measured in Grand Manan (1.17 x 10^{14} J). However, one reason why the energy density in Roseway Basin was greater was because the prey field was 3 – 4 times larger in area compared with Grand Manan Basin (280 km^2). A widespread prey field distribution may not be beneficial to right whale foraging; right whales would likely need to spend more

time and energy in Roseway Basin searching for food patches spread over a wider area than in Grand Manan Basin where the prey field is locally concentrated.

With this in mind, I investigated the possibility that right whales do not forage over the entire Roseway Basin habitat, and instead seek out high density prey patches that maximize their energy intake. The minimum energy density required for right whales to gain net energetic benefit is 10 kJ m^{-3} (Figure 3.31, Kenney *et al*. 1986). Under this threshold condition, $E = 4.4 \times 10^{13}$ J over an area of approximately 100 km^2 in Roseway Basin, and the Basin can support 88 - 104 whales for 136 days. This is within the range of the estimate of 'resident' whales (Vanderlaan et al. 2009) and is much more realistic than my first estimate.

My estimate of carrying capacity is near the maximum number of whales occupying Roseway Basin (107), which implies that 2008 was a very productive year for right whales in Roseway Basin. These prey patches were concentrated only in the deep Basin area where the slope water intrusion occurred (Figure 3.31), implying that the deep Basin was the best foraging area that year. However, we sighted only one right whale during our survey. Further, the historical sightings distribution of right whales is located along the southern slope, not in the deep Basin. Both of these observations suggest that there may be other constraints on right whale foraging besides a minimum energy density threshold that limits their foraging ability.

3.4.4 Oceanographic processes that aggregate right whale prey in deep Basins

My second objective was to investigate the sources, retention mechanisms and smaller-scale aggregation processes affecting diapausing copepods within the Basin. Specifically, I posed three questions: Are slope water intrusions an important source of diapausing copepods to the Basin? Are the deepest parts of the Basin sites of closed circulation that passively aggregate and retain diapausing C5s? Do ocean fronts (both tidal fronts and water mass fronts) aggregate plankton in the Basin? I found evidence that each of these three physical processes occurred in 2008, often at different spatial scales, and can explain some of the variation in copepod abundance within Roseway Basin. Below, I address each process individually.

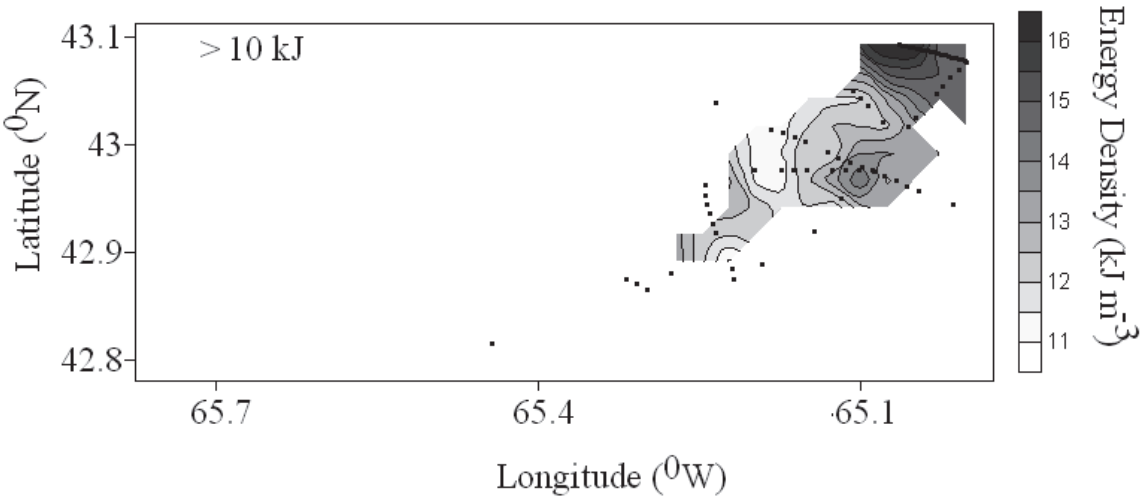

Figure 3.31 Planar distribution of averaged integrated copepod energy density (kJ m^{-3}) in September 2008 in the Roseway Basin over the 100 – 160 m depth stratum using only locations where energy density exceeded 10 kJ. The data were derived from each transect (see Figures 3.12 and 3.13). Data points are indicated with black dots on panels a and d. Where data points are depicted without contours under them, there was insufficient data to make an interpolation (see Section 3.2.4).

3.4.4.1 Are slope water intrusions an important source of diapausing copepods to the Basin?

The relative contributions from different Scotian Shelf copepod sources to Roseway Basin depend on production and advection from upstream at the surface in winter, spring and summer (Tremblay and Roff 1983, Herman *et al*. 1991, Head *et al*. 1999, Zakardjian *et al*. 2003). All Shelf sources, e.g., other Shelf Basins and subsequent Shelf production, GoSL outflow, slope intrusions at the surface in spring, are contributing to the diapausing copepod population in Roseway Basin, but what I measured at the end of summer at the western-most Shelf Basin was the result of all those processes. Thus it is not possible to elucidate specific sources and their relative contributions as was done in Sameoto and Herman (1990) and McLaren *et al*. (2001) in Emerald Basin, or most recently modeled at broad scales by Zakardjian *et al*. (2003) for the Scotian Shelf. What I was able to capture, however, is the effect of deep slope water intrusions in summer that bring diapausing copepods onto the Shelf from the continental slope diapausing populations. One of the clearest associations between diapausing *Calanus* spp. and hydrography in Roseway Basin was the spatial association between copepods and slope-influenced water, and the dominance of *C. finmarchicus* in the deep Basin is indicative of a slope water influence. This does not directly show that deep slope water intrusions in summer are important diapausing copepod sources. However, inferentially, the presence of slope-influenced water at the entrance of a channel connecting Roseway Basin to the continental slope, and that is contained the highest concentration of *Calanus* spp. encountered in the Basin, suggests that intrusions from the slope through the deep channels in summer are a significant source of copepods to the Basin.

Copepods overwintering on the continental slope can do so at depths exceeding 700 m (Visser and Jonasdottir 1999), presumably to use the cold temperatures to minimize metabolic rates while in diapause. Their internal density must increase for them to sink to such depths from surface waters; this could be accomplished by accumulating food in their stomachs (Visser and Jonasdottir 1999) and by regulating their internal ion concentrations (Sartorius *et al*. 2010). If the animals are swept into the relatively shallow Scotian Shelf Basins during their descent over the continental slope, they would afterward be found in water of the highest possible density approaching as

close as possible the high density environment of continental slope deep water. This is one plausible interpretation that explains the very strong correlation between diapausing copepod abundance and water mass density (Figures 3.26 to 3.28).

The absence of copepods from cold, fresh BW that flooded the western end of the Basin could occur for several reasons; one plausible explanation is that BW is not sufficiently dense to retain diapausers, and copepods entering diapause in the BW either sink to the seafloor or are swept into the deep Basin, which is filled with higher density slope-influenced water. BW is probably an upstream source of copepods to Roseway Basin, since its biological indicator, the Arctic *C. hyperboreus*, was found in relatively high concentrations in the deep Basin. Those animals could have mixed with continental slope populations of *C. finmarchicus* at the surface upstream of Roseway Basin, as observed by Tremblay and Roff (1983), then sank into the Basin when they entered diapause.

Interannual variation in *Calanus* spp. abundance at depth in Roseway has been hypothesized to explain the absence of right whales there in some years (Patrician and Kenney 2010). Processes that affect water mass density in the bottom of the Basin, for example by increased volume transport of the BW or variation in the frequency and strength of slope water intrusions, could also affect the copepod concentrations in the Basin by varying the density of bottom water in Roseway; for example if the water becomes so low in density that the copepods sink out of the water column. If, as I propose, summer intrusions of deep slope water are an important source of copepods to Shelf Basins, variation in the frequency and strength of slope intrusions could also have a significant impact on the Roseway Basin independent of the density variation in the habitat. Water mass density could then be an indicator of *Calanus* spp. abundance, but not its cause.

3.4.4.2 Are the deepest parts of the Basin sites of closed circulation that passively aggregate and retain diapausing C5s?

In late-summer when diapausing copepod abundance is high, Roseway Basin contains a gyre-like circulation maintained by baroclinic response to larger-scale forcing. The center of the gyre is the deepest part of the Basin (Figure 3.24), where I found high

concentrations of copepods (Figure 3.31). Thus, the deepest parts of the Basin are sites of closed circulation that passively aggregate and retain diapausing C5s.

3.4.4.3 Do ocean fronts (both tidal fronts and water mass fronts) help aggregate plankton in the Basin?

Frontal dynamics appear to play a key role in accumulating diapausing copepod patches within the larger aggregation in the Basin. Accumulation of copepods at or near fronts occurred in several places in the Basin. 'Plankton behavior' in this case appears to be the tendency for copepods to sink to depths of neutral buoyancy in the densest possible water. 'Physical dynamics' in this case could include the deviation of current direction (e.g., upwelling or downwelling) at numerous vertical fronts within the Basin where, for example, slope-influenced water met Shelf water, or where mBW intruded into the Basin and met slope-Shelf mixed water that had intruded onto the Scotian Shelf earlier in the year. The front along the southern boundary certainly contributes to variation in the smaller scale patchiness of copepods diapausing in that area (Figure 3.9). It is also an area where the long axis of the tide is oriented across-isobath and this could affect the current dynamics in the area. Copepod accumulation on the Basin side of the front at every high tide is a predictable accumulation mechanism that right whales could exploit and which may help make the area the best foraging ground in the Basin. This is a novel finding; frontal associations of diapausing copepods at depth have not previously been examined on the Scotian Shelf since hydrographic and diapausing copepod data have not been collected at similar spatial resolutions or at resolutions fine enough to resolve such associations (e.g., Sameoto and Herman 1990).

3.4.4.4 Upslope tilting of the prey field at the southern margin

A novel finding in this study was the prey field cross-isopycnal tilting to reach shallower depths along the southern boundary than it did in both the deepest parts of the Basin and the northern boundary (e.g., Figure 3.12b). This tilting was measured across several transects over different time periods, so it seems to be maintained through at least weekly time scales. The upper (shallow) limits of this structure are probably related to the tilting in the upper layer of isohalines and isopycnals. However, at depth, the

isopycnals along the southern boundary turn downwards at a front, meaning that to maintain the 'tilted' structure, the copepod aggregation must cross isopycnals on the southern slope (Figures 3.26 and 3.27). It is not clear why this tilting across isopycnals at depth occurs, but I postulate that it is maintained through time through a dynamic steady-state mechanism acting to constantly push the copepods across isopycnals up the slope. Alternatively, if the major copepod source is off-Shelf, then the copepods on the slope may be new arrivals brought there by an intrusion over the bank. Here, I summarize the insights gained from this analysis, then I will explore the dynamics of the process in more detail in Chapter 4 using current, CTD and copepod data collected concurrently across the southern slope.

(1) The prey field tilts upslope on the southern boundary, and this upslope tilting feature crosses isopycnals that are tilted in the opposite direction at depth. This is a large-scale feature that was observed throughout the survey.

(2) There is a cross-isobath tidal ellipse on the southern slope, and an along-isobath residual current flowing toward the northeast that is generated by baroclinic response to larger-scale forcing.

(3) There is a front on the southern slope that separates vertically stratified water that is a mixture of all three water masses on the Basin slope, from vertically mixed slope-influenced mBW on the bank.

(4) When the tide is at its down slope position on the southern slope, there is a patch of copepods at depth, presumably created because copepods cannot cross the front and instead accumulate on the Basin side. This patch moves upslope and thins as the mixing front moves upslope with the tide. On the upslope tidal phase, concentrations were high at shallower depths, which may be due to water column mixing since that was also the location of a front (Fig. 3.10a,b,g,h).

3.5 Conclusions

In summary, I met my primary objective stated in Section 3.1 by defining and identifying the Critical Habitat for right whales based on their prey field distribution and the processes that aggregate prey in the Roseway Basin Critical Habitat. Further, my high resolution co-located copepod and hydrographic sampling allowed me to meet my second objective concerning the sources, retention and accumulation of prey within the habitat. Oceanographic processes that affect the right whale prey field in Roseway Basin include slope water intrusions, the water mass density field, gyre circulation and fronts. This is also the first large scale oceanographic survey of Roseway Basin, and hence advances general knowledge of the biological and physical oceanography on the Scotian Shelf.

This is a precedent setting study in marine conservation, for the North Atlantic right whale is the first marine species in Canada for which the biological and physical components of identified Critical Habitat will have been characterized robustly, at multiple scales. Already, there are effective conservation measures in place to protect whales from lethal vessel strikes in both Critical Habitat areas, and efforts are currently underway to protect whales from fishing gear entanglements in both areas (e.g., Vanderlaan *et al*. 2011). Once measures to mitigate entanglement are added to the current ship strike reduction strategy, Canada will have in essence created a Marine Protected Area for North Atlantic right whales without actually calling it a Marine Protected Area (Hinch and De Santo 2011).

Chapter 4

Tidal and Residual Current Influence on Copepod Aggregations Along a Sloped Margin in Roseway Basin

4.1 Introduction

The highly endangered North Atlantic right whales experience significant mortality from fishing gear entanglement and vessel strikes (Kraus and Rolland 2007). Measures to reduce these threats continue to increase through legislation, implemented as recently as 2008, that protects their feeding and breeding habitats (e.g., Vanderlaan and Taggart 2009, Vanderlaan *et al*. 2011). Conservation strategies should be based on the best available habitat data, however our understanding of what constitutes right whale habitat is in some respects quite poor (Baumgartner *et al*. 2003). In particular, physical and biological mechanisms that create and maintain large aggregations of the primary right whale food, calanoid copepods, are not characterized for most habitats.

Grand Manan Basin in the Bay of Fundy is a right whale feeding habitat where, through the combined effort of several research programs, significant progress has been made in describing these mechanisms (e.g., Woodley and Gaskin 1996, Laurinolli 2002, Baumgartner *et al*. 2003a, Michaud and Taggart 2007, Aretxabaleta *et al*. 2008, Michaud and Taggart 2011). Together, these and other studies have found that the planktonic food is advected by tidal currents in the Basin that accumulate and maintain patches of *Calanus finmarchicus* stage-C5 at depths > 100 m to the benefit of foraging whales. Strong tidal currents advect C5s along the ~ 8 km tidal excursion (Michaud and Taggart 2011), and right whales have been observed to move with the tide, presumably to maximize their consumption of the advecting patches of food (Laurinolli 2002, Baumgartner *et al*. 2003). Patch integrity appears to be maintained at tidal scales and likely at weekly scales or more (Michaud and Taggart 2011). Annual maxima in right whale sightings in the Basin correspond with the timing of maximum C5 abundance at depth (Michaud and Taggart 2007) and also the maximum particle retentiveness of a seasonal gyre in the Basin that is partially maintained by tidal rectification (Aretxabaleta

et al. 2008). Further, the 20 year aggregate right whale sighting probability distribution in Grand Manan Basin is approximately elliptical and oriented parallel to the cross-isobath tidal ellipse with the distribution center located near the geographic center of the Basin (Figure 4.1b, d). This is strong evidence that advection by tidal currents consistently affects the distribution of whales and, by inference, their food on interannual time scales (Michaud and Taggart 2011). The maintenance of a dense, high energy food source by persistent tidal processes in Grand Manan Basin offers a simple explanation as to why approximately one third of all North Atlantic right whales return to the habitat to forage for approximately 3 to 4 months each year.

The right whale population is loosely divided according to habitat fidelity into those that repeatedly habituate the Bay of Fundy and those that do not (Schaeff *et al*. 1992). Many of the non-Fundy whales feed during late-summer in nearby Roseway Basin on the western Scotian Shelf (Baumgartner *et al*. 2003, Vanderlaan *et al*. 2008). Roseway Basin, like Grand Manan, maintains diapausing *Calanus finmarchicus* stage-C5 aggregations that are also co-located with the less abundant diapausing *C. hyperboreus* stage-C4 copepodids, each with enhanced energy content and maintaining neutral buoyancy at the depths > 90 m, where they rest (Chapter 3). Oceanographic conditions also exist in Roseway Basin that serve to accumulate and maintain the food resources that may be commensurate with the metabolic needs of whales and other plankton predators that habituate the Basin. However, some processes influencing the prey field in Roseway (specifically the influence of the tide and residual currents) likely differ from Grand Manan Basin because the water masses, tides, currents and bathymetry differ between the two habitats.

I demonstrated in Chapter 3 that, like Grand Manan Basin, there is basin-scale gyre-like circulation in Roseway Basin that is maintained at least partially by baroclinic processes and helps maintain the prey field aggregation over time. The right whale prey field is evenly distributed in the deepest part of both Basins, with the highest concentrations near the center of the gyre. A unique (i.e., not found in Grand Manan Basin) feature of the Roseway Basin is that the prey field is also concentrated along the southern slope, where the aggregation is tilted upslope to shallower depths. This slope aggregation appears to be important to feeding right whales because an observer in

Roseway Basin has the highest probability of sighting a right whale along the southern margins of the Basin between the 100 and 160 m isobaths (Vanderlaan *et al*. 2008, Figure 4.1a). Given the spatial and tidal coincidence of the concentrated prey field and the whales in Grand Manan (Michaud and Taggart 2011), the whale distribution in Roseway would suggest that the southern slope is the most favorable feeding ground. The southern slope is not the area with the highest prey concentrations, however concentrations do increase when the tide is at its most down slope position (high tide) through prey accumulation on the Basin side of a tidal front.

I was unable to identify in Chapter 3 the mechanism by which this slope aggregation is maintained. It seems to be an unstable system since the copepods tend to seek higher density water in the deep Basin, yet they have to cross isopycnals toward less dense water to achieve the depth distribution observed on the southern slope. Since the density distribution at depth in the Basin is not sufficient to explain the slope aggregation, I hypothesized that the current system may play a role in a steady state, dynamic process that constantly pushes copepods upslope. Baroclinic circulation models show that the southern margins of Roseway have tidal ellipses oriented normal to the isobaths and a weak residual (total current – tide) flowing along-isobath (Hannah *et al*. 2001).

Physical mechanisms associated with a tidal front on a slope with a cross-isobath tidal ellipse have been hypothesized to maintain an aggregation of plankton in Grand Manan Basin and on Georges Bank, though the dynamics were not explored. Michaud and Taggart (2011) hypothesized that a tidal front can act as a barrier to inshore advection of C5s on the margin of Grand Manan Basin. They proposed that upslope mixing of the neutrally dense C5s during flood tide, and their subsequent sinking during ebb tide, could maintain the aggregation near the front edge on the Basin margin. Consistent with this hypothesis, Lagrangian particle velocity estimated on the northern slope of Georges Bank suggested a cell pattern, with particles at depth and on-bank being advected towards the surface and particles in the upper water column being advected off-bank and downwards (Wishner *et al*. 2006).

Asymmetric tidal mixing transport (ATMT) is a process by which a net horizontal transport of sinking zooplankton can occur by oscillatory tidal flows on a slope (Pringle and Franks 2001). The basic principle of ATMT is as follows: on the upslope phase of

the tide, cold water is forced over warm water, which creates turbulence that enhances the vertical mixing and resuspension of sinking particles into the water column where they experience a higher upslope velocity than near-bottom. On the down slope tidal phase, stratification is restored as warm water flows over cold water, the particles sink and are advected back down slope, but not as far as they were advected upslope because the near-bottom tidal velocities are retarded due to bottom friction. The result is a net transport, without any mean flow, *towards less dense water*, hence it is a steady state, dynamic mechanism that could cause upslope titling at the larger scale. In Chapter 3, I noted that on the upslope tidal phases, concentrations were high at shallower depths on the slope compared to the subsequent down slope phases, which is consistent with this hypothesis (Figure 3.10). I also found that the animals are most concentrated in higher density water, which suggests that in less dense water they tend to sink. A detailed diagnostic assessment of this mechanism requires simultaneously collecting, in time and space, data on water mass circulation, hydrography, and copepod abundance on the southern slope.

4.1.1 Objectives

The main objective of this chapter is to investigate the influence of tidal and residual currents on the right whale prey field in Roseway Basin using moored acoustic Doppler current profilers (ADCPs) deployed across the southeastern slope of the Basin during the period of annual maximum right whale occupancy in September. This is the first time ADCPs have been deployed in the Basin and I used them, along with other sampling and monitoring gear to address the following objectives. My first objective is to investigate variation in C4 and C5 concentration on the southern slope of Roseway in a Eulerian and, where possible, Lagrangian frame of reference, at high resolution and at the scale of the foraging whales. My second objective is to gain insights into the dynamics of prey movement and the forces responsible for this movement along the southern slope. My third objective is to test the hypotheses I developed regarding right whales and their food above that are based on the first two objectives.

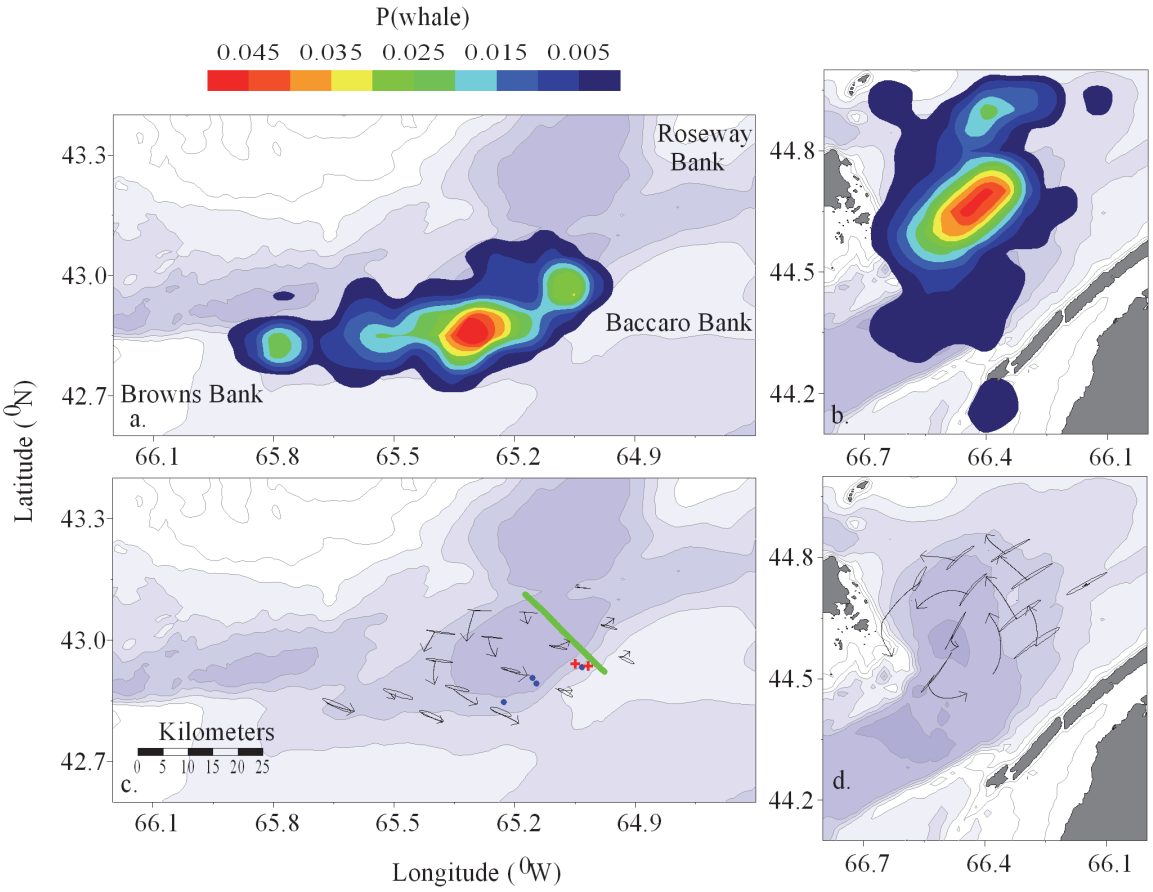

Figure 4.1 Bathymetric charts contoured at 25 m intervals, illustrating the relative probability distribution of right whales occupying (a) Roseway Basin and (b) Grand Manan Basin (after Vanderlaan *et al*. 2008), and (c), (d), modeled baroclinic circulation at 100 m depth in each Basin respectively based on WebDrogue ver. 0.66; Ocean Science Division, Bedford Institute of Oceanography, where line-arrows illustrate 60 h transport and direction for water parcels forced by the M2 residual and ellipses illustrate the M2 tidal ellipses, each for mid-September. Locations of ADCP and CTD mooring locations (red crosses), and biological net collections (blue circles) are illustrated on (c).

4.2 Methods

4.2.1 Field survey

Two RD Instruments Workhorse Sentinel ADCPs (hereafter RDI) equipped with four upward looking transducers and pressure and temperature sensors, were deployed in Roseway Basin during the period 04 through 13 September 2008 (day of year 248–257, hereafter *day*) from the R/V *Dominion Victory*. Each RDI was housed in a Streamlined Underwater Buoyancy System (SUBS, Open Seas Instrumentation Inc.) unit that was suspended 15 m above the seafloor, anchored by a train wheel, and recovered following activation of a remotely controlled acoustic release. Each SUBS unit was also fitted with an internally recording Seabird-37 MicroCat conductivity, temperature, depth (CTD) sensor and a three-transducer downward looking 1 MHz Nortek Aquadopp ADCP (hereafter Aquadopp). The Aquadopps were used in concert with the RDIs to collect full water column profiles of acoustic backscatter and current velocity, with the exception of a 4 m blanking region at the SUBS depth. Mooring and ADCP-specific frequencies, location, bottom depth and deployment period are provided in Table 4.1. The ADCPs recorded data using 1 m vertical bins and 2 minute ensemble intervals. The CTDs recorded data every 20 sec and the data were subsequently averaged over 2 minute bins. Moorings were separated by approximately one tidal excursion (2.7 km) across the southeastern slope of the Basin to measure cross-isobath variation currents, acoustic backscatter, pressure, temperature and salinity at a location where right whales have a high probability of being observed (Figure 4.1c).

Zooplankton samples were collected using a multiple opening-closing net system (BIONESS; Sameoto *et al*. 1980) to provide biological samples for calibrating ADCP acoustic backscatter. BIONESS was deployed at four locations along the southern margins during the ADCP deployment period (Figure 4.1c) and was equipped with seven 333 μm mesh nets, either a Seabird-19 CTD or Seabird-37 CTD, pitch sensors, two G.O. digital flowmeters, and an optical particle counter (OPC; Herman 1988, 1992). All casts began with an oblique net-tow to ~10 m above bottom and the remaining nets were opened consecutively every five minutes until the surface was reached. At one station all but one net were used to sequentially sample the same depth (~ 131 m). Samples were stored in 4 % buffered formalin and processed in the lab where all zooplankton were sub-

sampled, identified and counted. BIONESS-net and BIONESS-OPC zooplankton concentrations were estimated following the methods detailed in Chapter 3.

4.2.2 Relative zooplankton concentration estimation

The ADCP transducers were not calibrated and thus provided relative volume-scattering strength, and hence, only relative zooplankton concentration estimates. Relative zooplankton concentrations were estimated for each beam using an RDI-specific form of the sonar equation (Deines 1999):

$$S(z,t) = TS + C + 10\log_{10}((T_x + 273.16)\,R^2) - L_{DBM} - P_{DBW} + 2\alpha R + K_C(E - E_r) \quad (4.1)$$

where $S(z,t)$ is relative zooplankton concentration (dB) at each depth z and time step t, TS is the frequency-specific zooplankton target strength, C is a factory estimated calibration coefficient, T_x is transducer temperature, R is slant range (m), L_{DBM} is $10\log_{10}$(transmit pulse length), P_{DBW} is $20\log_{10}$(transmit power), α is the frequency-specific absorption coefficient of water, E is echo intensity, E_r is the factory measured real time reference level for the echo intensity, and K_c a factory measured beam-specific constant that converts E to units of dB. S (z,t) was then converted into linear space using $s(z,t) = 10^{S(z,t)/10}$. Units of $s(z,t)$ are number of dominant scatterers m^{-3}. The linear metric is used for the remainder of this chapter.

The depth-structured BIONESS-net and BIONESS-OPC data indicated that diapausing copepods were concentrated in a 30 m-thick layer at ~100+ m depth (Figure 4.2a). Eleven of the BIONESS nets collected zooplankton samples between 75 and 150 m depth. The zooplankton target strengths required to convert ADCP echo intensity to relative zooplankton concentration were estimated using data from the eleven deep nets. Considering all the zooplankton taxa in the nets and using standard weak scattering models for zooplankton (e.g., Lavery *et al*. 2007), I found that within the layer of interest (75 m - 150 m depth), 86 % (standard deviation, SD = 12, n = 11), 82 % (SD = 18) and 85 % (SD = 12) of acoustic scattering at the 300, 600 and 1000 kHz frequencies respectively was due to a combination of *Calanus finmarchicus* stage C5 and *Calanus*

Table 4.1. Upward-looking RDI Acoustic Doppler Current Profiler (ADCP) frequency, mooring location, bottom depth (instruments are 15 m above seafloor), deployment period and other instruments attached to two moorings, including downward-looking Aquadopp ADCPs and Conductivity, Temperature, Depth sensors (CTD), deployed in Roseway Basin during Day of Year 248 through 257, 2008.

Mooring	Location	Bottom Depth (m)	ADCP frequency (kHz)	Deployment Period	Other Instruments
Shallow Slope	42.936 -65.016	112	600	249 - 257 (8 d)	1 MHz Aquadopp Seabird-37 CTD
Deep Slope	42.941 -65.049	134	300	248 - 257 (9 d)	1 MHz Aquadopp Seabird-37 CTD

hyperboreus stage C4 (hereafter CF5 and CH4 respectively). Sub-samples of CF5 and CH4 (n = 1000) were taken from the deep nets, photographed and their lengths and widths digitally sized. The size distributions of these two species were combined, scaled for relative concentration and used to estimate the average frequency-specific target strength (*TS*) of a 'typical copepod' needed for Eq. 1, using the Distorted Wave Born Approximation (DWBA) model for copepods developed by Stanton and Chu (2000, Figure 4.3). Target strengths were not strongly frequency dependent; however a different estimate of average target strength was made and used for each instrument frequency. Subsequently, $s\ (z,t)$ was averaged among beams to provide a single value for each ADCP.

I quantitatively defined the depth interval of the deep copepod layer using the acoustic backscatter data by creating a frequency histogram of $s\ (z,t) > 3.14 \times 10^{12}\ m^{-3}$ at depth (z) for all ADCP observations. The zooplankton were most concentrated in the 90 to 130 m depth layer at the deep slope mooring (Figure 4.2b) and in the 80 to 110 m depth layer at the shallow slope mooring (Figure 4.2c). Subsequently, for each mooring and at each time step, I depth-averaged $s\ (z,t)$ over the zooplankton layer defined above (interpolating through the blanking region), and divided each value of the resulting time series $s\ (t)$ and the original matrix $s\ (z,t)$ by the minimum value of the time series; i.e., $s_{rel}(t) = s(t) / \min(s(t))$ and $s_{rel}(z,t) = s(z,t) / \min(s(t))$, to provide an easily interpretable variable showing the changes in relative concentration over time. Thus, s_{rel} represents a scaling factor with respect to the minimum concentration in the series; e.g., a value of 10 is 10-fold greater than the layer-averaged minimum concentration measured over the deployment period. The echograms of $s_{rel}\ (z,t)$ are provided in Figure 4.4. An attempt was made to use co-located BIONESS and OPC data to estimate the 'real' minimum concentration and to convert s_{rel} into absolute concentration. However I opted to use s_{rel} because the absolute concentration is very sensitive to error in the minimum concentrations estimated by the BIONESS (net estimates) and OPC (optical estimates).

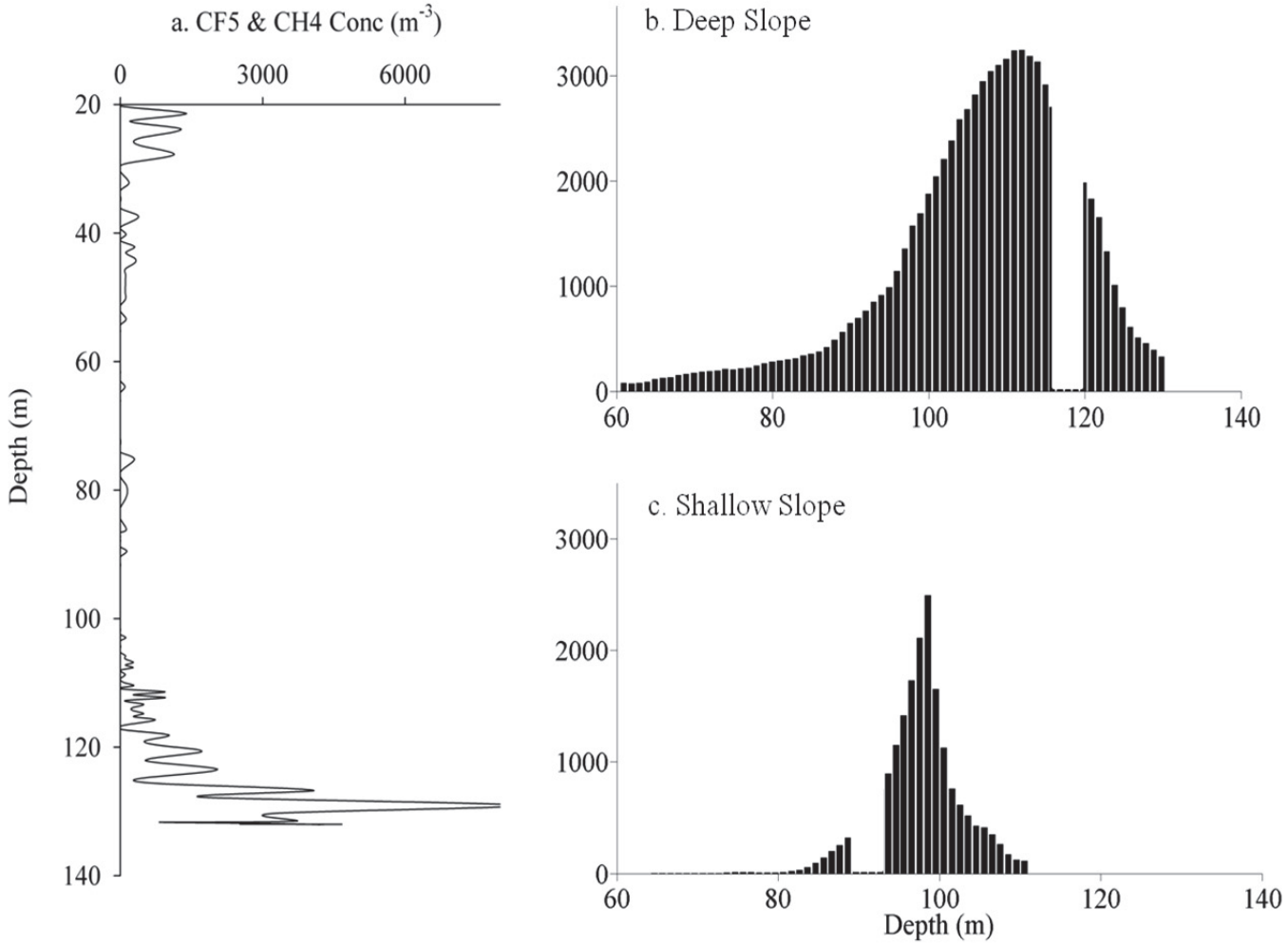

Figure 4.2 An example (a) of the depth distribution of *Calanus finmarchicus* C5 and *C. hyperboreus* C4 concentration (m^{-3}) based on BIONESS OPC-derived concentration at one location on the southern slope of Roseway Basin in 2008, and frequency histograms of the number of relative zooplankton concentration estimates, $s(z,t) > 3.14 \times 10^{12}$ m^{-3} , over the entire deployment period as a function of depth (z) between 60 and 140 m for the (b) deep slope and (c) shallow slope ADCP moorings where absence of some bars represent the no data regions between the RDI and Aquadopp ADCPs.

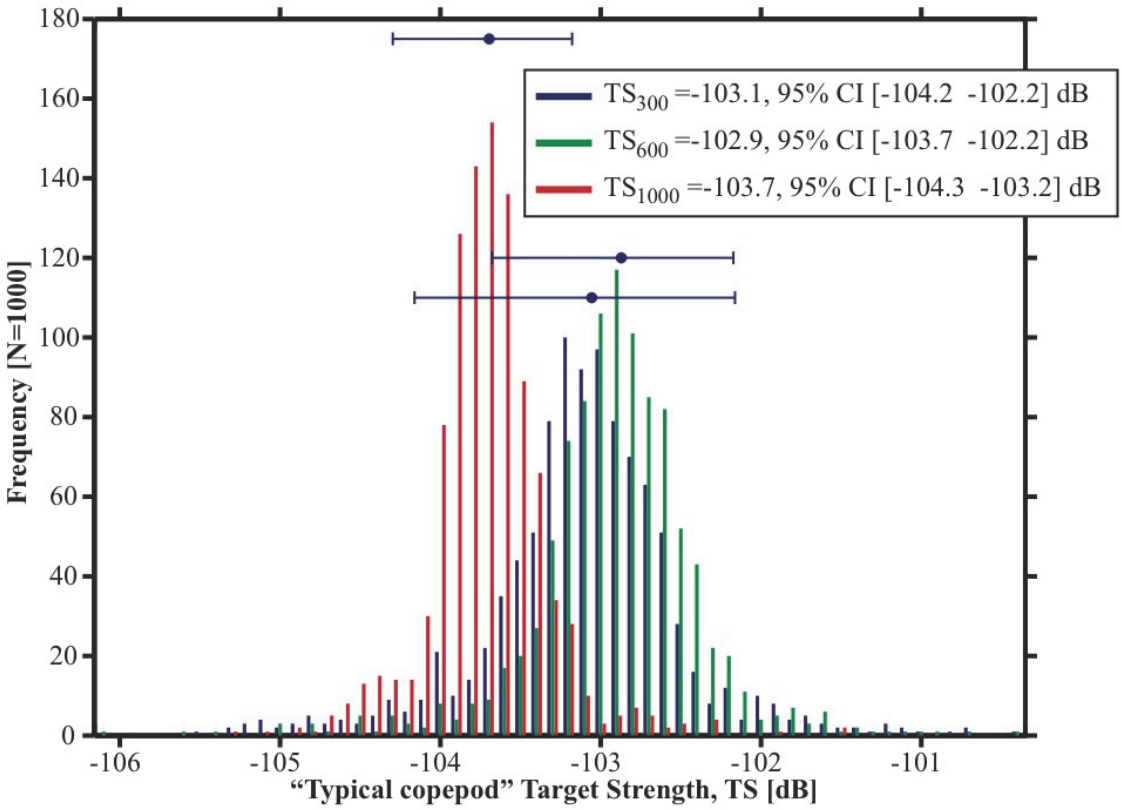

Figure 4.3 Histograms of target strength (*TS*) for a 'typical copepod' estimated from the combined size distribution of *C. finmarchicus* C5 and *C. hyperboreus* C4, corrected for relative concentration of each species. Samples were collected in BIONESS nets below 90 m depth in Roseway Basin. Average +/- 95 % CI target strengths for the beam frequency – specific (300, 600 and 1000 kHz) distributions are the horizontal blue bars.

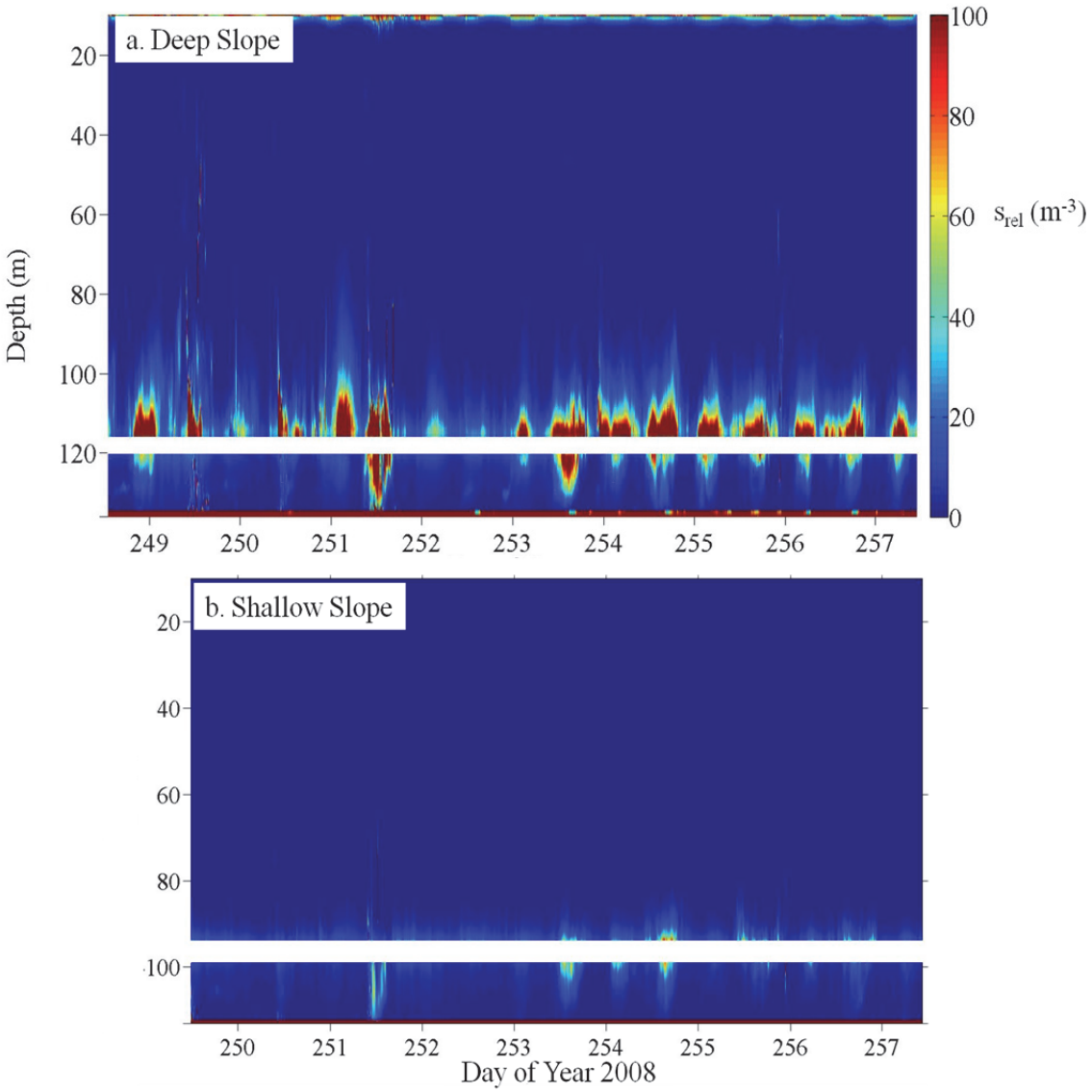

Figure 4.4 Time series of depth-dependant relative plankton concentration (s_{rel}, m^{-3}) collected with Acoustic Doppler Current Profiler (ADCPs) at the deep slope (a) and shallow slope (b) moorings in Roseway Basin between day of year 249 and 257, 2008. The white horizontal bar in each sectional plot illustrates the 4 m no data region between the upward and downward looking ADCPs.

4.3 Results

4.3.1 Hydrography

At the ADCP moorings, water mass temperature, salinity and density varied tidally and across a front that moved over the ADCPs during the first half of the series. Density (Figure 4.5a) and salinity (Figure 4.5c) varied by ~0.3 units over the time series, while temperature (Figure 4.5b) varied by approximately 2^{o}C. Both temperature and salinity contributed to the density variation, but at different times one or the other was the larger contributor. Water density at depth varied at a semi-diurnal tidal scale and decreased more-or-less monotonically throughout the first half of the series (Figure 4.5a). Density increased during ebb tide (upslope) and decreased during flood tide (down slope), consistent with tidal variation expected for a cross-isobath density gradient on a slope. There were similar and significant linear decreases in density before day 253 at each mooring described by σ_t = 37.5 - 0.0459 *day* at the deep mooring and σ_t = 39 - 0.0518 *day* at the shallow mooring (r^2 = 0.76 and 0.81, respectively, $p < 0.001$). Thereafter the density variation was tidally dominated and remained stationary for the remainder of the 9 day deployment period. During the declining phase the semi-diurnal variation in density was damped across some tidal periods. Change in density associated with low tides 1, 2 and 6 were similar in amplitude to those of the second half of the series, while changes associated low tides 3–5, 7 and 8 had reduced amplitude. This pattern was observed at both moorings, though dampening was greater at the shallow mooring. Density variation was more similar between moorings when the tidal signal was most damped (i.e. the cross-isobath density gradient decreased), suggesting that the same water mass was observed at both moorings during those times (e.g., tidal cycle 4 in Figure 4.5a).

Temperature, salinity and density variation through time at each mooring within and between series using T-S diagrams, revealed at least three water masses on the southeastern slope of Roseway Basin during the deployment period. During the first half of the series, the T-S signature illustrated a mixture between colder (~5.8 ^{O}C) and saltier (~33.25) water from the deep Basin that had greater influence at low tide (water mass 1, Figure 4.6), and warmer (~7.8 ^{O}C), fresher (~33.15) water from upslope that had greater influence at high tide (water mass 2, Figure 4.6). Water mass variation between high and

low tide was roughly cross-isopycnal, except during the 'replacement period' addressed below. Toward the middle of the time series, the influence of water mass 1 declined and the influence of water mass 2 increased, causing water temperature at both slope moorings to increase steadily from ~6.2 to ~7.5 ^{O}C while salinity and density decreased.

From *day* 252 and 253, there was a relatively abrupt change in the water mass characteristics at both moorings as water mass 2 began to be replaced by a colder (~5 ^{O}C), fresher (~32.95) water mass (water mass 3, Figure 4.6). Water mass 3 was similar in temperature but fresher than water mass 1. Replacement by water mass 3 began at the deep slope mooring, and within one tidal cycle, water mass 2 disappeared from the T-S signature during low tide on *day* 253. Water mass 2 subsequently disappeared at the shallow mooring during low tide one tidal cycle later. At both moorings water mass 2 disappeared less quickly from the upslope water observed at high tide. Water mass 2 was completely replaced by water mass 3 at the deep slope mooring by *day* 254 and at the shallow mooring by *day* 256. The change in hydrographic properties was a Basin-wide phenomenon; a small change in temperature was measured mid-Basin by using a sensor deployed at ~150 m depth (data not shown). With the water mass replacement and the absence of the front, variation in T-S and density became predominantly tidal (Figure 4.5a,b,c) and followed the consistent, cross-isopycnal gradient created by the mixing line between the end-member water masses 1 and 3 (Figure 4.6). As opposed to the replacement period, this tidal gradient was salinity driven with very little change in temperature. This can be seen in Figure 4.5b and c where the temperature signal is gradually damped at the end of the series, while the salinity signal is amplified.

In relation to the three major water mass types identified in Roseway Basin in Chapter 3, water mass 1 identified here is a mix of intermediate Bottom Water (iBW) and modified Bottom Water (mBW) that dominates the SE slope at 90 – 130 m depth (Figure 3.16, red markers). Water mass 3 is the same mix of iBW/mBW, but with some Bottom Water (BW) from shallower depths, which lowers the salinity and matches the signature of water at 70 m (Figure 3.16, red markers). Water mass 2, the 'warm front', is both warmer and less saline than water mass 1, and does not have the signature of any water mass I identified in Chapter 3. It may be formed by surface mixing of the warm, fresh Gulf of St Lawrence water that I identified in the Basin above the thermocline.

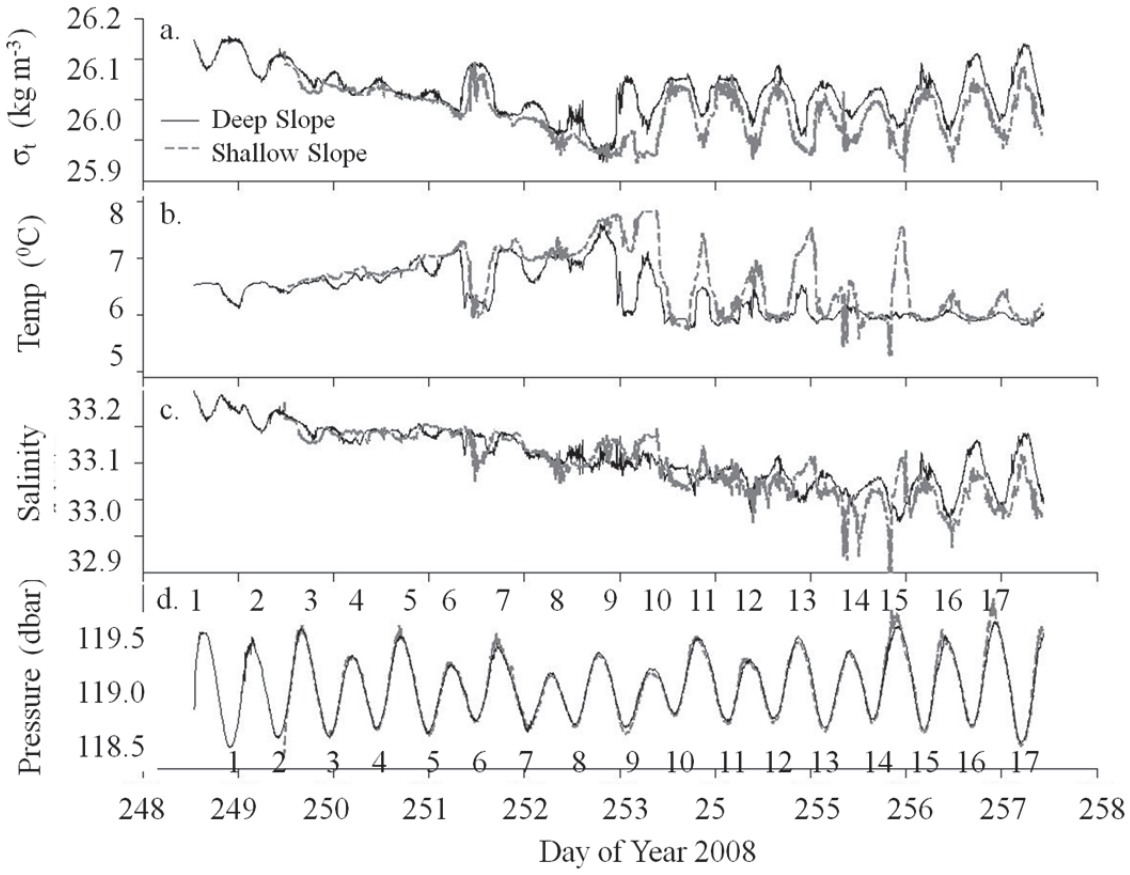

Figure 4.5 Time series of (a) density (σ_t, kg m^{-3}), (b) temperature (^oC), (c) salinity and (d) Aquadopp ADCP pressure (dbar) at the shallow (grey dashed line) and deep slope (solid line) ADCP moorings on the southern slope of Roseway Basin during day of year 248 through 257, 2008. The shallow slope pressure series is offset +22 dbar for direct comparison with the tidal amplitude pattern at the deep slope mooring. Tide sequence numbers referred to in the text are provided on (d).

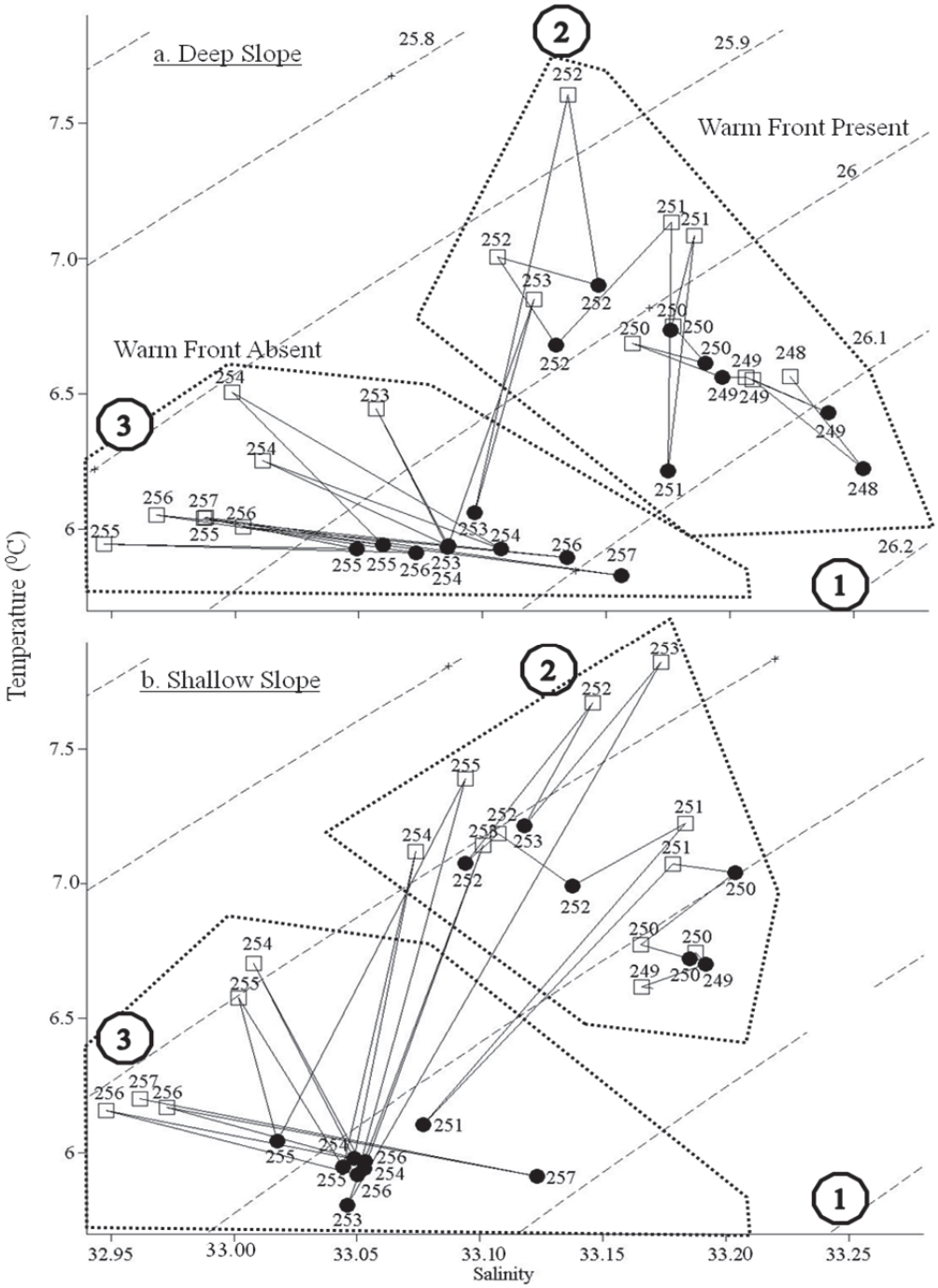

Figure 4.6 Temperature (^{o}C) and salinity, TS diagrams, derived from CTD time series data collected at the deep (a) and shallow slope (b) moorings, where each datum represents the T-S state observed at each semi-diurnal high (open squares) and low tide (closed circles) on day of year 248 through 257, 2008 (labeled), where solid lines join the tidal sequence. The dashed lines represent the σ_t isopycnals with magnitudes provided in (a), water mass identity end-members referred to in the text are labeled 1, 2, 3 and periods when the warm front was present and absent are encompassed by a dotted polygon and labeled in (a).

4.3.2 Velocity and inferred displacement

Tidal variation in the velocity measured by the ADCPs was dominated by the M2 tide with the long axis of the tidal ellipse being ~3 km and oriented cross-isobath at both moorings (deep: 2.76 km, 320^0 True; shallow: 3.36 km, 316.5^0 True) (t-tide Matlab program, Pawlowicz *et al*. 2002). To separate the effects of tidal and residual velocities, the horizontal current velocity was decomposed into along-isobath [+$V(z,t)$, toward the northeast], and cross-isobath [+$U(z,t)$, upslope] directions. Below I consider both the velocities averaged over the depth interval defining the zooplankton layer (i.e. bulk transport of the layer), and later the more complex vertical structure. I primarily used velocity in the form of the cumulative displacement (i.e. the time integral, or progressive vector diagram) of both the depth-specific *V(z,t)* and U*(z,t)*, where $d_A(z,t) = \sum_{t'=1}^{t} A(z,t')$ and layer-averaged *V(t)* and *U(t)*, where $d_A(t) = \sum_{t'=1}^{t} A(t')$ and A = V or U. Plotting displacement makes it easier to identify pattern in the residual than plotting the velocities because changes in the residual are small at short time scales relative to the amplitude of the tidal changes. Raw velocities are provided for the reader's reference in Figures 4.7 and 4.8.

At the deep mooring, layer-averaged $U(t)$ varied between 15 and 29 cm sec^{-1} among tidal cycles at maximum ebb (upslope) and between 14 and 35 cm sec^{-1} at maximum flood (down slope). Layer-averaged velocity was greater at the shallow mooring by ~4 cm sec^{-1} in both the upslope and down slope directions; there it varied between 16 and 38 cm sec^{-1} at maximum ebb and 13 and 41 cm sec^{-1} at the maximum flood. The layer-averaged tidal excursion, represented by $d_U(t)$, was highly variable among tidal cycles, ranging from ~1 to 6 km and partially dependent on the spring-neap cycle (neap tide occurred on *day* 252).

There were no significant tidal components to the layer-averaged $V(t)$, so I assumed that the majority of variation in *V(t)* was non-tidal and was due to the residual current (the 'residual' is current velocity left over after the tide is removed). *U(t)* contained both tidal (U_{tide}) and residual (period >3 d, U_{resid}) variation. I separated the layer-averaged variation due to the tidal and residual flows in $d_U(t)$ by fitting a polynomial. The best-fit polynomial was order 3 at both the shallow mooring ($d_{Uresid}(t)$ =

$0.0587*day^3$ - $44.5813*day^2$+$1.129x10^4*day$ - $9.5321x10^5$, r^2=0.93) and the deep mooring ($d_{Uresid}\ (t)$ = $0.0626*day^3$ - $47.4597*day^2$+$1.1994e^4*day$ - $1.0103x10^6$, r^2=0.90). The 3rd order polynomials accounted for variation at frequencies lower than 1/4 to 1/6 cycles day^{-1}. This is a much lower frequency signal than the semi-diurnal tide, meaning that the polynomial captured the low frequency residual ($d_{Uresid}\ (t)$, Figure 4.10), and the tidal variation ($d_{tide}\ (t)$) was explained by the regression residuals (i.e. $d_{tide}\ (t) = d_U\ (t) - d_{Uresid}\ (t)$, Figure 4.9). The cumulative non-tidal displacements, $d_{Uresid}\ (t)$ and $d_V\ (t)$, were combined to estimate the cumulative displacement of the total 2-D residual current $d_{resid}\ (t)$, illustrated in Figure 4.10.

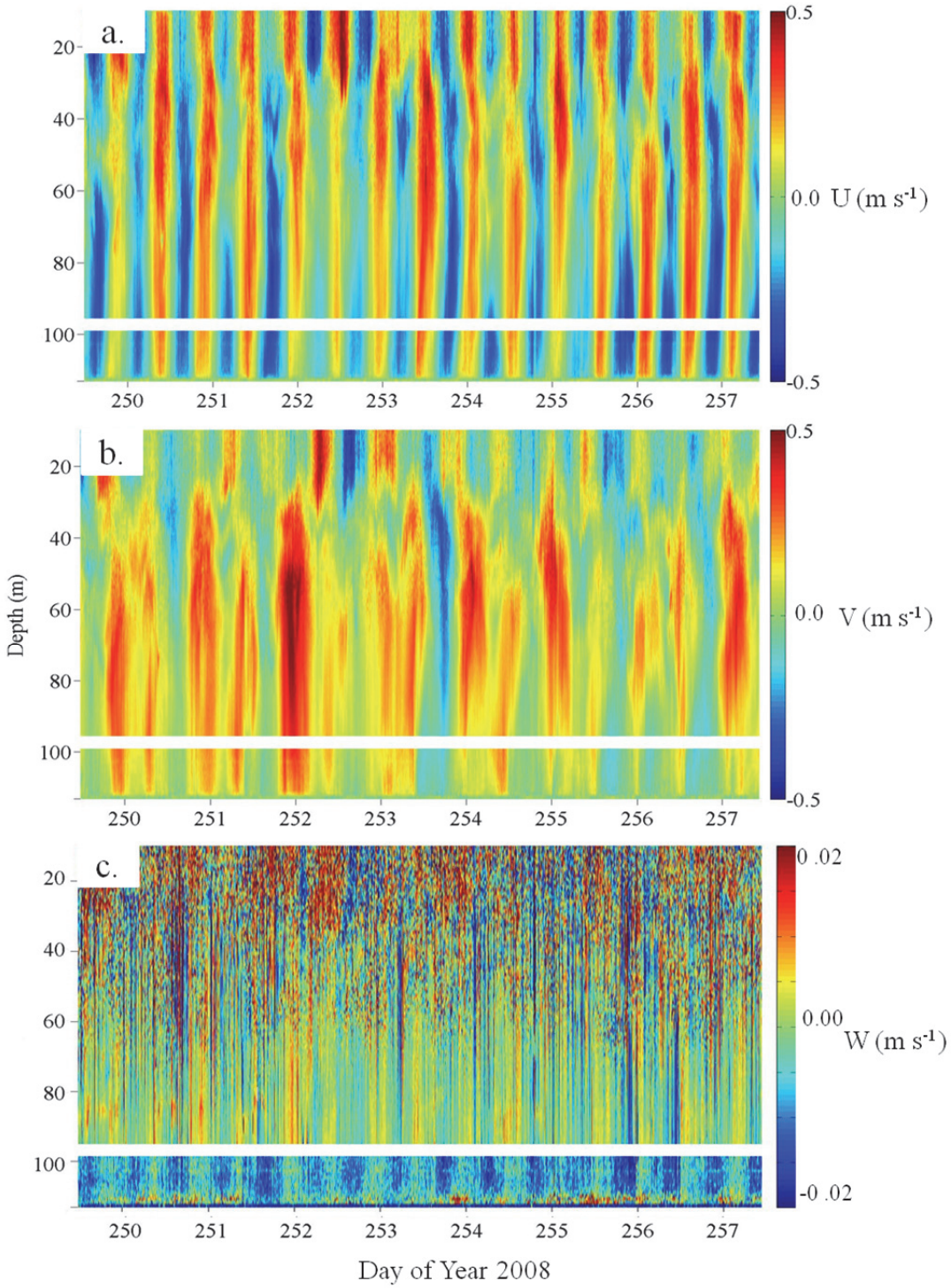

Figure 4.7 Time series of depth-specific (a) cross-isobath velocity (U, m s^{-1}), (b) along isobath velocity (V, m s^{-1}) and (c) vertical velocity (W, m s^{-1}) collected between 10 and 118 m depth using an upward- and downward-looking ADCPs moored 15 m above the seafloor at the shallow slope location on the southern margin of Roseway Basin. The white horizontal bar in each sectional plot illustrates the 4-m no data region between the upward- and downward-looking ADCPs.

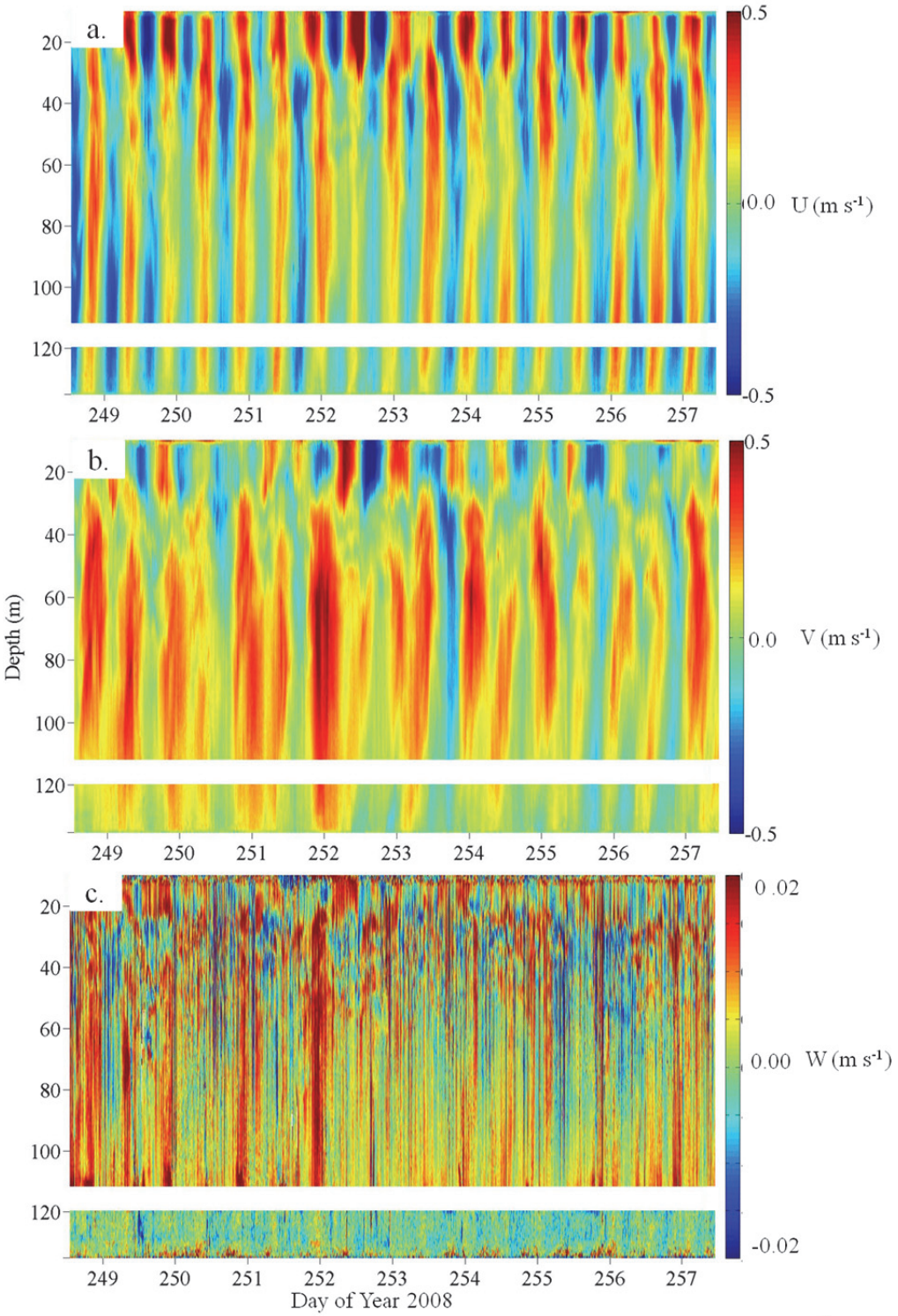

Figure 4.8 Time series of depth-specific (a) cross isobath velocity (U, m s^{-1}), (b) along isobath velocity (V, m s^{-1}) and (c) vertical velocity (W, m s^{-1}) collected between 10 and 135 m depth using upward- and downward-looking ADCPs moored 15 m above the seafloor at the deep-slope location on the southern margin of Roseway Basin. The white horizontal bar in each sectional plot illustrates the 4-m no data region between the upward- and downward-looking ADCPs.

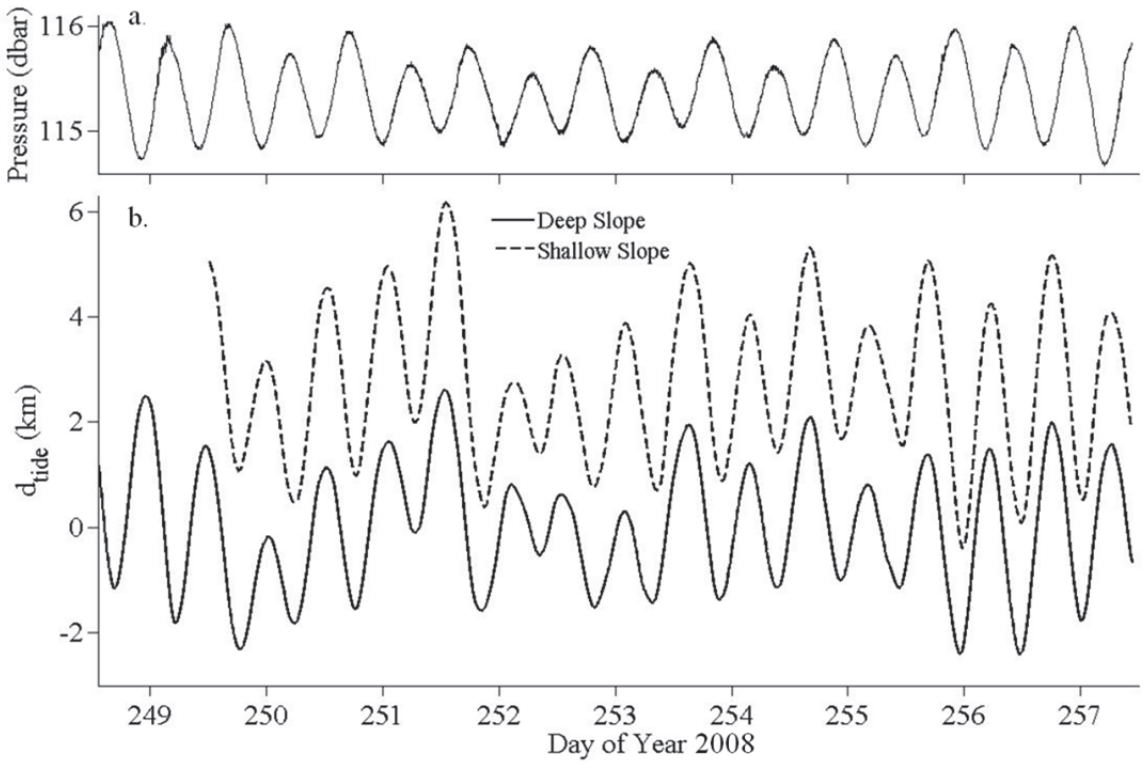

Figure 4.9 Water pressure (dbar) time series (**a**) at the deep-slope mooring and (**b**) the layer-averaged cumulative displacement of the tide, d_{tide} *(t),* km, collected at the deep- (solid line) and shallow-slope (dashed line) moorings in Roseway Basin during day of year 248 to 257, 2008 where the d_{tide} ordinate is labeled with respect to the deep-slope mooring and where the estimates for the shallow-slope mooring, located 2.7 km upslope from the deep-slope mooring, are offset +2.7 relative to the deep-slope mooring estimates.

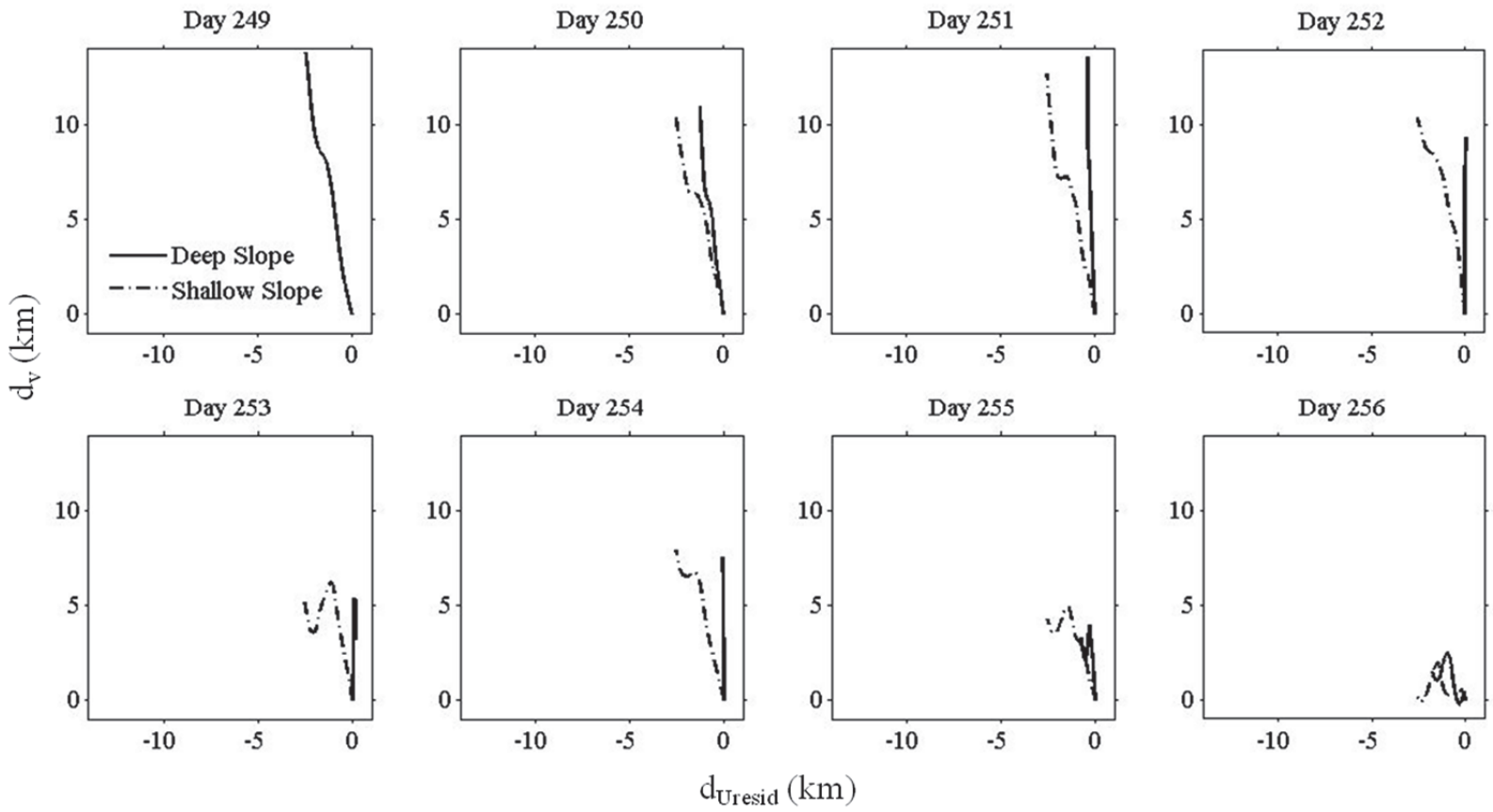

Figure 4.10 An 8 day sequence of 24 h layer-averaged cumulative-displacement (km) estimates for residual currents, $d_V\ (t)$ and $d_{Uresid}\ (t)$, measured at the deep- (solid line) and shallow-slope (dot-dash line) ADCP moorings where the displacement vectors are oriented in relation to the southern margin of Roseway Basin (Figure 4.1) with + $d_{Uresid}\ (t)$ upslope (across-isobath) to the southeast on the abscissa ordinate and +$d_V\ (t)$ along-slope (along-isobath) to the northeast on the ordinate.

During the first half of the deployment, the residual current flowed primarily northeast along-isobath, and was dominated by $d_V\,(t)$ at both moorings (Figure 4.10). A much smaller cross-isobath component transported water down slope into the Basin with greater transport at the shallow mooring than at the deep mooring; i.e., there was a cross-isobath gradient in $d_{Uresid}\,(t)$. Despite this gradient, there was no significant difference in the transport distance per day between the shallow mooring and the deep mooring (paired-t test, $P = 0.110$), because the influence of $d_{Uresid}\,(t)$ was small relative to $d_V\,(t)$ (Figure 4.10). The residual velocity was on average 10 cm s^{-1} (range -10 to 35 cm s^{-1}), and moved 10 to 15 km of water per day over the ADCP moorings during the first four days. On *day* 253, transport at the deep mooring began to slow, followed by the shallow mooring on *day* 254.

The above results concern the layer-averaged bulk transport, but the depth-specific $d_V\,(z,t)$ and $d_U\,(z,t)$ show transport variation within the zooplankton layer as well (Figure 4.11). The magnitude of $d_{resid}\,(z,t)$, illustrated by the total 2-D linear (non-tidal) variation in the $d_V(z,t)$ and $d_U(z,t)$ components for each mooring location (Figure 4.11) was smallest near-bottom and increased with decreasing depth to a maximum at ~70 m, then began decreasing again at ~60 m. In addition to changes in magnitude, the residual also changed direction from down-slope near the seafloor ($-d_{Uresid}\,(z,t)$) to along-isobath at ~80 m ($d_{Uresid}\,(80,t) = 0$), and to upslope above 80 m ($+d_{Uresid}\,(z,t)$), consistent with changes expected in a bottom Ekman layer. The change in direction, indicated by the magnitude of $d_{Uresid}\,(z,t)$, was more pronounced at the shallow slope mooring than at the deep slope mooring. Near-bottom (120 m at the deep-slope, and 100 to 110 m at the shallow slope) and near the end of the series ($d_V\,(z,t) \cong 40$ km at the deep slope and 30 to 50 km at the shallow-slope) $d_V\,(z,t)$ virtually stopped, while the magnitude of $d_U\,(z,t)$ remained relatively constant. This resulted in a strong down-slope transport at the shallow mooring, and almost no down slope transport at the deep mooring; consistent with the cross-isobath gradient in $d_{Uresid}\,(z,t)$ observed during the remainder of the series (Figure 4.11).

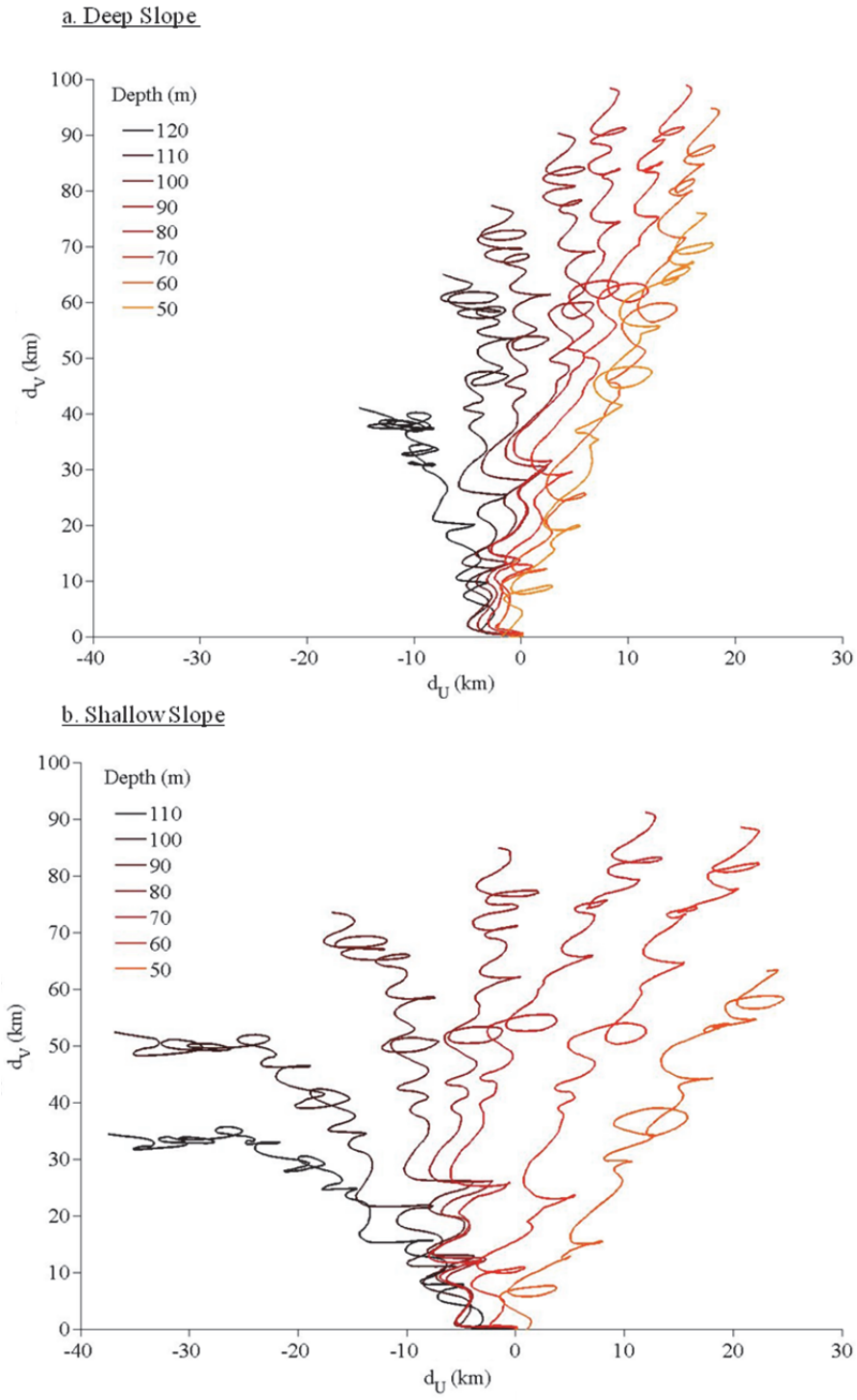

Figure 4.11 Colour-coded cumulative displacement estimates (lines) over the 9 day deployment period (km) in Roseway Basin at 10 m depth increments in the along-isobath, d_V *(z,t),* and cross-isobath d_U *(z,t),* directions at (a) the deep and (b) shallow slope moorings. Displacement vectors are oriented in relation to the southern margin of Roseway Basin (Figure 4.1) with + d_U *(z,t)* upslope (across-isobath) to the southeast on the abscissa and +d_V *(z,t)* along-isobath to the northeast on the ordinate.

The residual current appears to have been generated, at least partially, by density driven geostrophic flow and Coriolis rectification. As a first approximation, the contribution due to density driven flow to the magnitude of the along-isobath velocity (v) on the southeastern margin of the Basin was calculated using the sectional density data from transect-2 (Figure 4.12) and the thermal wind equations (Eq. 4.2). I made this calculation at 75 m, 100 m, and 125 m depths, assuming a level of no motion at 150 m depth; an example calculation for the 125 m isopleth is provided below.

$$\frac{\Delta v}{\Delta z} = -\frac{g}{\rho f}\frac{\Delta \rho}{\Delta x} \tag{4.2}$$

where z is depth (m), g is the acceleration due to gravity, f is the Coriolis coefficient, ρ is average water column density and $\frac{d\rho}{dx}$ is the horizontal change in density in a cross isobath (x) direction between 15 and 20 km along the transect. The data region is depicted by a black box in Figure 4.12. I estimate $v_{125} = 2$ cm s^{-1}, $v_{100} = 4$ cm s^{-1}, and $v_{75} = 0$ cm s^{-1}.

$\rho = 1025.9$ kg m^{-3} (estimated from Figure 4.12)

g = -10 m s^{-2}

f (45^0 latitude) = 10^{-4} s^{-1}

$\frac{\Delta \rho}{\Delta x} = \frac{0.04 \text{ kg m}^{-3}}{5000 \text{ m}}$ (estimated from Figure 4.12)

$\Delta z = -150\text{m} - (-125 \text{ m}) = -25 \text{ m}$

$\Delta v = v_{150 \text{ m}} - v_{125 \text{ m}}$

$v_{150 \text{ m}} = 0 \text{ m s}^{-1}$ (assuming a level of no motion at 150 m depth)

$$\frac{0 - v_{125 \text{ m}}}{-25 \text{ m}} = -\frac{-10 \text{ m s}^{-2}}{(1025.9 \text{ kg m}^{-3})(10^{-4} s^{-1})} \times \frac{0.04 \text{ kg m}^{-3}}{5000 \text{ m}}$$

Thus, v_{125} = + 0.02 m s^{-1} (into the page, toward the northeast in Figure 4.12)

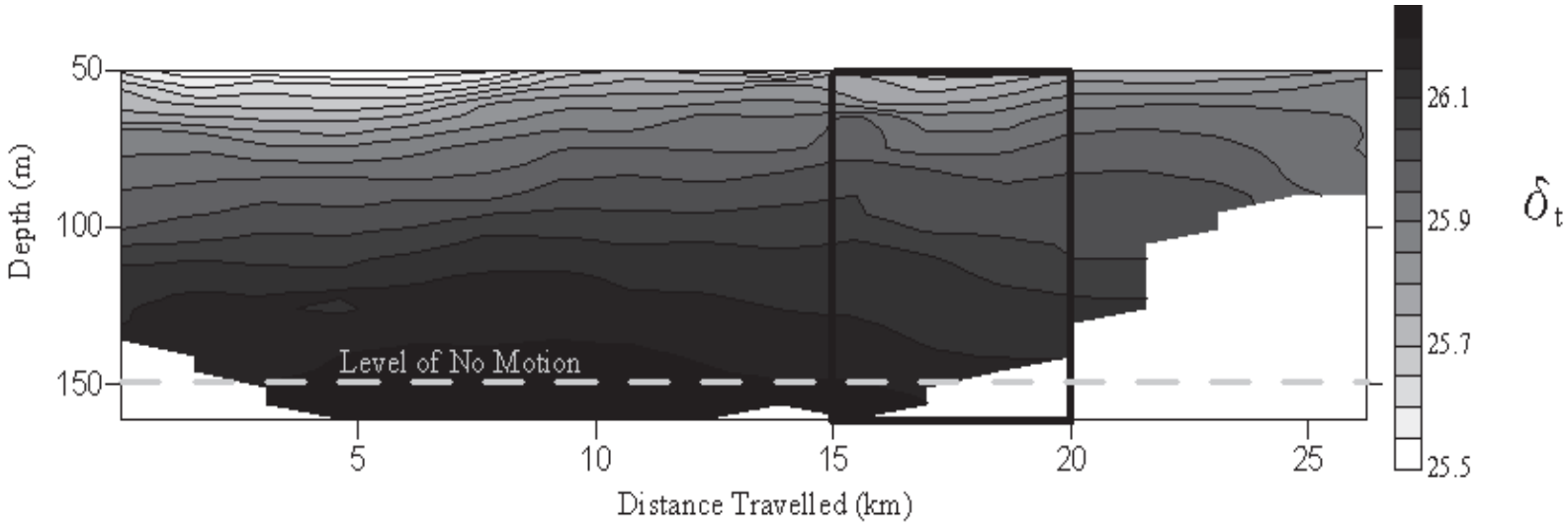

Figure 4.12 A water mass density (σ_t) section measured across Roseway Basin (reproduced here from Figure 3.22b) used to calculate the along-isobath residual velocity generated by the density field using the thermal wind equation (Eq. 4.2). The black rectangle encompasses the data region used for calculations The level of no motion was assumed at 150 m depth (dashed line). The transect line where these data were collected is illustrated in Figure 4.1c.

The density structure indicated a current of 2 to 4 cm s^{-1} on 11-September, amounting to ~1/3 of the series average along isobath residual flow along the southeast margin. This flow was strongest at 100 m depth. Coriolis rectification generates an along-isobath residual current by nonlinear tidal advection when there is a cross-isobath velocity gradient over a sloping bathymetry (Loder 1980). The southern slope region of the Basin has the necessary characteristics to generate rectified flow. These include a sloping bathymetry and a cross-isobath tidal ellipse (Figure 4.1), and a cross-isobath tidal velocity gradient (Figure 4.9). Since the rectification is generated by tidal currents, $d_{resid}(t)$ should vary in response to variation in the strength of the tidal velocities (Loder 1980). While $V(t)$ did not have any significant tidal components, the strength of the residual decreased rapidly after neap tide (*day* 252) when the tidal velocities also decreased (Figure 4.9 and 10). The contribution of Coriolis rectification to the total residual is estimated to be about 3 cm s^{-1} (B. Petrie, pers. comm., Bedford Institute of Oceanogaphy).

4.3.3 Problems estimating the vertical velocities

At each mooring, horizontal currents measured by the upward-looking RDI ADCP and the downward-looking Aquadopp ADCP were in good agreement (Figure 4.7 and 4.8). The vertical velocities ($W(z,t)$) however, did not agree between the two instruments at either mooring. The patterns were similar between instruments, but the RDIs always measured a larger positive $W(z,t)$ than the Aquadopps. On average, the RDIs measured deep-Basin (>60 m) velocities that were positive, and the Aquadopps measured near-bottom velocities that were negative; however, Aquadopp $W(z_{min},t) \neq -1*RDI\ W(z_{max},t))$. The reasons for the disagreement are unclear. It is possible, though it seems unlikely, that I measured real changes in $W(z,t)$ with depth and the transition zone between positive and negative velocities occurred within the 4 m 'no-data' region at both moorings. However, $W(z,t)$ did not decrease with depth above or below the 'no-data' region in a way that suggests such a transition; the change was abrupt. More likely, the disagreement is related to a technical issue. The magnitudes of $W(z,t)$ from all instruments were larger than the error velocities, meaning that the variation in $W(z,t)$ was not simply due to background noise. If the ADCPs were not oriented with the center axis

perfectly perpendicular to the seafloor and ocean surface, which could happen if the SUBS unit were unbalanced, then some of the variation in the horizontal currents could be instead measured as vertical currents. It seems unlikely though that both SUBS units could be unbalanced in the same way. In that case, I might expect (1) vertical currents to be abnormally large in amplitude, because horizontal currents are 1 - 2 orders of magnitude larger in amplitude than vertical currents, and (2) high correlation between the horizontal and vertical currents. The vertical currents I measured were not abnormally large on any instrument, averaging ± 3 mm s^{-1} at depth and reaching a maximum of ~2 cm s^{-1}. Horizontal and vertical currents were not well correlated (r<0.3) at any depth for either instrument at the shallow slope mooring or for the Aquadopp at the deep slope mooring. Horizontal and vertical currents near the transducer of the deep slope RDI were better correlated (r= 0.43) and this correlation declined with distance from the transducers. In summary, I am uncertain which instruments, if either, the Aquadopps or the RDIs, measured the vertical current magnitudes with accuracy or precision.

4.3.4 Plankton layer source and cross-slope width

The zooplankton layer below ~100 m originated down slope in the Basin and was pushed upslope on the southeastern side only during ebb tide (Figure 4.13). The relative zooplankton concentration estimates, s_{rel}, increased at both moorings when the tide began to ebb, first at the deep mooring and shortly thereafter at the shallow mooring. The concentrations reached maxima at around low tide at both moorings and then decreased; first at the shallow mooring and later at the deep mooring. During high tide, and throughout the series, s_{rel} remained consistently near the series minimum.

Although plankton concentrations increased with every ebb tide, the magnitude of the increase differed strongly among tidal cycles at both moorings. Below, I focus on the deep mooring only, though the trends were similar at the two moorings. During the first half of the series, concentrations at the deep mooring remained relatively low at low tide except during tides 2 and 6 where concentrations were 322- and 360-fold higher than the series minimum respectively (Figure 4.13). The lowest maxima in concentrations at the deep mooring were 6- to 13-fold higher than the minimum during low tides 3, 5, 7, 8 and 9. During the second half of the series the maximum magnitudes were more similar

among tidal periods. Though they did not reach the degree observed during low tides 2 and 6, the maxima during tides 11 through 17 were still between 28- and 54-fold higher than the series minimum. In the next section, I investigate the among tidal cycle variation between in plankton concentration and the physical environment.

When s_{rel} is examined as a function of the cumulative cross-isobath displacement of the tidal current, $d_{tide}(t)$, the concentration distribution of the zooplankton layer for the entire series becomes apparent in water mass space (Figure 4.14). The concentration distribution in water mass space thus indicates that the moorings were located at a depth on the slope of the Basin where they captured a horizontal boundary of the zooplankton layer, assuming that the average position of the water mass during the series was at the mooring locations (0 km, Figure 4.14). When the ADCPs sampled shallower water while the water mass was being transported 1 to 5 km down slope (negative $d_{tide}(t)$) from the deep mooring, s_{rel} consistently remained near the series minimum. It was only when the water was transported above ~1 km down slope (positive $d_{tide}(t)$) from the deep mooring that s_{rel} began increasing, indicating that the layer margin lay there, near the 120 m isobath.

Using the data illustrated in Figure 4.14**,** I estimate the minimum cross-isobath width of the zooplankton layer, assuming that the average position of the layer boundary lay ~1 km down slope of the deep mooring (as above), and that when the layer washed upslope over the ADCPs, the instruments measured the closest zooplankton boundary but not the farthest boundary because it was presumably located more than one tidal excursion down slope of the deep mooring. This is a valid assumption because zooplankton concentrations clearly increased exponentially as the water moved upslope over the deep mooring during ebb tide, but did not plateau or decline again as the water moved further upslope. Thus, I conclude that the minimum cross-isobath width of the layer is at least ~ 4 km, and likely greater because the exponential increase in s_{rel} only became readily apparent on the deep slope side of the observed water mass.

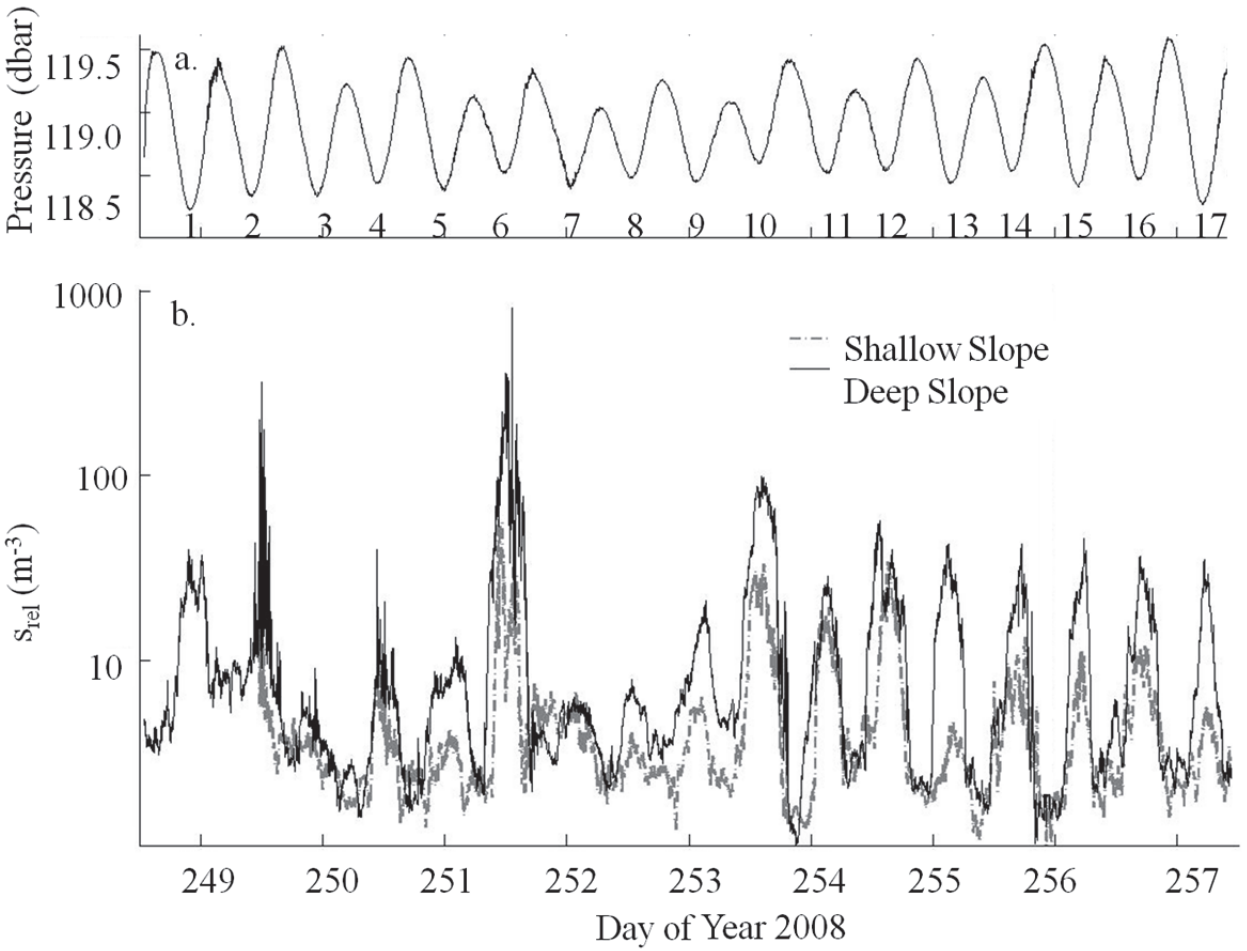

Figure 4.13 Time series of (a) water pressure (dbar) at the deep slope mooring, and (b) layer-averaged relative zooplankton concentration (s_{rel} *(t)*, m^{-3}) at the deep (solid black line) and shallow slope (grey dot-dash line) ADCP moorings. Low tide-sequence numbers referred to in the text are provided on (a).

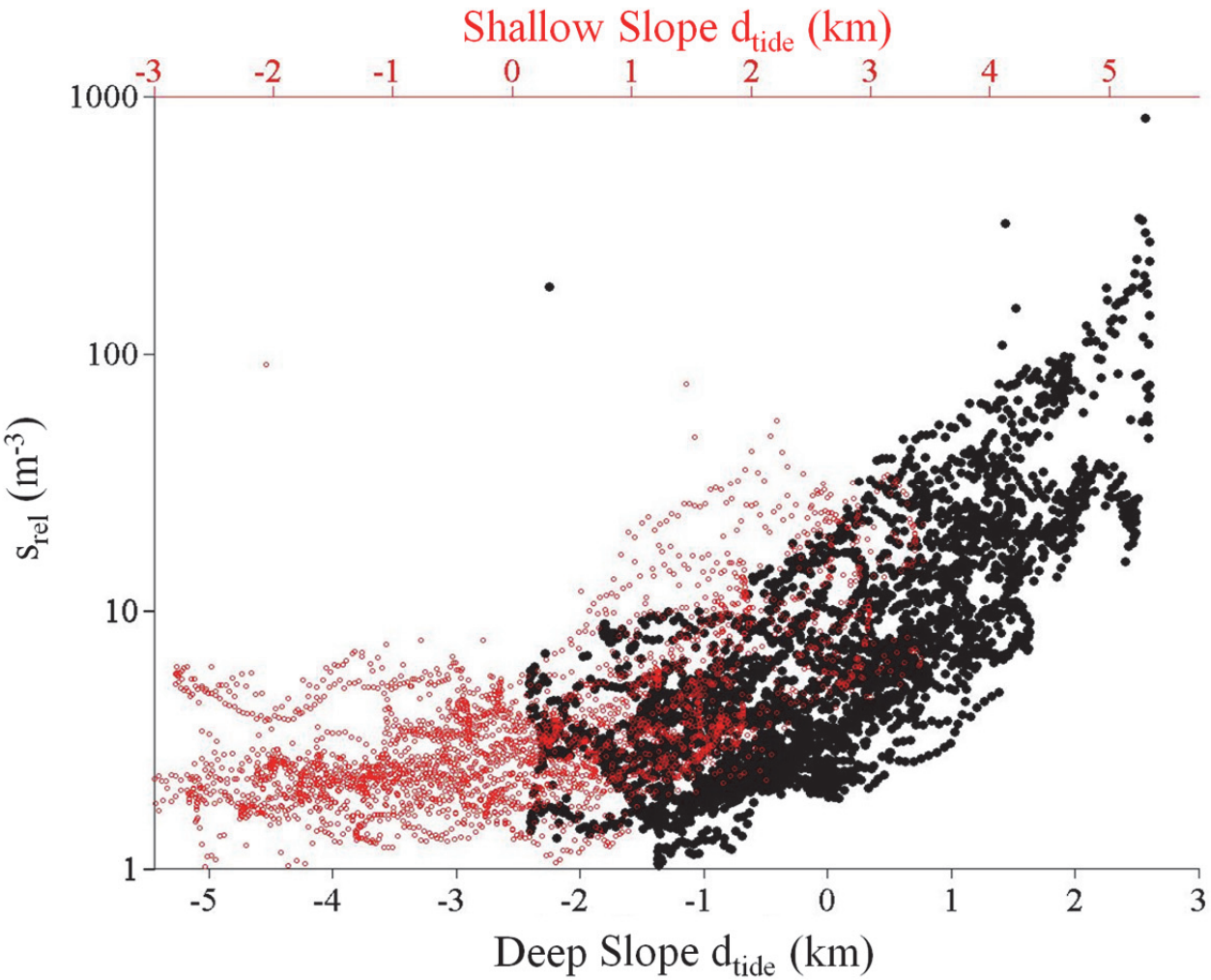

Figure 4.14 Change in layer-averaged relative zooplankton concentration (s_{rel} *(t)*, m^{-3}) estimates (every second datum only) in relation to upslope transport or excursion (km) of water, d_{tide} *(t)*, at the deep slope (black) and shallow slope (red) ADCP moorings, where the upper and lower abscissas are shifted with respect to their cross-isobath separation distance of 2.7 km.

4.3.5 Plankton relationships with physical variables

4.3.5.1 Tidal advection

Each of σ_t, $d_{tide}(t)$ and s_{rel} consistently varied with the semi-diurnal tide at each mooring location (Figure 4.5, 4.9 and 4.13) and the zooplankton were aggregated below the ~26 σ_t isopycnal that was advected with the tidal front. Thus, to further examine the variation in s_{rel} among tidal cycles, the log-transformed s_{rel} and σ_t anomalies were calculated and averaged over time between each maximum ebb and maximum flood tide (low tide-averaged) and the relations between the low tide-averaged s_{rel}, σ_t and the maximum upslope extent of the tidal excursion [positive $d_{tide}(t)$] among low tides were examined using linear regression where the data from both moorings were aggregated. For the analyses involving the density anomaly, it is relevant to note that the two moorings were separated on the density axis by 0.06 kg m^{-3}; the average density difference measured between moorings during the second half of the series. Regression results indicated that ~60 % ($P<0.001$) of the variation in zooplankton concentration among tidal cycles was accounted for by variation in the upslope advection of zooplankton in a density gradient (Figure 4.15). Therefore, processes that modulate the tidal excursion contribute to determining the concentrations of zooplankton available on the slope. Such processes are considered in the next two sections.

4.3.5.2 Along-isobath plankton distribution and advection

There was more variation in the upslope advection of water (containing zooplankton) among tidal cycles during the first half of the series when the along-isobath residual was strong (Figure 4.10 and 4.13). The along-isobath residual current, and the associated hydrographic changes, may have caused variation in zooplankton concentration on the slope directly through along-isobath advection of the zooplankton layer. Assuming advection was the only mechanism affecting zooplankton concentration (i.e., no accumulation or losses within the layer), the along-isobath flow should provide insights into the distribution of zooplankton in the along-isobath direction. In the remainder of this subsection I attempt to discriminate the possibilities that zooplankton were either associated with a particular water mass, or were randomly distributed, or uniformly distributed along-isobath.

First, I note that the residual current was accompanied by a near monotonic decrease in density as the warm, low density weak front moved across the ADCPs during the first half of the series (Figure 4.5). Second, two pieces of evidence link the front with the residual: a) each of the large daily $d_V(t)$, and consequently the large magnitude d_{resid}, and the weak front were persistent during the first half of the series only, and b) the front moved off-shelf (Figure 4.6) on the same day that the daily $d_V(t)$ began to decrease (Figure 4.10). If the zooplankton were associated with a particular water mass (e.g., σ_t >26 kg m^{-3}) being advected along-isobath, I would expect zooplankton abundance to vary between the periods when the warm front was present and when it was absent. The decrease in density over the period when the warm front was present spanned approximately the same range in density experienced between low and high tide when the warm front was absent (~26.1 to 25.9 kg m^{-3}). Therefore, I would expect to measure a decrease in zooplankton over the same time as the warm front progressed, at least comparable in magnitude to that observed between high and low tide when the warm front was absent (just over one order of magnitude change in zooplankton concentration). However, I found no clear associations between zooplankton abundance and the warm, low density front, and no significant trend in zooplankton abundance was found in the first half of the series (Figure 4.13, linear regression, $p > 0.1$ at both moorings). I conclude that hydrographic changes evolving from the warm front as it was advected along-isobath and across the ADCPs by the residual current were not sufficient to explain variations in zooplankton concentrations.

Figure 4.15 Least-square regression relations and associated statistics illustrating (**a**) relative zooplankton concentration, s_{rel} (m^{-3}) as a function of shallow and deep slope estimates of d_{tide} (km), (**b**) s_{rel} as a function of the shallow and deep slope density (σ_t) anomalies, and (**c**) shallow and deep slope density (σ_t) anomalies as a function of shallow and deep slope estimates of d_{tide}, where the shallow (red) and deep slope (black) estimates are bounded by ±1 SD where possible. Data from each mooring is presented on the same graph separated by the 2.7 km distance between moorings or by the average 0.06 kg m^{-3} σ_t difference between moorings.

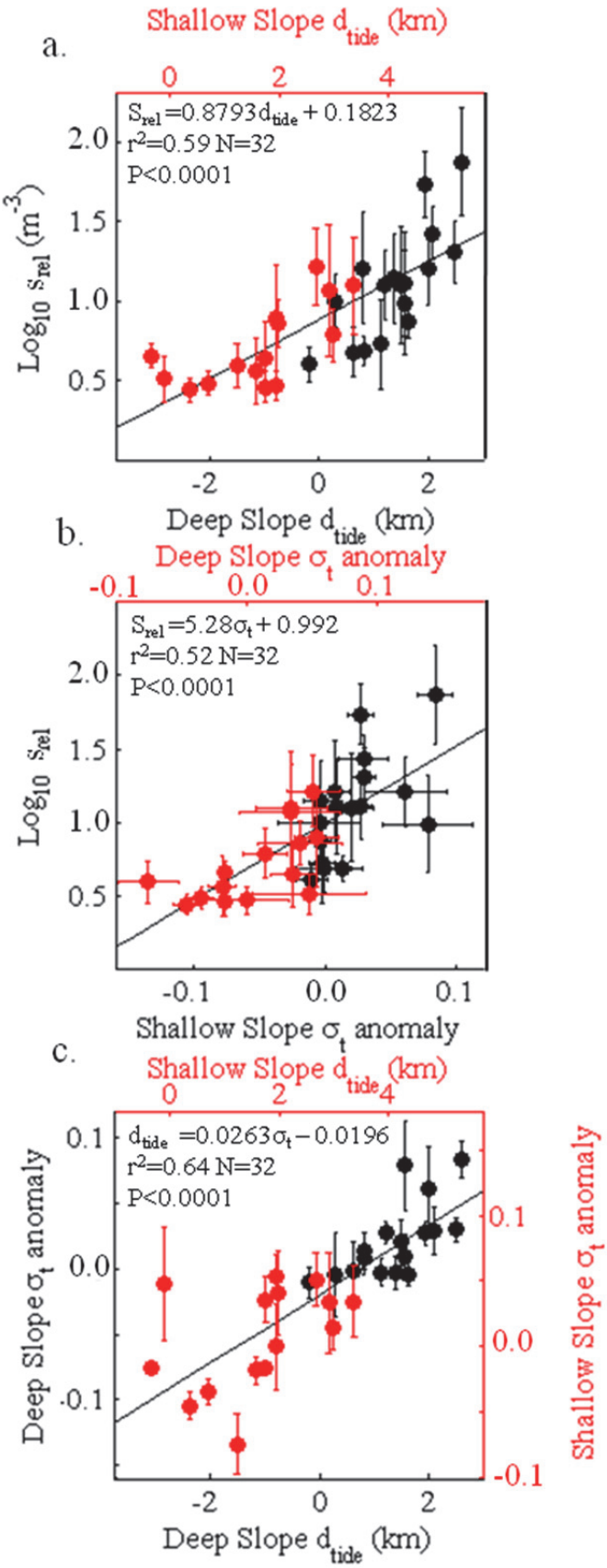
a.
Shallow Slope d_tide (km)
0
2
4
S_rel=0.8793 d_tide + 0.1823
r²=0.59 N=32
P<0.0001
Log10 s_rel (m^-3)
2.0
1.5
1.0
0.5
-2
0
2
Deep Slope d_tide (km)
b.
Deep Slope σ_t anomaly
-0.1
0.0
0.1
S_rel=5.28σ_t + 0.992
r²=0.52 N=32
P<0.0001
Log10 s_rel
2.0
1.5
1.0
0.5
-0.1
0.0
0.1
Shallow Slope σ_t anomaly
c.
Shallow Slope d_tide (km)
0
2
4
d_tide =0.0263σ_t − 0.0196
r²=0.64 N=32
P<0.0001
Deep Slope σ_t anomaly
0.1
0.0
-0.1
0.1
0.0
-0.1
Shallow Slope σ_t anomaly
-2
0
2
Deep Slope d_tide (km)

If zooplankton were randomly distributed along-isobath in patches that were smaller than the length scale of the along-isobath residual, I would expect to find no correlation between zooplankton abundance and the distance upslope traveled by the tide (maximum positive $d_{tide}\ (t)$) during the time period when along-isobath advection was strong. This was not the case; the relationship between zooplankton concentration and the upslope extent of the tidal excursion was the same (and statistically significant) regardless of the residual being strong or weak. The simplest explanation, and consistent with my observations, is that the length scale of a fairly uniform (at km scales; I do not address small-scale heterogeneity) zooplankton aggregation distributed along-isobath has a length scale greater than the along-isobath particle transport. In such a case, the along-isobath advection of the layer would not significantly change the concentration estimates at the ADCP locations over short time scales. The transport measured at the ADCPs varied within the zooplankton layer with a scale of 40 (deep) to 90 (shallow) km over my deployment period (Figure 4.11). Assuming a Lagrangian particle velocity of 2/3 the Eulerian velocity, which is valid for particles on a sloped boundary in a cross-isobath tidal velocity gradient (Loder 1980), the length scale of the layer in the along-isobath direction is 27 to 60 km. Roseway Basin is roughly 60 km in length along the southern margins and the ADCPs were located at approximately 2/3 this length (40 km) from the western margin (Figure 4.1). Thus, the southern margin to the west of the ADCPs is of insufficient length (~40 km) to accommodate a layer of zooplankton with the maximum length of ~ 60 km. This indicates some kind of copepod replenishment mechanism associated with the western margin of the Basin.

It is entirely possible that my assumption of a 2D slab within which zooplankton concentrations do not appreciably change over time is invalid, though the average concentrations (Figure 4.13) and transport estimates above (Figure 4.10 and 4.11) suggest otherwise. Nevertheless, I could, for example, consider that animals near bottom might be retained along the southern margin longer than animals at shallower depths due to the depth-related shear in the residual flow (Figure 4.11). I could also imagine one or more accumulating or dispersing mechanisms acting on the slope that serve to maintain concentrations at a certain level regardless of significant concentration variation in the source water. I visualized accumulation and dispersal with the movement of a tidal front

in Chapter 3 but the dynamics of this process were not examined, since I had no current velocity data. Similar kinds of processes have also been considered by others (e.g., Wishner *et al*. 2006, Aretxabaleta *et al*. 2008); these are explored below.

4.3.5.3 Asymmetric tidal mixing transport

Pringle and Franks (2001) identified several pieces of evidence that could be used to identify the relevant dynamics of asymmetric tidal mixing transport (ATMT) across a slope. My dataset is suitable (though I cannot use the vertical velocities) for testing this hypothesis because I had two ADCPs to measure cross-slope variation at tidal frequencies, I measured near-bottom tidal velocities (the process depends on the dynamics in the boundary layer) and finally, I measured a full water column profile of acoustic backscatter allowing me to identify patterns in layer thickness and height through the time series in relation to the tidal cycle. Below I provide the analytical results for the shallow slope mooring only, but the analyses were performed on both moorings and were very similar between moorings.

If ATMT were occurring, I expect that the vertical profile of plankton concentration should show that on the upslope tidal phase, the particles are higher in the water column than on the downslope tidal phase. I compared the vertical profiles of plankton concentrations between the maximum ebb (upslope) and maximum flood (down slope) tides at both moorings, and found no consistent difference in either the layer thickness or height in the water column between tidal phases at either mooring or during any tidal cycle (Figure 4.16).

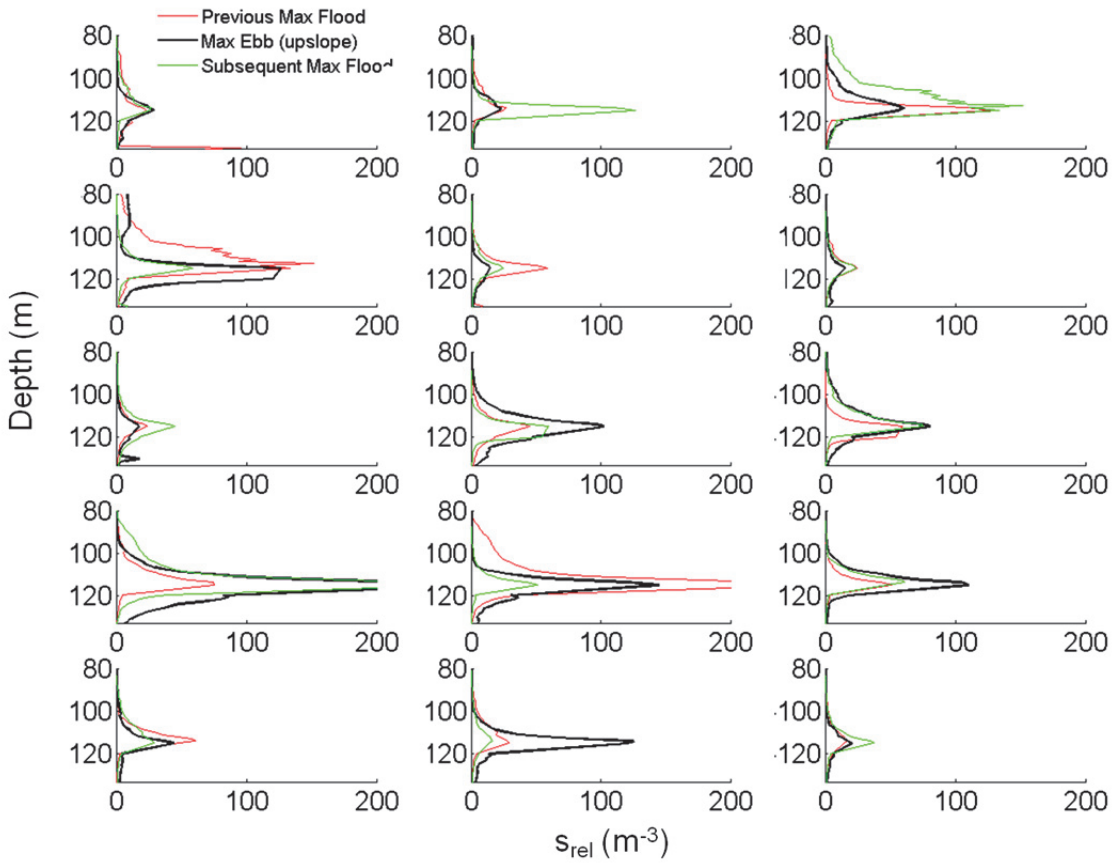

Figure 4.16. Comparison of the copepod layer height and thickness (s_{rel}, m^{-3}) between the maximum ebb (upslope) tide (black) and the previous (red) and subsequent (green) maximum flood (down slope) tides for every tidal cycle measured at the shallow slope mooring.

A second indication of ATMT is that stratification should be weaker on the upslope phase of the tide as cold water moves over warm water and generates vertical turbulent mixing, while on the down slope phase, stratification should be higher. I measured a crude first approximation of stratification by taking the difference in density between the two slope moorings at each maximum flood (down slope) and maximum ebb (upslope) tidal phase. I also assumed that the density I measured at the shallow mooring would be the same as density measured at the same depth above the deep mooring. I expected, if the hypothesis were correct, the difference in density between moorings to be smaller on the upslope tidal phase than the down slope. When I compared the differences in stratification between tidal phases using a t-test. I found no statistical difference in stratification between the upslope and down slope tidal phases (t = -0.51, df = 27, P = 0.614).

Thirdly, for ATMT to occur, the Rouse number (R) should be >1 on down slope phase, when particles are near bottom, and R should be <1 on the upslope phase of the tide when particles are spread throughout the water column. The Rouse number is a non-dimensional number $R = w_0 / (k\, u^*)$ that relates the sinking speed of a particle (w_0) to the turbulent velocity of the water column ($k\, u^*$) where k is the von Karman's constant (0.4) and u^* is the velocity scale of the eddies in the bottom boundary layer. When $R > 1$ ($w_0 > k\, u^*$), the particles will be clustered near the bottom, and when $R < 1$ ($w_0 < k\, u^*$) particles will be spread throughout the water column. I do not know what the sinking speed of my particles was in relation to the density field, which is a limitation, so I speculated that they sink at a constant rate on the slope because they are far above their desired depth of neutral buoyancy (Chapter 3). I will assume a constant sinking rate for this approximation of 1 mm s^{-1} which has been observed for scallop larvae (Chia *et al.* 1984). This means that variation in R will be determined primarily by the dynamics of u^* on different tidal phases.

The parameter u^* is related to the tidal currents ($U(z)$) in weakly stratified regions near the bottom by the following equation (Pringle and Franks 2001):

$$|U(z)| = \frac{u^*}{k}\log\left(\frac{z+z_o}{z_o}\right) \qquad (4.3)$$

where z_0 is about one tenth of the length scale of bottom roughness. Typical values of z_0 are 10^{-3} m and I used this value in my calculations.

First, I calculated the vertical profiles of the *U(z)* (Figure 4.17) averaged over all maximum ebb tides and separately averaged over all maximum flood tides, similar to Figure 5 in Pringle and Franks (2001). From these profiles I estimated the bottom boundary layer thickness (h_{bbl}) to be ~10 - 20 m (~90 – 110 m depth at the shallow mooring), which contains the plankton layer. I then estimated u^* within the bottom boundary layer (Figure 4.18). I found that $u^* \sim= 0.06$ m s^{-1} on the down slope tidal phase and is smaller at $u^* \sim= 0.045$ m s^{-1} on the upslope tidal phase, primarily because the tidal currents are stronger on the down slope than the upslope tidal phase. This is close to the $u^* = 0.02$ m s^{-1} estimated by Pringle and Franks (2001) for Georges Bank.

Already my values of u^* are indicative that *R* will be smaller on the upslope than the down slope phase, which is not consistent with the expectation for ATMT. At a constant sinking speed of 1 mm s^{-1}, R = 0.05 on the upslope tidal phase, and R = 0.04 on the down slope tidal phase. This means that on both phases of the tide, particles tend to be mixed into the water column. This could easily be so; they could be mixed by turbulent processes in the boundary layer on the upslope tidal phase, and mixed at the edge of the tidal mixing front as it moves down slope on the opposite phase. For *R* to exceed 1, in this case, the sinking rate would have to be greater than ~2 cm s^{-1}, which seems unrealistically high.

The validity of the Rouse number is questionable without knowing the sinking rate of particles under different density conditions. For example, if the boundary layer is well mixed on the upslope tidal phase, with uniform density throughout, the sinking rate is more likely to be constant. On the down slope tidal phase when stratification is restored, sinking rate would likely decrease as copepods sink toward higher density water and became more neutrally buoyant. Also, the realized sinking rate will depend on the vertical current magnitude and direction, which the Rouse number does not take into consideration. Nevertheless, it does not seem likely that in this system particles would cluster near bottom. Instead, they would tend to be spread throughout the boundary layer, consistent with the vertical profile I observed.

On consultation with the author of the ATMT paper, he agrees that based on my analysis, ATMT is not operating on the southern slope of Roseway Basin (P. Franks, pers. comm., Scripps Institution of Oceanography).

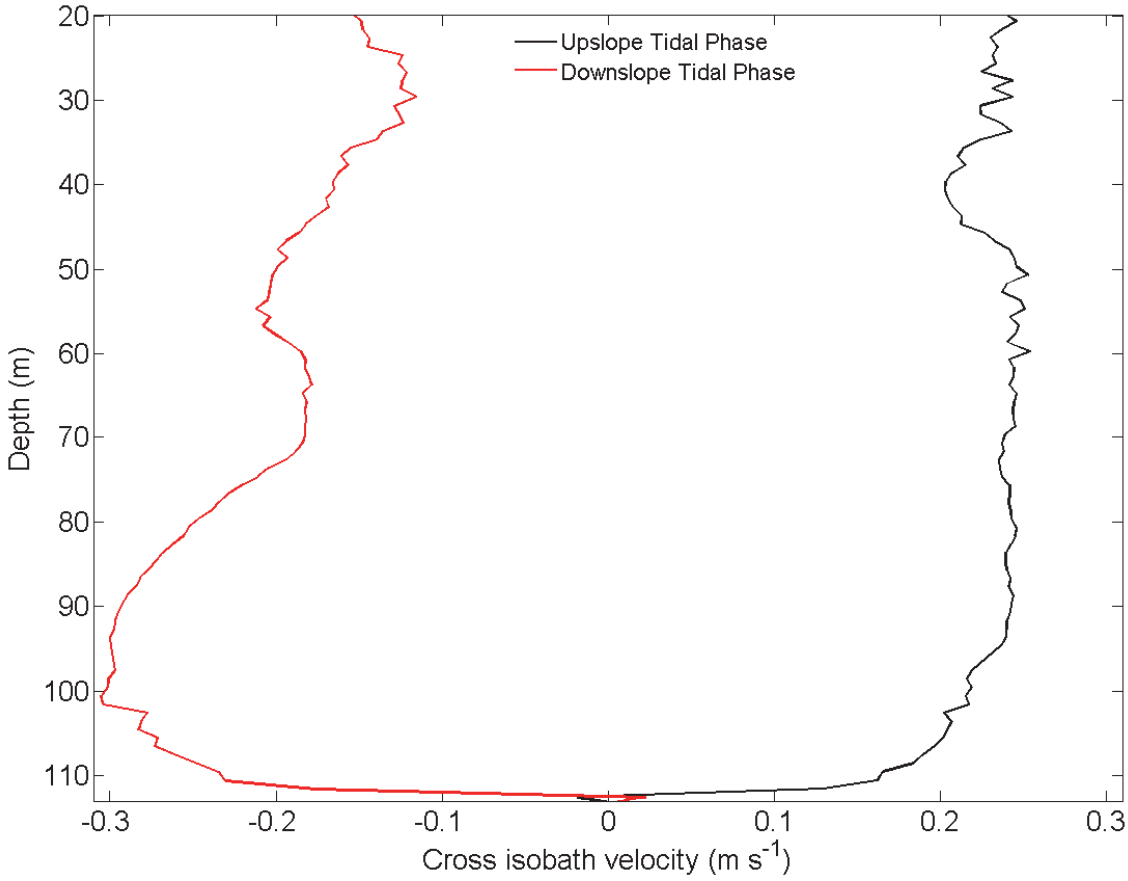

Figure 4.17 Average vertical profile of the cross isobath velocity (*U(z)*, m s^{-1}) at the shallow slope mooring, averaged over all maximum ebb (upslope) tidal phases (black) and maximum flood (down slope) tidal phases (red). The bottom boundary layer occurs between 100 and 112 m depth, where the velocity slows from bottom friction.

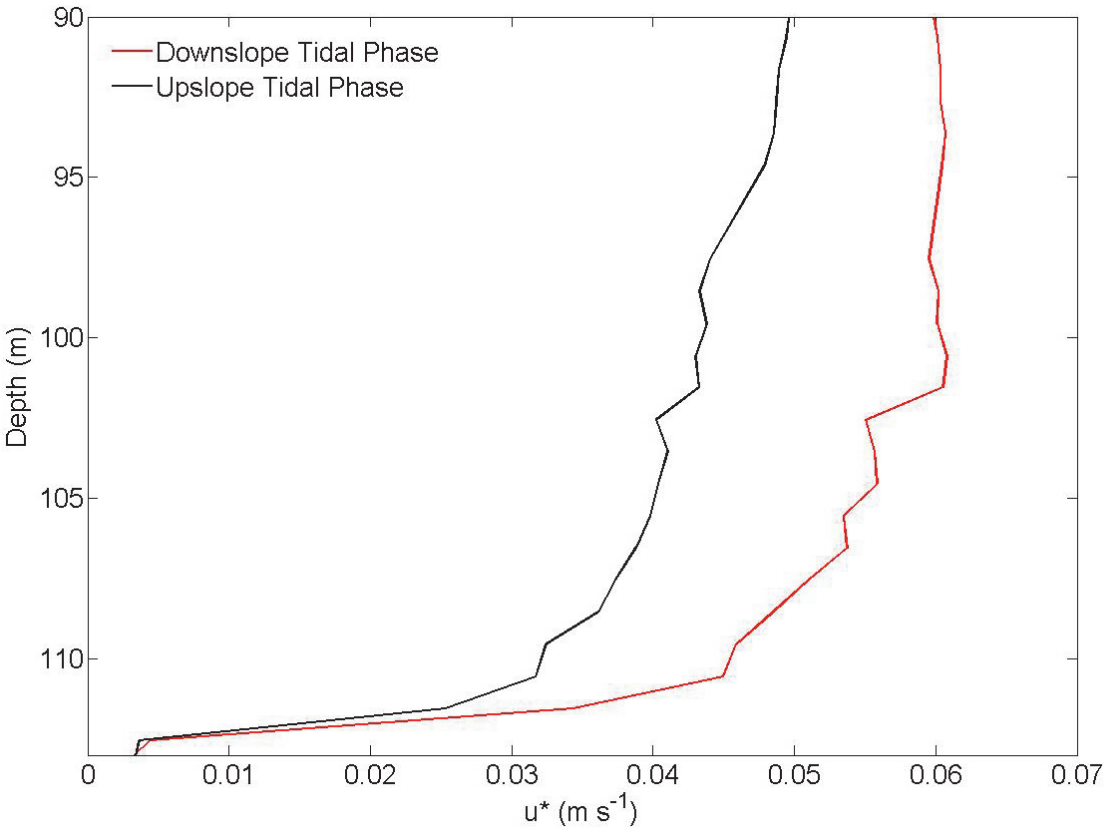

4.18 Vertical profile of the turbulent mixing parameter u^* in the bottom boundary layer at the shallow slope mooring.

4.3.5.4 Zooplankton accumulation on the slope: a simple model

Zooplankton accumulation generated by a coupling of current velocities and vertical velocities generated by zooplankton through sinking, floating or directed swimming has been demonstrated by modeling studies (e.g., Franks 1992). Thus, is it possible that patches of diapausing copepods could accumulate through a combination of current velocity and maintenance of vertical position imposed by the copepods? Assuming that the diapausing copepods are neutrally buoyant in water of a certain density to which they have become physiologically acclimatized (i.e., they have achieved neutral buoyancy), then it is reasonable to conclude that if they are advected above or below this density they will return to their original vertical position, in density space, by sinking or rising back to their "preferred" depth of neutral buoyancy. To examine this proposed accumulation mechanism on the sloped margin of Roseway Basin, I extended my 2D analyses above to include the vertical and horizontal structure in the current velocity estimates. My goal was to determine the effects of sheared *dU/dx* and *dU/dz* on plankton concentrations within the layer, and provide insights into the dynamics behind (1) the accumulation and dispersal of copepods on the Basin side of the tidal mixing front (Chapter 3) and (2) the 'tilting' of the prey field upslope on the southern Basin margin (Chapter 3).

Having the two ADCP moorings deployed cross-isobath, and within one tidal excursion (i.e. they overlapped in water mass space), allowed me to infer flow-fields within the domain between the mooring at each time step of my deployment and thus to examine the horizontal structure of currents in the cross-isobath dimension (*dU/dx*). Vertical structure (*dU/dz)* was included based on each of the ADCP horizontal currents measurements at 1 m depth resolution (*z*-layers) throughout the water column. I initially developed a simple 1D flow-field model using my measured cross-isobath velocities (*U(x,z,t)*, where x = cross-isobath position, z = depth, t = time). The equations of continuity cannot be satisfied in this simple model; my purpose is to identify fundamental processes and then develop hypotheses that can be compared with my observations of the prey field and tidal front movement across the boundary in Chapter 3. First, I linearly interpolated U (m s^{-1}) between the two moorings at each *z*-layer (1 m) between 50 m and the bottom at every 2 min time step. I restricted the model domain to below 50 m because, 1) copepods were not aggregated at the shallow depths, and 2) current estimates

in the shallows (farther from the transducers) had large uncertainties. My moorings were located on a slope; bathymetric steering of the currents near bottom meant that interpolating between the same depths at both moorings was not appropriate for all depths, particularly those near bottom. Therefore, depth pairs between moorings were selected by assessing correlations in current velocity at all time steps between each possible depth pair. Pairs that were well correlated (highest r^2) were then selected and used in the interpolation. The interpolation resulted in a matrix of cross-isobath velocities at each time step for each *z*-layer and 100 m horizontal spacing in the cross-slope direction.

I initialized the flow field model with particles uniformly distributed across the *z*-layers using the 100 m cross-isobath (*x*) resolution (Figure 4.19), similar to Franks (1992), and tracked those particles through the flow field model for a full tidal cycle between two maximum ebb tides. Particles leaving the domain were problematic as I had no current information external to the domain. To minimize the problem I proceeded as follows: a) only the deep slope half the model domain was seeded with particles, consistent with the observations, b) the period for a model run was restricted to one tidal cycle because a significant proportion of the particles would leave the domain and not return over longer periods due to the cross-isobath residual, (c) maximum ebb tides were chosen as time boundaries, though alternatively the time period between maximum floods would achieve the same result if the shallow slope half of the model were seeded with particles, and (d) if particles left the model domain at the deeper or shallower boundaries, they were assumed to advect at the same speed they experienced at the model boundary. Particles were permitted to be transported along the sloped bottom. Density stratification was not initially considered. The model was run over each tidal cycle throughout the 9 day current data series.

The results of the modeling are presented graphically (Figure 4.19) for three of the many tidal cycles representing a range of the different physical oceanographic conditions observed in the along-isobath residual current: 1) cycle 3; when there was a strong along-isobath current, 2) cycle 10; when the along-isobath current began to slow at neap tide, and 3) cycle 17; when there was no along-isobath current below 100 m (see Figure 4.5 showing the oceanographic conditions and tide-sequence numbering). Note

that the state of the along-isobath current when I transected the southern slope in Chapter 3 (Figs 3.9 and 3.10) was in a 'weak along-isobath current' state, similar to cycle 10. On the completion of each model run I calculated the depth averaged particle-to-particle horizontal distance (an estimate of *dU/dx* since the particles are initiated with equal spacing) for each of the ebb and flood tidal phases to quantify zones of apparent particle compression or decompression (as defined by Franks 1992) relative to the initial state. Because the 1-D model precludes continuity equations, the terms compression and decompression describe only the change in particle-to-particle distance; i.e., apparent compression does not equal particle accumulation and apparent decompression does not equal particle dispersal. Putting the compression and decompression zones into a more formal context requires a more sophisticated 3-D model and analysis.

Despite the simplicity of the 1-D model, some interesting and recurrent patterns in the cross-isobath particle distribution are apparent. During the initial upslope (ebbing) tidal phase, there was either a small compression or small decompression among particles, but as low tide approached, more decompression occurred (Figure 4.19, Hour-3). This is consistent with the thinning of the copepod layer on the upslope tidal phase I observed previously (Figure 3.9). During the down slope (flooding) tidal phase the particles were always compressed and compression tended to increase near bottom (Figure 4.19, Hour-6 and Hour-9). This is consistent with the forming of the copepod patch at depth on the down slope tidal phase I observed previously (Figure 3.9). However, when the along-isobath current was strong, the upslope tidal phase (ebbing) was also, on average, in a compressive state. During the tidal cycle I transected in Chapter 3, there was no along-isobath current, so I missed this time-varying property. Finally, when decompression occurred on the upslope phase, it was always less than the compression apparent on the preceding down slope phase. Taken together, these results show that particles will compress in a cross-isobath direction over time, creating a convergence zone for water on the slope that is maintained through time.

Compression or decompression occurs because of cross-isobath gradients in the cross-isobath currents (i.e., *dU/dx*). Compression on the down slope phase of the tide can easily be explained by the gradient in tidal currents between moorings (Figure 4.9). Faster moving water at the shallow mooring, pushing on slower water deeper in the

Basin, will create an apparent compression. The absence of an equal and opposite decompression on the upslope phase that should result from the same gradient, however, is more difficult to explain. One part of the explanation comes from the cross-isobath component of the residual flow, which below 80 m depth is always directed down slope regardless of tidal phase (Figure 4.11). This residual is greater in velocity at the shallow mooring than at the deep mooring and works against the decompressive gradient on the upslope tidal phase. This residual also explains why compression is greatest near bottom, where the cross-isobath residual is strongest (Figure 4.11).

When the along-isobath residual was present, a compressive 'sweet spot' occurred in the 75 to 120 m (Tide 3 in Figure 4.19) depth layer that encompasses the highest concentrations of copepods (Figure 4.2). Below 120 m, particles tended to be swept down slope by the cross-isobath residual (Figure 4.11). Above 75 m, they were swept toward the open ocean as the residual current veers seaward in the upper Ekman layer (Figure 4.11). Within the 75 – 120 m layer I observed little to no vertical shear in the cross-isobath currents and this would serve to help maintain the vertical integrity of advecting zooplankton patches as they are transported along the slope. This simple mechanism could help maintain high concentrations of diapausing copepods on the slope.

Figure 4.19 Particle-tracking model results for three tidal cycles (tide sequence numbers shown in Figure 4.4 and 4.9) representing periods of strong along-isobath current (Tide 3, left panels), slowing of along-isobath current at neap tide (tide 10, middle panels) and no along-isobath current (tide 17, right panels), where in each case the evolution of particle compression and decompression is illustrated from initialization at ~ maximum ebb tide through 3 h increments of the tidal cycle to ~maximum flood tide. The abscissa, *X,* represents the cross-isobath transport distance (km) with respect to the deep slope ADCP and the ordinate, *Z,* is depth (m) below surface. The model domain is outlined with a grey line that reflects the sloping bottom that was linearly interpolated between the seafloor depths at each ADCP location.

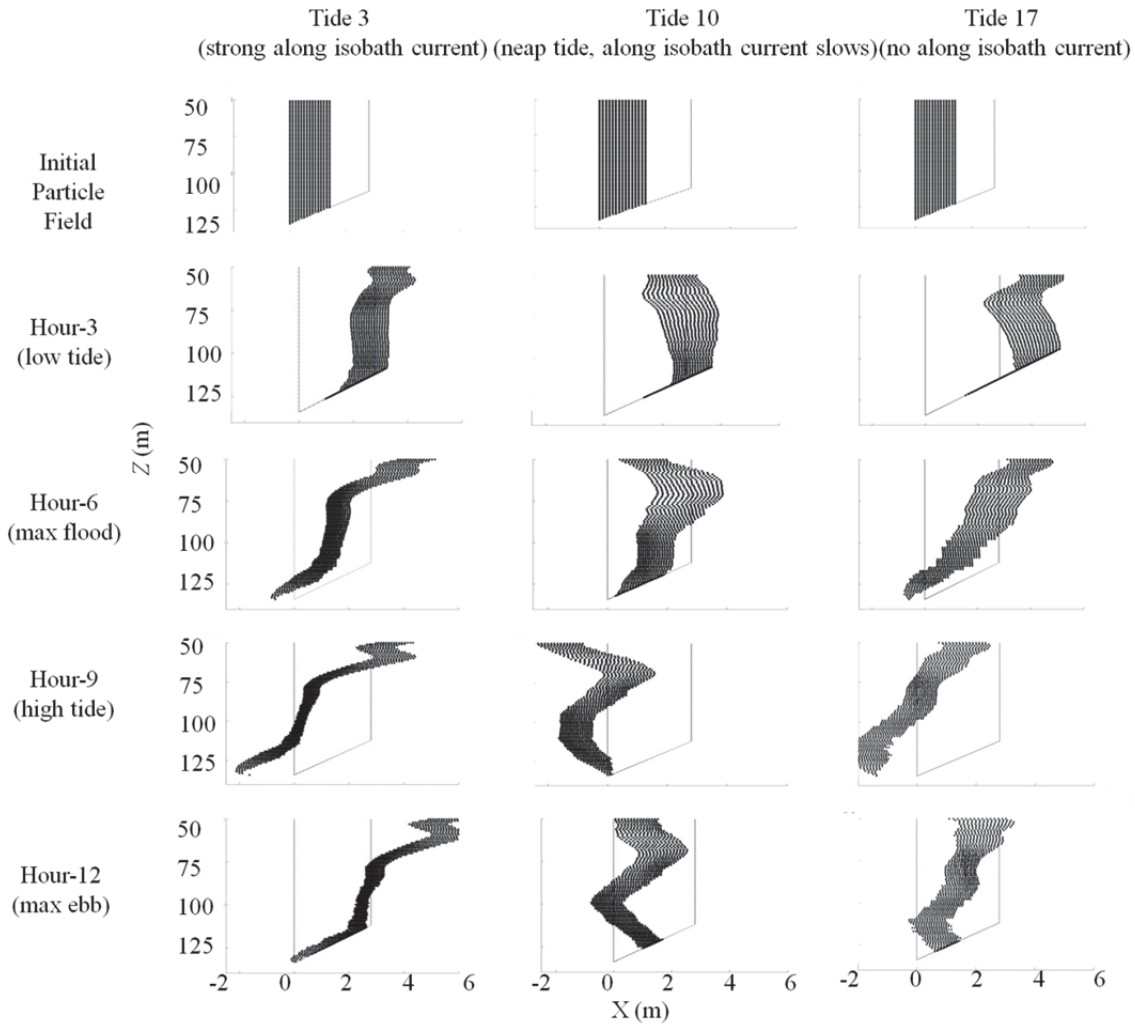
Tide 3
(strong along isobath current)
Tide 10
(neap tide, along isobath current slows)
Tide 17
(no along isobath current)
Initial Particle Field
Hour-3 (low tide)
Hour-6 (max flood)
Hour-9 (high tide)
Hour-12 (max ebb)
Z (m)
50
75
100
125
-2
0
2
4
6
X (m)

4.4 Discussion

I have shown that copepods diapausing at depth in the southern slope region of Roseway Basin were advected by a cross-isobath tidal current that converged on the slope, where they were advected along-isobath by a residual flow on the stratified side of a front. The animals were generally evenly distributed in an along-isobath direction, and new individuals advecting along-isobath with the residual flow appeared not to be retained along the slope for more than a few days based on the along-isobath current velocities. The Eulerian description of the habitat provided valuable insights (e.g., relationship between tidal advection and copepod concentration), but adequate characterization of the mechanisms affecting the right whale prey field required the additional Lagrangian description of the biological and physical environment that was provided by the particle model. Below, I use this information to provide further insights into hypotheses developed in Chapter 3 concerning sources and retention mechanisms for copepods along the southern slope, the physical dynamics at the southern slope that promote prey aggregation and the potential of the southern slope as the most favorable feeding ground for right whales in Roseway Basin.

The Eulerian velocity on the southern slope margin of Roseway Basin was equivalent to a transport distance of 10 - 15 km day^{-1} during the first 4 days and, assuming the Lagrangian particle velocity is 2/3 of the Eulerian velocity due to Stokes Drift (Loder 1980), individual copepods will not be retained along the 60 km long slope for more than ~7 d. Tidally rectified flow around the nearby Browns Bank occurs year-round with no strong seasonal signal and varies primarily, as I also found, in response to tidal forcing (Smith 1989). Density driven flow also occurs to some degree throughout the year (Loder *et al*. 1997, Hannah *et al*. 2001). As suggested above, there must then exist a mechanism near the western end of the Basin that provides continuous copepod replenishment of the high concentrations of copepods swept along-isobath by the residual on the southern slope. The three possible mechanisms for copepod replenishment to the deep water on the southern slope are not mutually exclusive: a continuous surface supply, continuous along-isobath flow and recirculation within the Basin.

4.4.1 Continuous surface supply

In relation to surface supply, the copepod population at depth can be replenished vertically as new individuals in the surface layer enter diapause and sink below ~75 m depth. These individuals most likely originate upstream either in the Gulf of St Lawrence, from populations associated with other Shelf Basins on the eastern Scotian Shelf, or slope waters intruding onto the Shelf in spring (Herman *et al*. 1991, Head *et al*. 1999). These "source" populations are then advected to the western Basins, including Roseway, by Shelf circulation. The paucity of appreciably high concentrations of copepods in the surface layers on the Shelf suggests that this supply, measured as point estimates, is diffuse in time and space and cannot alone replenish the large concentrations advected along the southern slope (Figure 4.2; see also Herman *et al*. 1991).

4.4.2 Continuous along-isobath through flow

Copepods concentrated at depth along the southern margin of the Basin may be replenished by an along-isobath flow entering the Basin from the western margin between the deep channel separating Browns Bank and Nova Scotia and flowing along the southeastern slope to exit the Basin at the eastern margin via the channel separating Baccaro and Roseway Banks (Figure 4.1a). Smith (1989) measured inflow to Roseway Basin on the northern flank of Browns Bank that was generated by rectification around the Bank. Eastward flow at depth in the Browns Bank - Nova Scotia channel in summer is suggested to be dynamically related to deep inflow from the Northeast Channel (Hannah *et al*. 2001), and thus, the copepod source may be populations over-wintering on the Scotian Slope that enter the Shelf region and Roseway Basin via the Northeast Channel.

This hypothesis, however, is not consistent with the water mass structure in the deep Basin shown in Chapter 3, which shows that the slope water in the deep channel separating Browns Bank and Nova Scotia is essentially cut off from Roseway Basin by the Bottom Water mass that cuts south across the western Basin margin (Figure 3.14, 3.20 and 3.26). Thus I conclude that, based on my evidence, deep channel separating Browns Bank and Nova Scotia will not be able to replenish copepods on the southern slope of Roseway Basin at weekly time scales.

4.4.3 Basin recirculation

In Chapter 3 I showed evidence of a gyre in Roseway Basin. Gyre re-circulation is the most likely mechanism by which copepods are replenished at the western end of the southern slope at weekly scales. The gyre is then an important component to the maintenance of the prey field over longer time scales for two reasons; (1) it helps retain copepods below the sill depth in the Basin over long time periods, and (2) it replenishes copepods to the southern slope, where right whales are most often sighted. It is not, however, sufficient to explain why the southern margin of the Basin is frequented by right whales, particularly when the highest prey concentrations occur at the NE end of the Basin near the gyre center. Similar to Roseway, copepods in the nearby Emerald and Lahave Basins are aggregated with a generally uniform kilometer-scale distribution at depth in these basins, and surface supply, coupled with at-depth circulation is postulated to maintain the aggregations (Herman *et al*. 1991). Although not addressed by Herman *et al*. (1991), their data also illustrate elevated concentrations on the southern slopes of both the Emerald and Lahave Basins at depths of between 150 m and 200 m that are shallower than the mid-Basin concentrations. Slope aggregations of this type are likely overlooked as they are small features relative to the mid-Basin aggregations. As suggested above, gyre-like recirculation, coupled with a copepod accumulating mechanism acting on the slope, could explain such distributions in these other Shelf basins.

4.4.4 Prey field dynamics of the southern slope

I showed using my particle model that apparent compression of copepods can occur in a cross-isobath direction, particularly when the along-isobath residual is strong. It is also possible that the slope is an actual compression zone, which is one type of accumulation zone (also as defined by Franks 1992). Though continuity was not enforced in my model, I know that when the particles are compressed in a cross isobath direction, they will decompress in an along isobath direction. If all the water that converged in the cross isobath direction was subsequently advected in an along isobath direction, no concentration changes would occur in the layer. But I also know that some of the water converging on the slope will advect vertically. The vertical currents measured by the ADCPs at the deep mooring were either consistently directed toward the surface

(assuming the RDI data are reliable) or consistently directed downward (assuming the Aquadopp data are reliable) throughout the time series. Copepods compressing on the slope and advected upward or downward must sink, float upwards or swim to maintain their vertical position at depth in relation to the density field, else be advected out of the Basin in the upper water column or sink to the bottom. I speculate that cross-isobath compression coupled with vertical position maintenance could act to accumulate copepods at depth on the sloped margin. Testing this hypothesis will require mapping the cross-isobaths density field using a time series of CTD sections, modeling copepod buoyancy in relation to the density field, and extending the flow field model to 3 dimensions with continuity and conservation compliance (e.g., Aretxabaleta *et al.* 2008).

Below, I summarize the information about the dynamics of the southern slope in relation to the right whale prey field into a narrative about the copepod's travel along the southern slope of Roseway Basin.

- The Basin as a whole is populated by ontogenetic descent of copepods from upstream sources on the Shelf
- Gyre recirculation brings copepods continuously to the southern slope at the western end of the Basin.
- The along isobath residual, as part of the gyre circulation, advects these copepods along the isobath, toward the northeast.
- As they are advected, the tide moves the copepods up and down slope.
- On the down slope tidal phase, copepods are compressed at the front edge, and on the upslope phase, the copepods are washed upslope and the layer decompresses. On the upslope tidal phases, concentrations are high at shallower depths due to water column mixing at the tidal mixing front (Figure 3.9, 3.10).
- The down slope compression of the prey is always greater than the upslope decompression, so that as the copepods move along isobath, they accumulate over time. This is partly due to the cross isobath component of the residual (U_{resid}).
- When the along-isobath flow is present, within the 75 – 120 m layer there is little vertical shear in the cross-isobath currents and this would serve to help maintain the vertical integrity of advecting zooplankton patches as they are transported along the slope.

Despite my detailed examination of the prey field dynamics along the southern boundary, the reason behind the prey field upslope tilting and the relative stationarity of its position throughout my survey, remains unexplained. I found no evidence that Asymmetric Tidal Mixing Transport is operating on the slope, and I know of no other hypotheses regarding a steady state, dynamic process that could maintain the tilted structure through time. I have discovered how copepods are transported to the slope region, and how they move through the slope region, but not how their depth distribution in relation to the density field can be maintained, apparently regardless of tidal state. The smaller-scale dynamics of the slope are related to the tide, yet no tidal variation is reflected in the larger aggregation (Figure 3.12), nor was any mechanism by which the copepods are constantly 'pushed' toward lighter water identified. I noted in Chapter 3 that the shallow depth limit to the tilting appears to be set by the cross-Basin tilting of isopycnals and isobaths in the upper layer. Perhaps, then, the larger-scale circulation patterns and not the smaller-scale dynamics specific to the slope govern the larger distribution of the prey field.

Despite this shortcoming, I have gained insights into the reasons why the southern slope may make a favorable feeding ground for right whales. From the data I have collected and analyzed in Chapters 3 and 4, I speculate that the southern slope of Roseway Basin is a favorable feeding ground for right whales for two reasons:

(1) The depth distributions of the 'tilted' slope aggregations relative to the deep Basin aggregations make the former more beneficial to feeding whales despite the slope being relatively small in area and hence a smaller but more concentrated prey field. Such a benefit may be related to there being a depth limit below which the energy gained by the whales feeding at greater depth does not outweigh energy expended by diving to greater depth, thus favoring foraging at the relatively shallow (<120 m) regions of high copepod concentration. Such a limitation may explain why right whales are rarely observed in the deeper Emerald and Lahave Basins, despite these Basins containing high concentrations of copepods. I caution, however, that right whale occupancy estimates for these other basins are essentially non-existent, though there is some evidence that right whales occasionally occur in Emerald Basin (Mellinger *et al*. 2007).

(2) The combination of the tide, the front on the southern slope, and gyre circulation cause predictable accumulation of copepods at tidal frequencies along the entire southern slope boundary. The tide accumulates copepods every tidal cycle, while the gyre circulation moves this aggregation along isobath and replenishes new individuals to the system. The dynamic forcing of the cross-isobath residual (U_{resid}) is relevant to this interpretation because it, along with the cross-isobath tide, contributes to the generation of an apparent compression zone (as defined by Franks 1992) for copepod-filled waters on the slope as they move along-isobath. How is it generated? That the cross-isobath residual did not slow near bottom after neap tide with the along-isobath residual, and remained relatively stable throughout my monitoring period, indicates that the two residuals (d_V and d_{Uresid}) were not completely dynamically related. The cross-isobath residual was also not a local or ephemeral event as my observations are consistent with those of Smith (1989) for the northern flank of nearby Browns Bank. The cross-isobath residual is thought to originate from buoyancy fluxes associated with the barotropic and baroclinic tidal interactions on a slope (Ou and Maas 1986), meaning that this flow should be stronger in steeper areas than in areas with a weaker bathymetric gradient. If it is a general mechanism on sloped boundaries on the Shelf, such a flow could generate convergence zones for zooplankton on other steep slopes on the Shelf, including in Lahave and Emerald Basins.

A relevant question to ask is why the whales are not more frequently sighted in the NE corner of the Basin, where I observed the highest concentrations of copepods? I speculated based on my analysis in Chapter 3 that the large deep Basin prey patch occurred during an ephemeral event, a slope water intrusion, which probably occurred recently before my survey. I speculate that it was a recent event since there was no mixing between the off-Shelf water and the Shelf water, whereas in other parts of the Basin there was evidence of Shelf-slope water mixing, which would occur over time. If that intrusion had not occurred, or if I had surveyed a month later after the water masses within the Basin had more mixing time, that large patch may not have existed but rather the prey concentrations may have been homogeneously higher throughout the Basin. The southern slope processes, related to the tide, are predictable processes that the whales can rely upon to accumulate prey into larger patches and reach shallower depths. Also, I only

measured these processes near neap tide; at spring tide the effects are likely amplified to the greater benefit of the whales.

4.5 Summary and Conclusions

I met my first objective to investigate variation in C4 and C5 concentration on the southern slope of Roseway in a Eulerian and, where possible, Lagrangian way, at high resolution and at the scale of the foraging whales. Diapausing copepod aggregations on the southern slope of Roseway Basin are advected cross-isobath with the tide. Individual copepods do not remain on the slope for long because they are advected along-isobath by the residual flow. The fact that high copepod concentrations are maintained on the southern slope, despite along-isobath emigration, implies that there must be one or more replenishing and concentrating mechanisms. I showed that gyre recirculation of copepods within the Basin is the most likely replenishing mechanism. My second objective was to gain insights into the dynamics of prey movement and the forces responsible for this movement along the southern slope. I provided evidence that tidal advection at a front, coupled with along isobath advection and shear in the horizontal currents accumulate copepods predictably along the southern slope region of the Basin at tidal frequencies. The accumulation of the copepods makes the slope region a beneficial feeding ground for right whales relative to the rest of the Basin, and thus explains why the highest probability of sighting a right whale occurs along the southern slope and not elsewhere. This addresses my final objective, which was to interpret the data with regard to right whale foraging.

Chapter 5

Interannual Variation in the Roseway Basin Right Whale Critical Habitat: 2007 - 2009

5.1 Introduction

In Chapters 3 and 4, I described the spatial and temporal variation in the distribution of copepod abundance in Roseway Basin using extensive survey data collected in a single year. However, these habitat characteristics vary among years because cycles of biological production and water mass advection on the Scotian Shelf exhibit strong seasonal variation. Thus, it is important to assess how representative a single year survey of right whale habitat may be in relation to data collected over multiple years. Multi-year sampling can answer questions such as: was the single year of sampling done in a relatively productive year for right whale prey? Was it an exceptionally poor year in terms of prey production? Does the western Basin margin always have many fewer copepods than the central-eastern Basin?

If the prey field in Roseway Basin exhibits substantial interannual variation, this is likely to influence annual right whale abundance in the Roseway Basin Critical Habitat. For example, in the late 1990s, some researchers contend that right whales abandoned Roseway Basin for a number of years (Brown *et al.* 2001). The same researchers hypothesized that Roseway Basin was abandoned because there were fewer *Calanus finmarchicus* in the Basin during those years. This hypothesis was addressed by Patrician and Kenney (2010) who used Continuous Plankton Recorder (CPR) data collected in the surface layer of Roseway only, to infer diapausing *C. finmarchicus* abundance at depth among three periods: before, during, and after the abandonment. They concluded that average *C. finmarchicus* abundance at the surface was lower during the abandonment period than either before or after the abandonment. Further, they attributed variation in surface layer density as well as the variation in *C. finmarchicus* abundance to decadal-scale variation in water mass advection onto the Scotian Shelf that is linked to decadal-scale circulation changes in the region. However, the lack of *in situ*

biological data (i.e., diapausing copepods at depth) meant that the interpretation was restricted in scope to very broad-scale processes. Multi-year sampling of the Roseway Basin habitat that is directed at the diapausing copepod population is required to provide further insights into the role of prey field variation in the interannual habitat occupancy by right whales.

An assumption of the above studies, and also in other research linking right whale population dynamics to their prey, is that the average abundance of *C. finmarchicus* measured across a habitat provides an adequate estimate of the prey available to right whales in that habitat. However, when predictive relationships are drawn between the habitat-averaged prey concentration (or their indicators) and right whale calving rates or habitat occupancy, the relationships are either qualitatively inferred (e.g., Payne *et al.* 1990, Costa *et al.* 2006), are non-significant, or leave a large portion of the variance in right whale dynamics unaccounted for (e.g., Greene and Pershing 2004, HLista *et al.* 2009, Pendleton *et al.* 2009, Patrician and Kenney 2010). Further, the mechanistic relations among whales, copepods and the physical environment cannot be characterized using these studies because the sampling resolutions and indices are inadequate (i.e., net samples are localized, CPR estimates reflect only the surface layer, or the indicators such as *Chl a* are distantly removed from copepod indices). While the goals of such studies are typically to predicatively model right whale population dynamics for conservation purposes, the conclusions reached indicate that such goal will rarely be achieved based on the methods used, because the models do not describe the right whales niche with the appropriate resolution, precision, or accuracy.

To advance research in this area, Baumgartner *et al.* (2007) proposed that if the mechanisms of prey aggregation within a habitat were spatially variable, then the amount of food available to right whales will not depend solely on large-scale average prey abundance estimates. Aggregation is necessary because right whales must consume a minimum of 10 kJ m^{-3} of energy to gain a net energetic benefit from feeding (Kenney *et al.* 1986). However, right whales have no behavioral mechanisms that aggregate prey, as some other whale species do (e.g., humpback whales). As a consequence, right whales rely completely on the environment to aggregate their food into higher concentration patches at smaller spatial scales within their feeding habitats. The proposal by

Baumgartner *et al.* (2007) was based on information collected during large-scale sampling of *C. finmarchicus* in the Gulf of Maine, western Scotian Shelf (including Roseway Basin) and Grand Manan Basin, which suggested that *C. finmarchicus* was more abundant in the year 2001 than in 2000 (Greene and Pershing 2004, Baumgartner *et al.* 2003a). However, *C. finmarchicus* concentrations near feeding right whales were 2-fold higher in concentration in 2000 than 2001, the aggregative mechanisms measured (surface horizontal temperature fronts) were stronger in 2000 than 2001, and right whale occupancy was higher in 2000 than 2001 (Baumgartner and Mate 2003). The authors cautioned that their conclusion was somewhat speculative as their sample size was limited, however, the merit of the study was in providing the scientific background for further research into the regional interannual variation in the mechanisms of prey aggregation.

Baumgartner and Mate (2003) also made some interesting observations concerning the smaller-scale spatial relationships among right whale occurrence, water mass density and *C. finmarchicus* concentration in Roseway and Grand Manan Basins that is relevant to describing variation at the interannual scale. The above authors observed that the probability of sighting a right whale was higher when the depth of the bottom mixed layer (BML) was shallower (i.e., BML was thicker). In contrast, they observed that *C. finmarchicus* became more abundant or more discretely concentrated as BML depth increased (i.e., the BML became thinner). This implied that the right whales do not forage in the areas of highest *C. finmarchicus* concentration, but rather where *C. finmarchicus* are aggregated at shallower depths. Hence the year-to-year variation in habitat suitability of Roseway Basin could be a function of both the average prey abundance in the habitat, and the strength of copepod aggregation processes that are related to water mass density (e.g., BML depth).

5.1.1 Objectives

The first objective of this chapter is to describe the spatial distribution of copepod abundance and hydrography in the Roseway Basin from surveys conducted in 2007 and 2009. Using these and the analyses from the 2008 survey presented in Chapters 3 and 4, the second objective is to quantify interannual variation in the abundance, distribution,

size- and stage-structure of copepods in Roseway Basin among the years 2007 through 2009. The third objective is to investigate the oceanographic factors that are related to this interannual variation. This third objective is divided into two parts: 1) I first examine large scale processes that affect the habitat-average abundance and distribution of copepods, including temperature and food-dependent copepod production on the Scotian Shelf and water mass advection; 2) I examine interannual variation in copepod aggregating mechanisms within the habitat wherein I include water mass density and its relationship to copepod buoyancy, prey field 'tilting' at the southern margin and its variation at tidal frequencies (Chapter 4), as well as slope water intrusions, and the occurrence of ocean fronts.

5.2 Methods

5.2.1 Sampling

Three surveys were performed in Roseway Basin in late-summer between 2007 through 2009 aboard the R/V *Dominion Victory*. The 2007 survey was exploratory, designed to inform more extensive surveys undertaken in 2008 and 2009. Methods and results are presented here for the 2007 and 2009 surveys, with reference to the 2008 survey where necessary (Chapter 3). Each survey consisted of biological sampling with nets and optical plankton counters (OPC), and hydrographic sampling with CTDs.

Zooplankton samples were collected at several stations during each survey (Table 5.1) using a Bedford Institute of Oceanography Net and Environmental Sampling System (BIONESS; Sameoto *et al.* 1980). In 2007, the BIONESS stations were spread across the Basin (Figure 5.1b) while in 2009, they were co-located at the western end of the Basin (Figure 5.1d). The 2007 and 2009 BIONESS surveys followed precisely the same procedure as the 2008 BIONESS survey described in Chapter 3, with one minor difference. In 2008 we did not collect flowmeter data due to conducting cable problems, whereas in 2007 and 2009 flowmeter data were collected to estimate volume filtered through the nets. Most BIONESS tows were vertical profiles, but in 2007 (station-B06) and 2009 (station-B01) the small-scale horizontal variation in the deep layer was sampled, in the same way as station-B02 in 2008 (Figure 3.7). All BIONESS tows in 2007 were collected during daylight hours. In 2009, BIONESS stations B01 and B02

were collected during the day, while B03 was collected at night. All BIONESS-OPC profiles were smoothed with a moving average filter, first with a 5 s window, then a second time with a 7 s window. Whenever possible vertical CTD casts were deployed using a Seabird-25 CTD; vertical profile data will be shown only for the 2007 survey (Figure 5.1b).

In 2008 and 2009, zooplankton abundance-at-size estimates, particularly for the *C. finmarchicus* C5 and *C. hyperboreus* C4 combined size distribution, were obtained using an Optical Plankton Counter attached to a V-fin along with a digital flowmeter and a Seabird-37 microCAT CTD (Towed Underwater Biological Sampling System, TUBSS). No TUBSS data were collected in 2007. The general sampling procedure for the 2008 - 09 TUBSS surveys, and details specific to the 2008 survey, are provided in Chapter 3. Below I provide details specific to the 2009 survey. In 2009, sampling was limited to two cross-Basin transects (transect-11 and -12) ~18 km in length on opposite sides of the Basin, interrupted by one along-Basin transect 52 km in length that transected the middle of the Basin (transect-13) (Table 5.2, Figure 5.1d). Transect-12 crossed transect-13 at the 15 km mark at the western Basin margin, whereas transect-11 crossed transect-13 at the 40 km mark near eastern end of the Basin. TUBSS data were collected during the day (transects-11 and 12) and at night (transect-13).

In 2009, TUBSS data (plankton particle size frequency, depth, pitch), CTD data and GPS navigation/flowmeter data were recorded in real time and logged at 0.5 s, 1 - 2 s and 1 s intervals, respectively. CTD, GPS and OPC data streams were integrated post-deployment at 1 second intervals. Data recording and storage were interrupted at ~1 h intervals to obtain files of manageable size and data interruption was generally less than 3 s. Volume filtered was determined using the product of flowmeter speed, elapsed time and OPC sampling tunnel cross-sectional area where the latter was corrected for instrument pitch. Flowmeter speed was systematically lower when TUBSS was deployed downward, leading to higher depth-specific zooplankton particle concentrations relative to the subsequent upward tow. Michaud (2005) observed the same phenomenon using the same equipment during a similar survey in Grand Manan Basin, attributing it to 'shielding' of the flowmeter by the tow body during nose-down descent. Separate

empirically derived calibration equation were applied in each case to correct the downward flowmeter estimates (upward = 1.02•downward + 0.37, P <0.001, $r^2 = 0.78$).

5.2.2 Zooplankton taxonomic, size frequency and energy content analyses

The details of these procedures are provided in Chapter 3. Energy content data were only collected in 2007, and the 2007 energy estimates were applied to TUBSS-OPC concentration estimates in the 2008 and 2009 surveys to obtain energy density (kJ m^{-3}) estimates in those years.

5.2.3 TUBSS-OPC data analysis

Details of the TUBSS-OPC data analysis for 2008 and 2009 are provided in Chapter 3. The 2008 and 2009 BIONESS-OPC data were regressed against the BIONESS-net data (Figure 5.2a), and this relationship was used to calibrate the TUBSS-OPC. No equivalent net correction was applied to the 2007 BIONESS-OPC data because the relationship between the BIONESS-OPC concentration and BIONESS net concentration was not different from 1:1 (Figure 5.2b). The 2007 data were not included in the calibration in Chapter 3 because 1) the copepod concentrations collected in 2007 were 2 - 3 times higher than in 2008 - 09 (Figure 5.2b), so any calibration using all three years would be unfairly weighted by the 2007 data, and 2) there were no TUBSS-OPC data collected in 2007.

5.2.4 Energy Density of the C5 prey field

Details methods for determining energy density in the C5 prey field are provided in Chapter 3 under section 3.2.6, and were applied to the 2008 and 2009 data.

5.2.5 Interannual comparison 2007 – 2009

Using the analyses from 2007 and 2009 (this Chapter) and 2008 (Chapters 3 and 4), I make comparisons among years for a number of variables. First, I compare the biological data in terms of copepod abundance, stage-structure, size frequency, and species composition. I then compare the major water masses and their relative hydrographic properties in relation to copepod variation.

Table 5.1. Survey periods and the numbers of BIONESS tows, vertical CTD casts and TUBSS transects performed during each survey conducted in 2007, 2008 and 2009.

Year	Cruise dates (mm/dd)	BIONESS tows	Vertical CTD casts	OPC/CTD transects
2007	09/10 – 09/17	7	20	0
2008	09/04 – 09/13	4	6	10
2009	08/17 – 08/27	3	1	3

Table 5.2 Summary characteristics of each transect sampled with TUBSS in Roseway Basin during 17 through 27 August 2009, including start and end dates and times (ADST) and latitudes and longitudes, as well as nominal transect headings and extents and the maximum sampling depths.

Year	Transect No.	Start Date (mm/dd)	Start Time (hh/mm)	End Date (mm/dd)	End Time (hh/mm)	Start Lat	Start Lon	End Lat	End Lon	Heading	Length (km)	Max depth sampled (m)
2009	11	8/26	09:16	8/26	14:00	43.053	-65.211	43.053	-65.208	NW	18.28	166
	12	8/25	09:40	8/25	13:30	42.931	-65.340	42.790	-65.245	SE	19.70	144
	13	8/25	21:44	8/26	07:57	42.825	-65.499	43.095	-65.041	NE	52.35	157

Figure 5.1 Bathymetric chart of Roseway Basin survey design, showing (a) the distribution of the relative probability (P) of observing a right whale in Roseway Basin (adapted from Vanderlaan *et al*. 2008), where the dashed line represents the boundaries of the provisional Critical Habitat and the solid rectangle represents the boundaries of (b-d). Panels b-d show the zooplankton prey field survey executed in 2007, 2008 and 2009, respectively. Each BIONESS tow location is identified by B0x labels and solid lines denote the TUBSS transect survey tracks, each of which is identified by numbers 1 - 10. Isobath contours are spaced at 10 m and the 100 m contour is labeled in (b). The 24 hour transect line is depicted by a red line in (b).

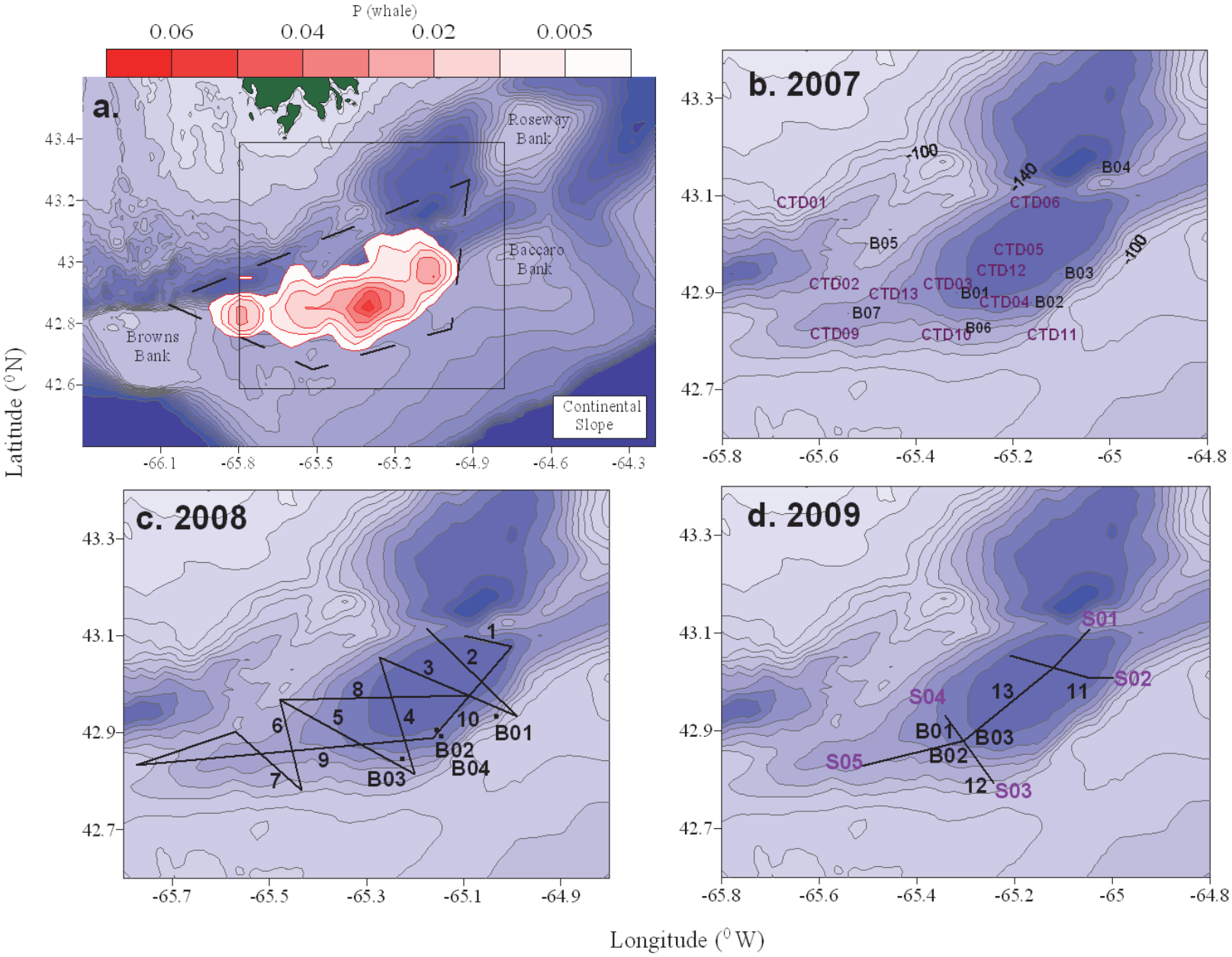
P (whale)
0.06
0.04
0.02
0.005
a.
Roseway Bank
Baccaro Bank
Browns Bank
Continental Slope
b. 2007
CTD01
CTD02
CTD03
CTD04
CTD05
CTD06
CTD09
CTD10
CTD11
CTD12
CTD13
B01
B02
B03
B04
B05
B06
B07
-100
-140
c. 2008
d. 2009
S01
S02
S03
S04
S05
Latitude (°N)
Longitude (° W)

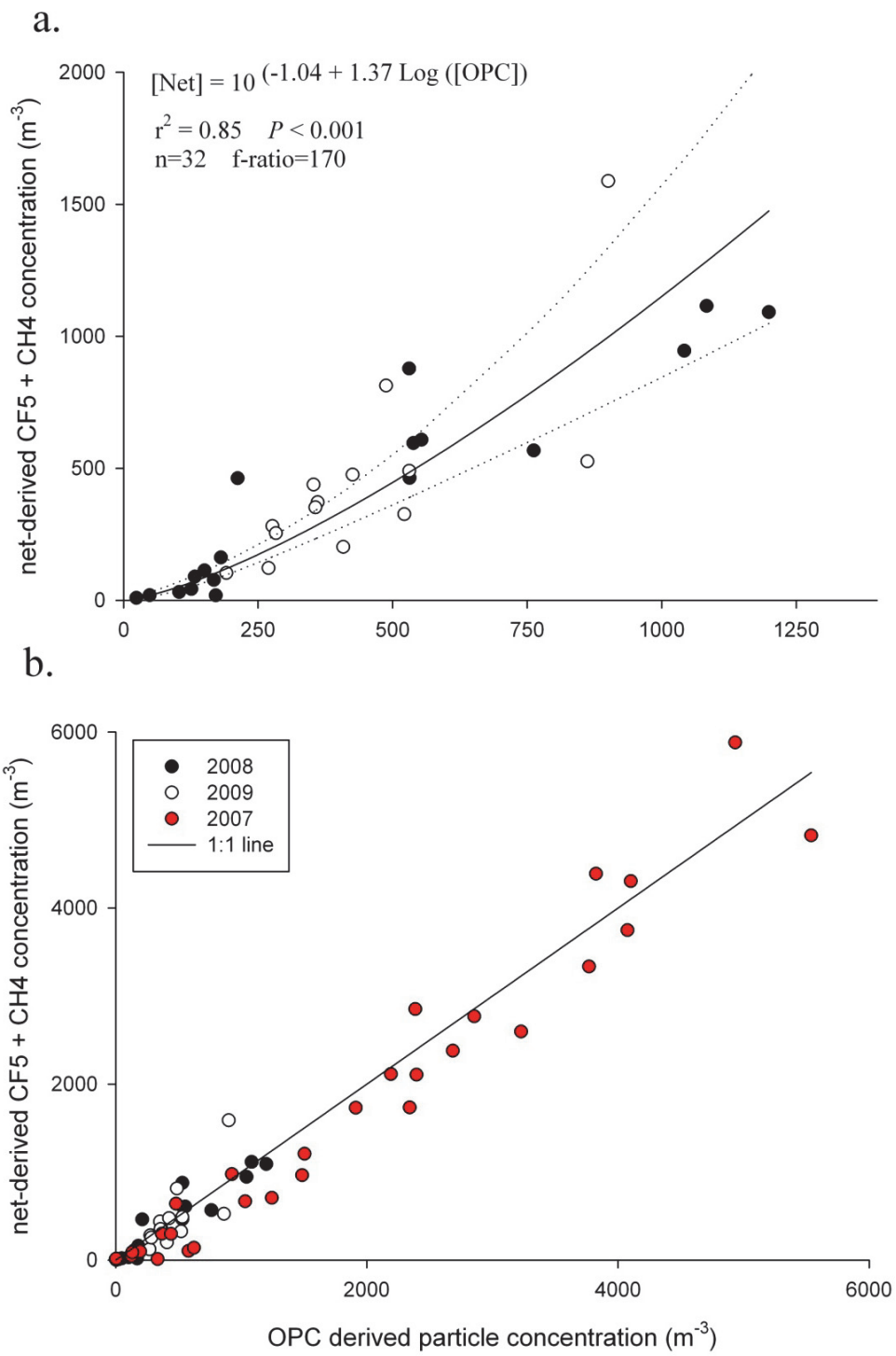

Figure 5.2 (a) Regression-based calibration of the BIONESS-OPC and corresponding BIONESS-net derived *C. finmarchicus,* CF5 and *C. hyperboreus* CH4 concentrations using data from 2008 and 2009, where dotted lines denote the 95 % confidence intervals around the prediction. (b) The variables are the same as in (a), but include all data from 2007 through 2009. The 1:1 line is plotted in (b).

5.3 Results

5.3.1 2007 field season

5.3.1.1 Copepod distribution and abundance

Vertical profiles of copepod abundance measured using BIONESS net samples at stations B01 - B05 and B07, indicate that 2007 was a highly productive year for *Calanus* spp. and particularly *C. finmarchicus* in Roseway Basin (Table 5.3). Late stage *C. finmarchicus* (C4, C5, adult males and females) were abundant at all stations. The diapausing *C. finmarchicus* C5s dominated the copepod assemblage at depths >100 m and were followed by *C. hyperboreus* C4s, *C. glacialis* C5s and *C. finmarchicus* C4s. Concentrations of *C. finmarchicus* C5s at depth at stations B01, B02, B03 and B07 were exceptionally high, ranging between 1683 and 4041 m^{-3}. Adult male and female *C. finmarchicus* concentrations were also elevated (10 to 100 m^{-3}) for the time of year and are indicative of an autumn generation. The absence of younger *C. finmarchicus* C3s and the high abundance of the later stages indicate that the majority of the copepods belonged to a single cohort with the majority in arrested development (assumed based on their depth distribution, stage-structure and lack of diel-vertical migration). Concentrations of the Arctic *C. hyperboreus* and *C. glacialis* species were also high in 2007, representing an average of 36 % (range 17 % to 65 %) of the total *Calanus* spp. abundance. The *C. hyperboreus* specimens were primarily C4s and rarely C5s while *C. glacialis* were primarily C5s and rarely adults. *Metridia* spp. and *Pseudocalanus* spp. were relatively rare in comparison to the multiple stages of the *Calanus* spp.

Vertical profiles of the combined *C. finmarchicus* C5 and *C. hyperboreus* C4 (hereafter, diapausing copepods) concentration estimates derived from the BIONESS-OPC showed considerable variation among stations, with some features in common (Figure 5.3). At station B05, located on bank to the northwest of the Basin, the diapausing copepods were at relatively low concentrations throughout the water column to the maximum depth of 100 m. At station B07, located at the western Basin margin, the concentrations were low until they increased abruptly to ~12 000 m^{-3} at ~120 m depth and remained at >5 000 m^{-3} until the maximum sampling depth of 140 m was reached; indicative of a concentrated ~30 m depth layer. Moving eastward toward deeper water, station B01 had a similar vertical concentration profile as at B07, though the rapid

increase in concentration did not occur until 120 m depth though the concentration layer was also ~30 m in depth (Figure 5.3). To the northeast and along the southern slope of the Basin, stations B02 and B03 had similar vertical concentration profiles markedly different from all other stations. Diapausing copepod concentrations at stations B02 and B03 increased gradually with depth, beginning at 40 m and reaching a maximum of ~8000 and ~12 000 m^{-3} at 140 m (50 to 100 m depth layer). The multi-modal depth distribution of concentration at station B03 was indicative of vertical patchiness within the relatively thick layer. The differences among vertical concentration profiles located near the western Basin margin (B07 and B01) and the central-Basin southern-slope (B02 and B03) were in agreement with the BIONESS net estimates (Figure 5.3, Table 5.3). At B01 and B07, the highest concentrations of *C. finmarchicus* C5 were found in a single deep-net collection below 115 m depth, while at B02 and B03, *C. finmarchicus* C5s were highly concentrated in all four net collections below 75 m depth. Finally, at station B04, located at the eastern Basin margin, concentrations were fairly low throughout the water column, with a moderate increase below 100 m depth to ~3500 m^{-3} after which concentrations below 100 m depth remained above 1000 m^{-3} (Figure 5.3).

Measures of diapausing copepod abundance at depth over a 1.2 km transect at station B06 on the southern Basin margin revealed both long (~100 m) and short (~50 m) spatial variation (Figure 5.4). At longer scales, concentrations steadily increased from ~1000 m^{-3} at the beginning of the transect, to ~3000 m^{-3} at the end of the transect. When the series was treated first with a high pass filter to remove the longer variations and then subjected to an autocorrelation analysis I was able to resolve a weak ($r = 0.3$) autocorrelation at a 50 m lag. Horizontal spatial variation in the physical properties at the 10 m – 1 km scale was relatively small at depth and most of the variation is related to depth of tow along the transect. There was no significant autocorrelation in these hydrographic variables, though this is addressed further in Section 5.3.1.3 below.

Table 5.3 Zooplankton species and stage assemblage concentrations (m^{-3}) based on BIONESS net samples collected at 6 stations (B01 - B05, B07) in 2007. Concentration estimates are provided for each of the depth integrated nets (left column) and the deepest net collection (right column), for each station.

Species	B01		B02		B03		B04		B05		B07	
Tow depth interval:	4-148 m	126-146 m	0-141 m	124-142 m	0-151 m	123-151 m	0–145 m	n/a	0-120 m	100-115 m	0-130 m	115-128 m
C. finmarchicus C3	0	0	0	0	0	0	0		0	0	0	0
C. finmarchicus C4	52	334	97	130	16	1549	12		7	12	91	385
C. finmarchicus C5	231	1683	790	1874	98	3728	94		71	115	1057	4041
C. finmarchicus M	4	49	3	10	2	101	5		3	9	8	0
C. finmarchicus F	15	12	57	58	112	29	8		9	2	23	27
C. hyperboreus	71	383	203	781	37	2240	10		10	69	170	824
C. glacialis	11	223	99	518	3	245	8		22	5	26	93
Metridia spp.	32	173	4	20	1	43	32		6	26	17	13
Centropages spp.	0	0	0	0	0	0	0		0	0	0	0
Pseudocalanus spp.	24	49	3	0	0	0	0		39	139	29	0
Total Mesozoop.	444	2921	1256	3391	271	7976	173		169	377	1420	5384
Macrozooplankton	<1	<1	0	0	0	0	0		0	3	11	40

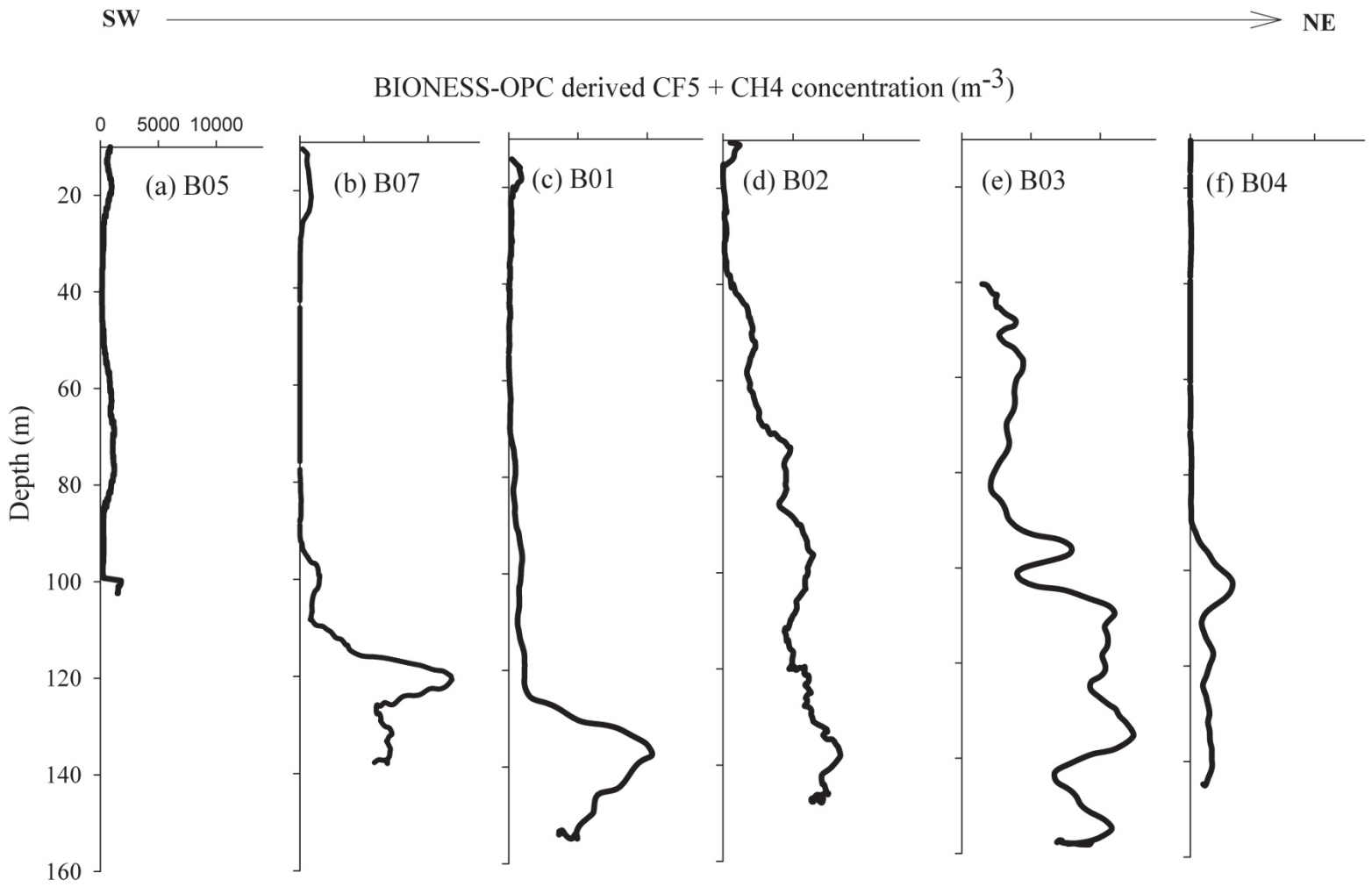

Figure 5.3 Vertical profiles of the BIONESS-OPC derived concentration of *Calanus finmarchicus* stage-C5, CF5, and *C. hyperboreus* stage-C4, CH4, collected at BIONESS stations B01-B05 and B07 that were distributed in a roughly SW to NE direction across Roseway Basin in 2007 (Figure 5.1b).

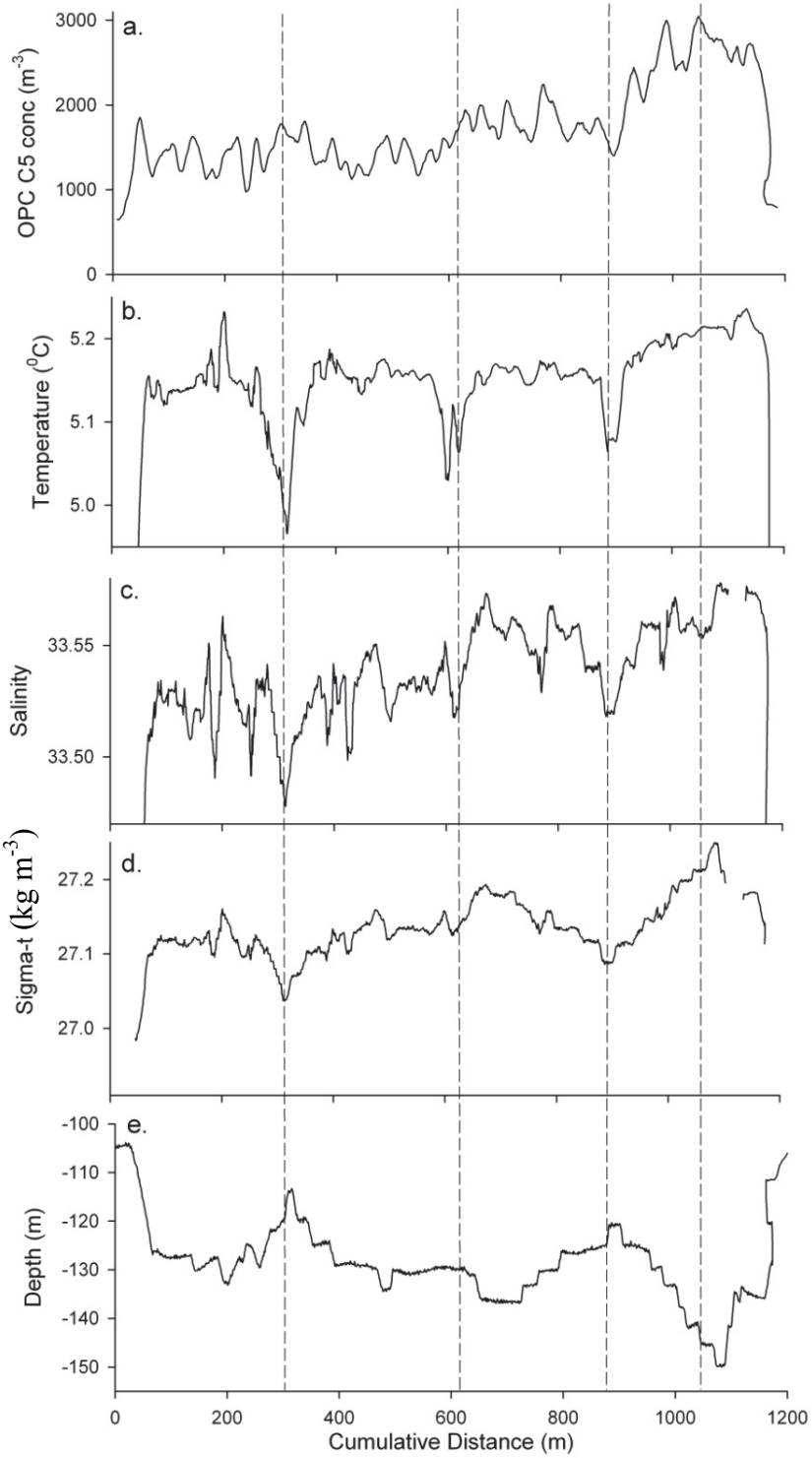

Figure 5.4 High resolution horizontal spatial variation at depth recorded at station-B06 in 2007 showing: (a) BIONESS-OPC derived diapausing copepod concentration; b) water temperature (^{o}C); c) salinity; d) σ_t (kg m^{-3}); and e) instrument depth (m). Peaks in the data are noted with dashed lines for comparison among panels.

5.3.1.2 Hydrography

The 2007 hydrographic survey results are presented as 3 sets of stations grouped by their location in a cross-basin direction (from SW to NE) for ease of comparison with the 2008 sectional profile data. Stations CTD02, CTD06 and B04 are grouped together and represent the hydrography along the northern Basin margin (Figure 5.5). Stations B07, CTD13, CTD03, CTD12 and CTD05 represent the mid-Basin hydrography (Figure 5.6). Stations CTD09, CTD10, CTD04 and B03 represent the hydrography along the southern Basin margin (Figure 5.7).

Overall, there was surprisingly little spatial variation in the T-S or density properties across or along the Basin. The general structure included warm, low salinity water near the surface sitting above a cold intermediate layer at 20 to 60 m depth. Below the cold intermediate layer, the water generally warmed and increased in salinity, until the T-S properties became relatively constant with depth below ~100 m. The largest spatial gradient was in the SW - NE direction, where in the SW the intermediate layer was absent and the water near-bottom was lower in density. Toward the NE the cold layer became more prominent, the pycnocline slope increased, and bottom density increased.

Water mass temperature along the northern margin was ~10 ^{o}C at the surface, and decreased with depth to the cold (min T = 2^{o}C) intermediate layer at 20 - 80 m (Figure 5.5a-c). The thermocline was more pronounced at the NE end of the Basin. The water then remained cold until the seafloor at the western margin (Figure 5.5a) or warmed with depth in the central Basin (Figure 5.5b). We lost communication with BIONESS at station B04 below 90 m (Figure 5.5c) but it appears to follow the same trend as at station CTD06. Salinity at all three stations was lowest at the surface and increased monotonically with depth. Below 100 m at station CTD06, the water became very uniform, maintaining a constant T-S profile with depth. At the western end of the northern margin, density was fairly uniform with depth, whereas to the east there was a clear pycnocline at 20 m. Density at depth was higher at the eastern end than the western end of the northern margin. The trends described above also apply to the SW - NE trend along the middle of the Basin (Figure 5.6) and along the southern margin (Figure 5.7) and are substantiated by the T-S diagram for the profiles at station CTD06 on the NW

margin, station CTD05 collected mid-Basin, and station CTD04 collected on the SE margin (Figure 5.8). They are virtually identical below 70 m.

The water masses at depth in Roseway Basin in 2007 are described by a simple two end-member system that transitions between Basin Water (BW, $T = 2^{o}C$, $S = 32.5$, $\sigma_t = 26$ kg m^{-3}), which dominates at 50 m depth, and intermediate Basin Water (iBW, $T = 6^{o}C$, $S = 33.8$, $\sigma_t = 26.7$ kg m^{-3}), which dominates in the deep Basin (Figures 5.8 and 5.9). No modified Bottom Water (mBW) was present in Roseway Basin in 2007, as was present in 2008 (Figures 3.15 and 3.16). Basin Water originates from the Gulf of St. Lawrence (GoSL) and is carried along the Scotian Shelf by the inner arm of the Nova Scotia Coastal Current. Intermediate Basin Water also originates from the GoSL, but its path from the GoSL to the Shelf is along the Shelf break, where it is influenced by slope water before intruding on-Shelf periodically through deep channels. Within the deep water (90 - 120 m) of the eastern and central Basin, there was only Intermediate Basin Water, while at the western margin, Basin Water was dominant at depth (Figure 5.9).

Horizontal spatial variation at the 10 m – 1 km scale was also very small at depth (Figure 5.4). Most of the variation can be explained by the tow depth as we moved along the transect. There was no spatial autocorrelation in the hydrographic variables.

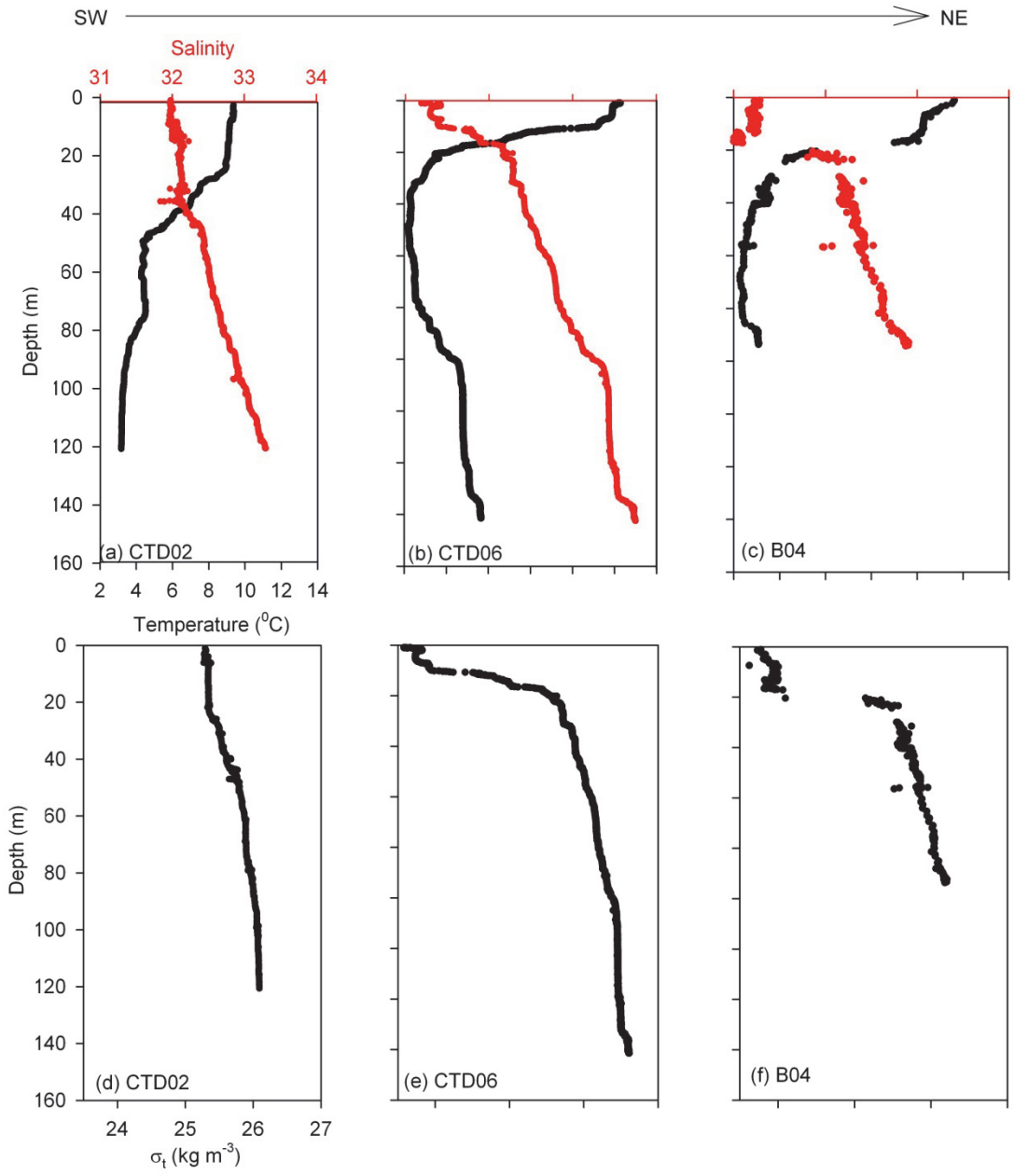

Figure 5.5 Vertical CTD profiles collected at stations CTD02, CTD06, and B04 in 2007 along the northern margin of Roseway Basin. Panels (a) through (c) show the temperature and salinity while panels (d) through (f) show the density. Profiles are presented in a SW to NE direction, and the locations are provided in Figure 5.1.

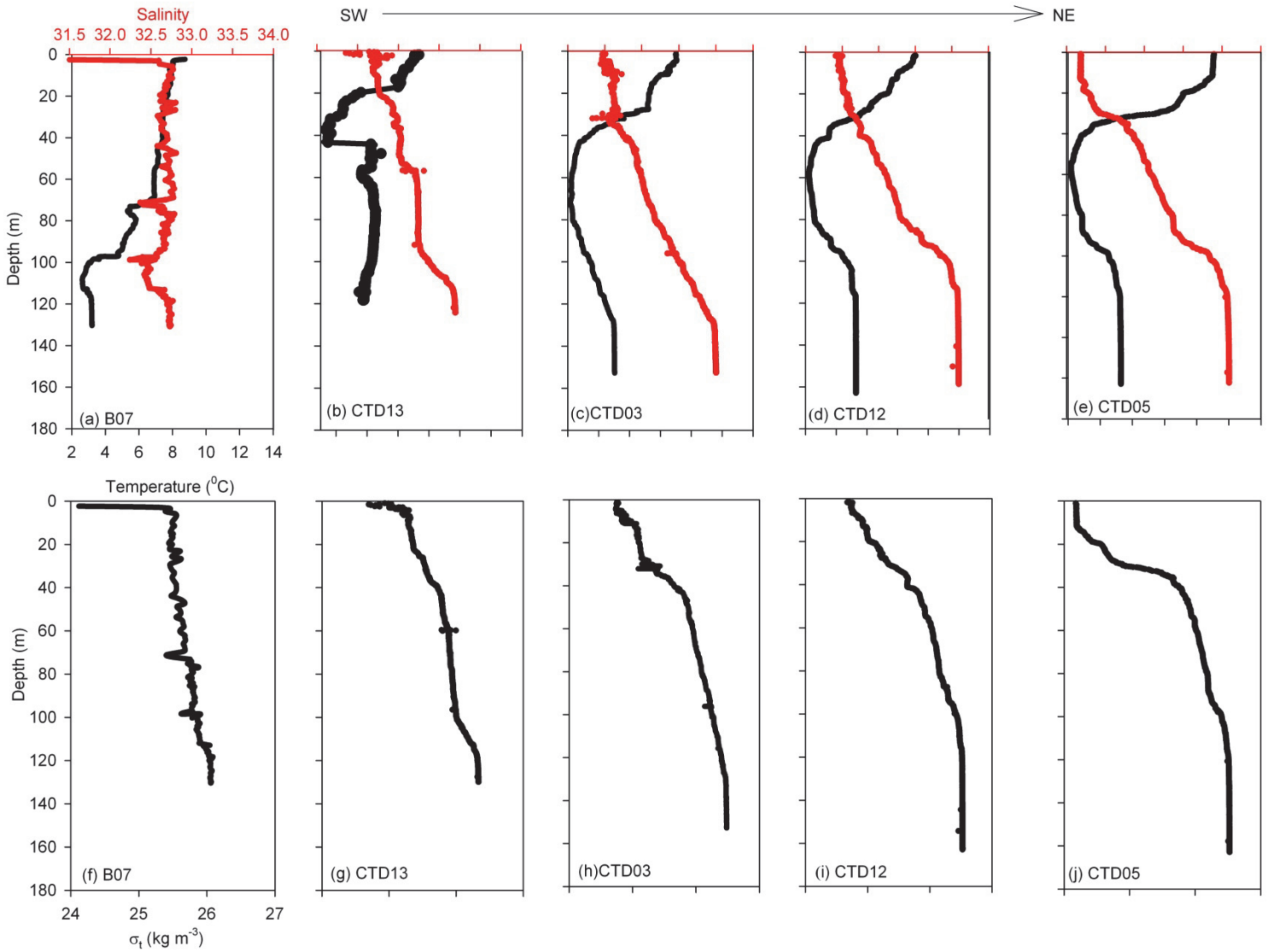

Figure 5.6 Vertical CTD profiles collected in 2007 at stations B07, CTD13, CTD03, CTD12 and CTD05 that transect the middle of Roseway Basin in 2007 in a SW to NE direction. Panels (a) through (e) show the temperature and salinity while panels (f) through (j) show the density. The locations are provided in Figure 5.1.

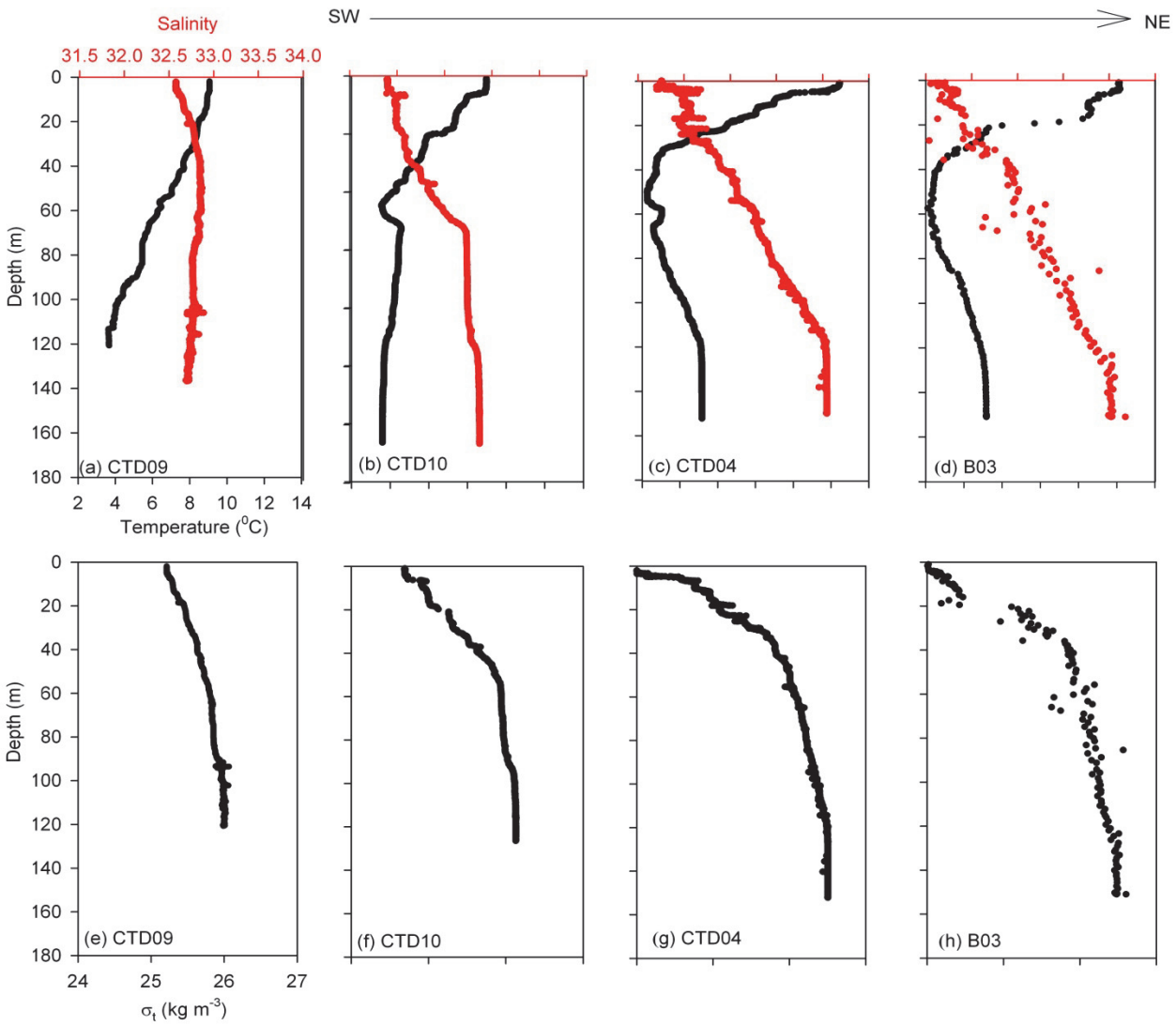

Figure 5.7 Vertical CTD profiles collected in 2007 at stations CTD09, CTD10, CTD04 and B03 that transected the southern boundary of Roseway Basin in 2007 in a SW to NE direction. Panels (a) through (d) show the temperature and salinity while panels (e) through (h) show the density. The locations are provided in Figure 5.1.

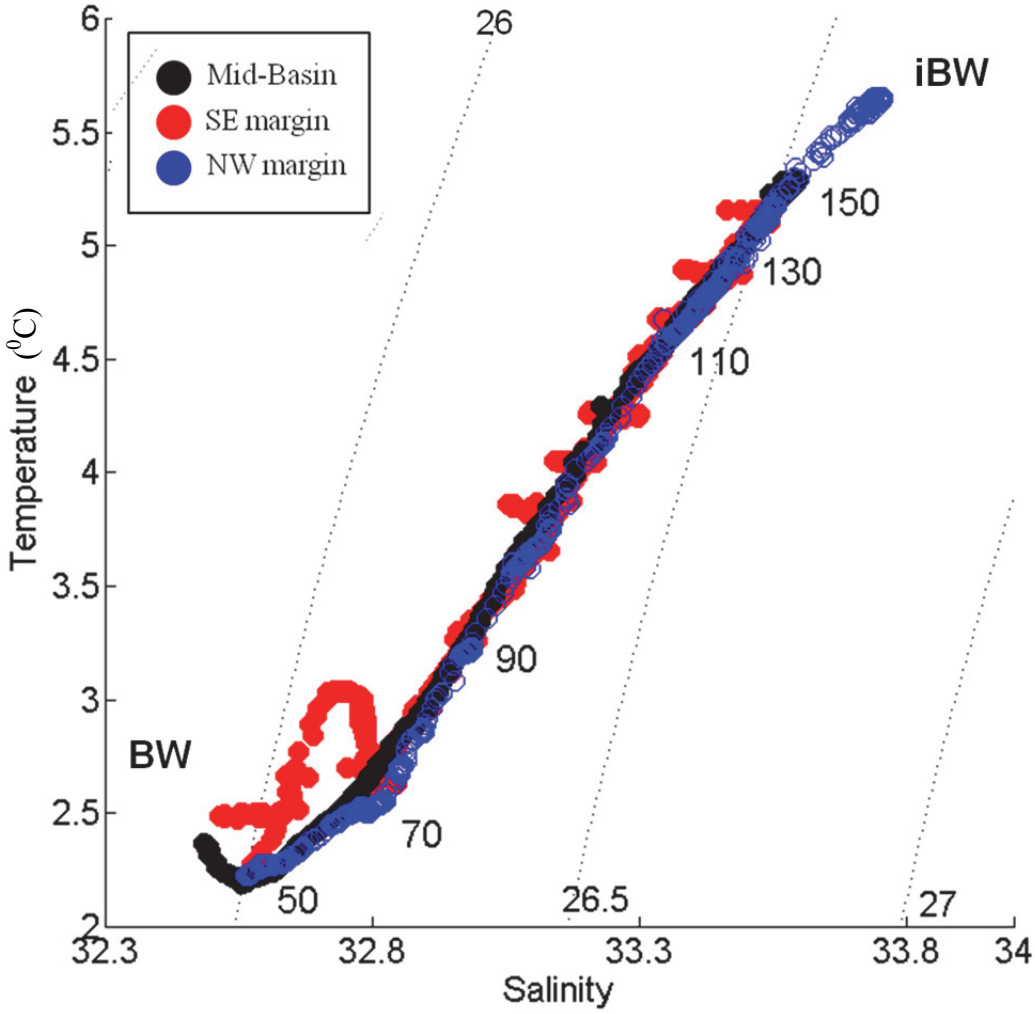

Figure 5.8 Vertical temperature-salinity profiles >50 m depth collected at station CTD06 on the NW margin (blue), station CTD05 collected mid-Basin (black), and station CTD04 collected on the SE margin (red) of Roseway Basin in 2007. Water mass end-members are shown, where BW = Basin Water and iBW = intermediate Basin Water. Depths are labeled at 20 m intervals. Dotted lines depict the σ_t isopycnals, which are spaced at 0.5 kg m^{-3} and labeled.

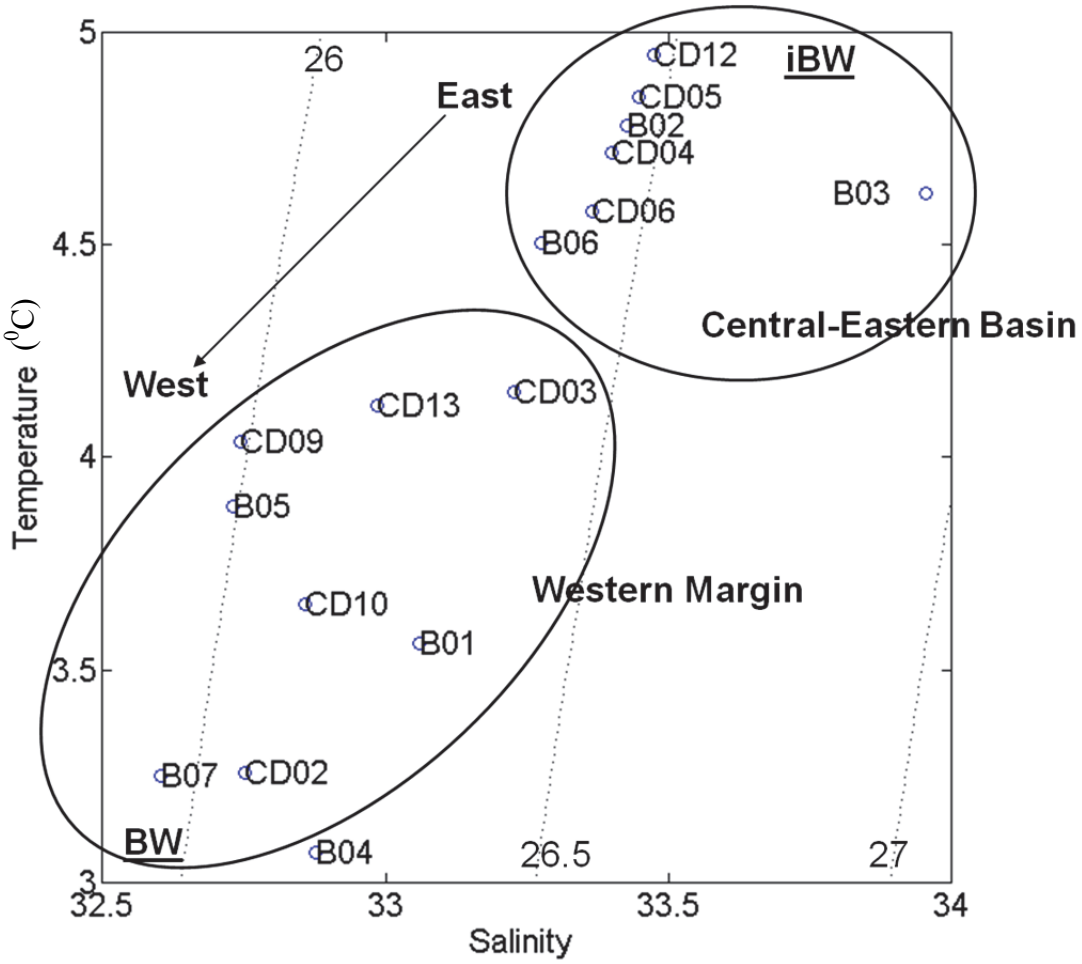

Figure 5.9 Temperature-salinity diagram from each CTD profile collected in Roseway Basin in 2007 with the Seabird-CTD (CDxx) or BIONESS-CTD (B0x) and averaged over the 90 - 120 m stratum (locations are in Figure 5.1). Water mass end-members are displayed, where BW = Basin Water and iBW = intermediate Basin Water. Dotted lines depict the σ_t isopycnals, which are spaced at 0.5 kg m^{-3} and labeled. The major geographical groupings of profiles are circled and identified as being from the western margin or the central-eastern margin.

5.3.1.3 Copepod - hydrography relationships

Cross-correlation analysis between the de-trended diapausing copepod concentration and hydrographic variables along the horizontal transect at depth (Figure 5.4) was used to examine km scale spatial associations between the prey and hydrography. The best cross-correlation was between water mass density and copepod concentration. These were correlated (r = 0.38) with a lag of 200 m and out of phase by 30 m. The primary determinent of the density variation was variation in the depth of tow, indicating that the dominant scale of variation is vertical and not horizontal, consistent with other results presented earlier.

The co-located profiles of diapausing copepod concentrations and water mass density show that the 1026 kg m^{-3} isopycnal may be a vertical density barrier below which the diapausing copepods aggregate. At stations B07 and B01, each with no strong pycnocline, the copepod concentrations were low throughout the upper water column and then increased abruptly at depth (120 and 130 m respectively), whereas at stations B02 and B03 the concentrations began to increase with depth from below the pycnocline, reaching maxima at or below 100 m (Figure 5.10). At station B07, with no pycnocline, density was generally low throughout the column and did not reach the 1026 kg m^{-3} until 110 m, where copepod concentration abruptly increased. At station B01, with a weak pycnocline at 50 m, density did not reach 1026 kg m^{-3} until ~80 m depth, where copepod concentrations began to increase (Figure 5.10). The maximum concentration at B07 was coincident with a density of 1026.2 kg m^{-3}. At stations B02 and B03, copepod concentrations were elevated below the 50 m pycnocline where density at the bottom of the pycnocline was 1026 kg m^{-3}. At station B03, the multimodal maximums in concentration (10 000 m^{-3}) were associated with densities near or above 1026.2 kg m^{-3}.

The relationship between water mass density and the vertical copepod distribution coincides with water mass variation among stations. At the western end of the Basin (B01 and B07), BW was dominant at depth, while at the eastern end of the Basin (B02, B03 and B06), iBW dominated at depth (Figure 5.8). I demonstrated in Chapter 3 that in 2008, the diapausing copepods were associated with iBW and not with the less dense BW.

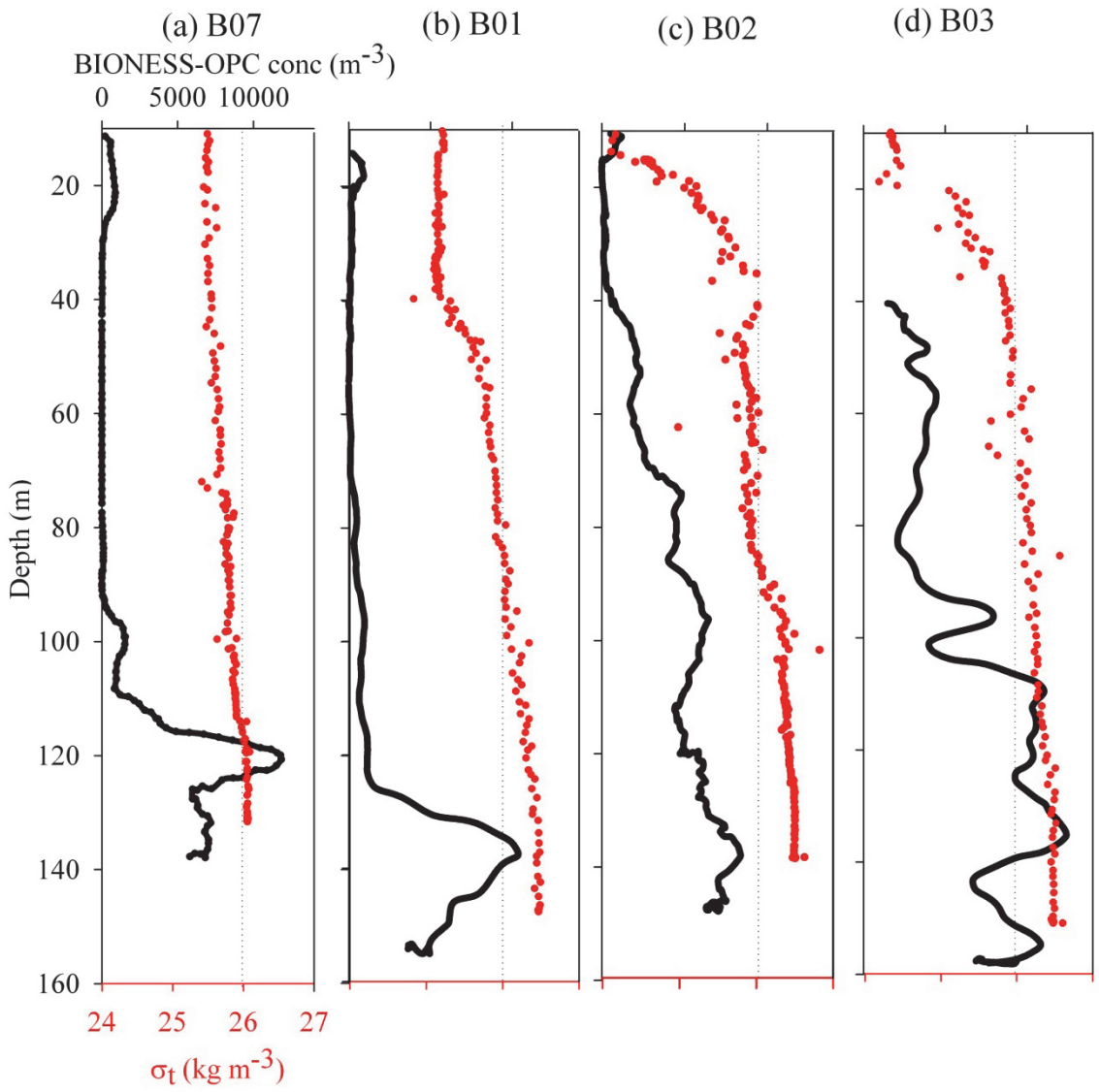

Figure 5.10 Vertical profiles of BIONESS-OPC derived concentrations of *Calanus finmarchicus* stage-C5, CF5, and *C. hyperboreus* stage-C4, CH4, (black) and water mass density (σ_t, kg m^{-3}) (red) collected at BIONESS stations (a) B07, (b) B01, (c) B02 and (d) B03 in 2007. The 26 kg m^{-3} σ_t isopycnal is referenced with a dotted line on each panel.

5.3.2 2009 field season

5.3.2.1 Mesozooplankton distribution and abundance

The surface copepod layer

Based on the outcome of the 2007 and 2008 surveys, it was decided to focus the BIONESS and TUBSS sampling effort in 2009 on the deep Basin where diapausing copepods aggregate. Unexpectedly, post-cruise analysis of the 2009 BIONESS-OPC data from three separate vertical profiles showed that the 20 to 50 m layer (referred to as the 'surface layer' to discriminate it from the 'deep diapausing layer') contained large concentrations of CF5-sized animals (Figure 5.11a-c). A deep (presumed diapausing) copepod layer was present near-bottom, though concentrations were very small in comparison to the surface layer.

At station B01 in 2009, all nets were opened at depth to collect data on km-scale variation in the deep copepod layer (Table 5.4). At depth, C5s dominated the abundance, but all other species and stages measured in 2007 (Table 5.3) and 2008 (Table 3.3) were also present, and in greater abundance, in 2009. This indicated that the system was more diverse than other years (e.g., no *Centropages* spp. in 2007). At station B02, collected during daylight, the surface layer (0 - 29 m depth) contained relatively high abundances (200 - 700 m^{-3}) of *C. finmarchicus* C3s and C4s (Table 5.5). There were also many *C. finmarchicus* C5s in the surface layer, indicating that not all C5s were diapausing at the time of sampling. At station B03, sampled at night in a vertically structured manner, *C. finmarchicus* C3s, C4s and adult females were concentrated near the surface, and there was no clear evidence of a deep C5 layer; instead the C5s were distributed at low abundance throughout the water column (Table 5.6). While there was no clear evidence of a deep layer in the deep nets at B03, the BIONESS-OPC did measure a weak deep layer that was vertically thicker and shallower at night than during the day (Figure 5.11b, c). During night sampling (B03, Figure 5.11c), the OPC concentration at the surface was greater and closer to the surface than during the day (B02, Figure 5.11b), presumably reflecting diel-vertical migration. High abundance of early stage *C. finmarchicus*, abundance of C5s in surface nets, and diel-vertical migration all indicated that the cohort of copepods measured in 2009 was at an earlier phase of development than that which observed in 2007 and 2008.

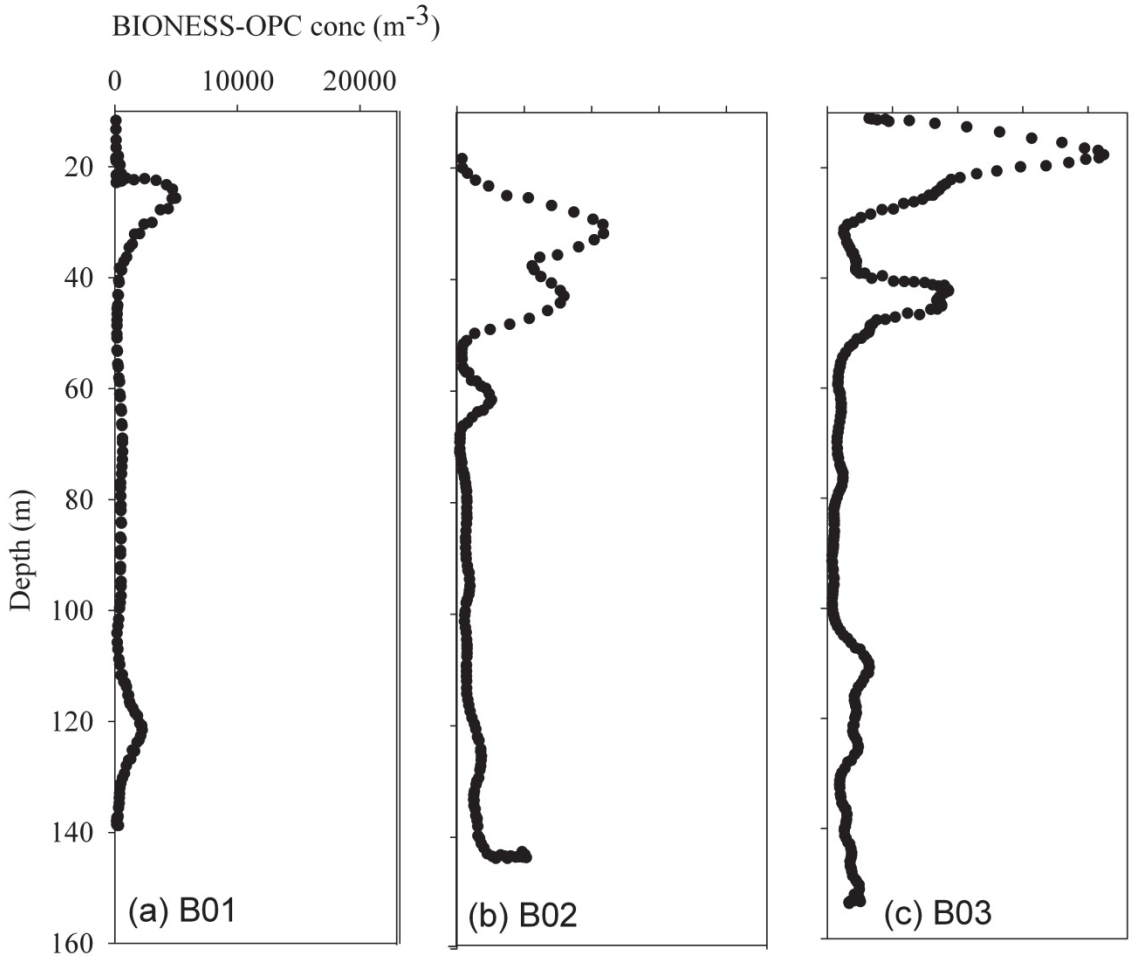

Figure 5.11 Vertical profiles of BIONESS-OPC derived concentrations of *Calanus finmarchicus* stage-C5 and *C. hyperboreus* stage-C4 sized particles collected at BIONESS stations (a) B01, (b) B02 (daytime sampling) and (c) B03 (night sampling) during the 2009 survey of Roseway Basin. The geographic location of each profile is depicted in Figure 5.1d.

Table 5.4 Zooplankton species assemblage and concentrations (m^{-3}) in 2009 collected with BIONESS at station B01 during daylight hours. B01 consisted of one depth integrated net and four nets that opened and closed at depths > 110 m. Depth intervals of each net are provided.

Tow depth interval:	0 - 139 m	118 - 136 m	118 - 122 m	116 - 121 m	115 - 131 m
Calanus finmarchicus C3	27	0	1	0	0
Calanus finmarchicus C4	62	5	1	2	1
Calanus finmarchicus C5	115	354	414	445	326
Calanus finmarchicus M	2	3	5	4	3
Calanus finmarchicus F	13	5	4	4	3
Calanus hyperboreus	8	17	26	33	27
Calanus glacialis	1	12	14	28	14
Metridia spp.	21	49	27	58	70
Centropages spp.	6	0	0	1	0
Pseudocalanus spp.	13	10	8	21	16
Total Mesozooplankton	291	494	527	648	504
Macrozooplankton	<1	4	2	1	2

Table 5.5 Zooplankton species assemblage and concentrations (m^{-3}) in 2009 collected with BIONESS at station B02 during daylight hours. Depth intervals of each net are provided.

Tow depth interval:	0 - 136 m	125 - 135 m	106 - 130 m	21 - 105 m	0 - 29 m
Calanus finmarchicus C3	6	3	0	56	144
Calanus finmarchicus C4	51	8	19	547	673
Calanus finmarchicus C5	465	1467	745	522	497
Calanus finmarchicus M	7	8	5	16	5
Calanus finmarchicus F	32	11	16	34	3
Calanus hyperboreus	31	142	74	4	0
Calanus glacialis	19	83	41	7	0
Metridia spp.	31	19	19	29	0
Centropages spp.	19	0	0	7	119
Pseudocalanus spp.	12	29	16	51	60
Total Mesozooplankton	748	1792	960	1609	1068
Macrozooplankton	1	8	5	2	0

Table 5.6 Zooplankton species assemblage and concentrations (m^{-3}) in 2009 collected with BIONESS at station B03 during the night. Depth intervals of each net are provided.

Tow depth interval:	0 - 146 m	129 - 147 m	70 - 131 m	46 - 71 m	0 - 46 m
Calanus finmarchicus C3	188	0	1	10	80
Calanus finmarchicus C4	358	16	11	10	139
Calanus finmarchicus C5	318	252	234	95	202
Calanus finmarchicus M	5	11	5	5	8
Calanus finmarchicus F	35	6	5	21	47
Calanus hyperboreus	8	31	22	9	0
Calanus glacialis	5	42	16	9	1
Metridia spp.	48	76	61	25	36
Centropages spp.	23	0	0	1	10
Pseudocalanus spp.	15	23	20	14	33
Total Mesozooplankton	1068	478	397	238	671
Macrozooplankton	0	2	0	2	2

The large discrepancy between the BIONESS-net concentrations of mesozooplankton at the surface (Tables 5.5 and 5.6) and the net-calibrated OPC-concentrations in the surface layer (Figure 5.11) indicated that the net calibration I developed for the deep layer does not apply to the surface layer. Since *C. finmarchicus* C3 and C4 overlap with the smaller end of the size distribution of *C. finmarchicus* C5, it is possible that the OPC size-range selection (bin classes 9 -16) estimated the abundance of all three stages. As in Baumgartner (2003), I addressed this possibility by examining the potential of 'masking' the small end of the C5 OPC-size frequency distribution by smaller animals at the surface layer compared with the deep layer (Figures 5.12 and 5.13). I determined in Chapter 3 that the combined size frequency distribution of *C. finmarchicus* C5 and *C. hyperboreus* C4 was normally distributed across OPC bin classes 9 - 16 (Figure 3.4). At 30 m depth at station B02, where the surface layer maximum occurred (Figure 5.12a), the OPC measured animals in bin classes 9 to 14, consistent with the presence of *C. finmarchicus* C5 (Figure 5.12b). However, there were also animals in bin classes 7 and 8, and in bin class 9 the number of animals measured was greater than expected if the distribution were normal (Figure 5.12b). This indicates that there was an overlap between animals encompassing size classes 7 - 9 (likely *C. finmarchicus* C3 and C4 based on our collections, and possibly other small species such as *Centropages* spp.) and animals in size class 9 - 14 (likely *C. finmarchicus* C5 based on our collections). Very few copepod-sized particles were measured at depths between 60 m and 120 m (Figure 5.12c, d, e). Particles in bin classes 10 - 13 became more abundant at 140 m, consistent with a deep diapausing layer. At station B03, collected during the night, the size frequency distribution at the surface layer maximum was normally distributed, but shifted to smaller OPC bin classes 4 to 9 with very few particles in the *C. finmarchicus* C5 size range (Figure 5.13b). A second local maximum occurred at 40 m depth, and that maximum was also dominated by particles in OPC bin classes 4 to 9 (Figure 5.13c). The rest of the water column had few particles in bin classes 4 to 12 (Figure 5.13 d-g). Based on these results, I concluded that the net-calibration I developed explicitly for the deep diapausing layer (Chapter 3) was not appropriate for the surface in 2009 due to the abundance of smaller species and earlier stages of *C. finmarchicus*.

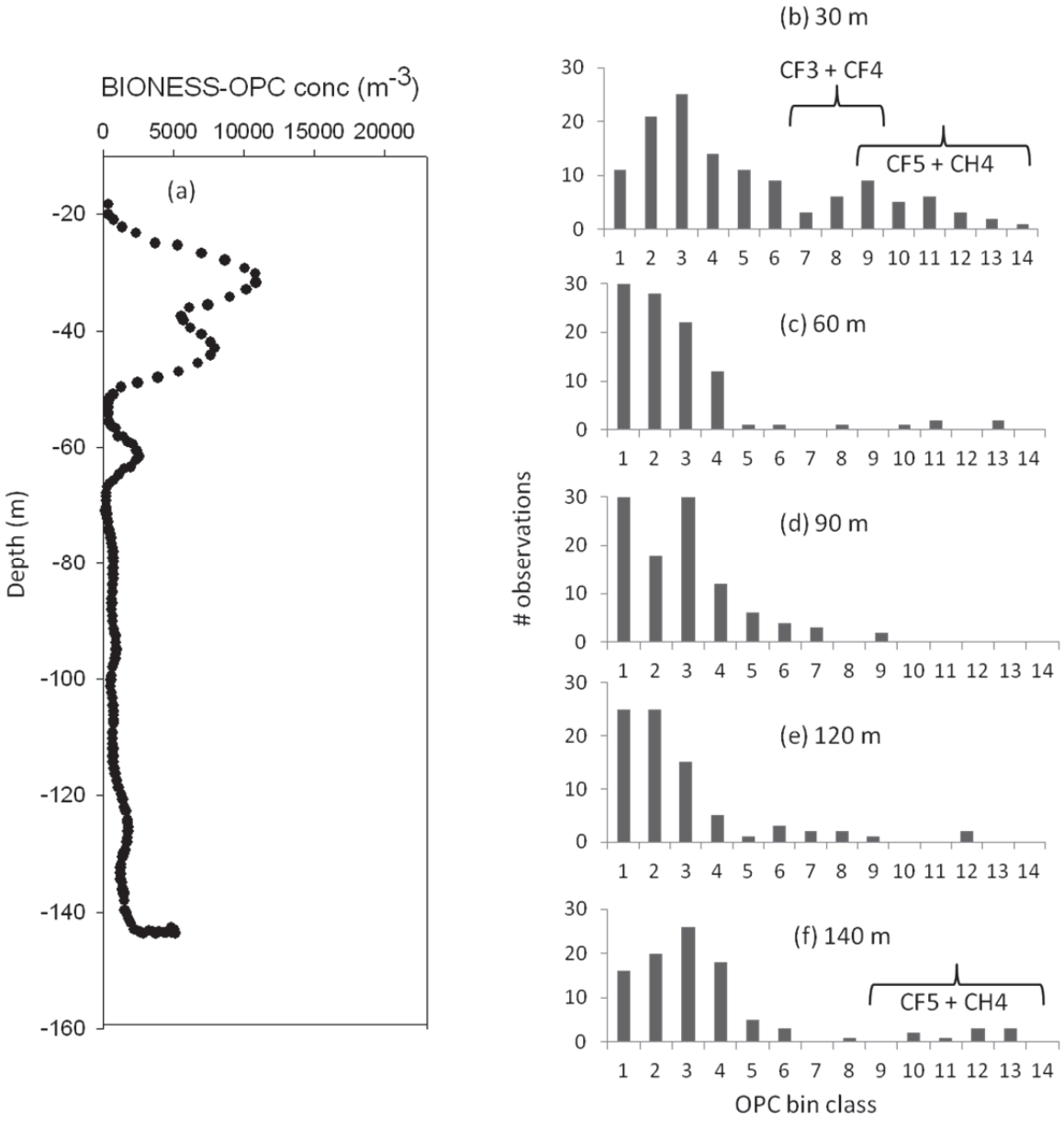

Figure 5.12 (a) Vertical profile of net-calibrated BIONESS-OPC concentration (m^{-3}) measured at station B02 (daytime tow) in 2009 is compared with the size frequency distribution of particles measured by the BIONESS-OPC over a 1 sec time interval at (b) 30 m depth, (c) 60 m depth, (d) 90 m depth, (e) 120 m depth, and (f) 140 m depth. For reference, the combined size frequency distribution of *C. finmarchicus* stage-C5 (CF5) and *C. hyperboreus* stage-C4 (CH4) falls within OPC bin classes 9 - 16 (see Figure 3.4). Masking of this distribution in OPC bin class 9 by younger stage *Calanus finmarchicus* (CF3 and CF4) is pictured in panel b.

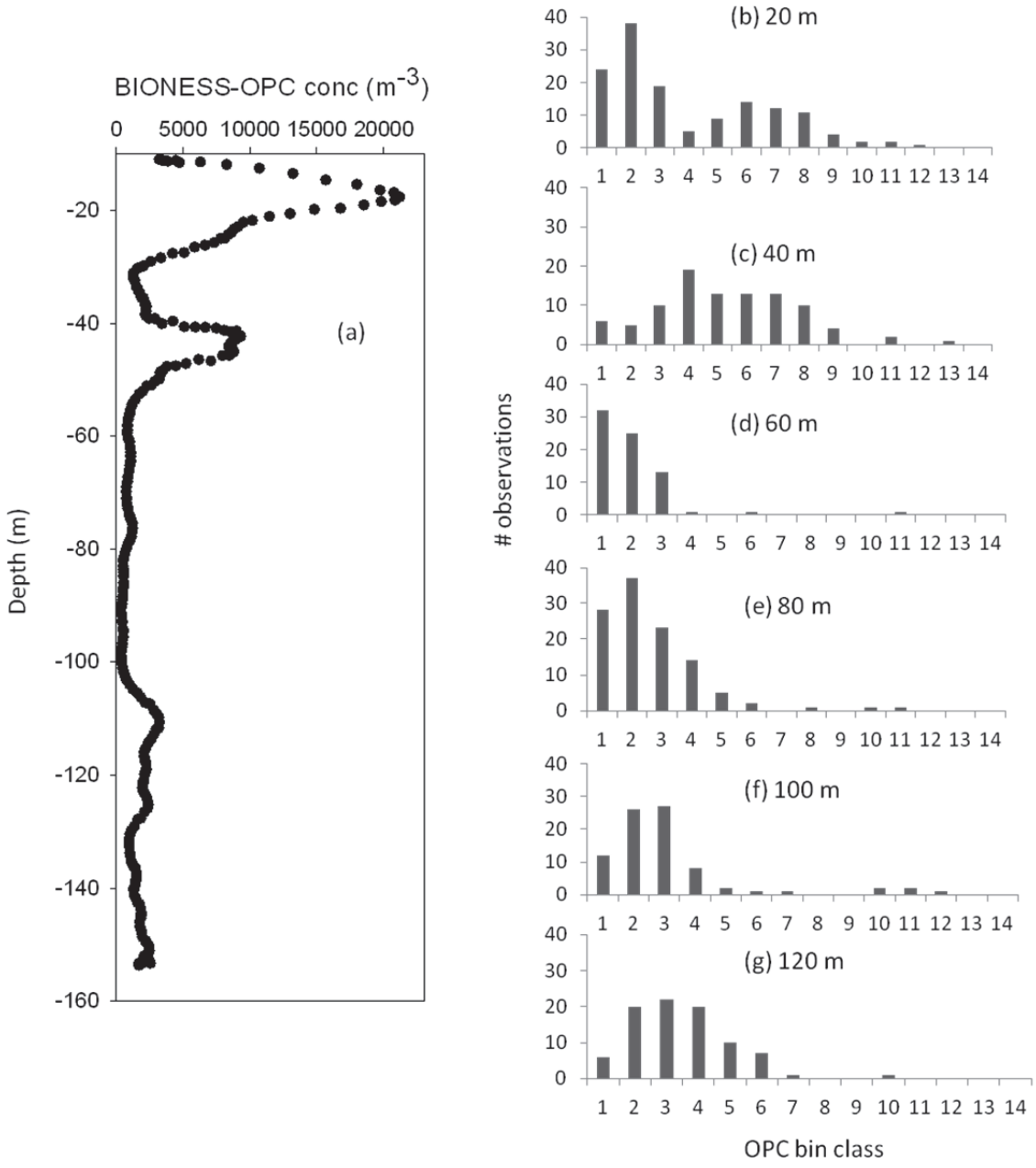

Figure 5.13 (a) Vertical profile of net-calibrated BIONESS-OPC concentration (m^{-3}) measured at station B03 (night tow) in 2009 is compared with the size frequency distribution of particles measured by the BIONESS-OPC over a 1 sec time interval at (b) 20 m depth, (c) 40 m depth, (d) 60 m depth, (e) 80 m depth (f) 100 m depth, and (g) 120 m depth. For reference, the combined size frequency distribution of *C. finmarchicus* stage-C5 and *C. hyperboreus* stage-C4 falls within OPC bin classes 9 - 16 (see Figure 3.4).

I was unable to develop a new calibration for the surface layer as I had only two surface layer collections in 2009, where at least three collections, and preferably more, are required. However, the un-calibrated OPC concentration estimates, integrated over the size range 4 - 14, may provide a first approximation of total mesozooplankton concentrations in the surface layer. To that end, I produced vertical profiles of un-calibrated OPC concentration estimates (bin classes 4 - 14) for the 0 - 60 m depth stratum at stations B01, B02 and B03 (Fig. 5.14). The results showed modest concentrations of 1000 – 2000 m^{-3} in the surface layer; much closer to the total mesozooplankton concentrations estimated using the net collections than the net-calibrated estimates shown in Figure 5.11.

In 2009, the TUBSS-OPC sampling was mostly limited to depths >50 m, though the surface layer was sampled at 5 different locations when TUBSS was deployed and retrieved at the beginning (S02, S04 and S05) and end (S01 and S03) of each transect, save transect-11 where OPC data were not recorded above 50 m during retrieval. At S02, S04 and S05, the data are reliable only below 10 m depth (equilibration at 10 m depth prior to beginning the tow). The locations of these surface profiles are illustrated in Figure 5.1d. The mesozooplankton concentrations measured in the surface layer by the TUBSS-OPC were similar at all five stations (Fig. 15). Concentrations peaked between 10 and 30 m depth at ~4000 m^{-3} and declined with depth thereafter. At stations S01, S02 and S04, the animals were more concentrated in the 10 to 20 m depths, whereas at S03 and S05 the animals were spread more evenly within the surface layer. This variation among stations is not easily attributed to diel variation or to a horizontal (e.g., east - west) gradient in concentration, and may be due simply to small-scale patchiness.

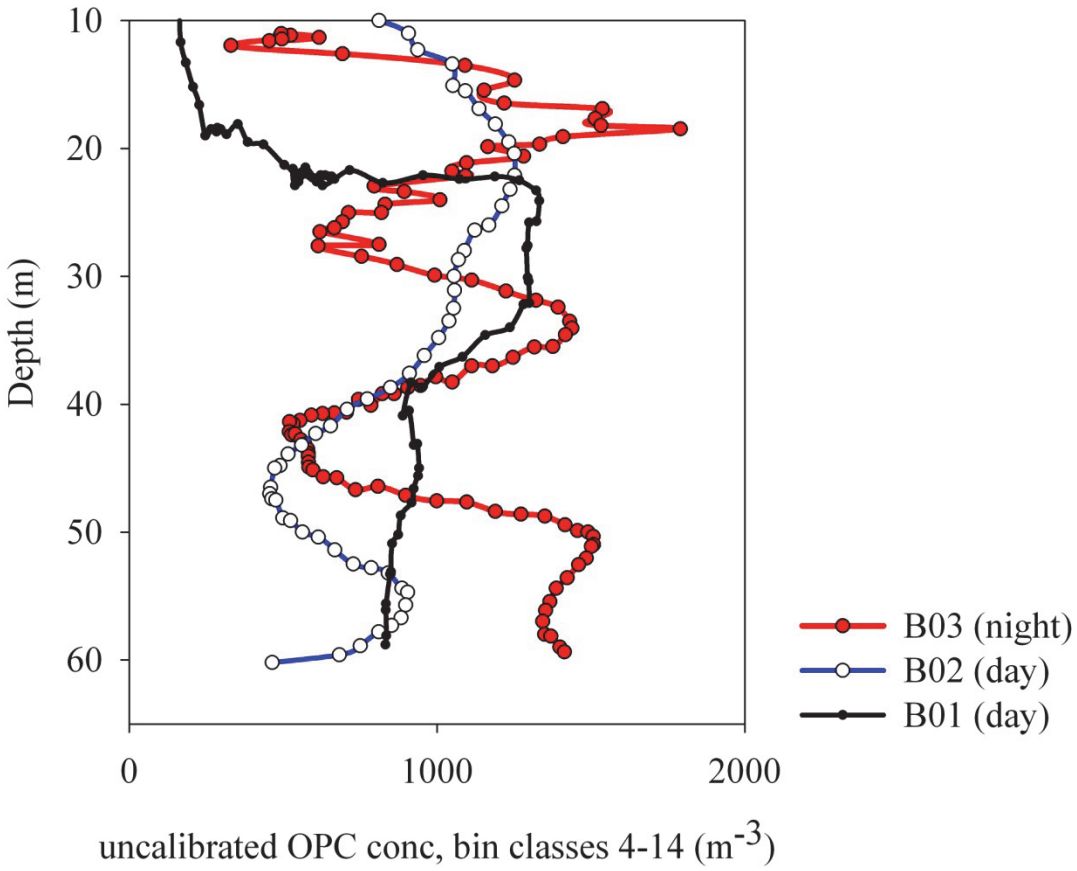

Figure 5.14 Vertical profiles of un-calibrated OPC concentration integrated over OPC bin classes 4 - 14 that encompasses approximately the size distribution of mesozooplankton collected with the BIONESS-OPC in the surface layer of Roseway Basin in 2009 at stations B01 (black), B02 (blue) and B03 (red).

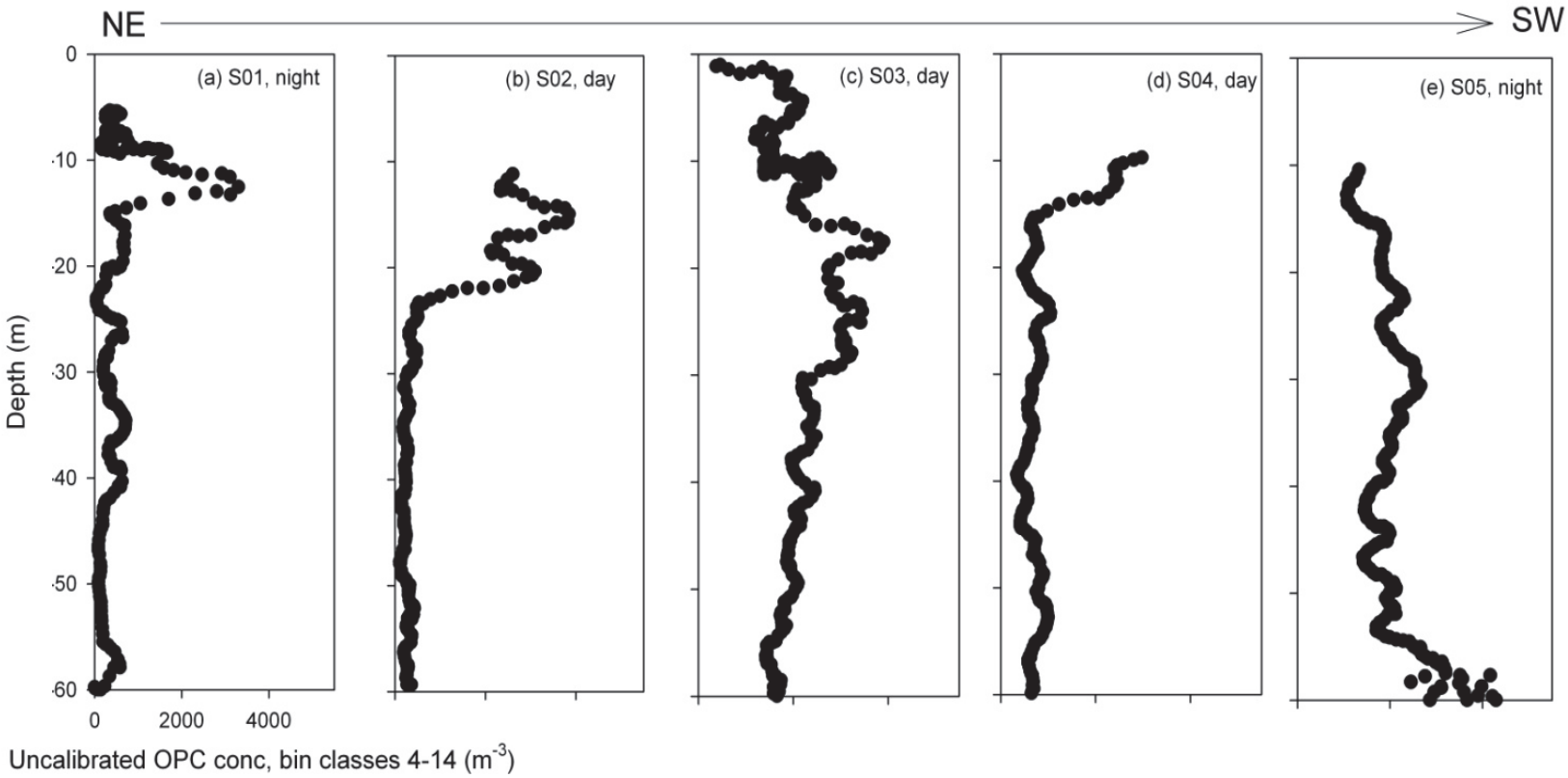

Figure 5.15 Vertical profiles of un - calibrated OPC concentration integrated over OPC bin classes 4 - 14 that encompasses approximately the size distribution of mesozooplankton collected with the TUBSS-OPC in the surface layer of stations S01, S02, S03, S04, and S05. The profiles are presented in a NE - SW direction.

The diapausing copepod layer

In 2009, the BIONESS-nets and BIONESS-OPC measured a deep layer of non-migrating copepods with concentrations exceeding 1000 m^{-3} in some locations. The species and stage composition of this layer was comprised primarily of C. *finmarchicus* stage-C5, with small concentrations of the cold-water species *C. hyperboreus* and *C. glacialis*. *Calanus hyperboreus* were stage-C4 and *C. glacialis* were stage-C5, as in 2007 and 2008. Thus it remains important that the OPC sampling design measured the small-scale (using BIONESS-OPC) and Basin-scale (using TUBSS-OPC) spatial variation in this deep, assumed diapausing, layer. Small-scale horizontal variation in the deep layer was measured along a 350 m transect (Figure 5.16a). As in 2007, concentrations along this transect varied between 500 and 3000 m^{-3}, and contained low and high frequency variation. At the low frequency, concentrations were lowest at the beginning of the transect at 140 m depth, and then increased as BIONESS ascended to 115 m depth. Concentrations remained fairly constant until BIONESS descended again at 270 m along the transect when concentrations decreased. At small spatial scales, the data varied by up to 2000 m^{-3} and were autocorrelated at a lag of 20 m.

The Basin-scale sectional distributions of diapausing copepod concentration (m^{-3}, Figure 5.17) and energy density (kJ m^{-3}, Figure 5.18) are presented for each transect. The patterns in both variables are, as expected, almost identical. Concentrations of diapausing copepods ranged from 0 to 5500 m^{-3}, and energy density ranged from 0 to 24 kJ m^{-3} at depth over the Basin. Transect-11 sampled the deepest regions of the Basin, and intersected transect-13 at the 40 km mark. During the day (transect-11) copepods were patchily distributed throughout the water column (Figures 5.17a and 5.18a), while at night at the same location (40 km mark on transect-13) the copepods were concentrated at depth (Figures 5.17c and 5.18c). It seems reasonable to speculate that the animals spread throughout the water column during the day were not diapausing. During the day, the diapausing and non-diapausing animals were mixed so that the deep layer was not clearly defined on transect-11, whereas at night the deep layer measured at transect-13 represented only the diapausing copepod population since non-diapausers had migrated to the surface layer at night.

Across transect-12 (day, Figures 5.17b and 5.18b) and -13 (night, Figures 5.17c and 5.18c) the copepods were concentrated in a layer below 100 m depth that extended to at least 10 m above the seafloor. Transect-12 was located at the western end of the Basin, and was transited at the same time of day as transect-11, one day later (Table 5.2). However, copepod concentrations and energy density across transect-12 were not distributed throughout the water column as they were on transect-11. The BIONESS-OPC vertical profiles at transect-12 showed a layer at depth and a layer at the surface during both day and night (Figure 5.11). This indicates that at the western end of the Basin, there were two distinct layers at all times and evidence of diel-vertical migration was weak; consistent with the BIONESS-OPC and TUBSS-OPC profiles. In the mid-Basin area, the animals were spread throughout the water column during the day, and concentrated in two distinct layers at night; evidence of strong diel-vertical migration of some animals. The total prey field was more concentrated in the deep Basin (transect-11) than near the western margin (transect-12), however the concentration and energy density of the deep diapausing layer was fairly evenly distributed throughout the Basin (transect-13).

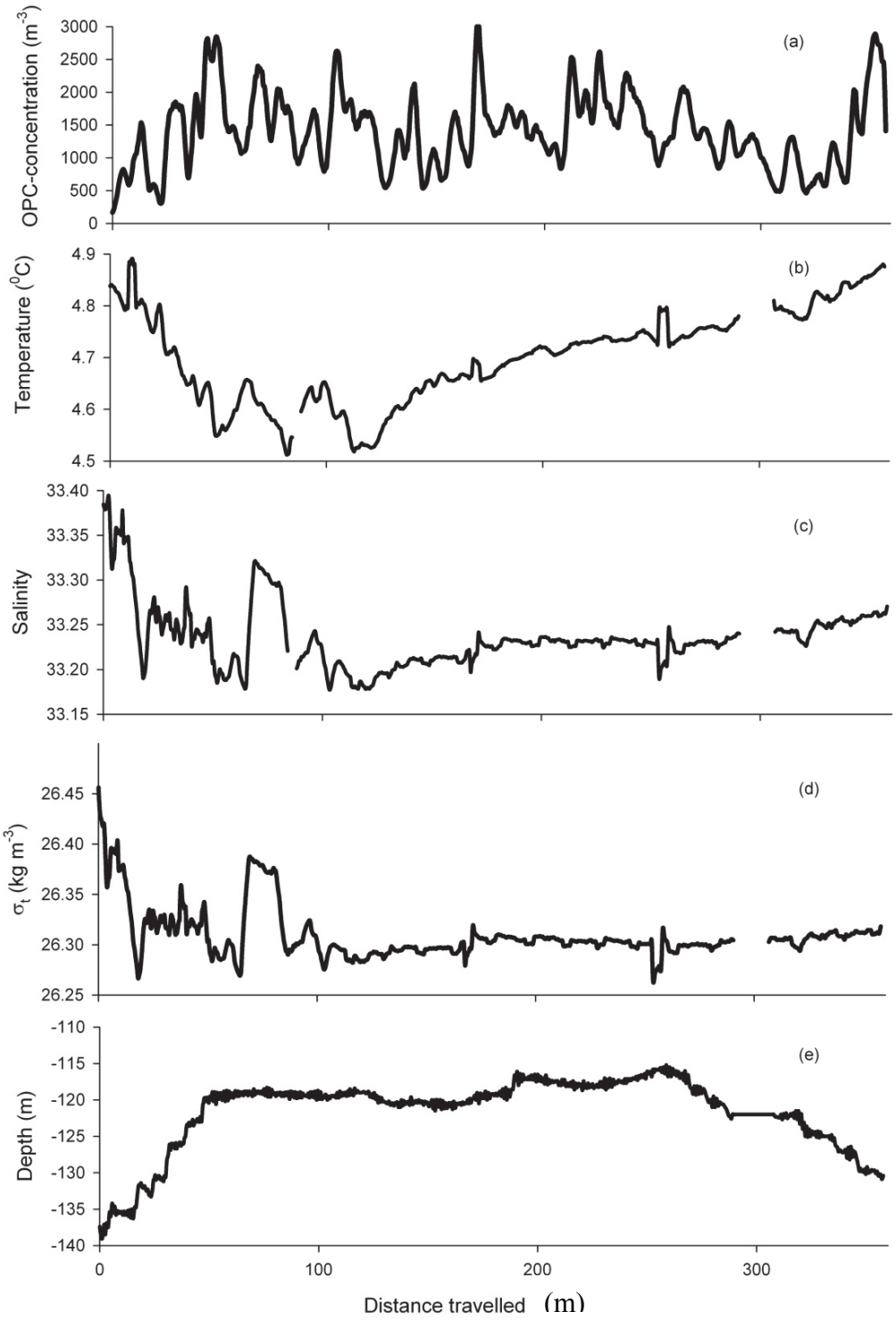

Figure 5.16 High resolution horizontal spatial variation at depth recorded at station-B01 in Roseway Basin in 2009 showing: (a) BIONESS-OPC derived diapausing copepod concentration; b) water temperature (^{o}C); c) salinity; d) σ_t (kg m^{-3}); and e) depth (m).

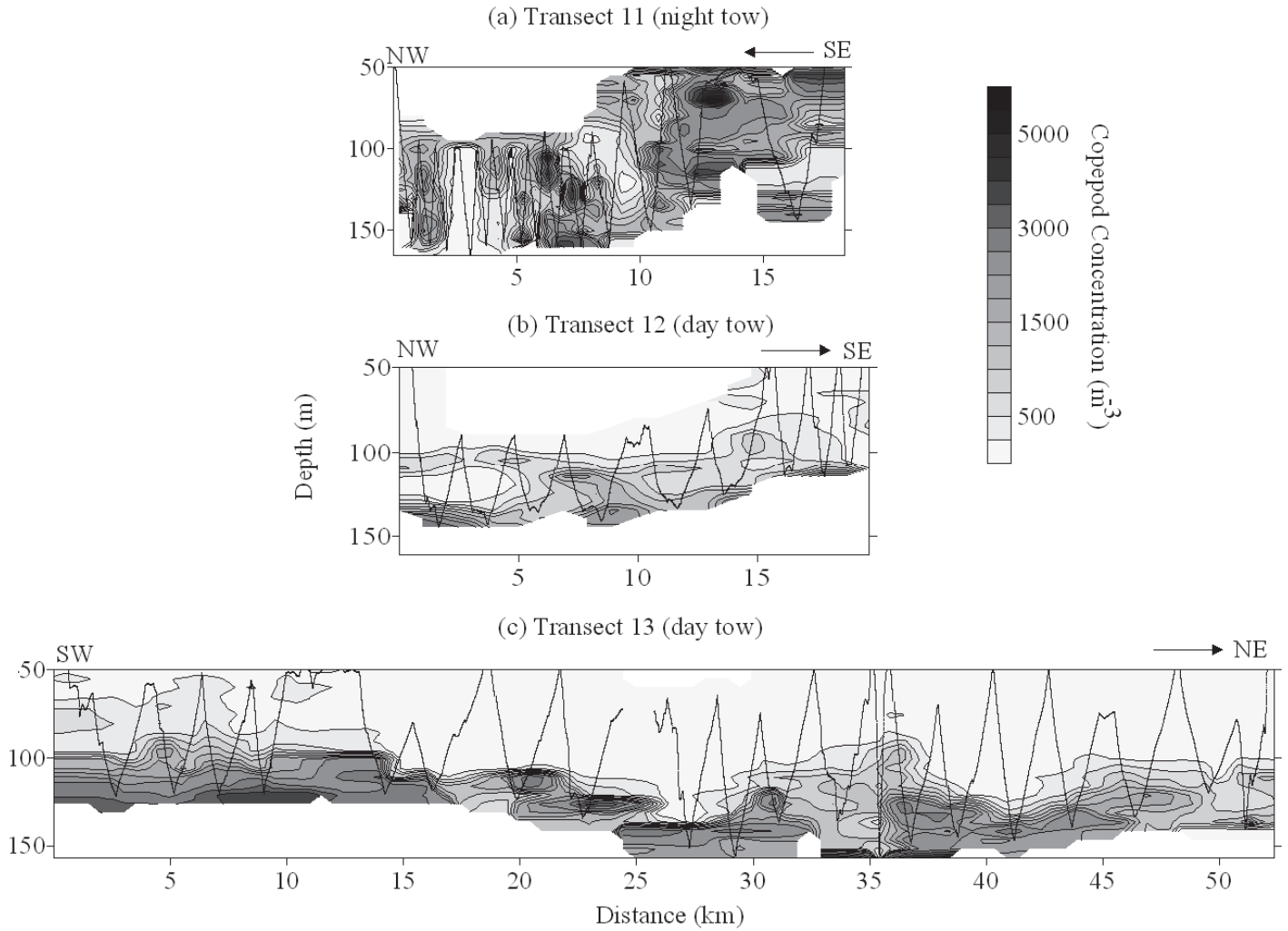

Figure 5.17 Sectional distribution of diapausing copepod concentration (m^{-3}), estimated using the TUBSS-mounted OPC in August 2009 in Roseway Basin along transects 11 through 13 (a through c). Transects (a) 11 and (b) 12 were oriented cross-Basin (NW - SE) and transect 13 was oriented along-Basin (SW - NE). Transect 11 was transited at night, while transects 12 and 13 were transited during the day; see Table 5.2 for the timing of each tow. The direction of each tow and the TUBSS-tow profiles are depicted here by arrows, and the geographic location of each transect in the Basin is pictured in Figure 5.1d.

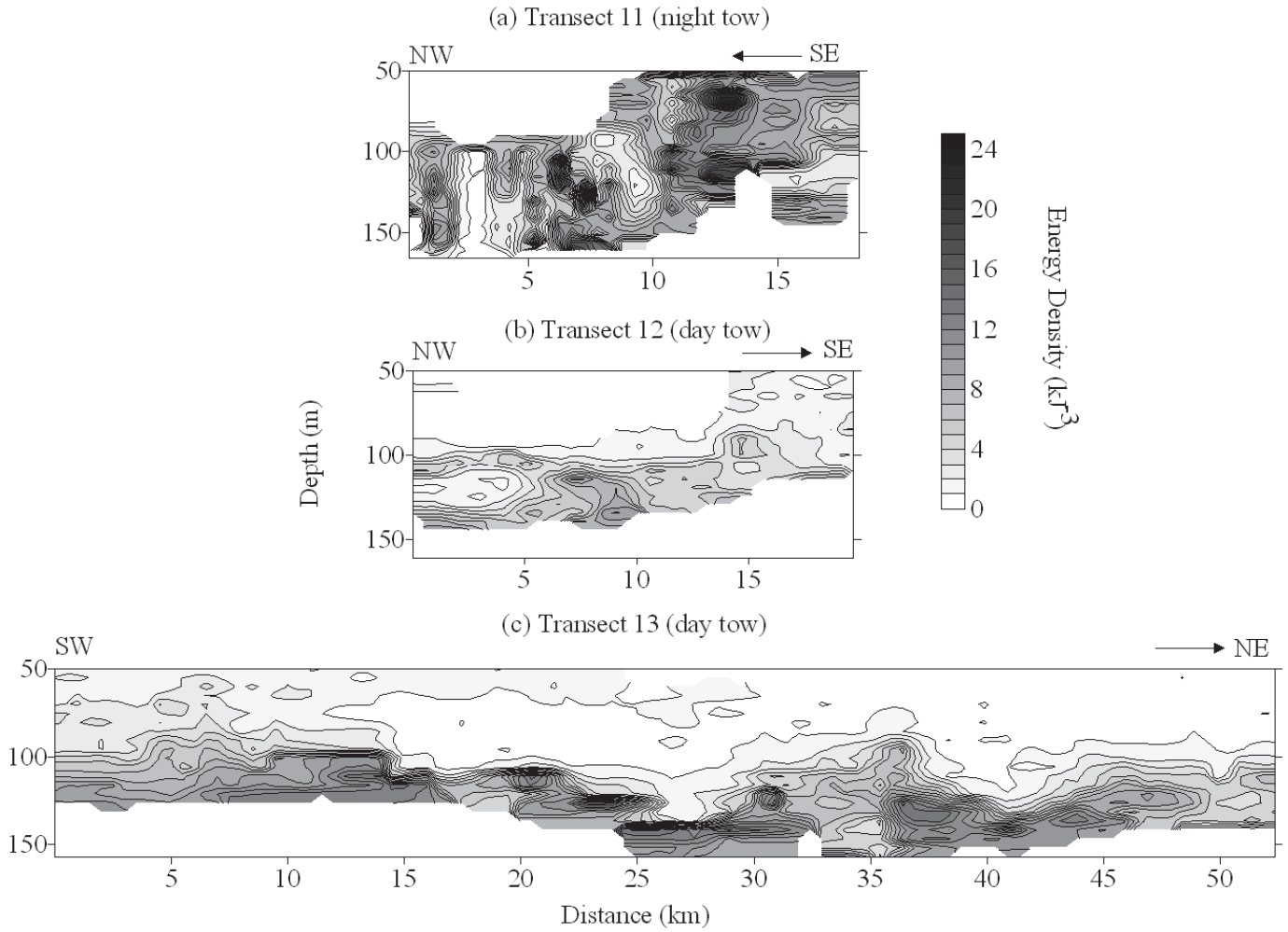

Figure 5.18 Sectional distribution of diapausing copepod energy density (kJ m^{-3}), estimated using the TUBSS-mounted OPC in August 2009 in Roseway Basin along transects 11 through 13 (a through c). Transects (a) 11 and (b) 12 were oriented cross-Basin (NW - SE) and transect 13 was oriented along-Basin (SW - NE). Transect 11 was transited at night, while transects 12 and 13 were transited during the day; see Table 5.2 for the timing of each tow. The direction of each transect and the TUBSS-tow profiles are depicted here by arrows, and the geographic location of each transect in the Basin is pictured in Figure 5.1d.

5.3.2.2 Hydrography

Vertical profiles with emphasis on surface layer (0 - 60 m) variation

Vertical profiles of hydrography were collected with the BIONESS-CTD at each BIONESS station, and the resulting patterns were similar among the three co-located stations. The BIONESS conductivity sensor is quite noisy, but the general patterns are clear. Water temperature was 14 ^{o}C at the surface, and decreased with depth to below 4 ^{o}C at 80 m over a weak and deep thermocline (Figure 5.19a-c). Temperature remained at 2 ^{o}C until 100 m depth where it increased to above 4 ^{o}C at the maximum sampling depth of 140 m. Salinity was near 32.5 at the surface and increased to 33 at 40 m depth. The salinity then decreased back to 32.5 at 60 m depth, then increased with depth reaching a maximum of 33.5 at the maximum sampling depth (Figure 5.19a-c). Water mass density was near 1024.5 kg m^{-3} at the surface, then increased over a weak and deep pycnocline between 10 and 60 m depth (Figure 5.19d-f). Thereafter it continued to slowly increase with depth to around 1026.2 kg m^{-3}.

Hydrographic profiles from the surface to 60 m depth were also collected with the TUBSS-mounted CTD at 5 locations in the Basin during TUBSS deployment and retrieval (as described above for stations S01 - S05, Figure 5.20). These provided a better description of the basin-scale variation in surface layer hydrographic properties than the co-located BIONESS-CTD data. The vertical patterns among these stations were similar to those measured at stations B01 - B03 (Figure 5.20). In water mass space, there was a clear along-basin NE - SW gradient in the water masses in the surface layer (Figure 5.21). Three water masses were present above 50 m; Basin Water (BW, T = 3.3^{o}C, S = 32.4, σ_t = 25.8 kg m^{-3}), modified Basin Water (mBW, T = 7.5^{o}C, S = 33.2, σ_t = 26 kg m^{-3}) and Gulf of St. Lawrence Surface Water (SLEW, T = 16^{o}C, S = 31.8, σ_t = 23.5 kg m^{-3}, Houghton and Fairbanks 2001). SLEW was dominant in Roseway at the surface with small contributions of BW and mBW. The proportion of SLEW decreased with increasing depth while, depending on location, mBW or BW became dominant at 50 m depth (Figure 5.21). At the eastern end of the Basin (stations S01 and S02), BW dominated at 50 m depth, while stations near the western Basin margin (stations S03 to S05) were influenced by mBW as well as BW.

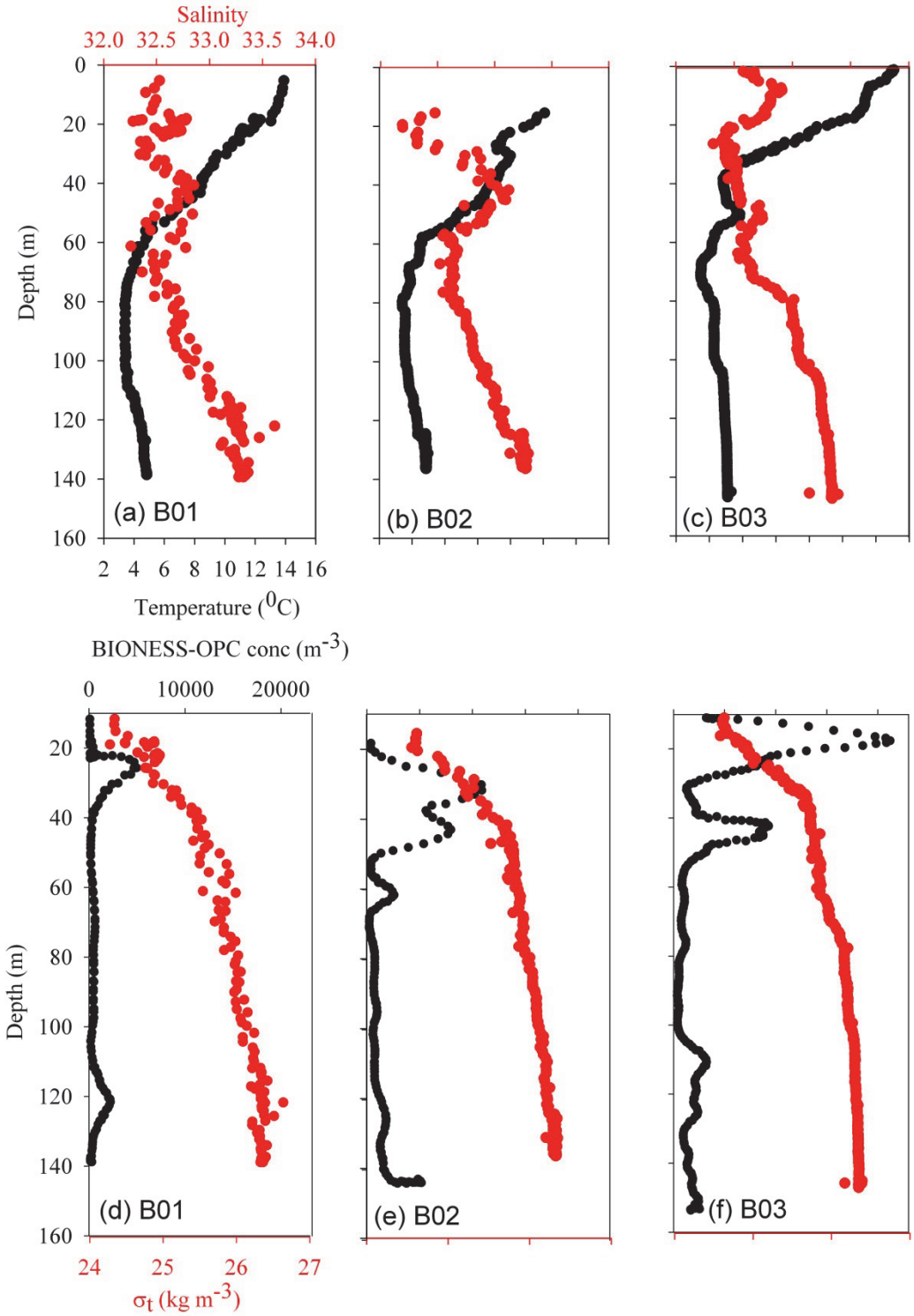

Figure 5.19 Vertical profiles of (a-c) temperature (black) and salinity (red) at BIONESS stations (a) B01, (b) B02 and (c) B03 and (d-f) BIONESS-OPC derived concentrations of *Calanus finmarchicus* stage-C5 and *C. hyperboreus* stage-C4 sized particles (black) and water mass density (σ_t, kg m^{-3}) (red) collected at BIONESS stations (d) B01, (e) B02 and (e) B03. The location of each profile is depicted in Figure 5.1d.

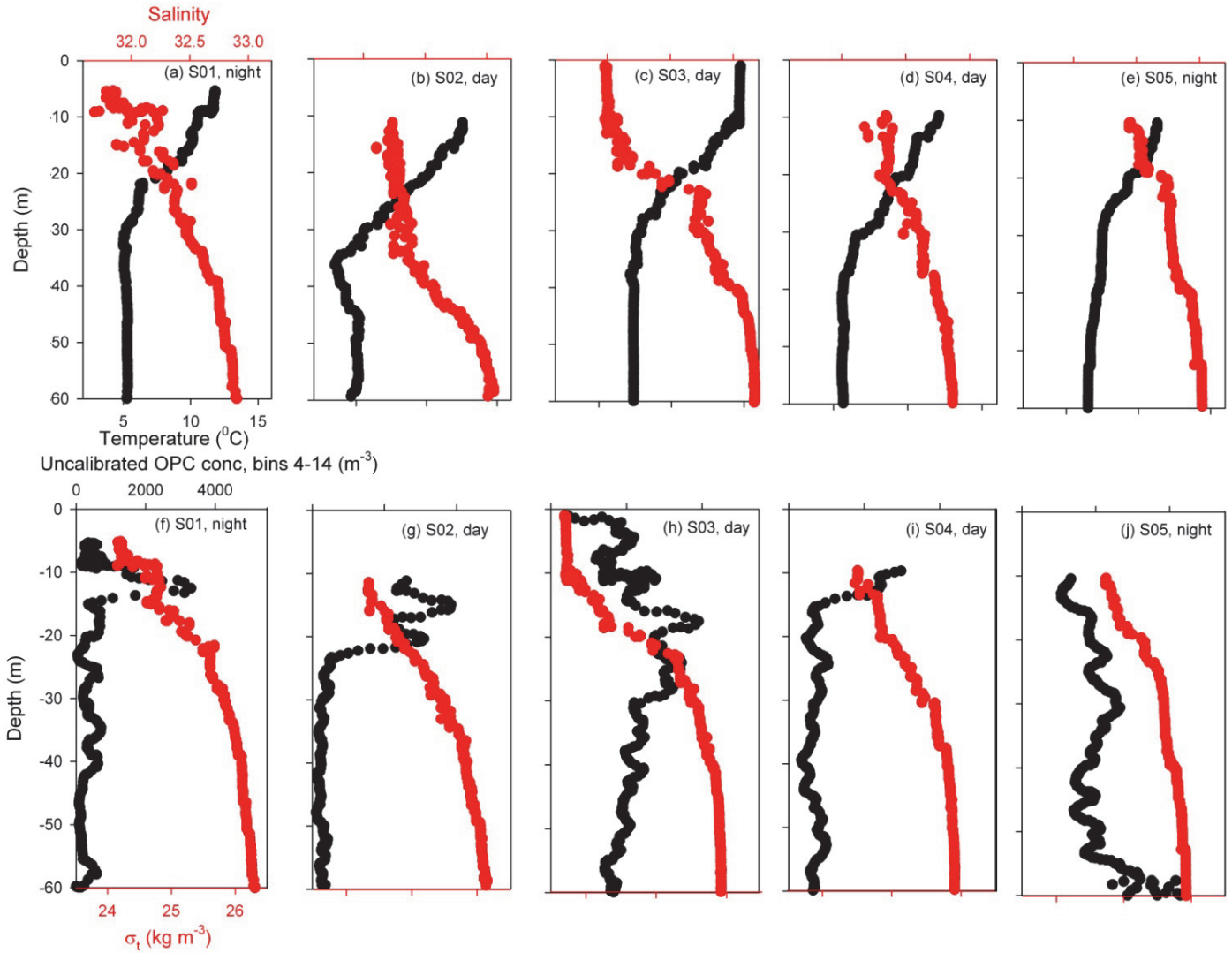

Figure 5.20 Vertical profiles of (a-e) temperature (black) and salinity (red) with the TUBSS-mounted CTD stations (a) S01, (b) S02, (c) S03, (d) S04 and (e) S05 are compared with vertical profiles of (f-j) TUBSS-OPC derived concentrations of *Calanus finmarchicus* stage-C5 and *C. hyperboreus* stage-C4 sized particles (black) and water mass density (σ_t, kg m^{-3}) (red) collected at TUBSS stations (f) S01, (g) S02, (h) S03, (i) S04 and (j) S05. The location of each profile is depicted in Figure 5.1d.

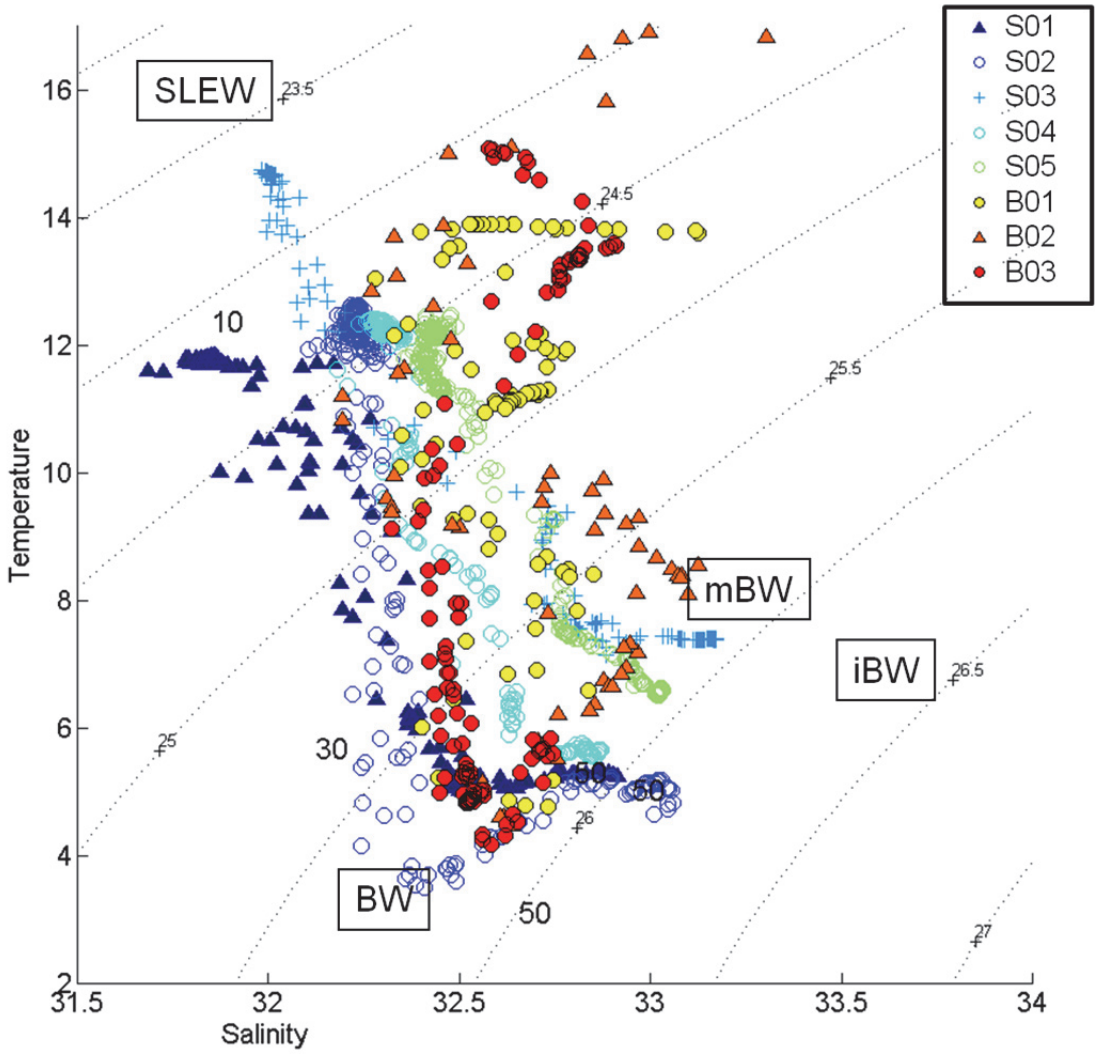

Figure 5.21 Temperature-salinity diagram showing hydrographic variation in the surface (0 - 60 m) layer of Roseway Basin in 2009 at stations S01 to S05 and B01 to B03. Stations symbols are color-coded, approximate locations of the 10 m, 30 m and 50 m depths are labeled, and end-member water masses Basin Water (BW), modified Basin Water (mBW), Basin Water (BW) and St. Lawrence Surface Water (SLEW) are labeled. Dotted lines depict the σ_t isopycnals, spaced at 0.5 kg m^{-3} and labeled.

Small and Basin-scale hydrography at depths > 50 m

As in 2007, small-scale horizontal variation in hydrography at a single depth in 2009 was very small; most of the variation across the 350 m transect was due to variation in tow depth (Figure 5.16).

The two cross-Basin transects (11 and 12) and the one along-Basin transect (13) in 2009 provided a general description of the basin-scale hydrography below 50 m depth. Across transect-11, at the eastern end of the Basin, where deepest, the water was relatively well stratified and less horizontally variable than along other transects (Figure 5.22). Temperature (Figure 5.22a) and salinity (Figure 5.22b) both increased with depth, and above 100 m depth there was little spatial variation in either variable along the transect. Below 100 m depth, the water warmed more slowly on the NW margin than on the SE margin and this resulted in a downward tilting of the isotherms and isohalines toward the NW. Toward the SE, the isotherms and isohalines remained generally horizontal below 100 m depth. The density section below 50 m was uninteresting and simply increased with depth with no evidence of a strong pycnocline and no horizontal variation, save a slight downward tilt near the NW margin that was more pronounced in temperature and salinity (Figure 5.22).

Along transect-12, located near the western margin of the Basin, there was considerably more cross-basin horizontal and vertical variation in hydrography (Figure 5.23). Near the NW margin, the water was relatively warm and fresh at 50 m depth, became warmer and salty at 90 m depth, then cooled and freshened near bottom (Figure 23a, b). The middle of the Basin contained relatively cold and fresh water that extended to 120 m where it then warmed slightly and became more saline. Near the SE margin, there was a strong vertical T-S front at ~15 km along the transect that separated the cold, fresh water the middle of the Basin from the warm (7^{o}C) and salty water near the SE Basin margin as it shoaled toward the bank. The density section showed a weak downward tilting of isopycnals near-bottom on both the NW and SE margins that is indicative of geostrophic flow at depth.

Along transect-13, that crossed the middle of the Basin in a SW to NE direction, there was again considerable spatial variation in the T-S properties that had a minimal effect on the density field (Figure 5.24). Near the SW Basin margin, between 0 and 15

km along the transect, the water was relatively warm and salty at all depths (Figure 5.24a, b). Deeper in the mid-Basin between 15 and 30 km, the cold, fresh water apparent on transect-12 above became dominant above 120 m, while below the water remained warm and salty. It was near this transition between warm-salty and cold-fresh water that the BIONESS–CTD profiles were collected and explains why, in the surface layer, there was more water mass variation at these stations than at the TUBSS stations around the Basin periphery (Figure 5.21). Between 30 and 40 km along the transect, the cold, fresh water shoaled, and the warm, salty water became dominant below 75 m depth. Between 40 and 45 km along the transect, the cold, fresh water deepened again, and for the remainder of the transect it shoaled, and the deep Basin became warmer and saltier. Again, there was evidence of weak isopycnal tilting where the cold, fresh water shoaled and then deepened, and also near bottom on the western margin between 10 and 25 m along the transect (Figure 5.24c).

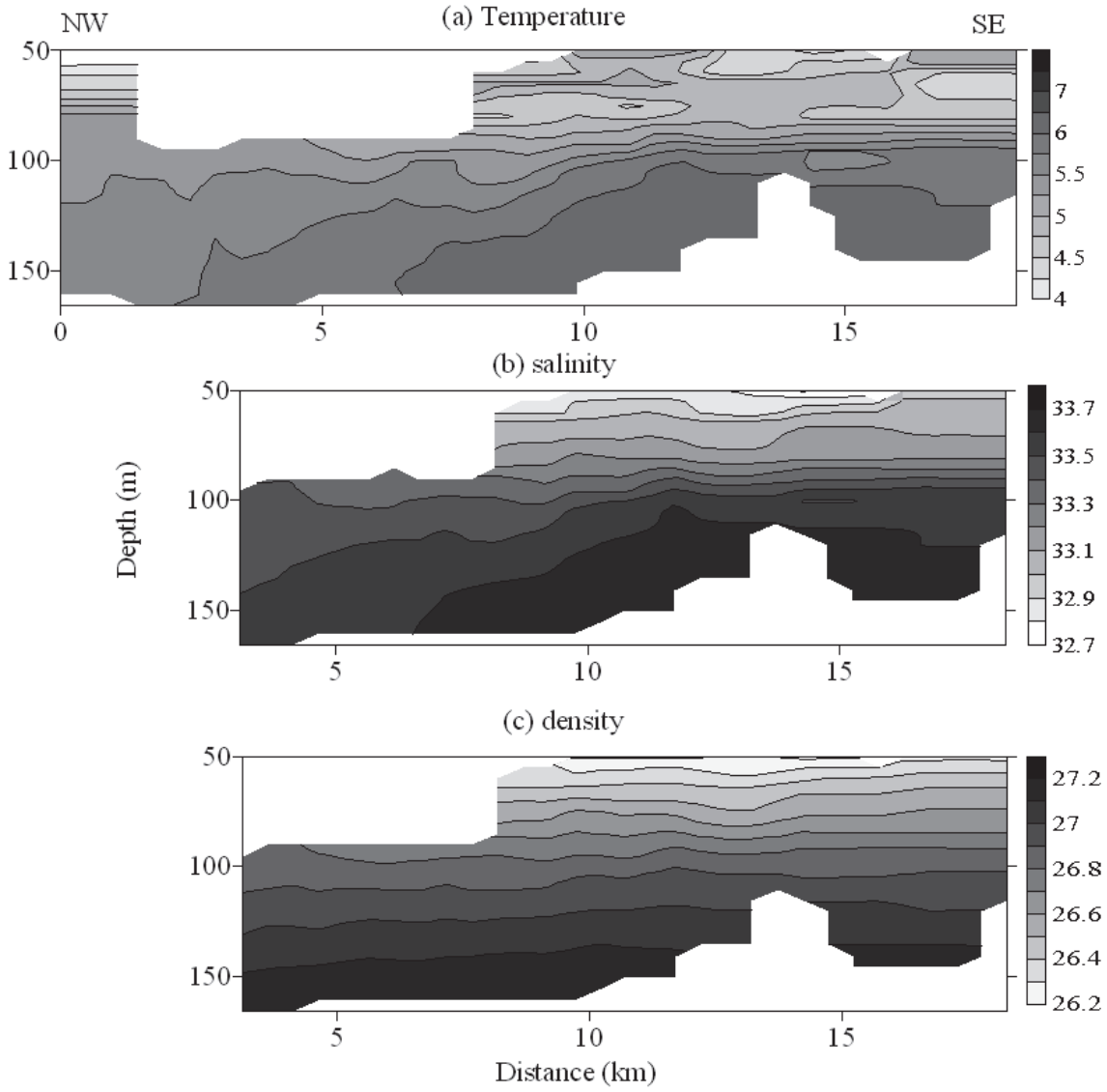

Figure 5.22 Sectional distributions of (a) temperature (^{o}C), (b) salinity and (c) density (σ_t, kg m^{-3}) estimated using the TUBSS-mounted Seabird-37 CTD in August 2009 in Roseway Basin along the NW to SE transect-11. The temperature transect is longer than the salinity and density transects because of a problem with the salinity sensor near the beginning of the transect. The TUBSS-tow profile is shown in Figure 5.16a, and the geographic location of the transect line is depicted in Figure 5.1d. The white regions are no-data regions.

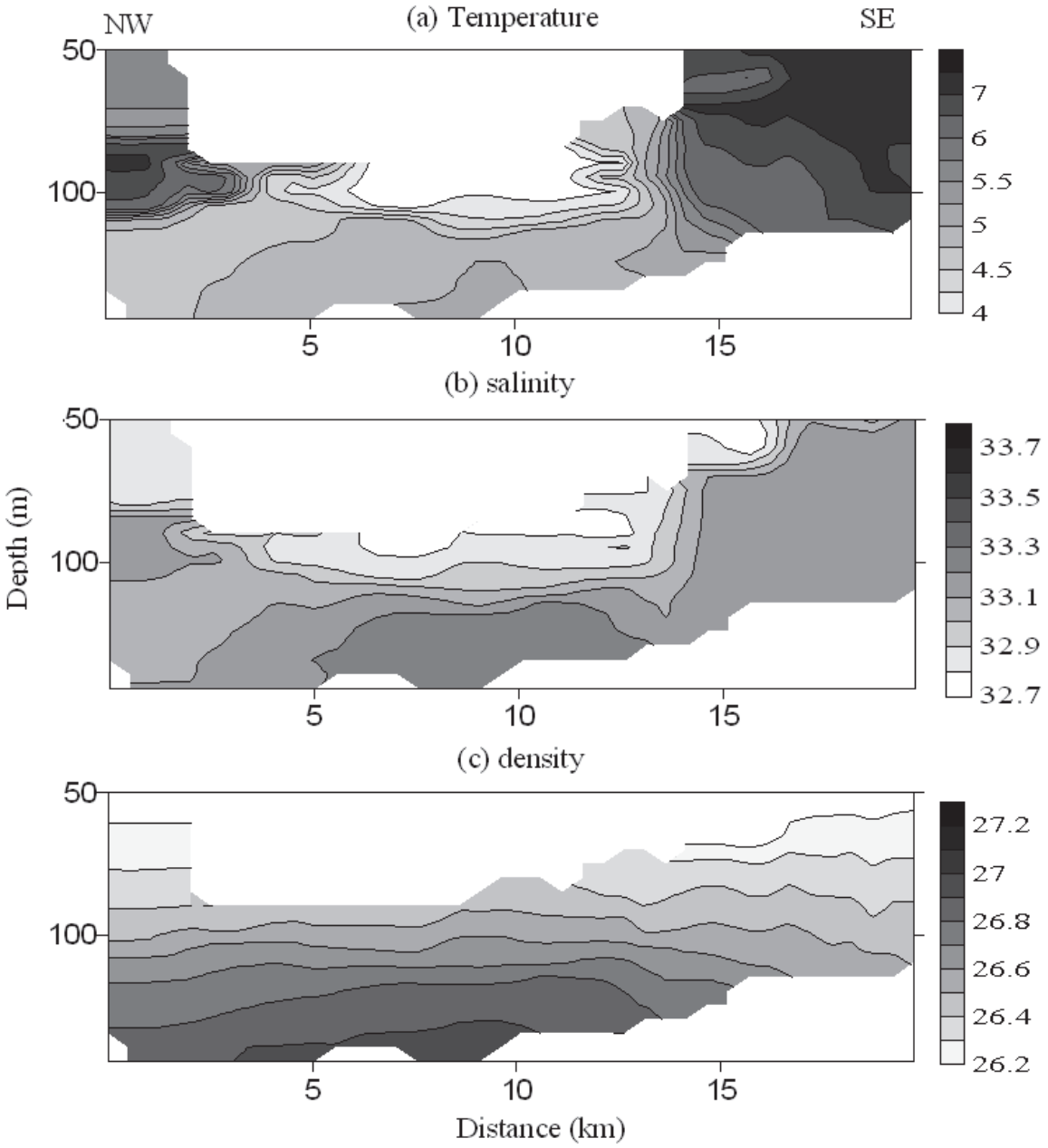

Figure 5.23 Sectional distributions of (a) temperature (^{o}C), (b) salinity and (c) density (σ_t, kg m^{-3}) estimated using the TUBSS-mounted Seabird-37 CTD in August 2009 in Roseway Basin along the NW to SE transect-12. The TUBSS-tow profile is shown in Figure 5.16b, and the geographic location of the transect line is depicted in Figure 5.1d. The white, un-contoured regions are no-data regions.

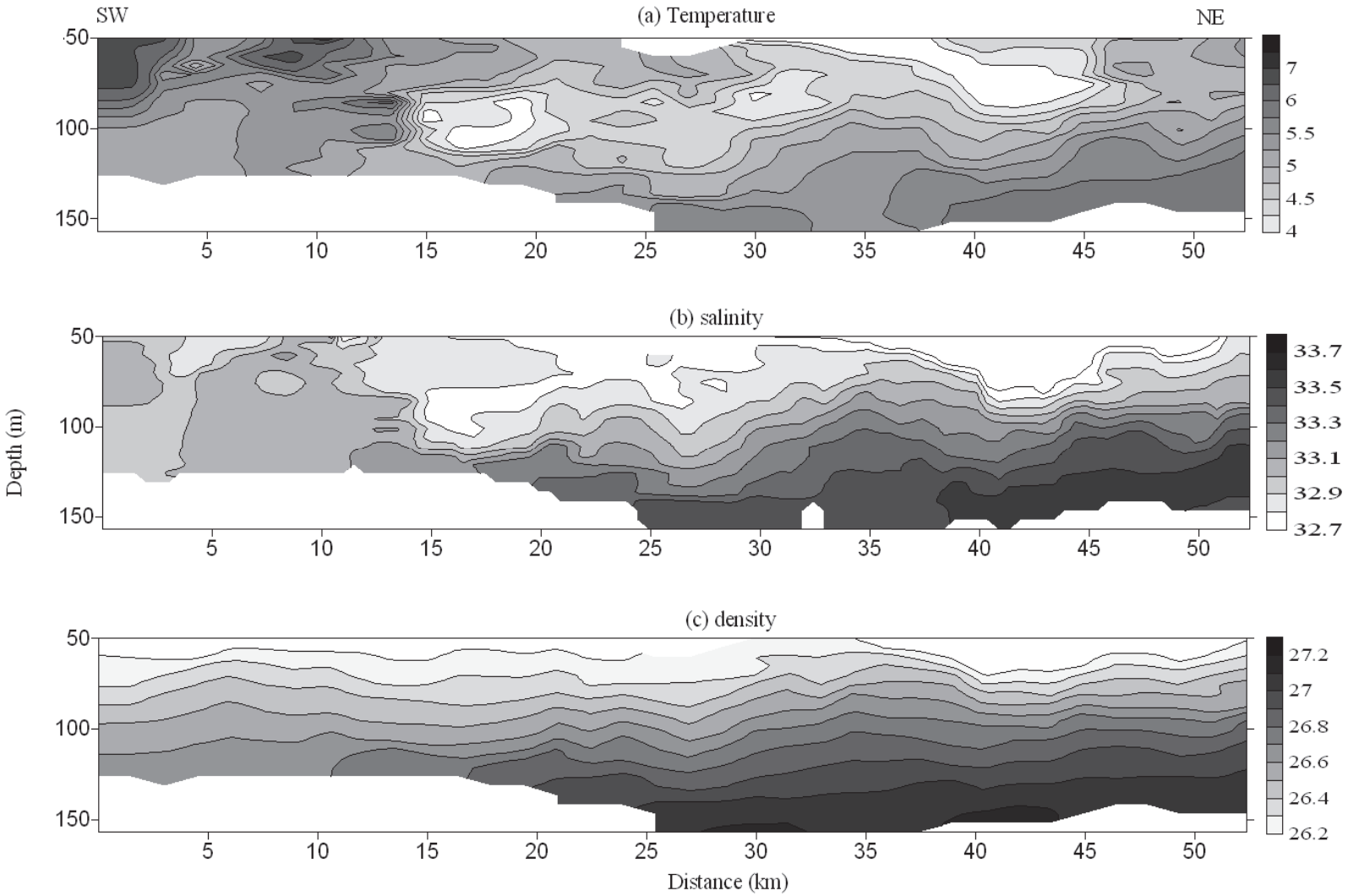

Figure 5.24 Sectional distributions of (a) temperature (^{o}C), (b) salinity and (c) density (σ_t, kg m^{-3}) estimated using the TUBSS-mounted Seabird-37 CTD in August 2009 in Roseway Basin along the NW to SE transect-13. The TUBSS-tow profile is shown in Figure 5.16c, and the geographic location of the transect line is depicted in Figure 5.1d. The white, un-contoured regions are no-data regions.

Three water masses were present at depth in Roseway Basin in 2009 (Figure 5.25); Basin Water (BW, $T = 3.3^{o}C$, $S = 32.4$, $\sigma_t = 25.8$ kg m^{-3}), intermediate Basin Water (iBW, T = 6.2^{o}C, S = 33.7, σ_t = 26.5 kg m^{-3}), and modified Basin Water (mBW, $T = 7.5^{o}C$, $S = 33.2$, $\sigma_t = 26$ kg m^{-3}). The water mass structure in 2009 differed from those of the two previous years, but had some characteristics similar to 2007, and some similar to 2008. As in 2007, in the deep Basin (transect-11), there was little NW - SE (cross-Basin) water mass variation (Figure 5.25a, compare with Figure 5.8). Here, the T-S diagram indicates a simple 2 - end-member system where BW dominated at 70 m depth in the proportion 50 % BW : 50 % iBW, and the proportion of iBW increased with depth to 100 % iBW at 130 m. Between 50 and 70 m depth the water was warmer than BW, indicating mixing with surface SLEW near the thermocline. At the western Basin margin (transect-12) the T-S diagram indicated a 3-end-member system, with less influence of iBW and more influence of BW and mBW than in the eastern Basin (Figure 5.25b). Also in contrast to the eastern Basin, at the western margin there was NW - SE (cross-Basin) variation in water mass structure. At the NW margin (Figure 5.25b, blue) the water was 50 % BW : 50 % mBW at 50 m. As depth increased, the proportion of mBW increased to 100 % mBW at 90 m. Thereafter the proportion of mBW decreased with depth until 130 m when the proportions were approximately 66 % BW : 33 % mBW and slightly more salty than at 50 m depth, indicating a small iBW influence. Mid-Basin (Figure 5.25b, black), the water was dominated by BW at 90 m depth. With increasing depth, the influence of BW declined while that of mBW increased. Along the SE margin (Figure 5.25b, red) the water mass was dominated by mBW at all depths, though there was a small influence of BW at the greatest depths.

Along- and cross-Basin variation in water mass structure, averaged over the 90 – 160 m depth stratum, showed very clearly the dominance of BW at the western and northwestern margins (Figure 5.26). Along the southern margin, the water masses were different at the western (transect-12) and eastern (transect-11) ends. At the western end, warmer, fresher mBW dominated at depth, whereas at the eastern end, colder, saltier and higher density iBW dominated. The general spatial distribution of hydrography in 2009 at the surface and at depth is summarized effectively in two simple diagrams that reflect the patterns described above (Figure 5.27).

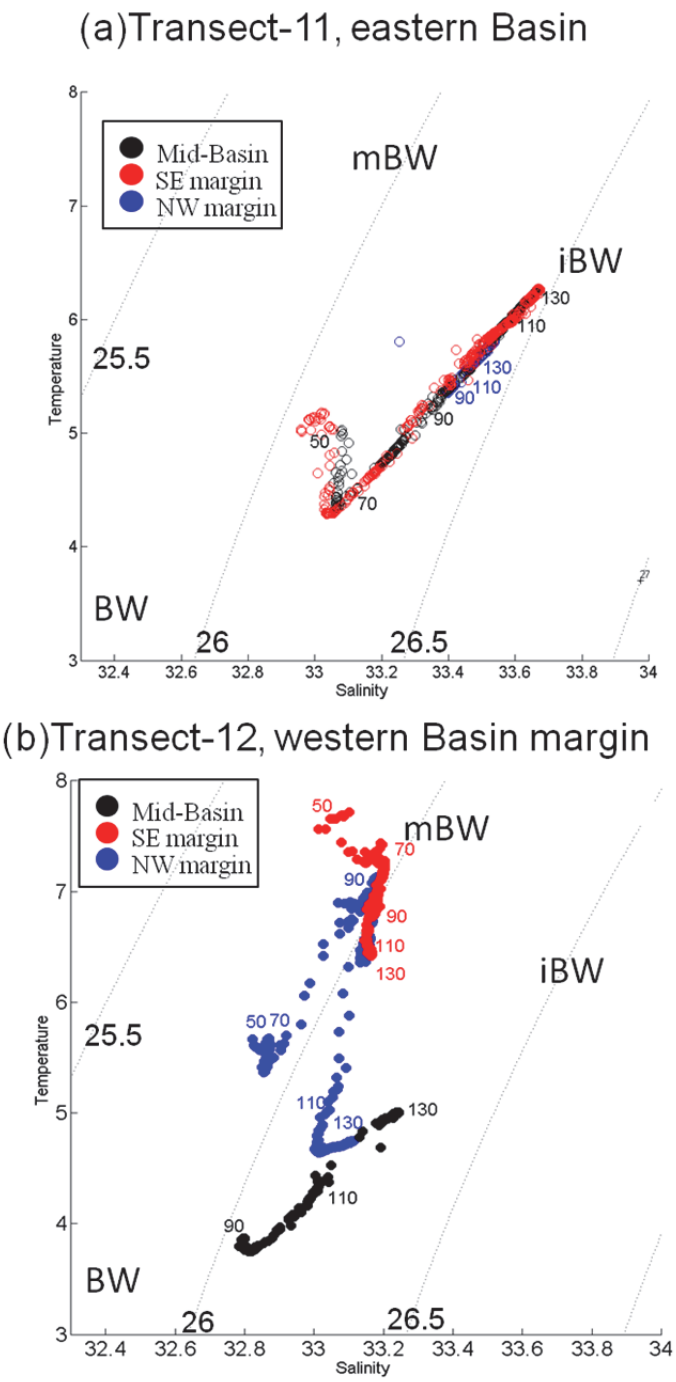

Figure 5.25 Temperature-salinity diagram of vertical temperature-salinity profiles collected with the TUBBS-mounted Seabird-37 CTD at >50 m depth across (a) transect-11 and (b) transect-12 at the NW margin (blue), mid-Basin (black), and SE margin (red) of Roseway Basin. In (a) the NW margin profile and in (b) the mid-Basin profile were collected only at depths >90 m. Water mass end-members are shown, where BW = Basin Water, iBW = intermediate Basin Water, and mBW = modified Basin Water. Depths are labeled at 20 m intervals. Dotted lines depict the σ_t isopycnals, spaced at 0.5 kg m^{-3} and labeled.

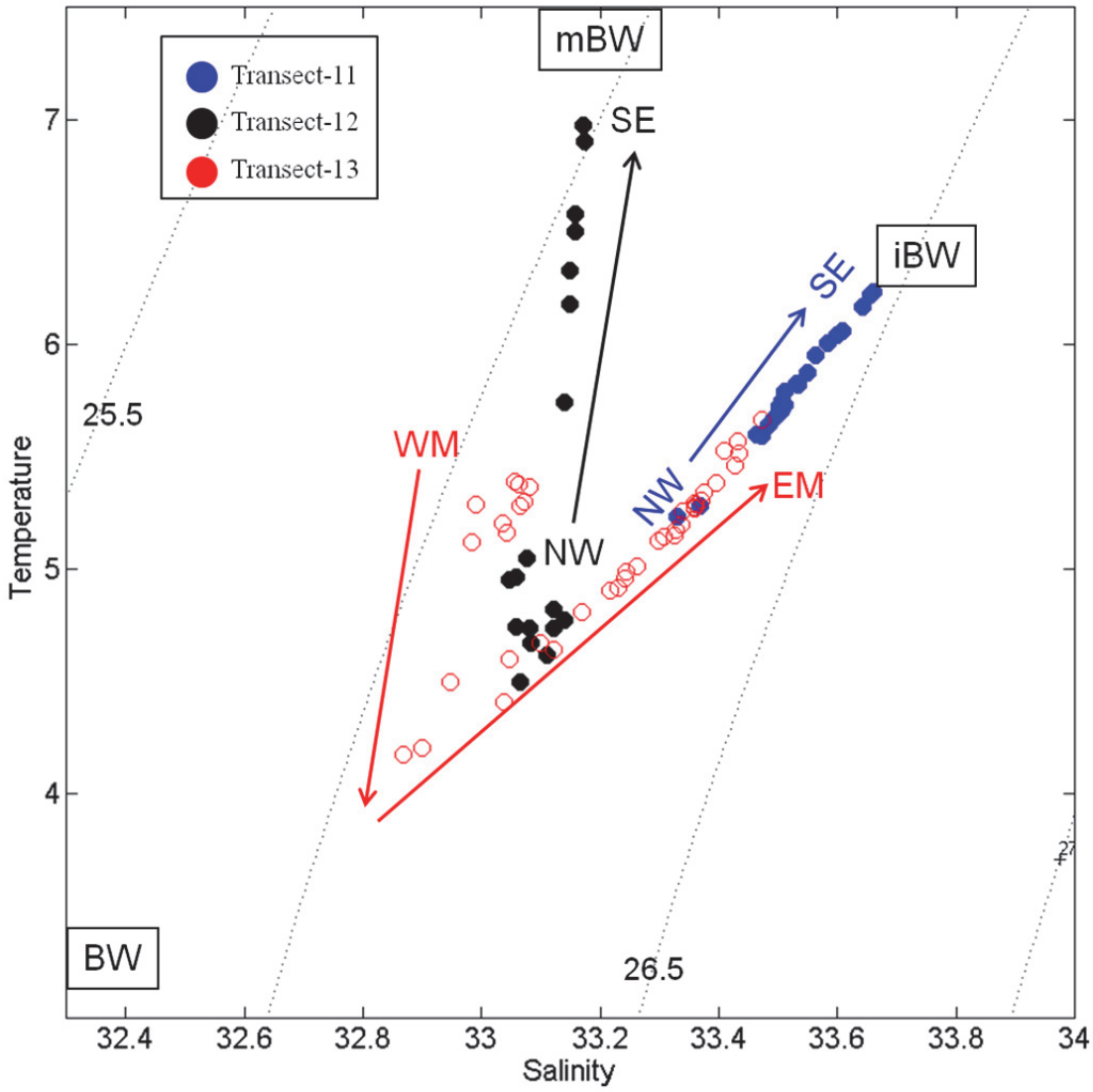

Figure 5.26 Temperature-salinity diagram of the deep water (90 - 160 m stratum) derived from the TUBSS-mounted Seabird-37 CTD along transects 11 (blue) 12 (black) and 13 (red). The direction of each transect is shown with arrows between the northeast (NW), southeast (SE), western Basin margin (WM) and eastern Basin margin (EM). Water mass end-members are shown, where BW = Basin Water, iBW = Intermediate Basin Water, and mBW = modified Basin Water. Dotted lines depict the σ_t isopycnals, spaced at 0.5 kg m^{-3} and labeled.

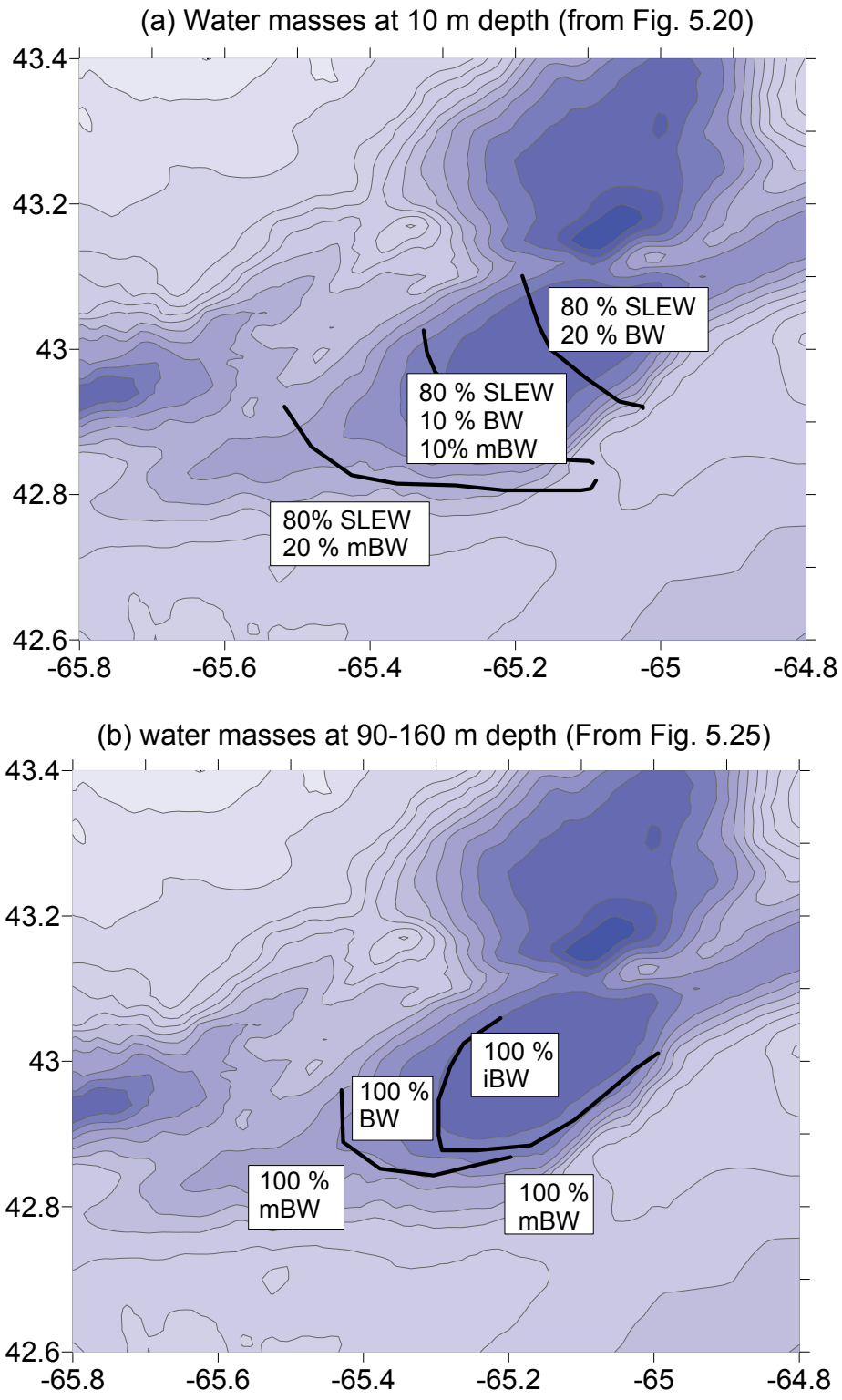

Figure 5.27 Water masses end-members in Roseway Basin in 2009, with their approximate relative contributions (%) based on T-S analysis in (a) the surface layer (10 m depth) and (b) the deep layer (90 – 160 m depth average). Black lines depict the approximate locations of water mass separation.

5.3.2.3 Copepod-hydrography relationships

Non-diapausing copepod population

In 2009, during the day at the eastern end of the Basin, non-diapausing copepods were spread throughout the water column below 50 m, whereas at the western end of the Basin, copepods were concentrated either at depth or at the surface (Figure 5.17a, b). This may be related to water mass variation in the east - west direction along the Basin. At the eastern end of the Basin, Basin Water was present only above 70 m depth and was diluted to 20 %; below 70 m iBW became dominant (Figure 5.25a). At the western end of the Basin, iBW was not present; BW penetrated the deep water mid-Basin and was flanked on either side by mBW (Figure 5.25b). This provides some evidence that the non-diapausing copepods, when at depth during the day, are associated more with iBW. It is possible that the non-diapausing copepods do not migrate to depths below the thermocline during the day at the western end of the Basin to avoid the very cold BW, which is ~13 ^{o}C lower than water near the surface.

However, at locations of the non-diapausers and above the pycnocline, there was no iBW, only warm, fresh SLEW throughout the Basin mixed with BW at the eastern margin and mBW at the western margin (Figure 5.27a). Animals in the surface layer, whether during the day or at night, were most concentrated within the pycnocline (Figure 5.19c-e, Figure 5.20f-g). These animals were measured in similar concentrations at all surface stations, indicating that they are not strongly and horizontally associated with particular water masses when in the surface layer.

Diapausing copepod population

Similar to other years, the diapausing copepods in 2009 were found in the deeper waters of Roseway Basin, where Intermediate Basin Water was dominant. The animals were also found at the western end of the Basin, at 0 km along transect-13, where mBW dominated at depth. The animals were not found in the Basin Water and this was particularly evident along transect-13 where the depth distribution of the deep layer varied inversely with the depth distribution of Basin Water (compare Figure 5.18c with Figure 5.24).

To examine the relationship between copepod energy density and water mass density, I assessed the sectional distributions of energy density as a function of water mass density below 50 m depth (Figure 5.28) as I had done 2008 in Chapter 3 (Figures 3.29 and 3.30). These sections showed that the copepod distribution in 2009 was not as closely related to the density structure as in 2008. There are likely two explanations for this. The first is that, based on the depth distributions and stage-structure of the population, not all the copepods were diapausing in 2009. Thus, they could migrate across isopycnals and hence be less associated with any depth of neutral buoyancy. Secondly, my analyses thus far have shown the 1026 kg m^{-3} isopycnal to be a biologically important upper limit to the diapausing copepod distribution. In 2008 this isopycnal was near-bottom, and the copepods collected just below it. In 2009, the 1026 m^{-3} isopycnal was shallower at 50 m depth, so diapausing copepods may not have been as restricted to the bottom layer in their search for high density water.

The presence of a surface population of *C. finmarchicus* C3s and C4s, and the paucity of evidence for any late-summer slope water intrusions that could re-supply the Basin, as in 2008 (Chapter 3), would be consistent with the copepods in the Basin being produced on the Scotian Shelf during the spring and the summer.

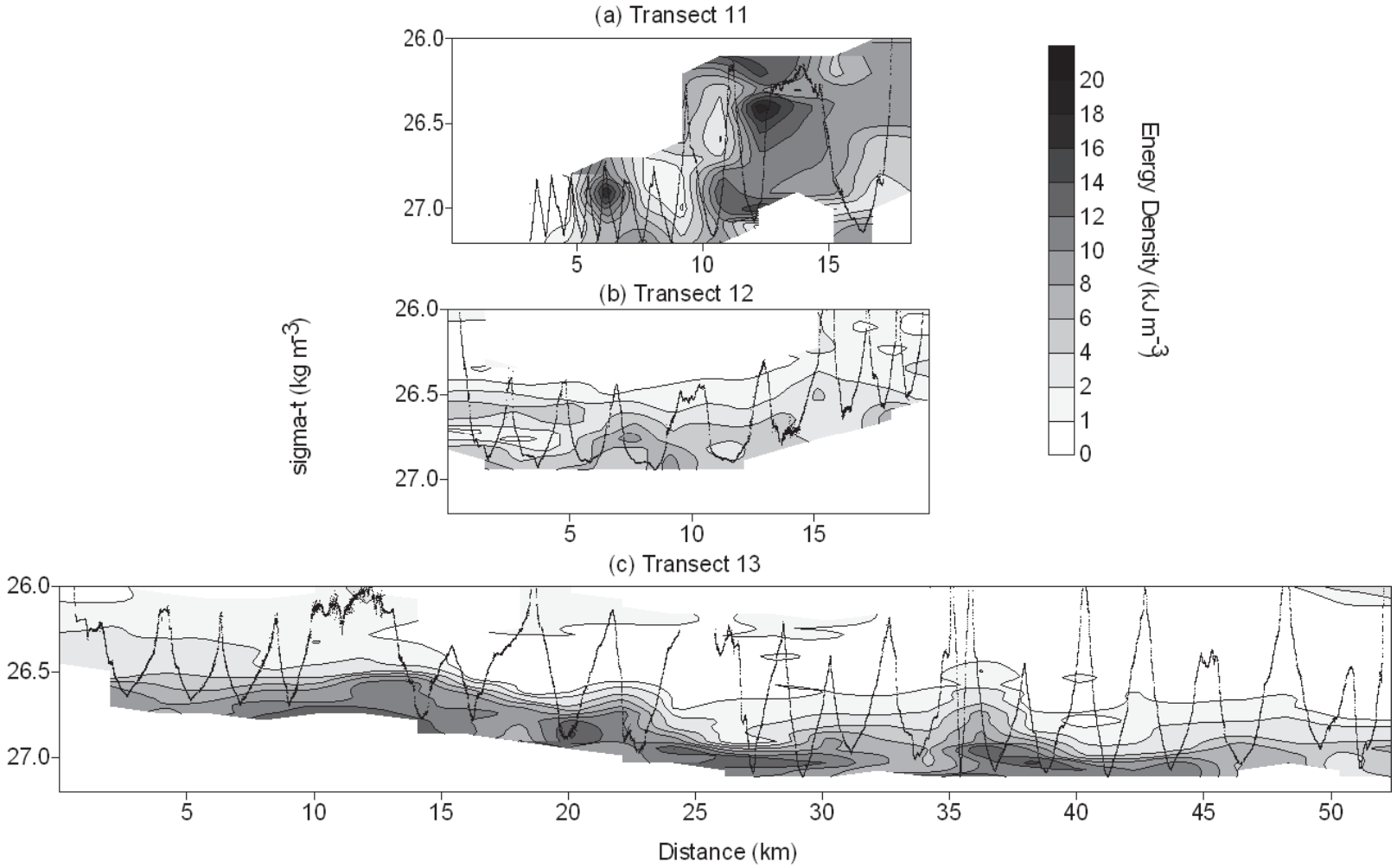

Figure 5.28 Sectional distribution of diapausing copepod energy density (kJ m^{-3}), as a function of distance along the transect (km) and water mass density (kg m^{-3}) below 50 m depth estimated using the TUBSS-mounted OPC in August 2009 in Roseway Basin along the transects 11 through 13 (panels a through c). Transects 11 (a) and 12 (b) were oriented cross-Basin (NW - SE) and transect 13 was oriented along-Basin (SW - NE). The direction of each tow is depicted, the TUBSS-tow profiles are plotted, and the geographic location of each tow in the Basin is pictured in Figure 5.1d.

5.3.3 Interannual comparison among 2007, 2008 and 2009 surveys

Below I discuss the similarities and differences in the biological and physical characteristics of Roseway Basin I determined among the three surveys. While I describe the variation as interannual for convenience, I recognize that the variation I describe could be associated with both interannual and intra-annual (e.g., survey timing in relation to biological production timing) processes. I address this in the discussion.

5.3.3.1 Calanus spp. size, stage structure, abundance and distribution

A comparison of the broad-scale patterns in *Calanus* spp. size, stage structure, abundance and distribution among the 2007, 2008 and 2009 surveys demonstrated that every year, the Roseway Basin system was similar in several important ways, and different in other equally important ways (Table 5.7). First I will discuss the similarities among years. Perhaps most importantly to right whales, every year a substantial population of diapausing *Calanus* spp. was aggregated at depth in the Basin. The copepod concentrations in the deep layer reached 5000 m^{-3} in 2008; the year with the lowest observed concentration. At least 74 % of the population in the deep layer consisted of *C. finmarchicus* stage-C5, followed by C. *hyperboreus* (primarily stage-C4) and finally *C. glacialis* (primarily stage-C5) (Tables 3.3, Tables 5.3 - 5.6). Based on the depth- and stage-structure of the *Calanus* spp., I estimated that at least 60 % of this population was in diapause during the time that right whales occupy the Basin in any given year, however I did not find a population of copepods that was 100 % diapausing at depth. Finally, every year right whales were sighted in the habitat during the survey. Thus I conclude that during all three years I surveyed Roseway Basin, it is possible that the copepod abundance and distribution I measured was sufficient to make the Basin a suitable feeding habitat for foraging right whales. However, the number of whales that the Basin could support and the length of time a whale could be supported was likely interannually variable.

There were also strong differences among years in all measured variables that could explain interannual variability in right whale occupancy timing and carrying capacity (Table 5.7). These differences show that the Roseway Basin habitat is very dynamic and the prey field details likely depend strongly on processes that occur at the

surface and external to the Basin. The year 2007 was the highest concentration year for copepods in Roseway Basin with the maximum concentrations estimated using BIONESS-nets at 6000 m^{-3} and by BIONESS-OPC at 12 000 m^{-3}. Using only the BIONESS-net data, a comparison of diapausing copepod concentrations among years showed that 2007 had significantly higher concentrations than in the latter two surveys (ANOVA, $P<0.001$, Figure 5.29). If I had used the TUBSS-OPC in 2007, I am confident I would have measured smaller scale aggregations exceeding 12 000 m^{-3}. The year 2009 had the second-highest copepod concentrations when both the surface and deep layer concentrations were added together (Table 5.7). In terms of energetics, the deep layer copepods contained a higher energy content than the surface layer, since diapausing animals are at their annual and life history maximum in lipid content. As I did not measure the energy content of animals in the surface layer, the total prey energy density available to right whales cannot be reliably estimated in 2009.

The year 2008 saw the lowest copepod concentrations in Roseway Basin (Table 5.7), however a slope water intrusion brought diapausing copepods in locally high concentrations from the continental slope into the Basin. The frequency of occurrence for slope water intrusions (as in 2008) is not known, and there was no evidence of such in 2007 or 2009. As slope water intrusions appear to be ephemeral and unpredictable events, it is not possible to know how frequently they may have resupplied the deep Basin with copepods in 2008 compared with the other two years, however it might be inferred if the dynamics that cause slope water intrusions (e.g., storms) are determined. Variation in the spatial extent of the diapausing copepod layer among years also made 2008 generally less lucrative from an energy perspective than the other two years. Diapausing copepods were present in high concentrations at the western, relatively shallow, end of the Basin in 2007 (Figure 5.11a, b) and 2009 (Figure 5.28b), but not in 2008 (e.g., Figure 3.13d).

The number of *C. finmarchicus* generations produced also differed among years. The number of generations and their identities as G_0 (emerging from overwinter), G_1 (first of the year) or G_2 (second of the year) can be identified based on prosome length frequency distributions (PL, McLaren *et al.* 2001). G_0 (mean PL at stage-C5 = 2.3 mm) are produced the prior year and die off in spring after producing G_1. The G_1 generation

(mean PL at stage-C5 = 2.6 mm) then produces a smaller G_2 generation (mean PL at stage-C5 = 2.3 mm, McLaren *et al.* 2001). Skewed or bimodal length frequency distributions from net collections indicate multiple generations that are mixed together (McLaren *et al.* 2001). In 2007, most animals were in diapause phase (stage-C5), and the prosome length frequency distribution of the diapausing C5s was normally distributed with a mean of ~2.3 mm (Figure 5.30a). This indicates that they were a single generation of primarily G2 individuals, although the slightly higher-than-normal abundance at 2.4 mm could be indicative of a less abundant G_1. The large number of adults (up to 100 m^{-3}) also present in Roseway indicates that a third, autumn generation would likely have been produced in 2007. In 2008, most animals were in diapause, however the length frequency distribution of C5s was larger than in 2007, bimodal (modes at 2.3 mm and 2.6 mm), and skewed toward larger size classes, indicating a mixture of G1 and G2 individuals at depth with a fairly strong influence of G_1 (Figure 5.30b). In 2009, it is likely there were three or more generations of *C. finmarchicus* based on the stage-structure and depth distribution of copepods. The length frequency distribution of C5s diapausing at depth had a mean of 2.2 mm and was again slightly skewed toward larger size classes, indicating a mix of G1 and G2 individuals with a greater dominance of G2 than in 2008 (Figure 5.3c). The length frequency distributions of *C. hyperboreus* C4 (Figure 5.30d-f) reflected the same interannual pattern as the *C. finmarchicus* C5.

The species composition of copepods diapausing in the Basin was also variable among years. In 2007 the proportion of cold-water *Calanus* spp. was quite high at 26 %, while in 2008 and 2009 the proportion declined. *C. hyperboreus* was always the dominant cold-water species and *C. glacialis* was rare. The entire system was more diverse in 2009 than in other years, with *Centropages* spp. *Metridia* spp. and *Pseudocalanus* spp. all being measured in relatively high abundance, though dispersed in the surface layer.

Table 5.7 Interannual comparison of *Calanus* spp. abundance, distribution and water mass associations in Roseway Basin among the years 2007, 2008 and 2009. Comparisons are made concerning the maximum *C. finmarchicus* C5 + *C. hyperboreus* C4 concentration measured in the deep layer by BIONESS nets (Max [Deep Net] (m^{-3})); maximum *C. finmarchicus* C5 + *C. hyperboreus* C4 concentration measured in the deep layer by the BIONESS-OPC (2007) or TUBSS-OPC (2008 & 2009) (Max [Deep OPC] (m^{-3})); approximate concentrations of the surface copepod population estimated from the BIONESS-OPC profiles (Figures 5.3 (2007), 3.6 (2008), and 5.14 (2009)), approximate average proportion of the *Calanus* spp. population that was in diapause based on stage-C5 abundance at depth (Tables 5.3 (2007), 3.3 (2008), and 5.4 – 5.6 (2009)), *C. finmarchicus* stage structure, average proportion of cold-water *Calanus* spp. compared to *C. finmarchicus* at depth, sources of *Calanus* spp. to the deep Basin and copepod-water mass associations.

Year	Max [Deep Net] (m^{-3})	Max [Deep OPC] (m^{-3})	Surface Population	Diapausing Population	*C. fin.* Stage structure	Cold-H_2O *Calanus* spp.	Source	Water mass Assoc.
2007	6000	12 000	None	90 %	C4s, C5s, adults	26%	unknown	iBW
2008	1100	5000	Isolated patches	99 %	Mostly C5s	19 %	Slope	iBW, fronts
2009	1600	6000	4000 m^{-3}	60 %	C3s, C4s, C5s	15 %	Shelf	iBW, mBW

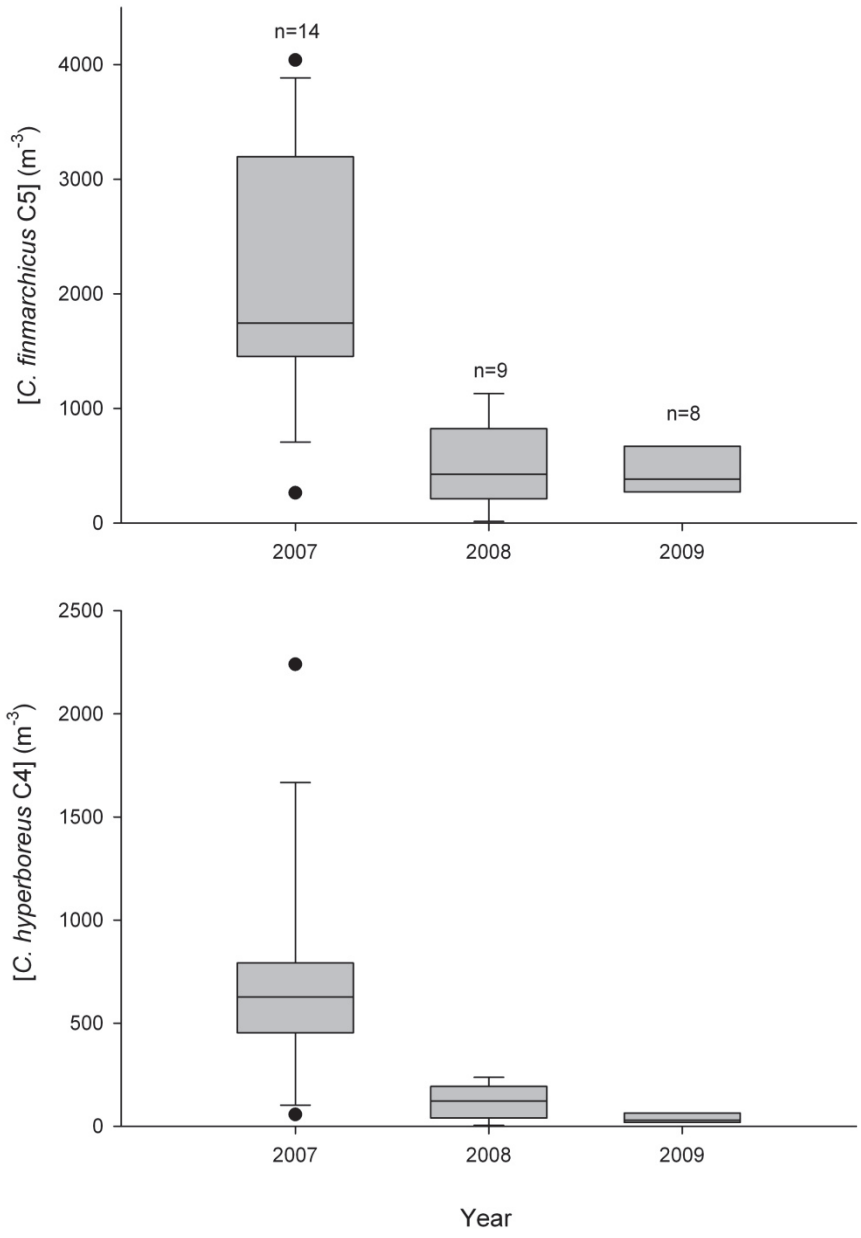

Figure 5.29 Box plot representation of interannual variation in the concentrations of (a) *C. finmarchicus* C5 and (b) *C. hyperboreus* C4 collected with the BIONESS nets at depths >100 m in Roseway Basin during the 2007 - 09 surveys. The median, interquartile range and outliers are provided.

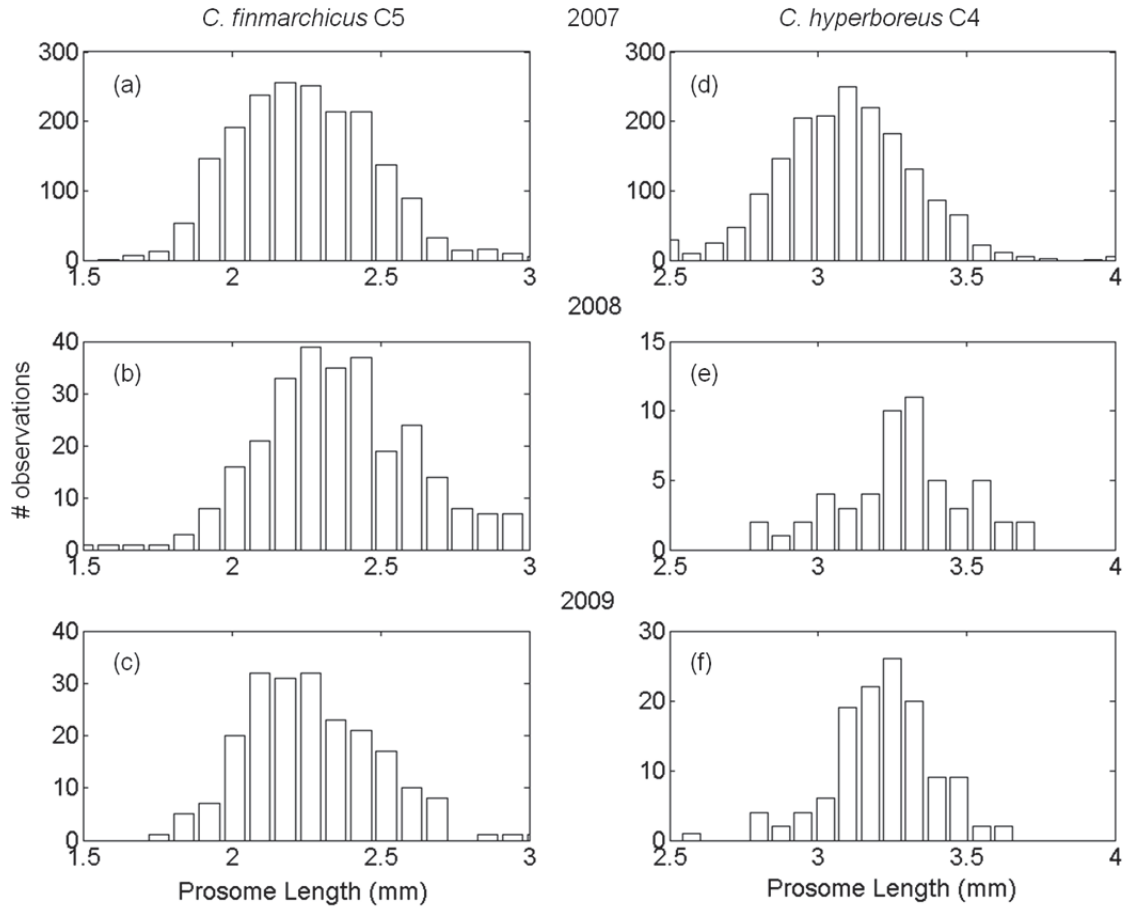

Figure 5.30 Frequency histogram distributions of interannual variation in late-summer prosome length (mm) of (a-c) *C. finmarchicus* stage-C5 and (d-f) *C. hyperboreus* stage-C4 among the (a, d) 2007, (b, e) 2008 and (c, f) 2009 field seasons.

5.3.3.2 Hydrography

Variation in the hydrographic properties of the end-member water masses (BW, iBW and mBW) and their relative contribution and distribution appears to be responsible for the basin-scale interannual variation in the deep waters of Roseway Basin. Each year, the hydrographic properties of each end-member differed (Table 5.8, Figure 5.31). In 2007, only 2 end-members were present (BW and iBW) while in 2008 and 2009 all three water masses were present. The lack of mBW in 2007 meant the water tended to be colder, especially along the SE margin where mBW was prominent in other years. The BW and iBW masses in 2007 were more saline and higher in density than in 2008 or 2009, and BW was 1 ^{o}C colder. Thus, the deep water of Roseway Basin in 2007 was cold, saline and dense compared to other years. Comparing 2008 and 2009, all three water masses were warmer and more saline in 2009, which meant that the entire water mass structure in the Basin was slightly denser than in 2008. There was a particularly strong contrast in the T-S properties of iBW between 2008 and 2009. The iBW water was very cold and fresh in 2008, possibly indicating greater mixing between iBW and BW in the deep Basin than I initially proposed in Chapter 3. Notably important to copepods in the Basin, each year the water only reached densities greater than 1026 kg m^{-3} when iBW was present.

Charts depicting the general horizontal spatial distribution and relative proportion of each end-member in relation to Basin bathymetry each year show that interannual variation in water mass distribution can be characterized based on how far into the Basin the mBW intruded over the southern bank (Figure 5.32). In all three years, the deepest part of the Basin was filled primarily with iBW. BW advected along the northern Basin margin, then turned south around the western Basin margin, possibly driven in that direction by bathymetric steering along the slope. At the western Basin margin, the BW abruptly stopped where it met slope water that dominated on the southern Basin margin and bank. In 2007, BW extended its influence across the entire southwestern margin, where it then mixed with iBW water on the southern margin and bank (Figure 5.32a). No mBW intruded over the bank or into the Basin in 2007. In 2008, the BW was abruptly cut-off at the southwestern margin by mBW that had intruded over the southern bank and margin, and into the deep water of the Basin on the SE margin (Figure 5.32b). In 2009,

the mBW mass was restricted to the bank, and both iBW and BW intruded farther south (Figure 5.32c).

Smaller-scale spatial variation in the water mass structure was also highly variable from year to year (Figure 5.33). In 2008, the water mass structure in the deep Basin was highly spatially variable; water mass fronts were prevalent throughout the Basin caused mainly by the mBW core that penetrated the middle of the Basin. In 2009, there were also water mass fronts in a cross-Basin direction at the western end of the Basin (transect-12, Figure 5.23), but at the eastern end of the Basin, where the majority of copepods aggregated, the water masses were spatially quite similar and stable (transect-11, Figure 5.22). The least amount of spatial variation in water mass structure occurred in 2007, likely because of the absence of mBW that year. For example, I compared the vertical profiles of hydrography collected mid-Basin, where the copepods were most highly aggregated, among the three survey years (Figure 5.33). It is easy to see from this comparison that 2008 was a markedly different year in the mid-Basin relative to 2007 or 2009, and the differences in the vertical water mass structure among years reflect the same pattern described above concerning the horizontal spatial structure.

As explained in Chapter 3**,** the downward tilting of isopycnals toward the Basin margins at depth in 2008 reflected geostrophic flow in the Basin that maintained a gyre-like circulation at depth. I also noted that this tilting at depth was partially caused by the dense slope water core that created higher density water at shallower depths in the mid-Basin compared to the margins (e.g., Figure 3.21, 3.22). In addition, the intrusion of higher density mBW over the southern bank, and the intrusion of lower density BW over the northern bank, caused the isopycnals in the shallower water to tilt upward on the southern margin and downward on the northern margin, causing westward flow in all directions above 100 m depth, though in reality, this only slowed the eastward flow, because baroclinicity only contributed ~1/3 of the total velocity (Chapter 4). I concluded that this structure aided in the tilting of the prey field upslope along the southern boundary, where it was susceptible to accumulation processes at a tidal mixing front.

Although I am unable to resolve the basin-scale density structure from the 2007 data, I can make a comparison between 2009 and 2008. In 2009, transect-12 and -13 showed downward tilting of isopycnals at the western end of the Basin (Figures 5.23c

and 5.24c), indicative of geostrophic flow along the margin. At transect-11, where in 2008 I observed the greatest isopycnal doming at depth, in 2009 the isopycnals were generally horizontal (Figure 5.22c), likely because there was no mBW core in 2009 to cause doming in the middle of the Basin. Hence there was no or reduced geostrophic flow along the southeastern margin in 2009. There was also no cross-basin tilting of isopycnals in the upper layer in 2009 because the mBW was restricted to the southern bank (Figure 5.32c) and it did not intrude onto the margin to tilt the ispycnals upward. Hence, two of the major processes that explained the large-scale distribution of copepods in Roseway Basin in 2008, the gyre-like circulation and upslope tilting of isopycnals on the SE slope, were not apparent in 2009. In addition, there was no evidence of slope water intrusions at the eastern end of the Basin in 2009, as there was 2008, to supply the deep Basin with high aggregations of copepods.

Table 5.8 Interannual comparison of water mass end-member hydrographic properties in Roseway Basin during late-summer 2007 - 2009. Water mass end-members are Basin Water (BW), intermediate Basin Water (iBW) and modified Basin Water (mBW).

Water Mass	Year	Temperature (^{o}C)	Salinity	σ_t (kg m^{-3})
BW	2007	2.0	32.5	26.0
	2008	3.0	32.0	25.5
	2009	3.3	32.4	25.8
iBW	2007	6.0	33.8	26.7
	2008	4.8	33.1	26.3
	2009	6.2	33.7	26.5
mBW	2007		Not present	
	2008	7.0	33.3	26.0
	2009	7.5	33.2	26.0

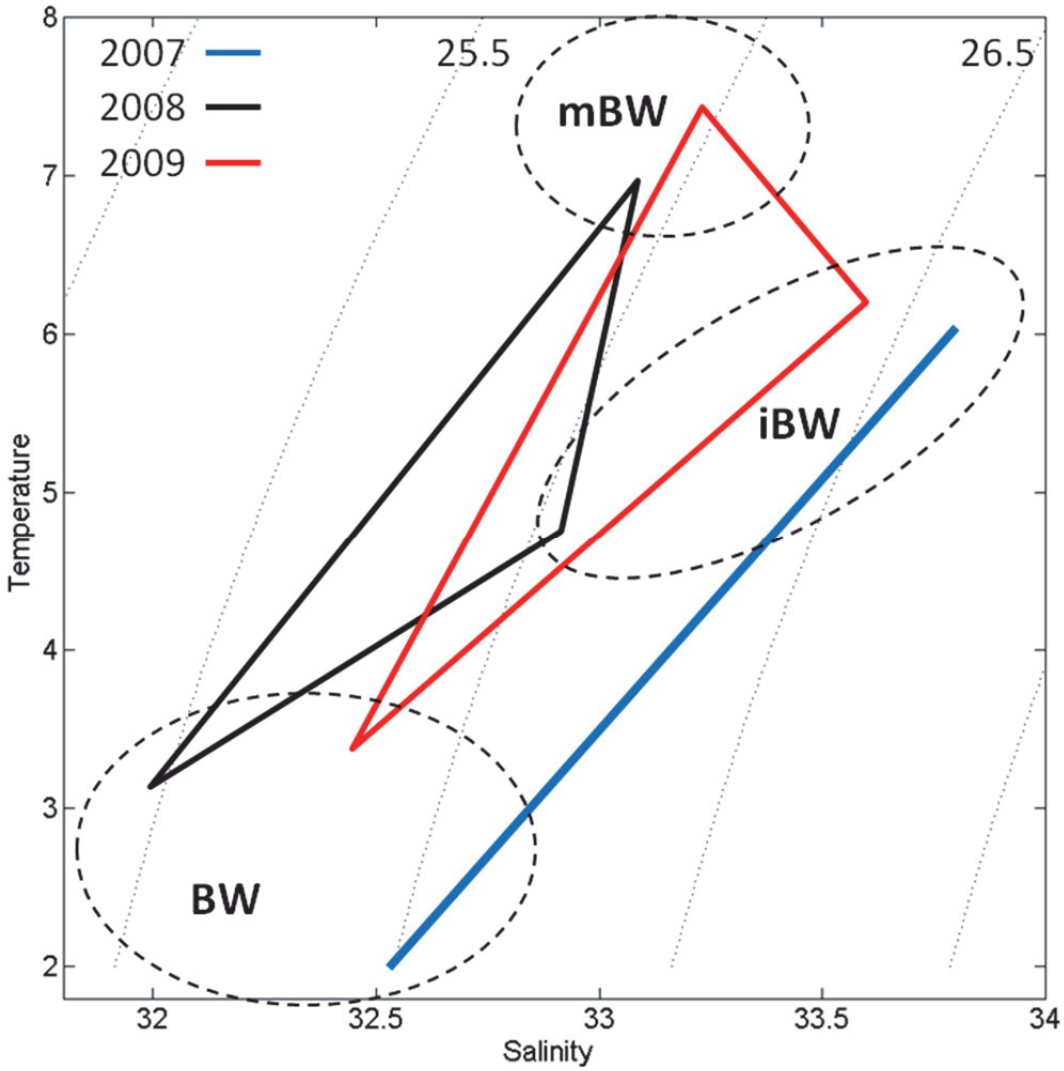

Figure 5.31 T-S diagram showing interannual variation in the water mass end-member hydrography in Roseway Basin. Lines are drawn between end-member T-S signatures within the same year (blue=2007, black=2008, red=2009) to show variation in the overall water mass structure in the Basin among years. Each end-member and its respective 2007 to 2009 T-S signatures are encompassed with a hatched line, and isopycnals are labeled.

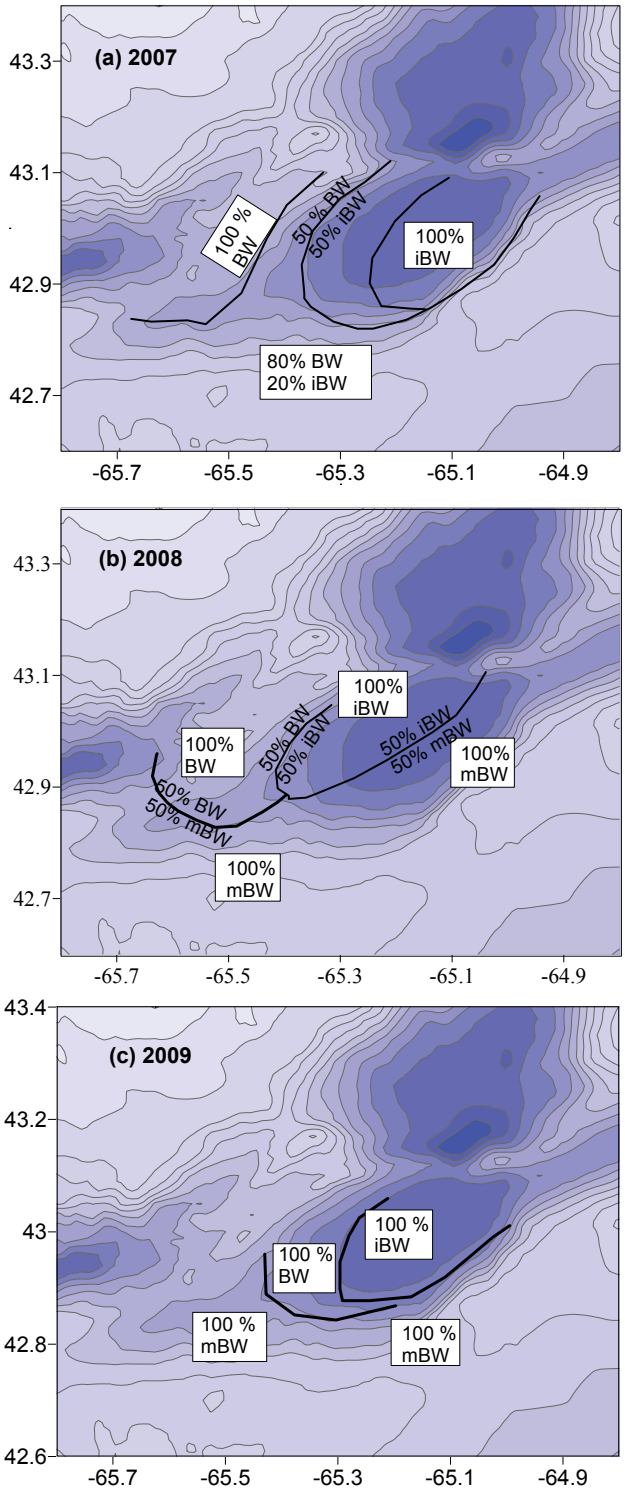

Figure 5.32 Charts of Roseway Basin illustrating the interannual variation in the general water mass structure in Roseway Basin averaged over the 90 – 160 m depth interval during late-summer in (a) 2007, (b) 2008 and (c) 2009. Approximate proportions are derived from the T-S diagrams presented in Figures 3.17, 5.9 and 5.26, respectively.

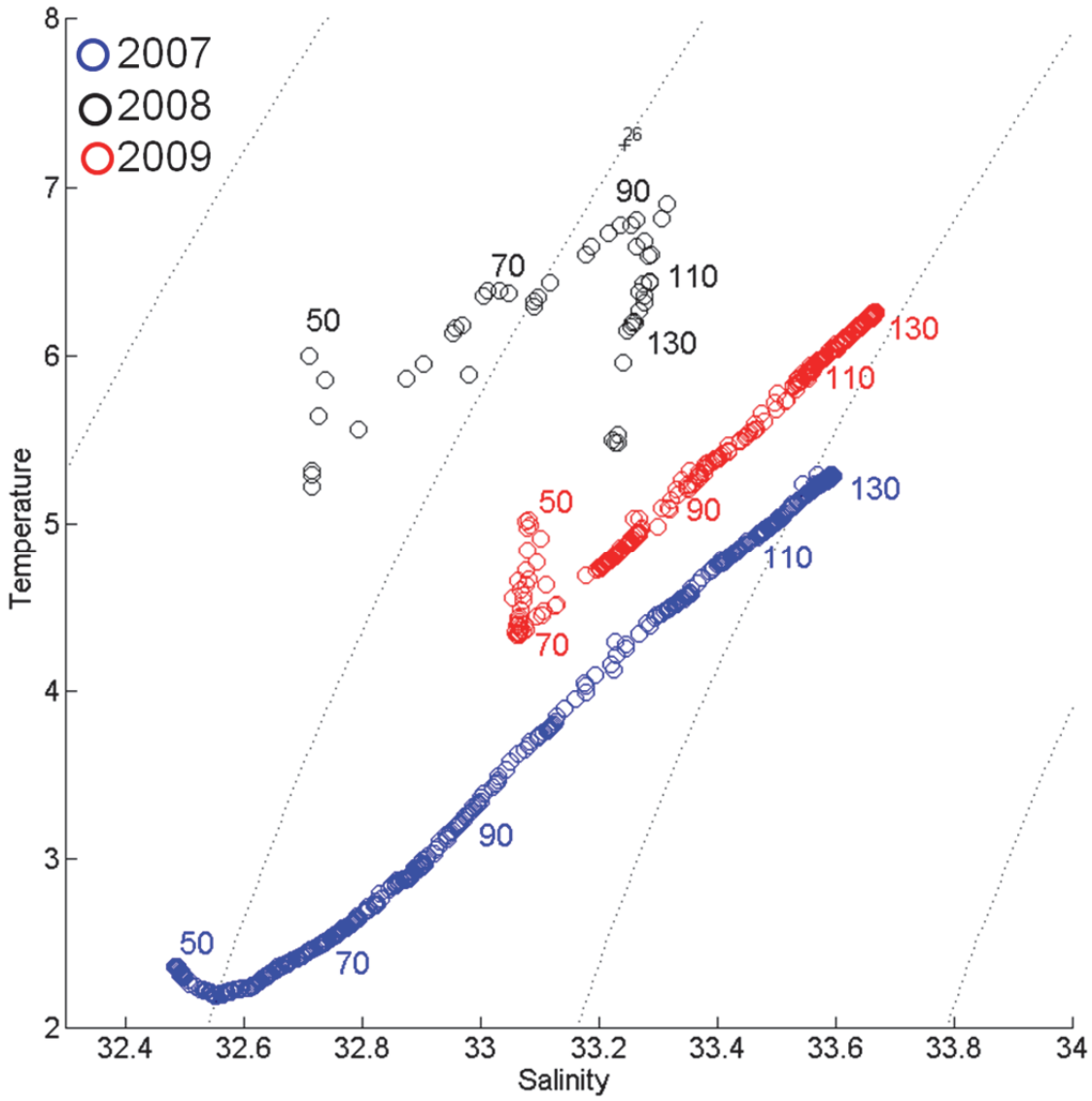

Figure 5.33 T-S diagram illustrating interannual variation in hydrographic profiles collected in approximately the same location near the center of Roseway Basin each year during late-summer in 2007 (blue), 2008 (black) and 2009 (red). The 50 m, 70 m, 90 m, 110 m, and 130 m depths are labeled on each profile.

5.3.3.3 Copepod - hydrography associations

There are two important aspects to consider when examining copepod - hydrography associations in Roseway Basin; one is the basin-scale abundance and distribution of copepods in relation to the water mass end-members, and the other is the smaller scale aggregations in relation to physical aggregative processes. I address each of these in turn.

Basin-scale associations

The strongest relationship I found in my analysis was that between the annual average copepod concentration and the presence and density of the intermediate Basin Water. Each year, intermediate Basin Water filled the bottom of the Basin, and the diapausing copepods were aggregated within that water. In 2007, the density of iBW was high, as was the average copepod concentration. The vertical distribution of copepods that year was clearly associated with water density; wherever the density reached 1026 kg m^{-3} or more, the copepods were concentrated. The layer was thick where the isopycnal was shallow, and restricted to a thin deep layer where the isopycnal was deep (Figure 5.11). In 2009, the density of iBW was lower than in 2007 concurrent with decreased copepod concentrations, and in 2008 the iBW was lowest in density and copepod concentrations were, on average, quite low and densely aggregated near-bottom where the 1026 kg m^{-3} water was also near-bottom. Along the southern slope in 2008, copepod concentrations exponentially increased in water with densities higher than 1026 kg m^{-3} (Chapter 4). The hydrographic relationships were not quite as clear or as strong in 2009 as in 2007 or 2008 due to the abundance of non-diapausing, vertically migrating copepods that were able to cross isopycnals; however the diapausing aggregations were situated below the 1026 kg m^{-3} isopycnal. I conclude that water of a 1026 kg m^{-3} density is biologically relevant and may be a density limit for diapausing copepod habitat at the basin-scale. Whether or not intermediate Basin Water is itself an important source of copepods to the Basin can only be speculated, however the lack of mBW in 2007 suggests that the Nova Scotia Current, which mixes with iBW along the southern slope as it leaves the Gulf of St. Lawrence, was stronger that year than other years, concurrent with very high average copepods concentration estimates.

Diapausing copepods were present in high concentrations at the western end of the Basin in 2007 (Figure 5.11a, b) and 2009 (Figure 5.28b), but not in 2008 (e.g., Figure 3.13d). The paucity of high concentrations at the western Basin margin in 2008 was explained by the presence of Basin Water at depths >100 m. BW was lower in density in 2008 than in 2007 or 2009 (Figure 5.32), so it is probable that this low density water at depth was an unfavorable environment for diapausing copepods.

Smaller scale associations and aggregative processes

In Chapters 3 and 4, I presented evidence of several processes that were operating to aggregate diapausing copepods into discrete patches in 2008. To review, these included the vertical distribution of the 1026 kg m^{-3} isopycnal, cross-basin tilting of the deep layer that pushed the animals upslope on the southern margin, a mixing front along the southern margin that aggregated and disaggregated a patch at tidal frequencies, replenishment of individuals to the southern slope by gyre-like recirculation, numerous water mass fronts that were present throughout the Basin, and a slope water intrusion. My analysis of the 2009 data across the southern margin showed that individual copepod patches were not retained in a single area over long time scales, but rather were advected around the Basin by the gyre-like circulation. I cannot assess whether most of these mechanisms were present in the other two years because the OPC/CTD surveys were less extensive and ADCPs were not deployed in 2007 or 2009. However, I can make some inferences based on the data available. All the data, and my analyses, suggest that in 2008, the mesoscale aggregative processes were stronger than in either 2007 or 2009. In the vertical, the depth of the 1026 kg m^{-3} isopycnal restricted animals in 2008 to thickly concentrated layers at depth, whereas in 2007 and 2009, the shallow depth distribution of this layer allowed copepods to be spread more evenly throughout the deep water column except near the Basin margins. In particular, there were localized areas at the western end of the Basin in 2007 where the 1026 kg m^{-3} isopycnal was deep and again copepods there were concentrated in a thick layer below this isopycnal at depth (Figure 5.11).

In 2008, a coupling between the gyre-like recirculation, cross-basin tilting of the deep copepod layer, and a tidal front, caused copepods to aggregate along the southern margin. I cannot properly assess whether these processes were occurring together in

2007 or in 2009. However, there was definitely no cross-basin tilting of the deep copepod layer in 2009, and no evidence of geostrophic flow along the southern slope set up by tilted isopycnals. In 2009, there was a tidal mixing front that separated well mixed mBW on-bank from stratified iBW across the southern slope at the western end of the Basin (transect-12, Figure 5.23) however no front was observed in the deep Basin (transect-11, Figure 5.22). I speculate that if the above processes were operating in 2009, their collective aggregative influence was substantially weaker than in 2008.

Vertical water mass fronts were observed at the western end of the Basin in 2009 where the BW mass meandered around the Basin margin. However, these were not nearly as prevalent as in 2008, when the mBW core created vertical temperature fronts throughout the Basin. I speculate that vertical water mass fronts were minimal in the Basin in 2007 since the mBW mass was not present. Slope water intrusions were also not apparent in 2007 or 2009, though these are ephemeral events. From these observations I conclude that the mesoscale aggregative processes in 2008 were stronger than either in 2007 or 2009.

5.4 Discussion

5.4.1 Summary of main findings

In summary, 2007 was a year of high diapausing copepod concentrations that included a large proportion of *C. hyperboreus*. Year 2008 reflected the lowest diapausing copepod concentration estimates and a smaller proportion of *C. hyperboreus*. The year 2009 was intermediate in relation to 2007 and 2008 with high abundance estimates of *C. finmarchicus* at the surface and in an earlier phase of development. Diapausing copepods were aggregated at depths below the 1026 isopycnal, that varied in its depth distribution from year to year with the proportion of intermediate Basin Water.

5.4.2 Copepod abundance in Roseway Basin in relation to Shelf production

The seasonal and interannual trends in both plankton abundance and physical oceanography in the North Atlantic show regional coherency due to the advective nature of the system and the fundamentally annual cycles of phytoplankton and zooplankton production (Johnson *et al.* 2012). These "regions" include, for example, Western Scotian Shelf, Eastern Scotian Shelf, Gulf of St. Lawrence, Fundy-Gulf of Maine, Labrador Sea, and the Newfoundland Shelf. Water mass variation tends to be coherent over broad horizontal scales both within and among adjacent regions, whereas both phytoplankton and zooplankton dynamics are coherent among sites within regions but can have opposing trends among adjacent regions (AZMP 2010). The variability I observed in large copepod abundance, stage-structure and spatial distribution in relation to water masses within the Roseway Basin indicated that the majority of those copepods were produced on the Scotian Shelf in spring and summer. Thus, interannual variation in average concentrations of copepods in Roseway Basin could be explained at least partly by variation in the temperature and phytoplankton-dependent production of copepods upstream (to the NE) of Roseway Basin earlier in the year and subsequent advection into the Basin.

Each year, scientists with the Atlantic Zone Monitoring Program (AZMP) and Northwest Atlantic Fisheries Organization (NAFO) collect and analyze biological, physical and chemical data based on standard surveys lines and stations from several sampling programs (e.g., groundfish surveys, AZMP, Continuous Plankton Recorder,

satellite remote sensing, etc.) to monitor regional-scale seasonal and interannual variability from the Labrador Sea to the Gulf of Maine. The data are reported in annual AZMP bulletins, NAFO Scientific Council Research Documents and CSAS Research Documents, and these annual reports are useful for interpreting the trends I observed in Roseway Basin in 2007 - 2009 within the larger Scotian Shelf/Gulf of St. Lawrence system. The most useful comparative data come from the Halifax Line and Halifax Station-2 (a fixed station), both in the Emerald Basin area ~100 km upstream of Roseway Basin, the Louisburg Line at the eastern extent of the Eastern Scotian Shelf ~ 300 km upstream of Roseway Basin, the Browns Bank Line, that transects the Shelf just southwest of Roseway Basin, and the NAFO statistical area 4X, that envelopes Roseway Basin.

5.4.2.1 2007 Comparison

In 2007, the physical dynamics on the Scotian Shelf were influenced by flow from the Arctic, bringing cold water copepod species to the southern extent of their range. The relative abundance of the cold-water *C. glacialis* had diminished between 2001 and 2006 near Halifax, presumably due to warming ocean conditions and a reduction in the Cold Intermediate Layer (CIL) (AZMP 2008). In 2007, this trend reversed on the Scotian Shelf. The CIL increased in volume and the biomass of the Arctic species *C. hyperboreus* increased; these are indicators of increased advection of Labrador Slope Water onto the Shelf (Galbraith *et al.* 2010, AZMP 2010, AZMP 2008, Petrie *et al.* 2008). The 0 to 100 m averaged temperatures at Halifax Station 2 were 2.1 standard deviations below the 1971 - 2000 average of 4.6 ± 0.6 ^{o}C (AZMP 2010) and Halifax SST was 1 ^{o}C below normal, making 2007 the 10th coldest year in 87 years (Petrie *et al.* 2008). Salinities at Halifax Station 2 were 0.5 above normal from 100 m to the bottom (Petrie *et al.* 2008). Bottom water temperatures in NAFO Fisheries Area 4X were 1.6 standard deviations below the 1971 - 2000 average of 7.4 ± 0.7 ^{o}C (AZMP 2010). Extreme temperature anomalies of 6 ^{o}C below normal were measured over the continental slope, and the Shelf-slope water front was 30 km south of its long-term average position of 100 - 200 km from the Shelf edge (Petrie *et al.* 2008). Overall, 2007 was a cold year in the region of Roseway Basin.

The most notable biological event in 2007 was a large magnitude and widespread spring bloom in April that reached near-record levels compared to the 1998 - 2006 average in the Gulf of St. Lawrence and on the Scotian Shelf (AZMP 2008). In some areas, the phytoplankton biomass was >4 fold higher than was observed over the previous 10 years. While the bloom was strong and widespread over the Scotian Shelf, its duration was short and phytoplankton biomass levels outside the bloom declined (AZMP 2008). During the bloom, high abundances of early-stage copepods were measured in the GoSL / SS region, and were composed of 60 – 90 % large calanoid copepods (Harrison *et al.* 2008, Johnson *et al.* 2012). The maximum in *C. finmarchicus* abundance was the highest since records began in 1999, although it came later in the year and was shorter in duration than usual at Halifax Station 2 (Harrison *et al.* 2008). Record high biomass levels of *Calanus hyperboreus* were present at Halifax Station 2 in spring (AZMP 2008). Later copepodid stages entered diapause in July, later than usual, and a second maximum of early copepodid stages occurred in September indicating a late-in-the-year generation. However, the burst of food and early-stage copepods did not appear to result in increased concentrations of late-stage copepods on the Scotian Shelf, because broad-scale trawl surveys on the Scotian Shelf in 2007 indicated that water-column averaged mesozooplankton abundances were below normal levels in July (Harrison *et al.* 2008, AZMP 2008).

Changes in the isopycnals occurred between 18 March and 04 April 2007, where the 25 and 25.5 kg m^{-3} sigma-t surfaces rose from 52 and 124 m to the surface and 44 m (Petrie *et al.* 2008). The authors surmised that this rising of isopycnals could have been due to strong onshore movement of water from off Shelf, and further proposed that the intrusion could supply the nitrogen needed to support the large and widespread phytoplankton bloom that year. This intrusion could also supply the Shelf with emerging adult copepods from the continental slope populations, thus explaining why the abundance of emerging adults was anomalously low in early spring before the intrusion (Harrison *et al.* 2008), yet record numbers of young were produced that year. This off-Shelf supply mechanism has been detected in late-winter/ spring in other years (Head *et al.* 1999).

The physical observations made by the AZMP group for the Scotian Shelf region were entirely consistent with the observations I made in Roseway Basin in 2007, and the biological observations were also consistent. The Shelf water masses I measured were cold and contained a significant population of *C. hyperboreus,* which is consistent with lack of warm modified Basin Water and increased input of colder-than-average Basin Water (Figure 5.32). A large bloom of phytoplankton in spring, contemporaneous with the emergence from diapause of breeding copepods (Zakardjian *et al.* 2003), explains the subsequent high production of early-stage copepods and second generation of copepods produced in spring 2007. And, since the water was cold that year, and growth is positively related to temperature in ectotherms, it also makes sense that these generations entered diapause late in the year (July). If the number of G_0 (emerging adults) were small in 2007 as estimated by Harrison *et al.* (2008), then the G_1 may have been relatively small as well, but produced a large G_2 due to the increased food availability in April. However, G_2 are not usually produced until June, and with the cold water and resulting long development time, it seems more reasonable that the G_1 generation was the abundant generation measured during the spring bloom. This would indicate that the Shelf was supplemented with G_0 from elsewhere, for example, the slope water intrusion.

Regardless of their origins, in the following exercise I demonstrate that the large number of early stage copepods measured on the Shelf in spring can account for the substantial number of diapausers I measured in Roseway Basin in September. The spring season average of *C. finmarchicus* was ~15 000 m^{-2} at each transect line on the Scotian Shelf, and I assume these resided primarily near the surface (Harrison *et al.* 2007, their Table 2). I assumed that all copepods (15 000 *C. finmarchicus* m^{-2}) in the waters over Roseway Basin (area ~1000 km^2) at the beginning of July sank and diapaused in the Basin. In addition there was constant replenishment of 15 000 *C. finmarchicus* m^{-2} for 31 days (July) at the northeastern end of Roseway Basin from horizontal advection into the Basin by a current of 0.01 m s^{-1} (this could replace the entire surface water of the Basin just less than once). I assumed that the surface water that was replaced and left Roseway Basin had no copepods (i.e., immigration only, no emigration). I also assumed, based on my data, that the animals diapaused in a layer 40 m thick at the bottom of Roseway, and that there was no immigration or emigration of diapausers at depth. Using these

assumptions I estimated that average concentration of diapausing copepods at the bottom of Roseway would be ~800 m^{-3}. During the spring maximum, the *C. finmarchicus* abundance at the Halifax Line was 210 000 m^{-2}. Under the same assumptions above, the average diapausing concentrations in the bottom of Roseway from the spring maximum alone would be 10 000 m^{-3}. It is likely that the actual number of copepods that enter diapause in Roseway Basin in late-summer will reflect the concentrations at the surface somewhere between the spring average and the spring maximum. The median concentration I measured in my nets was 1800 m^{-3} with maxima as large as 12 000 m^{-3}; this shows that it is feasible that the large number of early stage copepods on the Shelf in spring could have solely supplied Roseway Basin with its diapausing population in 2007.

The AZMP survey of 2007 reported overall low mesozooplankton biomass in deeper waters of the Shelf, although *C. finmarchicus* abundance was average (Harrison *et al.* 2008). These surveys generally do not provide adequate estimates of diapausing copepods because the surveys rarely sample the deep Basins and do so at large spatial scales insufficient to capture the diapausing aggregations (i.e., the patches are easy to miss). This would explain the apparent recruitment failure that year measured by the AZMP program despite the early-stage maximum in abundance. Harrison *et al.* (2008) also measured a small second generation produced in September 2007, consistent with the relatively large number of adult *C. finmarchicus* I found in Roseway Basin at that time (Table 5.3).

5.4.2.2 2008 Comparison

Year 2008 was again an anomalously cold year at the surface at Halifax Station-2, at depth in Emerald Basin, and at depth in NAFO Area 4X (containing Roseway Basin) (Petrie *et al.* 2009). However, at all three sites the water was warmer than in 2007; for example, deep Basin water in Emerald Basin was 1.2 ^{o}C warmer in 2008 than 2007 (Petrie *et al.* 2009). Outside of Halifax Station-2, the SST anomaly generally increased, leading to above-normal surface temperatures throughout the rest of the region (AZMP 2009). In addition, Area 4X was the only area to demonstrate significant warming (by 0.9 S.D.) near-bottom between 2007 and 2008; other areas were the same temperature or cooler in 2008 (AZMP 2009). The volume of the CIL was 1.7 standard deviations above

normal in 2008 but slightly lower than in 2007 (Petrie *et al.* 2009, AZMP 2009). The mBW mass was colder that year, however there was no mention of the presence or frequency of slope water intrusions onto the Shelf, nor mention of the position of shelf-slope front.

The record high and widespread spring bloom of 2007 did not recur in 2008, and as a result spring chlorophyll levels were, overall, at or below average (Harrison *et al.* 2009). Zooplankton biomass on the ESS in March was nearly the lowest observed on record, but notably, extremely high abundances of *C. finmarchicus* were measured at several stations at the offshore extent of the Browns Bank line in spring of 2008. Zooplankton biomass and *C. finmarchicus* abundance were anomalously low in May, and both exhibited late maxima (June - August, normally April - June) of near-average magnitude at Halifax Station 2. The maximum concentration of *C. finmarchicus* in June-August was normal at 60 000 m^{-2}, but 70% lower than the spring maximum in 2007. High *C. finmarchicus* abundance (~40 000 - 60 000 m^{-2}) then persisted in the summer and fall over the Shelf, but was primarily concentrated west of Halifax and near the Cabot Strait (Harrison *et al.* 2009). Cold water *Calanus* species (*C. hyperboreus* and *C. glacialis*) were more abundant than average at Halifax Station 2 but less abundant elsewhere on the Shelf. The authors concluded that 2008 was a more productive year for large copepods than 2007, but that this peak came later in the year and persisted into the fall, oddly, in the wake of a weak spring bloom.

The trends I observed in copepod abundance and water mass structure in Roseway Basin in 2008 were also consistent with the trends in the Shelf-Slope region that year. Shelf production of *C. finmarchicus* was relatively low in spring and was coupled with a long development time due to cold water is consistent with the relatively low (although still fairly substantial) average abundance of diapausing copepods at depth in Roseway Basin in September. Using the simple approximation above, and applying the 2008 average and maximum spring *C. finmarchicus* concentrations, I estimate that the Shelf could supply Roseway Basin with between 700 – 1000 m^{-3} *C. finmarchicus*, which is within the range I measured that year. The subsequent maximum in *C. finmarchicus* at the surface in summer on the Shelf is consistent with a supplement from the continental slope, that was measured in record numbers in spring. Although no slope water

intrusions were mentioned in the physical report, I provided evidence of a slope water intrusion into Roseway Basin in summer that supplemented the Basin with diapausing copepods from the slope. The upper waters of the western Scotian Shelf could also have been supplied at that time by animals that had not yet entered diapause due to the low temperature slope-water conditions and resulting delayed development. This slope water intrusion, if concentrated on the Western Scotian Shelf, would also explain why NAFO Area 4X experienced a significant warming of the bottom waters relative to other regions.

5.4.2.3 2009 Comparison

In contrast to 2007 and 2008, the year 2009 was entirely unremarkable in terms of the physical and biological characteristics on the Scotian Shelf that are relevant to this study. Bottom temperatures increased across the Scotian Shelf to near-average levels in 2009 (Petrie *et al.* 2010). Sea surface temperatures near Halifax were normal, and the volume of the cold intermediate layer decreased relative to 2008 and was less than the long-term average (AZMP 2010). There was no mention of slope water intrusions onto the Shelf in either winter 2008 - 09 (prior to the spring bloom) or summer 2009 (after the spring bloom). The magnitude of the spring bloom observed at Halifax Station-2 in 2009 (maximum: 670 mg m^{-2}) was considerably larger than the small bloom of 2008 (270 mg m^{-2}) and higher than the long-term average (470 mg m^{-2}). Bloom duration in 2009 (73 days) was also longer than the norm (44 days, Johnson *et al.* 2011), which means it could support more generations of copepods, particularly because development time would be relatively shorter due to the warmer temperatures compared to 2007 and 2008. Annual zooplankton anomalies were lower than normal in 2009, and the timing of the seasonal biomass maximum was normal or near normal (April - June, Johnson *et al.* 2011). Zooplankton biomass was lower than average or average throughout most of the year, with the exception of a higher-than-average spring biomass maximum in April. Both total zooplankton and *C. finmarchicus* abundance were relatively constant throughout 2009, with the highest abundance observed in the winter and fall, in contrast to the climatological annual cycle.

The seasonal trends on the Scotian Shelf in 2009 were also consistent with the abundance and stage-structure of copepods in Roseway Basin in September, and the

water mass temperatures. I measured deep diapausing populations as well as a surface layer populations composed of younger-stage individuals, indicating that multiple generations were produced in 2009. The longer-than-average spring bloom coupled with warmer surface temperatures could support multiple generations of copepods over the summer. The AZMP program also measured high *C. finmarchicus* concentrations in the fall, consistent with my observations. I found no evidence of slope water supplements to the Basin that year, nor was there mention of slope water intrusions across the Scotian Shelf that year. Thus, Shelf production was the only source of copepods to the Basin that year.

To summarize, the most important variables I found that explained the copepod abundance in Roseway Basin in 2007 – 2009 were the magnitude and duration of the spring bloom, the timing and frequency of slope water intrusions onto the Shelf, the number of emerging adults from the previous year, development time (related to water temperature), and number of generations produced. In 2007, the water was cold, the spring bloom was strong and widespread, and a large cohort of calanoid copepods was produced on the Shelf but disappeared relatively early, presumably to diapause in deep Basins on the Shelf. The year 2008 produced a small spring bloom and low copepod abundance in spring. Calanoid copepod concentrations peaked later in the year and reached very high levels by late-summer and fall, but the diapausing copepod concentrations in Roseway in 2008 were lower than in 2007. There is evidence that in both years, Shelf production alone was not sufficient to explain the seasonal trends in copepod abundance on the Shelf, or the variation in the diapausing population in Roseway Basin. The Shelf copepod population appeared to be supplemented by the slope population that was supplied by slope water intrusions onto the Shelf at different times of the year in relation to the spring bloom; in 2007 before the spring bloom (emerging adults), and in 2008 after the bloom (diapausers). In 2009 there was no evidence of slope water intrusions. Instead, the prolonged spring bloom and warmer ocean temperatures on the Shelf could support multiple generations of copepods in the surface layer, and this was reflected in the spatial distribution and stage-structure of copepods in late August in Roseway Basin.

Due to the sparse and variable nature of the data collection, the number of variables involved and few survey years, there is no robust statistical analysis I can do that will determine which combination of variables explains how many diapausing copepods were found in Roseway Basin in a given year. In Chapter 6, I further address this issue in more detail using a longer time series of data, and I include summary tables of all variables important to Shelf copepod production (see Tables 6.5 – 6.7).

5.4.3 Spatial distribution of copepods in the Basin: relationship with water mass density

A frequent assumption of right whale population dynamic studies is that average concentrations of *C. finmarchicus* measured across a habitat(s) provide adequate estimates of the prey available to right whales. Under this assumption, Roseway Basin was most lucrative as a feeding habitat to right whales in 2007, less so in 2009 (if both the surface and at-depth populations are considered), and least lucrative in 2008 (e.g., Figure 5.29). But, as proposed by Baumgartner *et al.* (2007), if the mechanisms of prey aggregation within a habitat were variable, then the amount of food available to right whales will not depend solely on large-scale average prey concentrations. Thus, when I evaluated interannual variation in the available prey in Roseway Basin between 2007 and 2009, I considered both average concentrations and aggregative processes. Below I consider the most relevant of the latter.

5.4.3.1 Biological relevance of the 1026 sigma-t isopycnal

The strongest and most universal aggregative process I measured in Roseway Basin was related to the depth of the 1026 kg m^{-3} isopycnal. Diapausing copepods were found below this isopycnal every year, and their vertical distribution changed depending on the depth of the isopycnal. Where the isopycnal was near-bottom, copepods were concentrated near-bottom, and where the isopycnal was higher in the water column, copepods were spread in a vertically thicker layer (e.g., Figure 5.11 a-c). Notably, diapausing *C. finmarchicus* also aggregate below the 1026 sigma-t isopycnal in the Grand Manan Basin, another major right whale habitat (Michaud and Taggart 2011).

Before I discuss how this process can influence right whale foraging, it is first appropriate to investigate what biological relevance the 1026 isopycnal might have as an environmental lower limit to diapausing Calanoid copepods. The most logical explanation is that at or above the 1026 isopycnal, diapausing copepods are negatively buoyant and sink, while below the 1026 isopycnal, they become neutrally or positively buoyant, and either stay at one depth or float upward. Buoyancy regulation in diapausing copepods is not well described since diapause has not been induced in the laboratory, however the role of lipids in buoyancy regulation has long been considered important. There are three main components to consider when measuring or modeling diapausing copepod buoyancy: (1) the animals have a large lipid sac (mostly wax ester), (2) they also have other biochemical constituents such as proteins and (3) they may or may not be able to regulate their internal ionic composition. Concerning (1) above, wax ester has some interesting buoyancy properties in relation to seawater. Its thermal expansion coefficient is much larger than seawater, and to a lesser extent, lipid compressibility with pressure is also greater than sea water (Yayanos *et al.* 1978). Based on the buoyancy properties of wax ester alone, late-stage copepods are generally positively buoyant at the surface (density = 910 – 915 kg m^{-3}), and as they move downward to colder, higher pressure water, they become negatively buoyant (Visser and Jonasdottir 1999). This means they cannot use lipids to help them sink when they enter diapause, however lipids will help them stay deep once they are resting.

The most compelling data that show the 1026 sigma-t isopycnal has biological relevance come from two experiments on *C. finmarchicus* and *C. hyperboreus* in settling columns designed to measure their internal density in relation to the seawater (e.g., Visser and Jonasdottir 1999, Kogeler et al. 1987). In the first experiment, live specimens of both species were caught every month for a year in the Fram Strait using a mid-water trawl, then placed immediately into a density column filled with seawater having an undisclosed temperature and a linear salinity gradient maintained using NaCl (Kogeler et al. 1987). The internal density of each animal was determined by the water density at which the animals stopped vertically moving (i.e., reached neutral buoyancy). The results showed that in September, during the time when the animals are entering diapause, their average internal density was not different from 1026 kg m^{-3} (Figure

5.35a). The animals increased in density in February as their lipids depleted during reproduction. In the second experiment, *C. finmarchicus* were frozen upon capture from the Faroe-Shetland Channel and later thawed before being placed immediately into a settling column with a density gradient established using seawater diluted with sugar (Visser and Jonasdottir 1999). The density of the animals was determined in the same manner as Kogeler et al. (1987). Afterward, the lipid and dry weight of each animal were measured, and the ratio of these two numbers was compared to the density of the animal (Figure 5.35b). As expected, the density of the animals decreased as the lipid/dry weight ratio in the animal increased. At the maximum lipid/dry weight ratio measured (γ=0.30), which is most comparable to the lipid content in the animals at time they enter diapause, the density of the animals was very close to 1026 kg m^{-3}. What these experiments show is that, as a first approximation, the 1026 isopycnal is near the density at which these animals reach neutral buoyancy *near the surface* (i.e. where the effect of pressure on lipids is negligible). It also predicts that below this isopycnal the animals will be positively buoyant, which is consistent with the predictions of modeling studies (see below). However, these studies answer part of the question, because my observations in Roseway Basin show that the animals are aggregated below the 1026 isopycnal (1026 – 1026.2), and not necessarily at it. These experiments are not perfect because they do not take into account the thermal expansion properties of wax ester, and they assume that the animals cannot regulate their buoyancy. But they do show that the 1026 isopycnal has biological relevance.

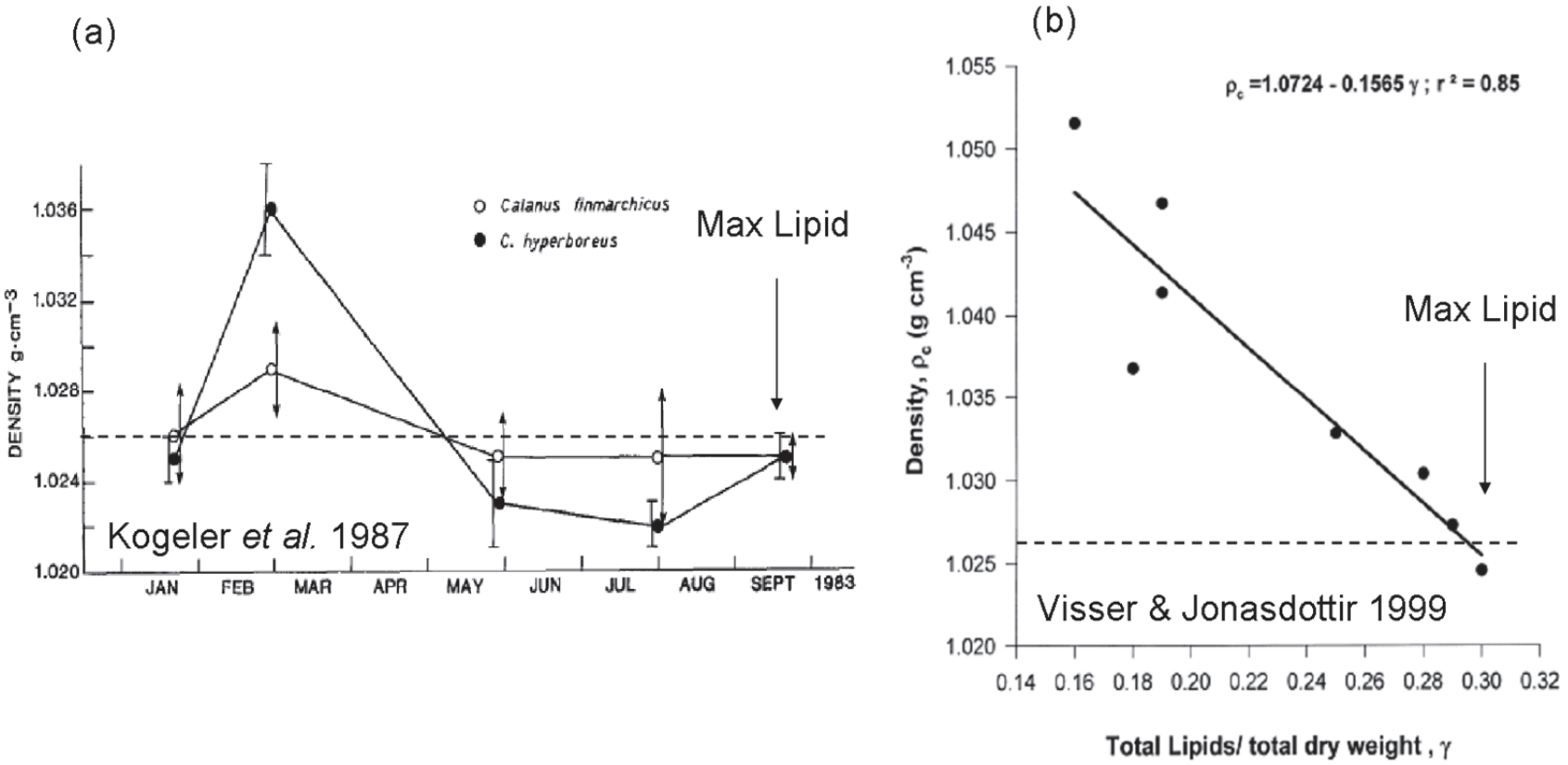

Figure 5.34 Density (g cm^{-3} = 10^{-3} kg m^{-3}) of Calanoid copepods derived from settling column experiments. (a) The monthly average (± 1 SD) density of *Calanus finmarchicus* (open symbols) and *C. hyperboreus* (closed symbols) collected in the Fram Strait (reproduced from Kogeler *et al.* 1987). (b) Density (ρ_c) of *C. finmarchicus* as a function of γ, its lipid to total dry weight ratio. The 1.026 g cm^{-3} isopycnal is depicted with a horizontal dotted line, and the point at which the animals are at their lipid maximum (i.e., as they enter diapause) are noted on each panel.

Copepod buoyancy models can help address some of the shortcomings of the two settling experiments discussed above. Copepod buoyancy modeling studies have been primarily concerned with temperature and pressure-dependent wax ester buoyancy; buoyancy properties of other tissues are estimated theoretically, and active ionic regulation by the animals is assumed negligible due to the paucity of data (Campbell and Dower 2003, Campbell 2008). Two diagnostic buoyancy models have been developed using *C. finmarchicus* populations that overwinter in the deep ocean waters (600–1000 m depth; Visser and Jonasdottir 1999, Campbell 2008). These models make the assumption that the animals are neutrally buoyant at depths of 600–1000 m depth, meaning they need to reach an internal density of between 1031.3 and 1032.8 kg m^{-3}. At the temperature and pressure range experienced by the animals at the relatively shallow Shelf Basin depths, these diagnostic buoyancy models predict that *C. finmarchicus* will be positively buoyant and will float toward the surface at ascent rates of ~100 m day^{-1} (Visser and Jonasdottir 1999). This is not realistic because many others, and my study, report the copepod populations can remain at depth in Shelf Basins for extended periods (September–February). The results of such diagnostic models do not extend to Shelf Basin populations (Campbell 2008).

Both models acknowledge that there must be some kind of active buoyancy regulation by the animals to aid in achieving their preferred depths and maintaining the that depth or density over the winter in the face of space and time variation in their external environmental density and decreasing internal lipid content. The fact that the animals can remain at depth in Shelf Basins over the winter, despite their lipid being positively buoyant, is consistent with this conclusion. A recent study shows that the diapausing copepod *Calanoides acutus*, an Antarctic relative of *C. finmarchicus*, can accumulate ammonium in exchange for the heavier sodium ion (Sartoris *et al.* 2010). This is a highly relevant finding because buoyancy properties appear to be extremely sensitive to biochemical composition (Campbell and Dower 2003). It is possible that the timing and state of knowledge is ripe for developing buoyancy measurements and models for diapausing copepods on the Scotian Shelf, particularly because of the relevance to the spatial distribution of diapausing copepods within Shelf Basins.

5.4.3.2 The influence of water mass density on right whale foraging

The 1026 sigma-t isopycnal can assist right whale foraging by restricting the vertical distribution of diapausing copepods and aggregating them in discrete, higher concentration, layers. The depth distribution of the 1026 isopycnal as a vertical aggregation mechanism for diapausing copepods can be approached from two directions in relation to its benefit to foraging whales. Assume that the total diapausing copepod abundance in Roseway Basin was the same in 2007 and 2008. The 1026 isopycnal was deepest in 2008 and the shallowest in 2007, making the copepod population more highly aggregated near-bottom in 2008 than in 2007 based on the above assumption. One might therefore conclude that, from the perspective of a right whale, the vertical aggregation process made the habitat more lucrative in 2008 than in 2007 because prey field was more vertically constrained in 2008. If this is so, then the strength of this process will be inversely proportional to the average water mass density of the habitat and to the volume of the Basin with density >1026.

However, I think that the benefit to right whales is a trade-off between higher concentration aggregations of prey in the habitat, and the depth distribution of those prey aggregations at the habitat margins (Figure 5.35). At the margins of the Basin, where the 1026 kg m^{-3} isopycnal approaches the sloped seafloor, copepods become aggregated in a vertically thinner layer than in the mid-Basin (e.g., Figure 3.11). As I demonstrated in Chapters 3 and 4, this isopycnal moves up and down in the water column with the tide at the margins (Figure 4.5), and at the same time copepods not only move up and down slope (Figure 4.13) but also accumulate and disperse at tidal frequencies (Figure 3.9), likely in response to the thickening and thinning of the water mass density layer on the stratified side of a water mass front. If this isopycnal meets the seafloor on the slope at a shallower depth, as happens when the density of water in the habitat is generally higher, then the accumulation and dispersal of copepods at tidal frequencies near the boundary between the seafloor and the 1026 isopycnal *will occur at shallower depths*, meaning the whales will not have to dive as deep to feed (Figure 5.35). However, in this case, the mid-Basin population would be lower in concentration than if the isopycnal were deeper. This trade-off will depend upon the relationship between how much energy a right whale spends diving, and how much energy is gained under the alternative aggregation

scenarios. If the whales gain more net energy feeding on a deep, highly concentrated prey population, then it would be more beneficial for the isopycnal to be deep. If the whales gain more net energy feeding on the shallow, less concentrated prey population, then it would be more beneficial if the isopycnal were shallow, as in 2007.

Shoaling of the 1026 isopycnal also opens up the entire western end of the habitat, which is shallow relative to the deep Basin. In 2007, at the western Basin margin (B07 and B01), the 1026 isopycnal was located at 80 m depth and a 30 m thick layer of copepods was concentrated in concentrations >10 000 m^{-3} below it (Figure 5.11). In 2008 in the same location at the western Basin margin (transects-5 to 7), the 1026 isopycnal was limited to a small parcel at ~110 m depth against the southern margin at transect 5 (Figure 3.22d) and had disappeared in favor of lower density water on transects-6 and 7 (Figure 3.23a, b). As a consequence, copepods were in very low concentrations and restricted in small patches against the southern slope (Figure 3.12d, 3.13a, b). The high density water in the Basin in 2007 made the western Basin margin a lucrative feeding area, whereas in 2008 the low density water meant that the 1026 was basically absent from the western margin, as were the copepods.

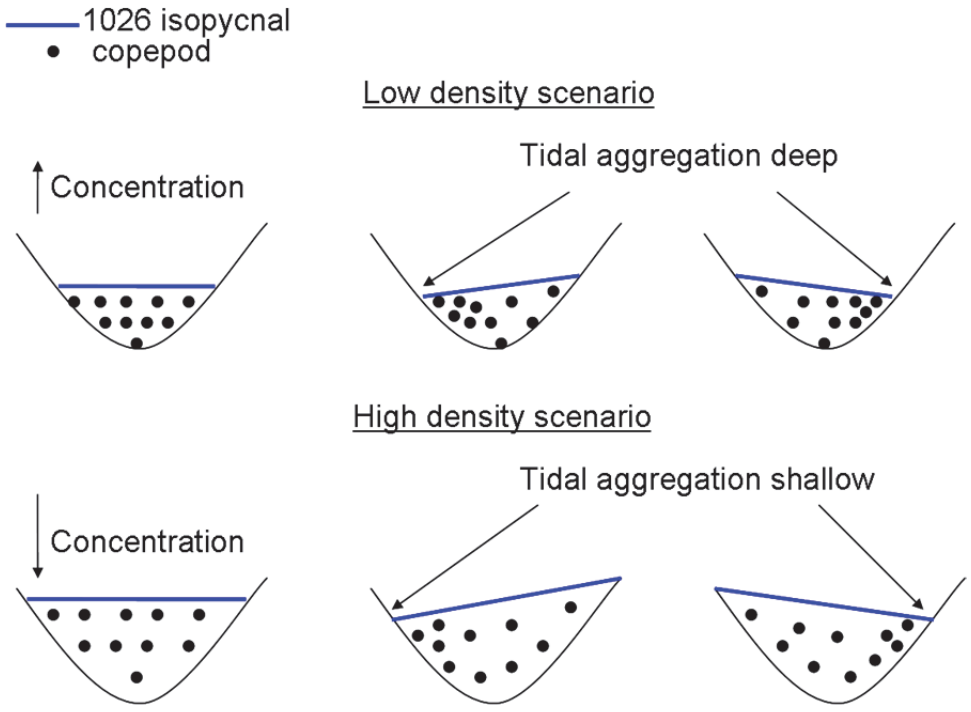

Figure 5.35 Alternative scenarios in which the mechanistic relationship between water mass density and diapausing copepod aggregation in a Basin influence right whale foraging, assuming the diapausing copepod abundance is the same under both scenarios. In the first scenario, the 'low density scenario', the water in the Basin is low in density such that the 1026 sigma-t isopycnal resides deep, and the copepods aggregate in high concentration near bottom. Under this scenario, as the isopycnal moves up and down at the Basin margins, aggregation of copepods at the margin occurs deep. In the second scenario, the 'high density scenario', the water in the Basin is high in density such that the 1026 sigma-t isopycnal resides shallow, and the copepods are lower in concentration because they are not as vertically restricted. Under this scenario, as the isopycnal moves up and down at the Basin margins, aggregation of copepods at the margin occurs shallow.

It appears, based on sightings records, that the whales in Roseway Basin prefer the southern and western margins (e.g., Figure 5.1a), which is consistent with a preference for shallower prey aggregations (thus favoring the 'high density' scenario). Further, Baumgartner and Mate (2003) found that the probability of sighting a right whale in the Grand Manan and Roseway Basin habitats was greater where the bottom mixed layer (BML) depth was shallower, consistent with my 'high density scenario' (Baumgartner and Mate 2003). Their observations of *C. finmarchicus* abundance in relation to BML depth are completely consistent with my observations; they found that the concentration of *C. finmarchicus* increased as BML depth increased, which I propose happens because the animals were restricted from above by a water mass density boundary. Baumgartner and Mate (2003) explained their results by concluding that right whales forage at shallower depths, even though the maximum in *C. finmarchicus* abundance is generally deep, because of the trade-off between energy expended diving and energy gained through feeding. All of this is consistent with my conclusions; but with my analysis I can now offer a mechanistic explanation for the observations.

The right whale preference for either scenario could further be quantitatively detected by comparing longer interannual time series of right whale abundance, copepod abundance and water mass density during late-summer. If a positive relationship between whale abundance and water mass density (or, better, average depth of the 1026 isopycnal) exists that is independent of any relationship between density and copepod abundance, then one may conclude that the high density scenario is correct. If a negative relationship is found between whale abundance and water mass density, then the whales may prefer the more concentrated mid-Basin population (low density) scenario. I address these postulates in Chapter 6.

5.4.4 Interannual variation in right whale Critical Habitat suitability

The analysis from the previous section demonstrates that it is impossible using prey field data alone to properly evaluate interannual variability in feeding habitat suitability to right whales. Overall, it appears that the right whale prey field was most lucrative to right whales in 2007 because the average copepod abundance in the habitat was highest that year and the density of the water was high, thus making high energy prey available at

shallower depths at the western and southern Basin margins. Based on average prey concentrations only, 2009 was less lucrative for right whales at the time it was sampled than 2007. The large, discrete layer of young stage copepods at the surface in 2009 would certainly be beneficial to the whales at the time sampled, and these would gain lipid energy over time and join the diapausing population later in the season. Thus the habitat was not yet at its maximum energetic value when measured in 2009. In 2009, the whales were observed along the southern and western margins (NARWC 2009), yet the surface layer was spread throughout the Basin. This indicates that the whales still had a preference for the diapausing copepod aggregation at the margins despite the availability of lower energy prey at the surface. Without knowing the relative energetic value of the surface population versus the population at-depth, and without knowledge of the right whales' foraging behavior and the energetic trade-off between deep diving and surface feeding, it is not possible to evaluate whether in one year the habitat was 'better' than another.

Finally, 2008 appeared to be the least lucrative year for right whales in Roseway Basin based on average prey concentrations. But again, arguments could be made that the habitat value was increased relative to the average density alone because copepod aggregative processes were strongest that year. The supplement from the slope, high frequency of water mass fronts and tilting of the prey field to shallower depths at the southern margin, were all processes that were not seen in the other years.

There are two major drawbacks to my study that limits its applicability to investigating interannual variability in the habitat suitability for right whale foraging. In the first, a major information gap occurred because no right whale abundance estimates are available for Roseway Basin in 2007 or 2008. Limited ship time did not allow surveys of both the habitat and the whales, and the North Atlantic Right Whale Consortium (NARWC) does not survey the Basin every year. Opportunistic sightings of 42 right whales in 2007 and 1 right whale in 2008, suggests that the feeding habitat was more lucrative during 2007. The NARWC did survey the habitat in 2009, and observed 44 right whales. The whale distribution that year beautifully demarcated the western and southern Basin margins, similar to the historical distribution of right whales in the habitat (Figure 5.1a, NARWC 2010).

The second major drawback of my study was the inability to link smaller-scale, within-habitat variation in the prey field dynamics to right whale foraging, because there was no directed sampling in the vicinity of right whales. It would have been very informative to have a second ship following the whales, recording their behavior and sampling the prey field near them, so that some of the hypotheses and scenarios presented in this discussion could be evaluated for their importance to feeding right whales. At the time, my goal was only to sample the 'potential niche', meaning the total prey available to right whales. I now believe this was an oversight on my part, and the 'potential niche' measured has much less applicability to foraging theory without linking it to the 'realized niche', meaning how the whales are actually using the habitat.

One hypothesis that can be addressed with my analysis is a hypothesis regarding the ephemeral nature of the Roseway Basin as Critical Habitat. It has been hypothesized that large variations in the number of right whales that return to Roseway each year can be explained because the habitat is extremely dynamic and experiences strong interannual variation in prey abundance. My dataset certainly shows that this habitat is interannually dynamic because both the average concentrations of diapausing copepods and the aggregative processes were different among all three years. Food available to right whales in the habitat is a function of a number of different variables and the absence of any one could reduce the energetic value of the prey field in a given year; i.e., very low water density, low Shelf production, and no slope water intrusions would appear most relevant. In the absence of any one of these factors, there could be few to no prey available to the whales.

5.4.5 Summary

In summary, the Roseway Basin right whale Critical Habitat exhibits a great deal of interannual variability. This variability was not limited to variation in average diapausing copepod abundance. During the three years of habitat survey, the abundance, stage-structure, species composition and aggregation locations of diapausing copepods were all different. The hydrographic structure in the habitat was also different every year, and as a consequence, the copepod aggregation mechanisms within the habitat also varied from year to year. All of this variation will likely affect how many whales the habitat can

support as well as the areas within the habitat that are the most beneficial foraging grounds. Thus, this analysis showed that simple measures of average abundance used in previous studies to predict right whale population variation have reached the limit of their applicability; more complex explanatory models that include the variables deemed important in this study are the future of this research area.

One major drawback of this study is the paucity of information concerning whale distributions and feeding preferences during the time the habitat was surveyed. This would require a second ship dedicated strictly to censusing right whales. A second limitation is the short nature of the time series. Examining a longer time series, that includes right whale data, may be beneficial to answering some of the hypotheses I proposed in this Chapter. Hence the next chapter, Chapter 6, examines a 20 year time series of interannual variation in right whales, copepods and hydrography in both the Roseway Basin and Grand Manan Basin right whale Critical Habitats. Although the time series are not spatially as well resolved as the data in this chapter, I use the baseline data developed in this and previous chapters to calibrate those time series.

Chapter 6

Historical Variation in Right Whale Habitat Occupancy (1987 – 2009) in the Late-summer Critical Habitats

6.1 Introduction

In Chapter 5, I assessed interannual variation in right whale habitat in Roseway Basin from 2007 through 2009. Two main hypotheses were formulated about the causes of this interannual variation and possible consequences for right whale foraging. However, the investigation was limited by the small number of years and by the lack of data on right whale abundance during 2007 and 2008. A longer time series of right whale habitat occupancy data in Roseway and Grand Manan Basin is available for most years between 1987 and 2009, and can be used to test the two main hypotheses developed in Chapter 5 in both these late-summer Critical Habitats (NARWC 2008). The ability to make adequate comparisons between right whale occupancy and habitats during 1987 - 2009 depends upon where and when the habitat data were collected. This necessitated extracting from archived samples and data for all calanoid copepod and hydrographic information available in the Critical Habitats collected during the years 1987 - 2009. Thus, this chapter focuses first on the data I was able to secure, their merits and inadequacies, and the feasibility of using them to address the two hypotheses developed in Chapter 5.

The first hypothesis was that habitat-averaged concentrations of right whale food in Roseway Basin varies interannually to a degree that could affect the number of whales that the habitat could support from a metabolic perspective and thus be reflected in the interannual variation in right whale occupancy. Previous studies have shown habitat-average prey density to be an important variable; however such variation alone is insufficient to explain variation in whale occupancy (i.e., it is a multivariate problem). In the past, when predictive relationships have been drawn between prey density estimates (or related indicators) and right whale calving rates or habitat occupancy, the relations are either qualitatively inferred (e.g., Payne *et al.* 1990, Costa *et al.* 2006), leave a large

portion of the variance unexplained (e.g., Patrician and Kenney 2010, HLista *et al.* 2009, Pendleton *et al.* 2009, Greene and Pershing 2004), or the correlations are significant but have no little or no biological or ecological meaning (e.g., Pershing *et al.* 2009). Right whale habitat occupancy may also depend upon the copepod aggregation processes that occur in the habitat, because right whales appear to rely on highly concentrated aggregations of their food (Baumgartner and Mate 2003, Baumgartner *et al.* 2007). As a logical follow up, my second hypothesis concerned the association between water mass density and aggregated prey near-bottom in the mid-Basin (the 'low density' scenario) or near-bottom at shallower depths at the Basin margins and varying at tidal frequencies (the 'high density' scenario), either of which may assist in right whale foraging and increase the number of whales the habitat can support.

6.1.1 Objectives

This chapter has two analytical and three ecological objectives. The first analytical objective is to examine the annual right whale survey data from the Roseway and Grand Manan Basins for the period 1987 through 2009 and determine which years have been surveyed with adequate effort to address my ecological objectives. Second, I investigate the availability of opportunistic habitat data (biological and physical) in each of the basins during the same period to determine whether the data are sufficient to address my ecological objectives. These data are then constrained in relation to whale survey effort, and the constrained data are the used to address the ecological questions.

The primary ecological objective of this chapter is to assess interannual variation in right whale occupancy in the Scotia-Fundy Critical Habitats, with an emphasis on the right whale 'abandonment period' in Roseway Basin during 1993 - 1999 (Brown *et al.* 2001). During this period, individual whales that were normally photographed in Roseway Basin during other years were observed in Grand Manan Basin, and a concurrent increase in the number of whales in Grand Manan Basin was measured in late-summer (Hamilton *et al.* 2007). However, the right whale distributional observations made using photo-identification data were not corrected for effort. Consequently, I first compare effort-corrected right whale survey data from transect surveys between the two Critical Habitats to determine if the effort-corrected data agree with the conclusions

drawn from the photo identification data. If the effort corrected data also show that Roseway Basin was abandoned during the 1993 - 1999 period, then I might expect that if habitat influences right whale occupancy, the effect of habitat will be most pronounced during the 1990s when the Roseway Basin habitat was abandoned. Thus, secondly I examine whether the variation in habitat occupancy inferred from such data can be explained by variation in the habitat.

There are two measures of habitat that may influence interannual variation in right whale occupancy, and my second ecological objective is to assess the importance of each. The first measure is habitat-average concentration of diapausing calanoid copepods. The second measure is the copepod aggregation process(es) related to water mass density as proposed in Chapter 5 (i.e. testing my 'high density' and 'low density' scenarios; see Figure 5.35).

My final objective is to examine whether diapausing calanoid copepod abundance in Roseway and Grand Manan Basins can be explained by variation in temperature- and phytoplankton-dependent copepod production in the Scotian Shelf – Gulf of Maine region. Diapausing copepod abundance might be greater on the Shelf in years with higher surface water temperature and greater primary productivity, because both of these promote faster individual copepod growth and shorter copepod generation time (Melle and Skjoldal 1998, Madsen *et al.* 2008, Moller *et al.* 2012). Faster individual growth and shorter generation time should both lead to greater population size because more generations can be produced during a season, and female fecundity is generally positively correlated with body size (Peters 1983). I hypothesized in Chapter 5 that diapausing copepod abundance in the Basins could be higher in years when slope water intruded onto the Shelf, because slope water intrusions supply the Shelf with copepods from the slope populations. Thus in this chapter I compare annual copepod concentration at depth in the Basins with the annual SST thermal integral, annual net primary productivity, annual spring phytoplankton bloom timing, duration and strength, and slope water intrusions (a proxy for copepod re-supply from the slope populations) on the Scotian Shelf (relevant to both Basins) and the Gulf of Maine (relevant to Grand Manan Basin).

6.2 The Grand Manan Basin study area

In the previous chapters, I provided background information concerning the Roseway Basin habitat; its bathymetry, prey field distribution, general circulation and hydrography. Here I provide similar background information relevant to Grand Manan Basin. Grand Manan is located at the head of the Gulf of Maine at the entrance to the Bay of Fundy and is ~80 km long and ~20 km wide (Fig. 6.1). Mid-Basin depths reach 220 m and right whales are annually present for 3 to 6 months within the 100 m isobath (Vanderlaan et al. 2008). Maximum whale abundance occurs during the August through September period, as is recorded for Roseway Basin.

Right whales in the Grand Manan Basin also feed on diapausing *Calanus finmarchicus* C5s that are concentrated at depths below 100 m (Winn et al. 1986, Baumgartner and Mate 2003). Energy ingestion for right whales in Grand Manan can account for ~70 % of their total annual food intake compared with 25% for the spring-early summer habitats in the Great South Channel and Cape Cod Bay (Goodyear 1986). The carrying capacity for Grand Manan in a high quality year is approximately 200 whales (Michaud 2005).

The general circulation pattern for Grand Manan Basin is documented from model simulations in several studies, notably Bumpus (1960), Greenberg (1983), and Aretxabaleta et al. (2009a,b). There are generally three water masses that contribute to the deep water in Grand Manan Basin: Scotian Shelf deep water carried into the Bay of Fundy via the inner arm of the Nova Scotia Coastal Current (NSCC), Shelf and slope water entering the region via the Northeast Channel (NECH), and Gulf of Maine recirculation. Depth-averaged residual circulation in Grand Manan is dominated by flow into the Bay of Fundy along the SE margin and flow out of the Bay along the NW margins (Geenberg 1983, Aretxabaleta et al. 2009a). Baroclinic model simulations in Grand Manan Basin demonstrated the existence of a persistent counterclockwise gyre, maintained by strong tidal rectification and density-driven circulation (Aretxabaleta et al. 2009a).

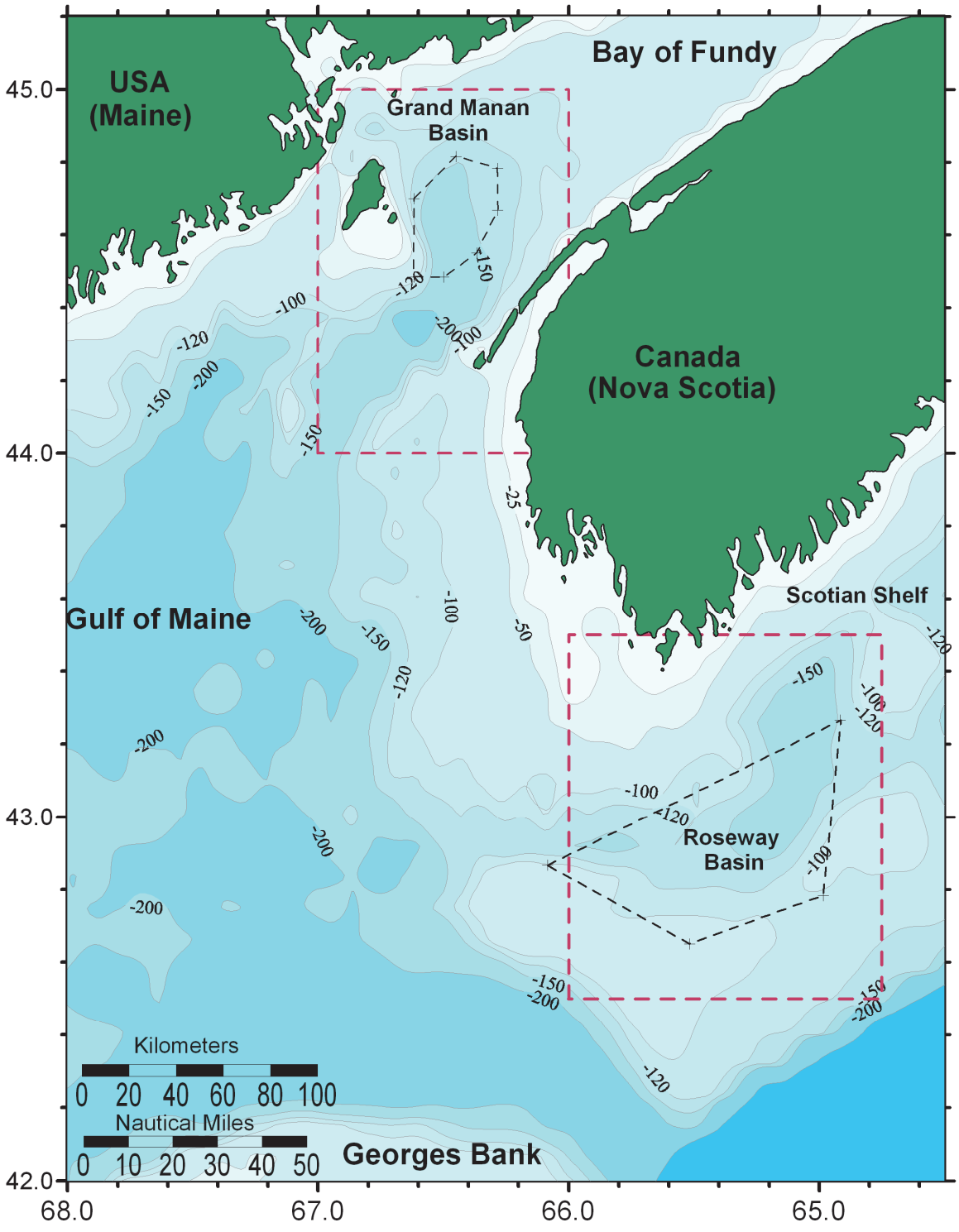

Figure 6.1 Bathymetric (m) chart illustrating the Grand Manan Basin and Roseway Basin right whale survey domains used by the North Atlantic Right Whale Consortium (red dashed line) and approximate prey field and hydrographic study domains used in this chapter (black dashed polygons). Prey field study domains approximately parallel the 120 m (Grand Manan) or 100 m (Roseway) isobaths.

6.3 Methods

6.3.1 Right whale survey data

Right whale surveys are conducted annually during summer in Roseway and Grand Manan Basins by the North Atlantic Right Whale Consortium (NARWC), a nonprofit organization in the USA composed of many scientists and institutions concerned with right whale conservation. An overview of the whale survey methodologies and quality control are provided in Brown *et al.* (2007), though the pertinent features are summarized here as in Vanderlaan *et al.* (2008). Survey platforms were primarily vessels and, secondarily, aircraft that followed systematic survey lines. Aboard vessels, observers used standardized methods and vessels travelled at ~12 knots (22 km h^{-1}) along typically N–S survey lines spaced at ~4 n miles (7.4 km); data used for analytical purposes were considered valid only when visibility was ≥2 n miles (3.7 km) and in sea state <4 in the Beaufort wind force scale (Vanderlaan *et al.* 2008). All right whales were counted and their locations geo-referenced. Aerial surveys were conducted as above using a Cessna® 337 Skymaster® flying at ~100 knots (185 km h^{-1}) at 230 m altitude along E–W survey lines spaced at ~5 n mile (9.3 km) intervals. Data were collected in Roseway Basin during one survey per year, usually in August or September, but sometimes in July or October. Data were collected in Grand Manan Basin during multiple surveys per year. The data were provided as cell-specific sightings (number of whales sighted) and effort (km surveyed) estimates across each 3' N latitude x 3' W longitude grid cell within the standard NARWC 20 x 20-cell grids (Grand Manan Basin; area = 2520 n $miles^2$, 8643 km^2) and 25 x 20-cell grids (Roseway; area = 3300 n $miles^2$, 11 319 km^2) as shown in Figure 6.1 (red dashed boxes).

Quality controlled right whale sightings and effort data collected during surveys described above for the period 1987 through 2009 were provided for each of the Grand Manan and Roseway regions by the NARWC (no survey data in 2007 and 2008 in the latter, NARWC 2005; see also Kenney 2001). The 2009 data are preliminary as the sightings data have not undergone quality control. Sightings data from Roseway Basin in 2009 have undergone one cursory edit by NARWC using photo-ID to eliminate repeat sightings of the same whale. The Grand Manan data have not been examined for repeat sightings of individual whales. As one in 4 whales was photographed twice per event on

average in Roseway (range 0 - 3 repeat sightings of a whale per event, n = 65 events) I assumed that the same number of repeat sightings per event occurred in Grand Manan Basin and adjusted those data accordingly. Nevertheless, whale sighting data may be overestimated during the 2009 surveys.

Right whale survey effort is highly inconsistent in space and time due to logistical limitations (e.g., ship time) and as a consequence, order of magnitude variability exists in the number of grid cells surveyed among years and between habitats. The spatial distribution of survey effort within each Basin also differs from year to year because not every grid cell within each study area is surveyed for right whales every year (Figure 6.2). Further, for a grid cell to be included as 'surveyed' in the NARWC database, a minimum 60 m of trackline must be monitored. To account for these issues in my analyses, the data were constrained in two ways. First, each grid cell is approximately 5.6 km x 4.1 km in area. For a grid cell to be included in my analyses, at least the median trackline distance for the Roseway Basin data (5.6 km $cell^{-1}$) had to be surveyed. This is equivalent to the ship transecting the entire length of the grid cell at least once. Second, I included only those grid cells that were surveyed at least 50% of the possible years for repeatability (12 of 23 years in Grand Manan and 10 of 20 years in Roseway; Figure 6.2). Ideally, it would be best to constrain the data to only those grid cells that were surveyed every year, but doing so would eliminate the Roseway Basin data; thus I had to compromise. In Grand Manan Basin, these constraints reduced the number of grid cells in my analysis from 375 to 79 (Figure 6.2a). In Roseway Basin, these constraints reduced the number of grid cells from 379 to 48 (Figure 6.2b).

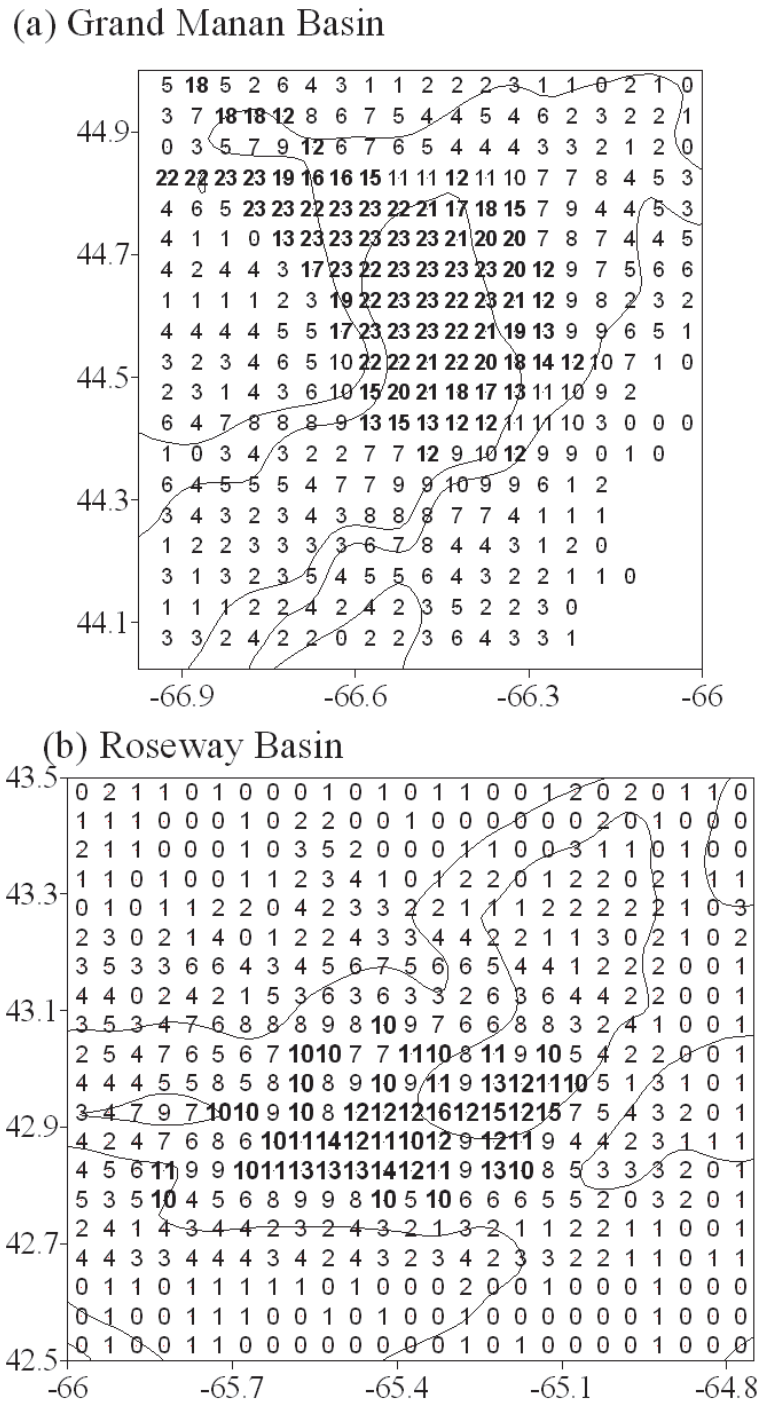

Figure 6.2 Number of years that each 3' x 3' grid cell within each right whale study area (red dashed boxes in Figure 6.1) was surveyed for right whales along at least 5.6 km of transect line per grid cell in (a) Grand Manan Basin and (b) Roseway Basin. Grid cells that were surveyed in at least 50 % of years are in bold; these were used for further analysis. The 100 m and 150 m isobaths are depicted with black lines.

The resulting time series of the total number of whales observed, number of grid cells surveyed, the kilometers surveyed, and average sightings per unit effort (SPUE, number of whales sighted per 1000 km surveyed), per grid cell, for each habitats are provided in Figure 6.3. Between 33 and 695 km were surveyed per year in the Roseway Basin habitat (Figure 6.3b); covering 48 grid cells (total area ~1100 km^2). Years with fewer than 10 grid cells of survey effort were considered marginal in providing reliable estimates of average SPUE. Thus the data from 1993, 1995, 1996, 1998, 1999, and 2001 in Roseway Basin were excluded from further analysis. This restriction did not exclude any years from the Grand Manan Basin data. It is noteworthy that the maximum number of grid cells surveyed in any year in Roseway Basin was 53 grid cells in 1990. This number is similar to the minimum number of grid cells surveyed in a given year in Grand Manan Basin (49 grid cells in 1994). Given that the Roseway Basin survey area is 30% larger than the Grand Manan Basin area, estimates in the Grand Manan Basin are clearly more reliable.

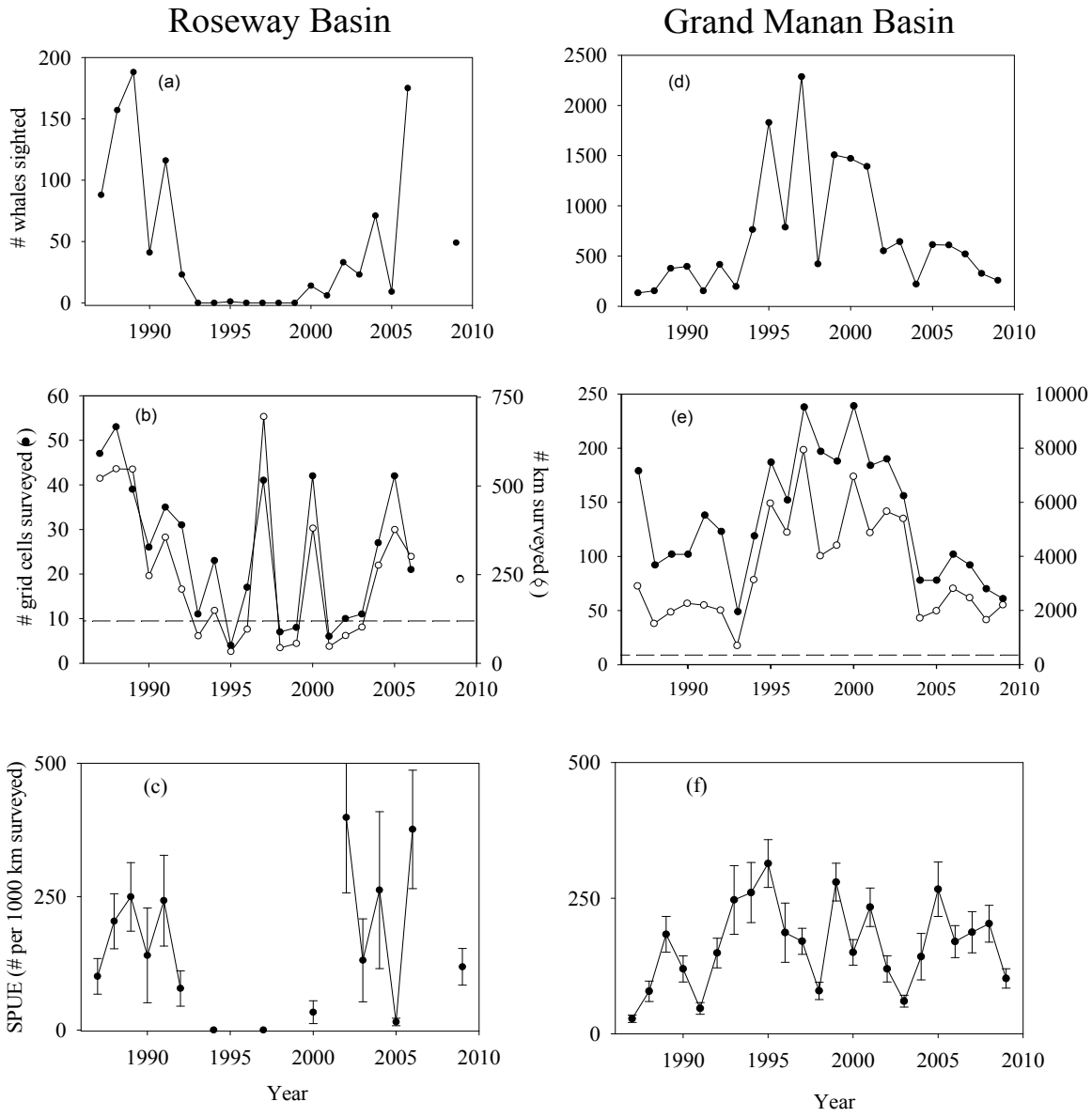

Figure 6.3 Time series (1987 - 2009) of right whale survey data from (a-c) Roseway and (d-f) Grand Manan Basins. Panels (a) and (d) depict the number of whales sighted each year, panels (b) and (e) show the number of 3' x 3' grid cells within each study area that were surveyed (closed symbols) and the total number of kilometers surveyed (open symbols), and (c) and (e) depict the per grid cell average (±1 S.E.) right whale sightings per unit effort (SPUE, number of whales per 1000 km surveyed). The dashed line in panels (b) and (e) represents the minimum amount of annual effort needed to make adequate SPUE estimates.

6.3.2 Copepod data

6.3.2.1 Data sources

Five sources contributed abundance estimates of total *Calanus* spp., *Calanus finmarchicus* C5s and *Calanus hyperboreus* C4s (Roseway only) from net collections in Roseway Basin and Grand Manan Basin in late-summer and autumn (July through November) during the period 1987 through 2009. Data were collected within the 100 m isobath in Roseway and the 120 m isobath in Grand Manan Basin (Figure 6.1). Data sources are detailed in Table 6.1.

Right whales exhibit fidelity to dive depths of approximately 120 m in Grand Manan Basin that is highly correlated with the depth of maximum C5 abundance (Baumgartner and Mate 2003). In previous chapters, I found that the prey field in Roseway Basin was generally restricted to below 100 m depth. The above information led me to consider 120 m as the minimum net tow depth required for depth integrated BONGO tows to adequately sample the right whale prey field, and samples collected with nets towed to a maximum depth shallower than 120 m were excluded from the analyses. Twenty three tows with maximum depths ≥25 m off bottom were also excluded, as it is possible that these tows may not have adequately sample the C5 layer. Such collections were considered statistical outliers (>1.5 times the interquartile range) in comparison with the frequency distribution of the collections in terms of their proximity to the bottom. The number of net collections in each year and habitat is provided in Table 6.2. No data were available in Roseway Basin for the years 1982, 1990, 1995 and 1997. No data were available in Grand Manan Basin for 16 of the 30 years.

My analyses in Chapters 2 through 4, as well as those of Michaud (2005) and Baumgartner and Mate (2003), all demonstrate that a single net collection in a given year is not representative of the annual average copepod concentrations across either habitat; the spatial variation in the prey field is far too high. As a consequence, for my analyses, I only use years when 3 or more net samples were collected in a habitat; this allowed me to at least calculate a variance term for each annual estimate. In Roseway Basin, my analyses are restricted to the nine years 1998 - 2001, 2005 - 2009 and in Grand Manan Basin they are restricted to the six years 1999 - 2002, 2006 and 2007. Almost all of these data were collected for four graduate theses; Michaud (2005), Baumgartner (2003),

Swaim (2008) and my study. Surveys were conducted in both habitats in 1999 - 2001 and 2006 - 2007, thus any comparison between habitats cannot extend far beyond the analyses presented in Baumgartner and Mate (2003) who compared right whale occupancy and copepod dynamics in both habitats between 1999 and 2001. All surveys included in my analysis were conducted in August or September, except the survey in Roseway Basin in 2000, when the survey was completed in July (Table 6.1).

6.3.2.2 Depth calibration

The majority of data provided by Michaud, Swaim and Baumgartner (Table 6.1) are depth integrated collections, and are used here as a relative index of prey abundance to examine interannual variability in the right whale prey field. Depth integrated samples underestimate the prey concentration available to right whales in the deep Basin habitats because the prey field is concentrated in a layer between approximately 100 m and 10 m above bottom. From my depth-structured net sampling, I estimate that on average 75 % of the prey field is located below 100 m depth. *Calanus* spp. concentration (m^{-3}) below 100 m was calculated for the depth integrated net collections as follows:

$$[Calanus_{>100m}] = \frac{[Calanus]_{wc} \times V_{wc} \times 0.75}{(D_t - 100\ m) \times A} \quad (6.1)$$

Where D_t (m) represents the maximum tow depth, A is the area (m^2) of the net opening, $[Calanus]_{wc}$ (m^{-3}) and V_{wc} (m^3) represent the water column integrated *Calanus finmarchicus* concentration and volume (A x D_{wc}) of the sampled water column respectively.

Any depth-structured tows (e.g., BIONESS) were used as-is, but only nets that collected samples below 100 m depth were included. Two time series were then generated, one for total *Calanus* spp. concentration and one for *C. finmarchicus* C5 + *C. hyperboreus* C4 (hereafter, diapausing copepod) concentration. Annual prey concentration was calculated by averaging prey concentrations among all tows within a year.

6.3.2.3 Gear Type biases

Variability in plankton mesh and gear size are important considerations due to sampling bias introduced through size-selective capture efficiency (i.e., net extrusion by smaller

animals and avoidance by larger; Anderson and Warren, 1991). The largest mesh size used during a survey was 505µm, and all smaller mesh sizes are too small to extrude the smallest measured *C. finmarchicus* C5 (width = 400µm). I found no difference in average prosome volume between C5s caught in nets fitted with 505µm mesh for which I had samples in-hand (n = 1008 C5s) and C5s caught in depth-integrated nets fitted with 333µm for which I had samples (n = 2335 C5s) (ANOVA $P = 0.327$). Less than 0.01% of C5s collected using a 333µm mesh were thinner than 505µm, indicating that the vast majority of C5s would not be extruded through the 505µm mesh, even if entering the mesh head-on. Finally, the smallest prosome width of a C5 caught with 333 µm and 505 µm mesh was 430 µm and 400 µm, respectively, indicating that even if a few individuals were thinner than the mesh size, extrusion was unlikely. From these results I conclude that individuals were retained once captured and under-sampling of smaller individuals due to variability in net mesh size was not a factor in biasing samples collected using a 505µm mesh.

Nets with wider mouth opening (gape) are more effective at capturing large plankton than smaller gape nets due to reduced avoidance (Anderson and Warren 1991; Pepin and Shears 1997). Samples used in this analysis were collected using nets equipped with either a 0.6 m, 0.75 m, or 1 m diameter gape. No samples were concurrently collected using different gape sizes, preventing empirical testing of gape size in relation to abundance. However, by August the majority of C5s are in diapause and may be considered as passive particles incapable of net avoidance, so I reasonably assume variability in net gape among collections does not affect capture efficiency.

Table 6.1. Sources of copepod abundance data collected in the Grand Manan and Roseway Basin feeding habitats between 1987 and 2009. Year and month when data were collected, as well as gear type and mesh size are provided.

Habitat	Data Source	Years (months)	Gear Type (diam. (m), mesh (μm))
Grand Manan			
	BioChem Database	2003(7) 2004(7)	Ring Net (0.75, 202)
	Josee Michaud (Taggart Lab)	2001(8) 2002(7,8,9,10)	BIONESS(0.6,333) BONGO(0.6, 333)
	Mark Baumgartner (2003)	1999(7,8) 2000(7,8) 2001(7,8)	MOCNESS(1,150) BONGO(0.6, 333)
	DFO Ichthyoplankton Survey	1987(11) 1989(10) 1990(11) 1994 (11) 1996(11) 1998(11)	BONGO(0.6, 505)
	Zachary Swaim (2008)	2006, 2007 (7,8,9)	BONGO (0.6, 300)
Roseway Basin			
	BioChem Database	1991(11) 1998(10)[1] 1999(7,10) 2000-2003(7,10)[1] 2004(7) 2005(7,10) 2006(7,10) 2007(7,10) 2008(7)[1]	BONGO (0.6, 333) BIONESS[1] (0.6, 243) Ring Net (0.75, 202)
	My Study (Taggart Lab)	2007(9) 2008(9) 2009(8)	BIONESS(1, 333)
	Mark Baumgartner (2003)	1999(8) 2000(7) 2001(8)	BONGO(0.6, 333)
	DFO Ichthyoplankton Survey	1987(10)* 1988(10) 1989(10,11) 1991(11) 1992(10) 1993(11) 1994(11)* 1996(11)	BONGO(0.6, 333*or 505)

*333um mesh size was used in years 1987 and 1994
[1]BIONESS used in years 1998 2003 and 2005

Table 6.2. Number of zooplankton net collections per year per habitat between 1987 and 2009. Collections that are included in my analysis are in bold.

Year	Roseway Basin	Grand Manan Basin
1977	0	1
1987	1	1
1988	1	0
1989	1	1
1990	0	1
1991	2	0
1992	1	0
1993	1	0
1994	1	1
1995	0	0
1996	1	1
1997	0	0
1998	**6**	1
1999	**6**	**7**
2000	**3**	**6**
2001	**9**	**50**
2002	2	**58**
2003	2	1
2004	1	1
2005	**7**	0
2006	**3**	**16**
2007	**30**	**13**
2008	**16**	0
2009	**9**	0

6.3.3 Hydrographic data at depth within the Critical Habitats

Temperature, salinity and density profiles for the Roseway and Grand Manan Basin study areas were extracted from the DFO Hydrographic Climate Database[4] maintained at the Bedford Institute of Oceanography in Dartmouth, N.S. The data are binned at a 1m depth resolution and encompass the late-summer (July through September) from 1987 through 2009, with some gaps. They include bottle (BT), conductivity, temperature and salinity (CTD), and space-time averaged batfish (BF) temperature and salinity data. The data were examined for duplicates, density inversions, extreme values, impossible depths and a number of other quality control measures by MEDS (MEDS Manuals and Guides #22, GTSPP Quality Control) and subsequently by me. Additional CTD profiles were collected by me in Roseway Basin during our 2007 through 2009 research expeditions and by others in Grand Manan Basin in 2002, using a SeaBird SBE-25 CTD. Again, because there was significant variation in survey effort among years, a year was only included in my analyses if more than three profiles and more than ten observations at depth were collected in a single year. This restriction eliminated years 1987 - 1989, 1992 and 1995 from the Roseway Basin data. It also eliminated nearly all years from the Grand Manan Basin data with the exception of 1999 - 2002, 2004 and 2005. Deep water time series were created by calculating the median temperature (T), salinity (S) and density (± 1 SD) of each tow, then calculating the median of each variable for all tows within each year below 100 m depth in Roseway Basin (to a maximum 180 m) and Grand Manan Basin (to a maximum 220 m). As my hypotheses are concerned primarily with water mass density, my results are discussed with a focus on density variation.

In addition to data from my primary study areas, I extracted late-summer (July - September average) time series data for the years 1987 – 2009 averaged spatially over a depth range of 100 - 200 m and over the Scotian Shelf system polygons containing the Nova Scotia Coastal Current (polygon SS06), continental slope water (SS34), coastal water at Halifax (SS14) and Northeast Channel (SS29) (Figure 6.4). Using these source water T-S data I was able to calculate the proportion of each end-member in Roseway Basin each year. I solved the following set of linear equations describing the relative

[4] http://www.mar.dfo-mpo.gc.ca/science/ocean/database/doc2006/clim2006app.html

contribution of each end-member to the Roseway deep layer temperature (Eq. 6.2), salinity (Eq. 6.3) and volume (Eq. 6.4):

$$aT_{NSCC} + bT_{slope} + cT_{Ro\_upper} = T_{Ro\_deep} \quad (6.2)$$

$$aS_{NSCC} + bS_{slope} + cS_{Ro\_upper} = S_{Ro\_deep} \quad (6.3)$$

$$a + b + c = 1 \quad (6.4)$$

where a, b and c are the estimated proportions, and subscripts represent each water mass. The proportion of water that each end-member contributed to produce deep water in Roseway was calculated annually between 1987 and 2009. At least one water mass was missing data in 1988 - 89 and 1997 so proportions were not calculated in those years.

Table 6.3 Roseway Basin. Number of temperature, salinity and density profiles and observations below 100 m depth collected per year between 1987 and 2009. Only years in bold were used for further analysis.

Year	Profiles	Temperature observations	Salinity/density observations
1987	6	12	6
1988	3	6	3
1989	2	3	3
1990	**14**	**109**	**101**
1991	**4**	**32**	**32**
1992	1	20	20
1993	**8**	**61**	**49**
1994	**8**	**43**	**43**
1995	3	19	19
1996	**10**	**108**	**108**
1997	**5**	**89**	**89**
1998	**9**	**303**	**303**
1999	**44**	**1066**	**958**
2000	**40**	**1362**	**1348**
2001	**44**	**1378**	**1374**
2002	**10**	**44**	**40**
2003	**7**	**72**	**69**
2004	**7**	**82**	**79**
2005	**42**	**1413**	**1277**
2006	**5**	**11**	**11**
2007	**21**	**1409**	**1408**
2008	**6**	**132**	**115**
2009	**7**	**243**	**242**

Table 6.4 Grand Manan Basin. Number of temperature, salinity and density profiles and observations below 120 m depth collected per year between 1975 and 2009. Only years in bold were used for further analysis.

Year	Profiles	Temperature observations	Salinity/density observations
1987	4	4	3
1988	0	0	0
1989	3	3	2
1990	0	0	0
1991	0	0	0
1992	0	0	0
1993	1	6	6
1994	2	3	3
1995	1	7	7
1996	0	0	0
1997	0	0	0
1998	0	0	0
1999	**21**	**868**	**867**
2000	**98**	**4626**	**4528**
2001	**97**	**4956**	**4954**
2002	**27**	**1497**	**1497**
2003	2	2	2
2004	**3**	**36**	**35**
2005	**26**	**1035**	**1035**
2006	1	2	2
2007	1	23	23
2008	0	0	0
2009	1	2	2

6.3.4 Temperature and phytoplankton-dependent copepod production model

I extracted two datasets from two sources to examine the relationship between diapausing copepod abundance in late-summer and temperature/phytoplankton (food) production in spring-summer in the Scotian Shelf – Gulf of Maine region during the years 1998 – 2009 for which I had copepod data. Temperature and phytoplankton data from the Scotian Shelf were compared with diapausing copepod abundance in late-summer in Roseway Basin since the Shelf is the primary source of copepods to the Basin. Temperature and phytoplankton data from both the Scotian Shelf and Gulf of Maine were compared with diapausing copepod abundance in Grand Manan Basin because water advects from both areas into the Basin.

I extracted monthly (Jan - Aug) sea surface temperature for the years 1998 – 2009 from the DFO Sea Surface Temperature Database. These data were spatially averaged over each of two polygon areas, SS14 (inner Scotian Shelf off Halifax) and SS44 (Gulf of Maine) (Figure 6.4). I chose these areas to represent the seasonal temperature conditions previously experienced by the animals because the areas are upstream of each Basin and near enough to each Basin that most copepods found within the Basins likely had to pass through these areas. I then calculated the annual thermal integral (^{o}C) from January 1 – August 31 by multiplying the monthly average sea surface temperature by the number of days in that month, then summing over all months. I use the thermal integral, rather than the average, because it represents the integration of conditions experienced over the entire growing season by the copepods, and thereby affects the diapausing copepod abundance at the end of the summer.

I also extracted annual net primary productivity estimates (gC m^{-2} yr^{-1}, 0 - 50 m) modeled for the Scotian Shelf and Gulf of Maine during the years 1998 – 2007 (Song *et al.* 2011) (Table 6.5). *In situ* spring phytoplankton bloom magnitude (mg Chl m^{-2}), onset timing (day of year) and duration (number of days) measured at Halifax Station-2 for the period 1999 - 2009 (Johnson *et al.* 2012) (Table 6.5). Again, annual primary productivity is the integral over the entire year, and should represent the integration of conditions experienced over the entire growing season.

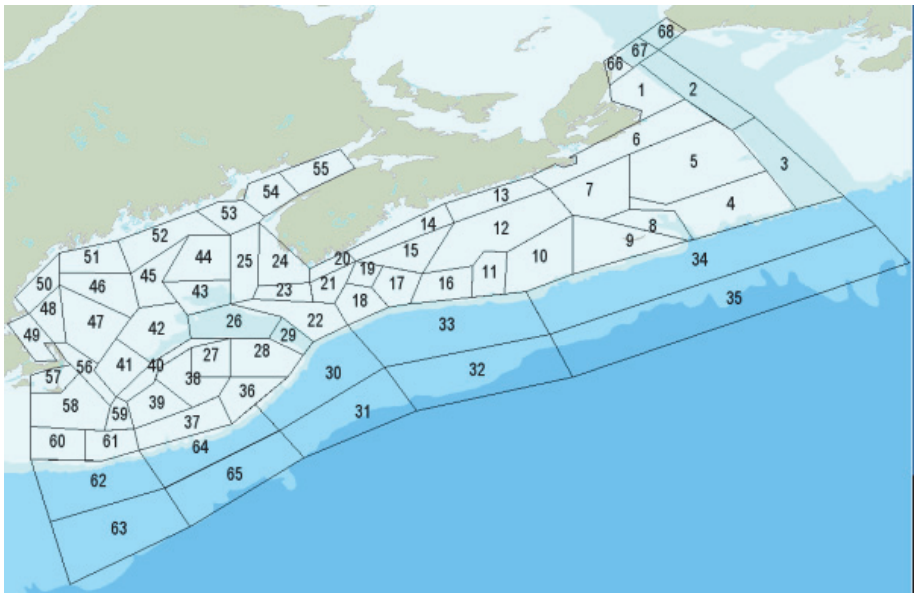

Figure 6.4 Map of polygon areas for the Scotian Shelf/Gulf of Maine (SS) used by the DFO Hydrographic Climate Database. Roseway Basin is located in area SS21, Grand Manan Basin is located in area SS54. I extracted sea surface temperature data for area SS14 (inner Scotian Shelf off Halifax) and SS44 (Gulf of Maine). Figure source: http://www.mar.dfo-mpo.gc.ca/science/ocean/database/doc2006/clim2006app.html.

Table 6.5 Time series of sea surface temperature (Jan - Aug thermal integral, ^{o}C•day) and net phytoplankton (1^{0}) productivity (gC m^{-2} yr^{-1}) on the Scotian Shelf (SS) and the Gulf of Maine (GoM) between 1998 and 2009. Time series of spring phytoplankton bloom dynamics are also provided for the Scotian Shelf (Halifax Station-2) only. These include bloom magnitude (mg Chl m^{-2}), onset timing (day of year) and duration (number of days).

Year	SS thermal integral (^{o}C•day)	GoM thermal integral (^{o}C•day)	SS net 1^{0} productivity (gC m^{-2} yr^{-1})	GoM net 1^{0} productivity (gC m^{-2} yr^{-1})	SS sp. blm. magnitude (mg Chl m^{-2})	SS sp. blm. onset (DOY)	SS sp. blm. duration (# days)
1998	1652	2009					
1999	1827	2250	127	144	160	40	67
2000	1827	2316	122	131	240	97	43
2001	1632	1956	128	141	278	72	53
2002	1764	2148	123	147	357	71	36
2003	1549	1966	125	135	664	78	46
2004	1508	1692	122	133	660	96	18
2005	1611	1840	121	136	633	90	9
2006	1868	2164	125	137	254	89	12
2007	1512	2020	124	135	939	76	35
2008	1783	2065			238	78	31
2009	1766	2178			662	75	43

6.3.5 Statistical analysis

The right whale SPUE (number of whales per 1000 km) per grid cell was highly skewed toward low values because there were many zeros in the dataset due to the rarity of sighting whales. The copepod concentration dataset was also significantly skewed, and variance was not equal among years. Annual average SPUE (averaged over all grid cells) and copepod concentration were compared separately within each habitat among years using non-parametric Kruskall-Wallace tests (one test of each variable per habitat). Annual anomalies are expressed in terms of the number of standard deviations from the series average (*z-value*). Comparisons of annual average SPUE and annual average copepod concentration were made between habitats using Pearson's correlation. The effect of interannual variation in average copepod abundance on annual average SPUE was assessed for each habitat using linear regressions of log transformed data (one test per habitat). Interannual trends in deep-Basin hydrography are described qualitatively. The effect of annual average water mass density on annual average SPUE was tested using linear regression of the log-transformed data. Finally, the influences of annual water mass temperature, primary productivity and slope water intrusions on diapausing copepod abundance were measured individually with linear regression, because the series were too short for multivariate analysis (too few degrees of freedom).

6.4 Results

6.4.1 Variation in right whale habitat occupancy

Average annual right whale SPUE varied by two orders of magnitude among years in Roseway (range 0 - 398 sightings per 1000 km) and one order of magnitude among years in Grand Manan Basin (range 60 - 313 sightings per 1000 km) between 1987 and 2009 (Figure 6.3c, f). There were significant differences in average SPUE among years within each habitat (Roseway: $H = 52$, $df = 14$, $P < 0.001$; Grand Manan: $H = 123$, $df = 22$, $P < 0.001$). In Roseway Basin, SPUE was greater than 2 standard deviations (S.D.) below the average of all observations during the years 1994, 1997, 2000 and 2005 (z values = -2.35, -3.20, -2.37 and -2.06, respectively). SPUE was greater than 2 S.D. above the average during years 1988, 1989, 2002, 2006 and 2009 (z-values = 2.08, 2.70, 2.58, 2.44, and 2.12, respectively). In Grand Manan Basin, SPUE was greater than 2 S.D. below the average during the years 1987, 1991, 1998, 2002 and 2003 (z-values = -6.07, -3.84, -2.49, -2.53, and -2.53, respectively). SPUE was greater than 2 S.D. above the average during 1995, 1999, and 2005 (z-values = 3.46, 3.33 and 2.96, respectively). SPUE was anomalous in both habitats in only one year; this occurred in 2005 when SPUE was low in Roseway Basin and high in Grand Manan Basin. This observation is reflected in that there was no statistically significant correlation between habitats with respect to annual right whale SPUE ($r = -0.305$, $P = 0.269$, Figure 6.5). However, the SPUE data do show that abandonment of Roseway Basin in the 1990s did result in an increased number of whales in Grand Manan Basin in 1994 and 1997.

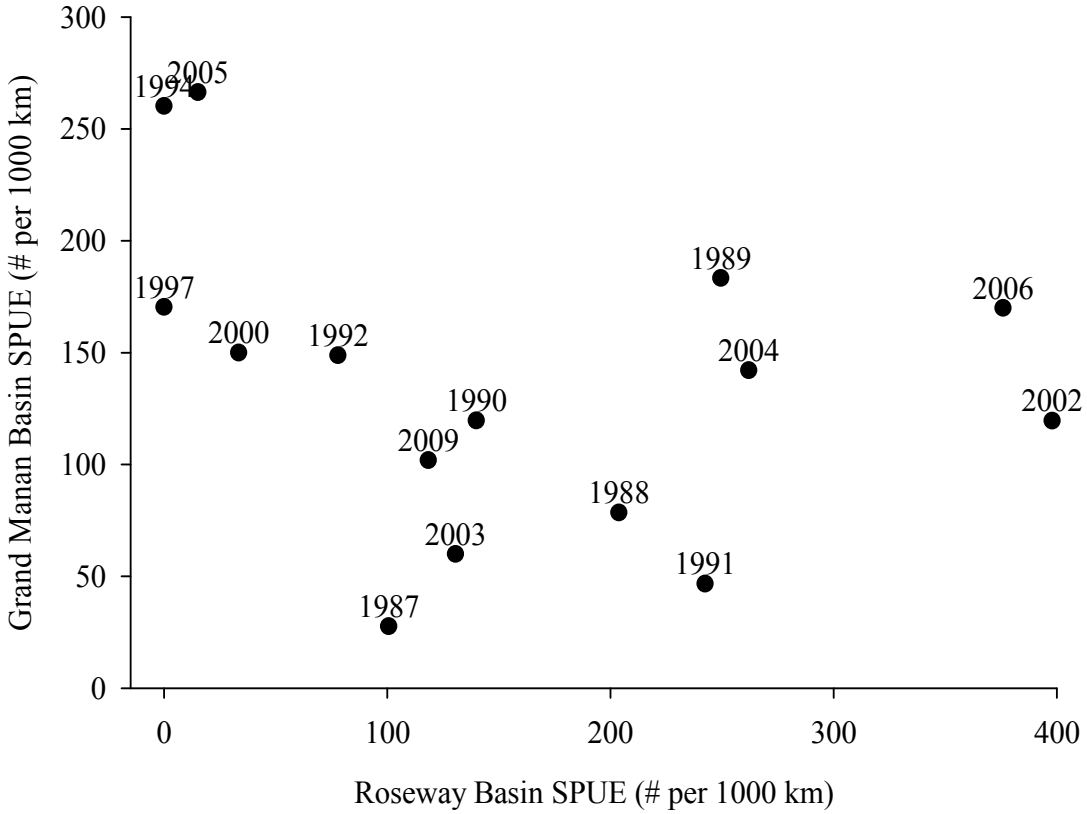

Figure 6.5 Scattergram of the relation between annual right whale SPUE in Roseway Basin and Grand Manan Basin for which there was no correlation (r = -0.305, P = 0.269).

6.4.2 Variation in copepod concentration

The time series of total *Calanus* concentration and diapausing copepod concentration were closely related (Figure 6.6), so I discuss the trends in diapausing copepod concentration only. Annual median diapausing copepod concentration varied by three orders of magnitude among years in Roseway Basin (range 81 - 2124 m^{-3}) and by two orders of magnitude among years in Grand Manan Basin (528 - 2076 m^{-3}) (Figure 6.6). There were significant differences in average copepod concentration among years in both habitats (Roseway: $H = 52.48$, $df = 8$, $P < 0.001$; Grand Manan: $H = 28.63$, $df = 5$, $P < 0.001$). In Roseway Basin, copepod concentration was greater than 2 standard deviations (S.D.) below the average of all observations during the years 1998, 1999, 2005 and 2008 (z-values = -3.46, -2.32, -2.89 and -2.48, respectively). Copepod concentration was greater than 2 S.D. above the average during 2007 only (z-value =5.55). In Grand Manan Basin, copepod concentration was greater than 2 S.D. below the average during the years 2000 and 2001 (z-values = -2.18 and -3.31, respectively). Copepod concentration was greater than 2 SD above the average in 1999 only (z-value = 3.31).

There were only 5 years when copepod concentrations were measured in both habitats during late-summer; 1999-2001, and 2006-2007. There was no statistically significant correlation between habitats with respect to annual diapausing copepod concentration ($r = 0.422$, $P = 0.479$, Figure 6.7). In 1999, Grand Manan Basin contained high copepod concentrations, while Roseway Basin contained low copepod concentrations. Thereafter, the two habitats were positively correlated; both contained low concentrations in 2000 and 2001, while both contained high concentrations in 2006 and 2007.

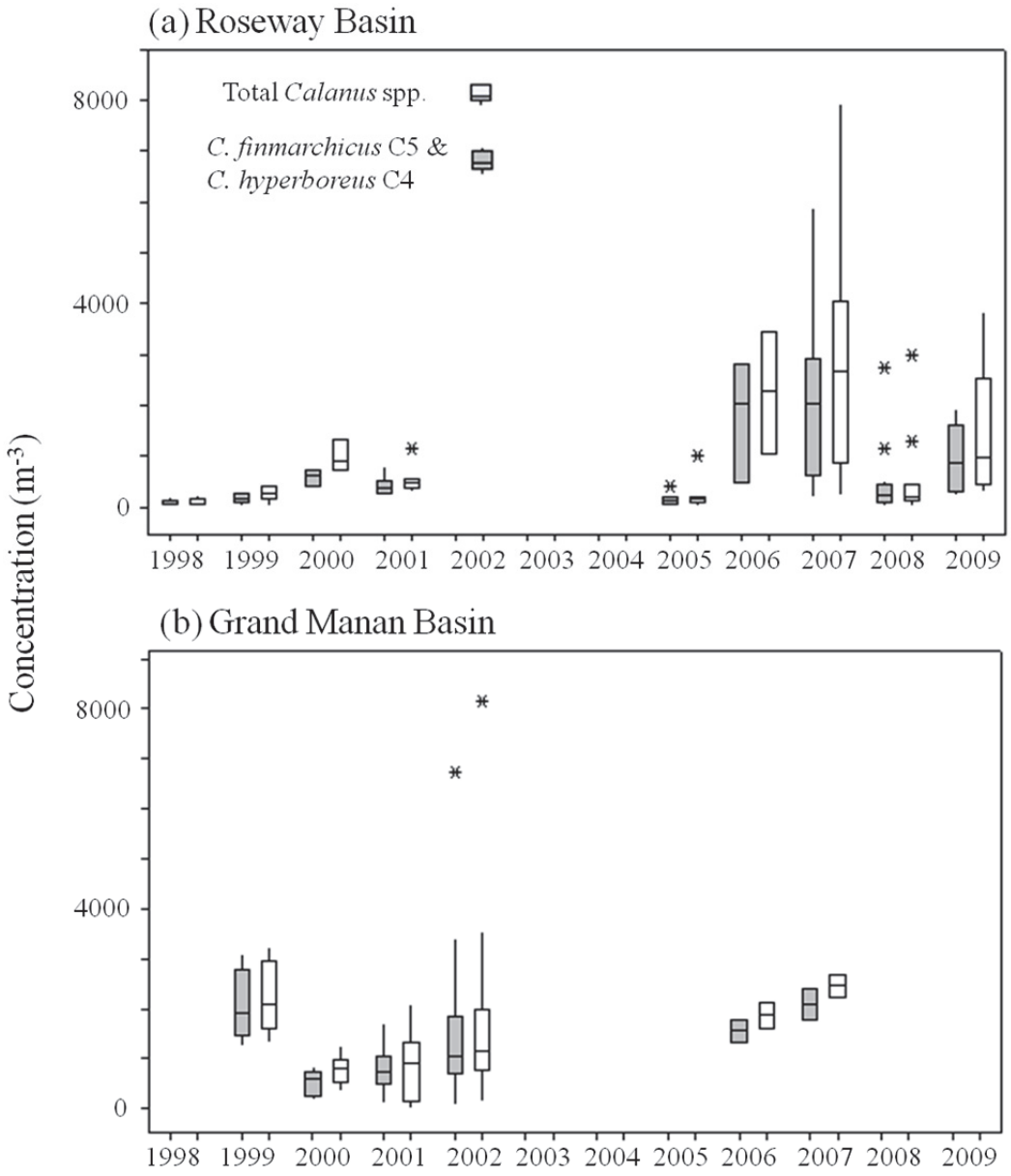

Figure 6.6 Time series (1998 - 2009) of annual late-summer total *Calanus* spp. concentration (white) and diapausing copepod concentration (grey) collected in (a) Roseway Basin and (b) Grand Manan Basin, and expressed as boxplots (median, interquartile range and outliers).

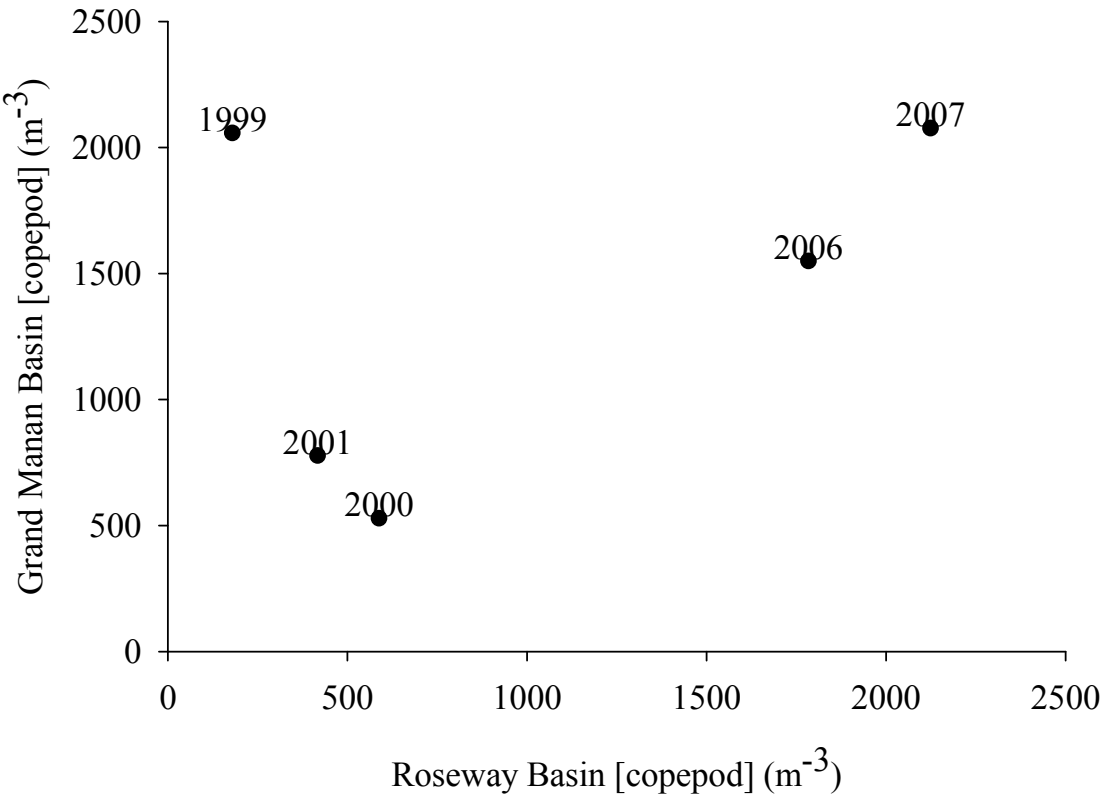

Figure 6.7 Scattergram of the relationship between annual late-summer diapausing copepod concentration (m^{-3}) in Roseway Basin and Grand Manan Basin. No significant correlation in copepod concentration between the two habitats exists (r = 0.422, P = 0.479).

6.4.3 Right whale habitat occupancy and prey availability

There were 5 years when both right whale SPUE and diapausing copepod concentration were measured concurrently with adequate effort in Roseway Basin; 1998, 2000, 2005, 2006 and 2009. Surprisingly, 93 % of the variation in right whale sightings per unit effort in Roseway Basin was accounted for by variation in habitat-average diapausing copepod concentration during those 5 years (*F-ratio* = 36.87, *df* = 4, *P* = 0.009, r^2 = 0.93, Figure 6.8). Consistent with this finding, 42 whales were opportunistically sighted in 2007 when diapausing copepod concentration was on average 2000 m^{-3}, and only a single whale was observed in 2008 when copepod concentrations were on average 400 m^{-3}.

There were 6 years when both right whale SPUE and diapausing copepod concentration were measured concurrently in Grand Manan Basin; 1999 - 2002 and 2006 - 2007. Unlike Roseway Basin, there was no relation between right whale SPUE and copepod concentration in Grand Manan Basin (*F-ratio* = 0.73, *df* = 4, *P* = 0.456, r^2 = 0.20, Figure 6.8). It would be relevant to compare the time series of whales and copepods in each habitat, however my dataset is too small for such a comparison. There were only two years, 2000 and 2006, when right whale and copepod data were collected concurrently in each habitat. Right whale SPUE and copepod concentration were both low in Roseway Basin in 2000 and both high in 2006 (Figure 6.8). In Grand Manan, copepod concentration showed a similar difference in magnitude between 2000 and 2006, however right whale SPUE was very similar in Grand Manan in both years. Interestingly, the overall interannual variation in average copepod concentration in Grand Manan Basin is similar to that in Roseway Basin, however, the concentrations did not reach very low values observed in Roseway Basin (Figure 6.8). The interannual variance in SPUE in Grand Manan Basin was lower than in Roseway Basin, and did not reach the low values estimated for Roseway Basin (Figure 6.8).

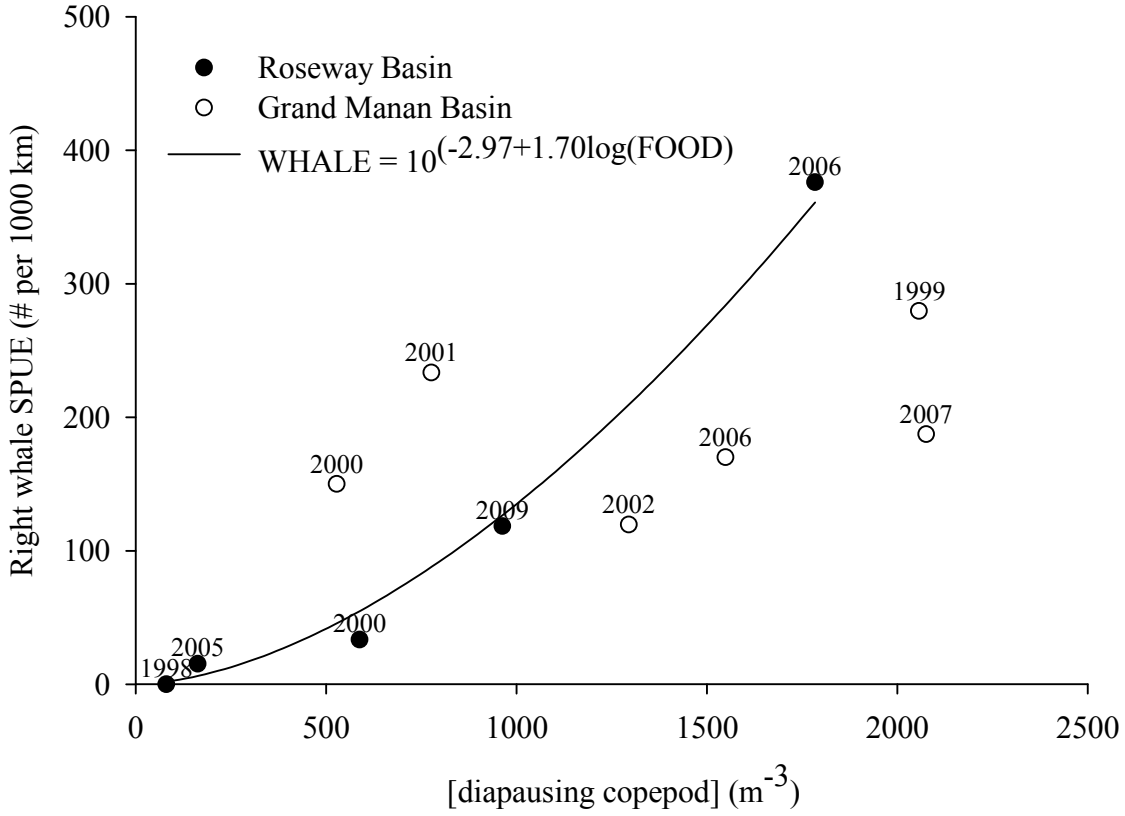

Figure 6.8 Annual late-summer right whale SPUE in Roseway (closed symbols) and Grand Manan (open symbols) Basins varies as a function of diapausing copepod concentration in Roseway Basin (the regression that is based on Roseway data only is depicted) but not Grand Manan Basin (no regression depicted).

6.4.4 Hydrography

6.4.4.1 Roseway Basin

The T-S properties at depths >100 m in Roseway Basin showed considerable interannual variation that was autocorrelated at a 4 year lag (Figure 6.9). Median annual late-summer temperature varies between 2 ^{o}C and 10 ^{o}C at the bottom of Roseway Basin. Temperature and salinity were positively correlated, and variation in salinity between 32.5 and 33.8 occurred concurrent with changes in temperature. Generally, water mass density increased over the time series, however it decreased in 2004 and 2008.

Three end-members contributed to the water mass characteristics observed in the deep water of Roseway Basin, and the relative contribution of each end-member varied among years (Figures 6.10 and 6.11). Most notably the deep basin water in each of the Grand Manan and Roseway Basins were closely associated with the 1026 kg m^{-3} isopycnal that is of significance to diapausing copepod concentrations as discussed in chapters 3, 4 and 5 above. The cold-fresh Nova Scotia Coastal Current (NSCC) end-member had a median temperature of 4 ^{o}C and median salinity 33.3 below 100 m (Figure 6.10), and dominated the deep water in Roseway, for example, in 1994 (Figure 6.11). The warm-salty continental slope water end-member had a median temperature of 9 ^{o}C and salinity 35.0 over the same depth range (Figure 6.10), and was most prominently represented in Roseway in 2003 (Figure 6.11). Each year the deep water mass in Roseway Basin had a T-S signature that fell roughly parallel to the mixing line between the slope and NSCC water masses, and the greatest interannual variation in T-S state occurred due to variation in the proportion of the slope-NSCC end-members (Figure 6.10). The slope water itself varied in temperature and salinity by approximately 6 ^{o}C and 1.6, while the NSCC water was much more consistent in T-S state. Slope water was particularly cold and fresh in 1989, 1991, 1994 and 2004. The density of slope water was unusually low in 1994.

The third end-member was warm (7 ^{o}C), fresh (32.1) and much less dense than the other two. This water mass pulled the deep water in Roseway Basin to the warm-fresh side of the slope-NSCC mixing line in Figure 6.10. It originated in the warm, fresh and low density upper layer above the deep water in Roseway (Figure 6.10, open circles), and it likely contributes to the deep water mass through vertical mixing. Because the T-S

state of deep water in the NSCC upstream of Roseway, offshore of Halifax, lies between Roseway and slope water, this demonstrates that most of the cross-Shelf mixing of slope water occurs upstream of Halifax. As the water moves along-Shelf, it gradually mixes with surface water, creating an along-shelf gradient of decreasing deep water density from northeast to southwest.

The climatological proportions of each end-member in Roseway were 19 % NSCC (range 0 - 38 %), 21 % slope water (range 0 - 47 %), and 60 % upper layer water (range 44 - 92 %). Below I describe interannual trends in the proportion of each end-member with an emphasis on the periods before, during (1994 - 1999) and after Roseway was abandoned by right whales (Figure 6.11). In the four years prior to the 1994 Roseway abandonment, the proportion of NSCC water observed in Roseway was below average or zero. During this time, the contribution of slope water was variable in its contribution but always present. Slope water was particularly well represented in 1991 and 1992. The proportion of upper layer water increased between 1987 and 1990, and in 1991 it fell. In 1993, upper layer water made up 92% of the deep layer.

Between 1994 and 1999 (Roseway abandonment years), the NSCC contribution was comparatively high, particularly in 1994, 1996 and 1998. Slope water contributed little in 1993, 1995 and 1996. The proportion of upper layer water remained near average (65%) throughout the abandonment period and until 2003, although it was particularly low in 1994 and 1998. Between 1998 and 2002, the contribution of NSCC water declined and the proportion of slope water increased. In 2002 and 2003, no NSCC water was found in Roseway and slope water was well represented. The opposite trend was observed in 2004. In 2005 neither water mass was well represented, while the upper layer water dominated. The year 2006 saw equal contributions of both end-members, and in 2007 and 2009, NSCC contribution was high while slope contribution was low. Note that the Roseway system was reduced to a two end-member system in 1987, 1991, 1993, and 2002 - 2004.

6.4.4.2 Grand Manan Basin

The time series of water mass characteristics in the deep (100 - 200m) layer of Grand Manan Basin has many missing years and as a consequence patterns are difficult

to identify, but when compared with Roseway Basin important trends emerge (Figure 6.9). The two habitats were positively correlated in their water mass properties, indicating they respond to similar forcing mechanisms; however Grand Manan Basin water is warmer and lower in density than Roseway Basin water. Interannual variation in all water mass characteristics is smaller in Grand Manan than in Roseway.

Water in Grand Manan Basin has similar contributors to its character as water in Roseway with the former having more time to mix and evolve because it is farther away from the GoSL and slope water end-members. It is possible that Roseway Basin waters make an advective contribution to Grand Manan waters, and both are supplied with water from the inland arm of the NSCC and slope water as well. Higher temperatures might occur in Grand Manan Basin because as the water travels between habitats it mixes with warm-fresh upper layer water and warm-salty slope water from the NECH (Figure 6.10). A mix of upper layer and NECH water masses produces water that is similar in salinity to Roseway Basin, but higher in temperature. This is the simplest explanation for the observed relationship between the two habitats. However, there are strongly shared elements in both because both advective pathways can be traced to the Gulf of St. Lawrence and NSCC with mixing and exchange with modified Basin Water, and this makes the degree of connectivity difficult to assess using T-S characteristics as a tracer. The increased complexity and multiple sources of slope water to Grand Manan Basin precludes the decomposition of the components in the manner I performed on the Roseway water.

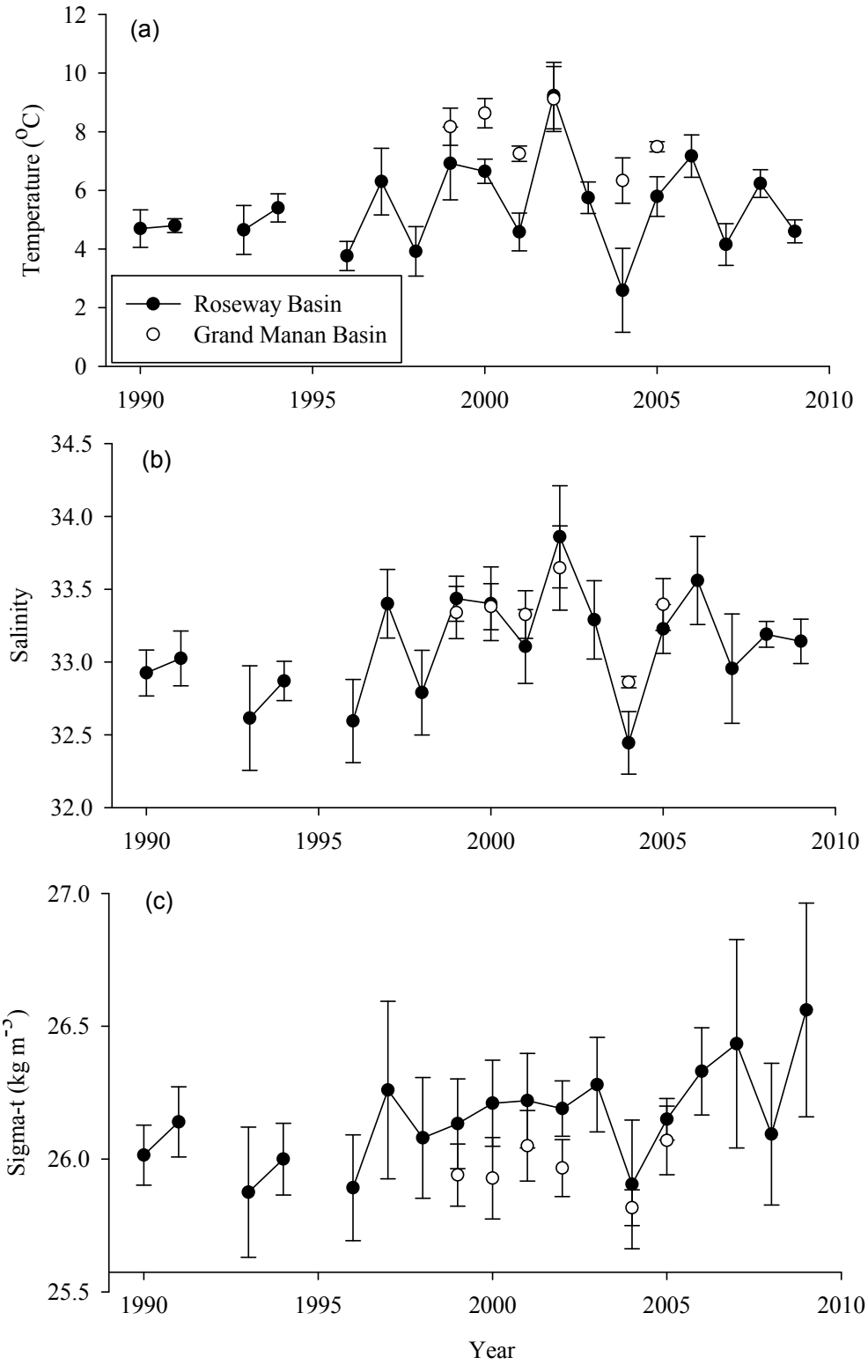

Figure 6.9 Time series of median (±1 SD) water mass (a) temperature, (b) salinity, and (c) sigma-t collected below 100 m depth in Roseway Basin (closed symbols) and Grand Manan Basin (open symbols).

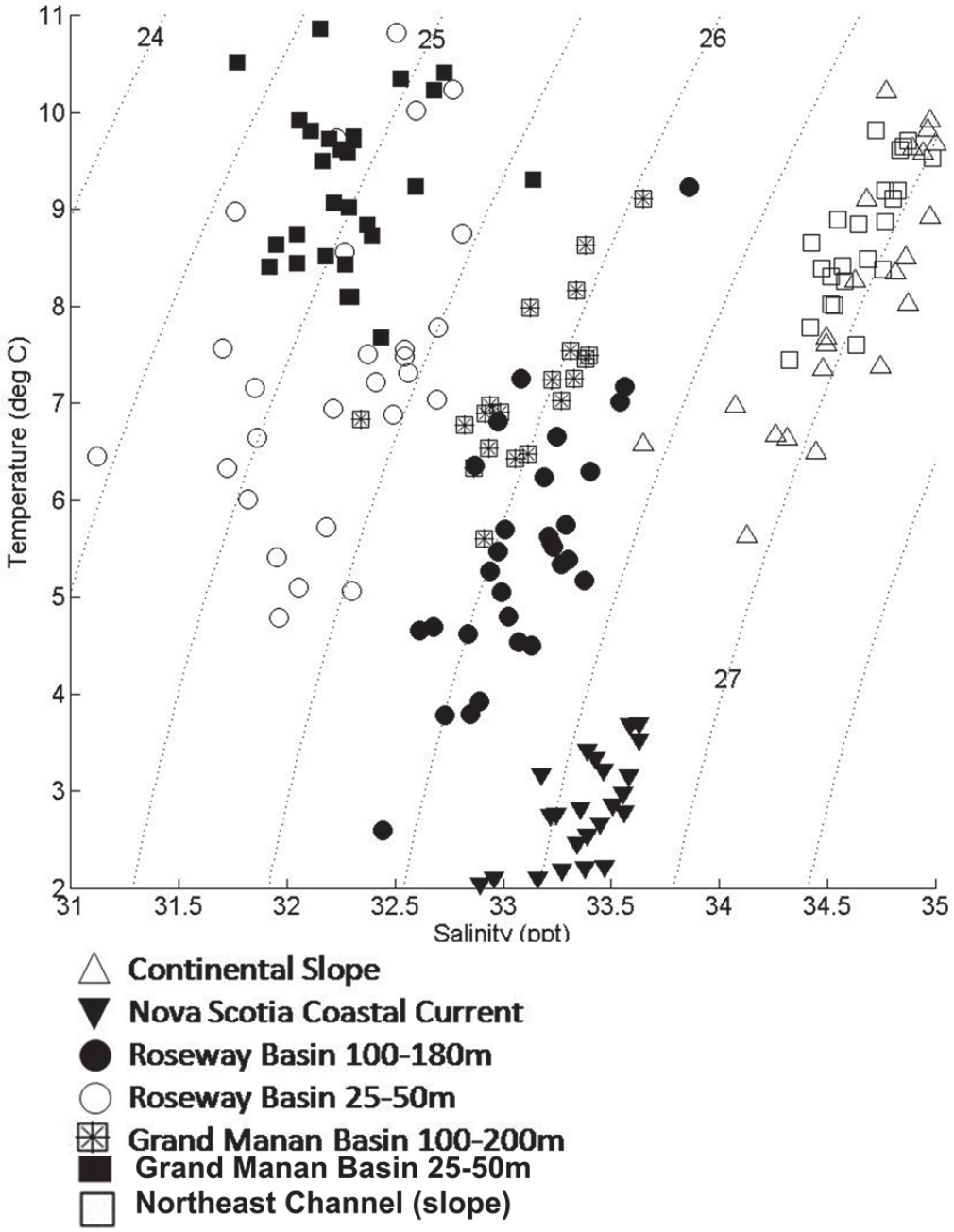

Figure 6.10 Temperature-salinity diagram showing median annual summer deep-water temperature and salinity below 100 m in Grand Manan Basin (hatched squares) and Roseway Basin (closed circles), 25 - 50 m depth in Roseway Basin (open circles) Nova Scotia Coastal Current 100 - 200 m (closed inverted triangles), Continental Slope water 100 – 200 m (open triangles) encompassing the years 1987 through 2009. Dotted lines are lines of constant sigma-t ($s,t,0$) and range between 1024 and 1027.5 kg m^{-3} (bold numbers).

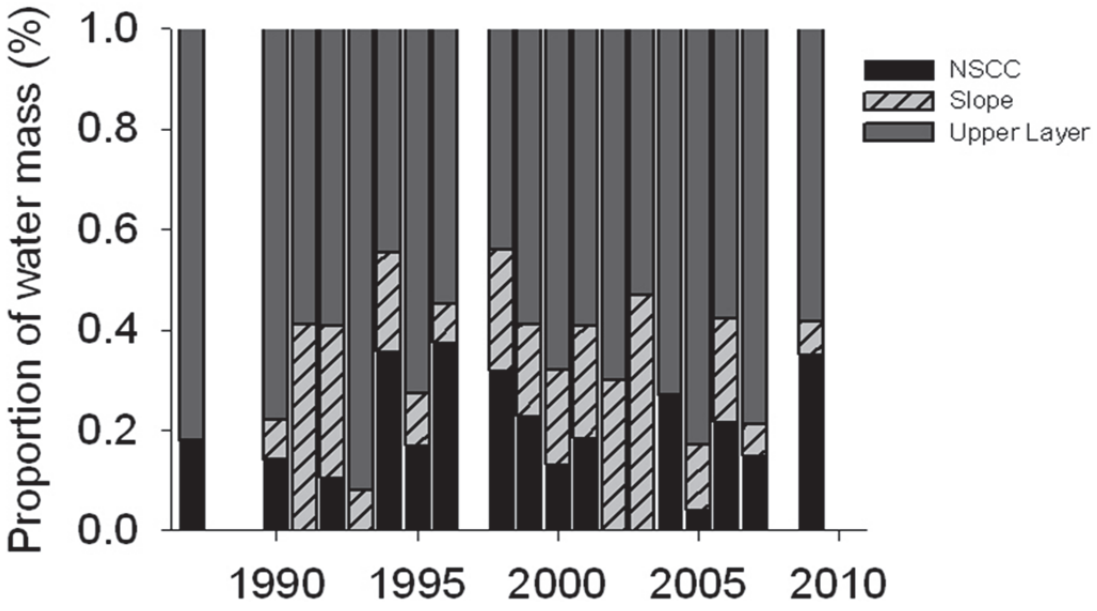

Figure 6.11 Proportion of each end-member water mass that contributes to deep (>100 m) water in Roseway Basin.

6.4.5 Hydrographic variation and right whale occupancy

I hypothesized in Chapter 5 that water mass density is relevant to the aggregation of copepods within deep Basins, and to the benefit of foraging whales. I proposed two alternative scenarios in which water mass density could affect right whale foraging and, as a consequence, the number of whales the feeding habitat could support, which could in turn affect whale abundance as estimated using the SPUE index. In the high density scenario, copepod aggregations may be available at shallower depths along the Basin margins where right whales prefer to feed. In this case, I would expect right whale SPUE to be positively correlated with density (Figure 5.36). In the low density scenario, copepods may aggregate near-bottom in high concentrations because they are vertically restricted by low density water. In this case, I would expect right whale SPUE to be negatively correlated with water mass density. I found no evidence of either expected relation (Figure 6.12).

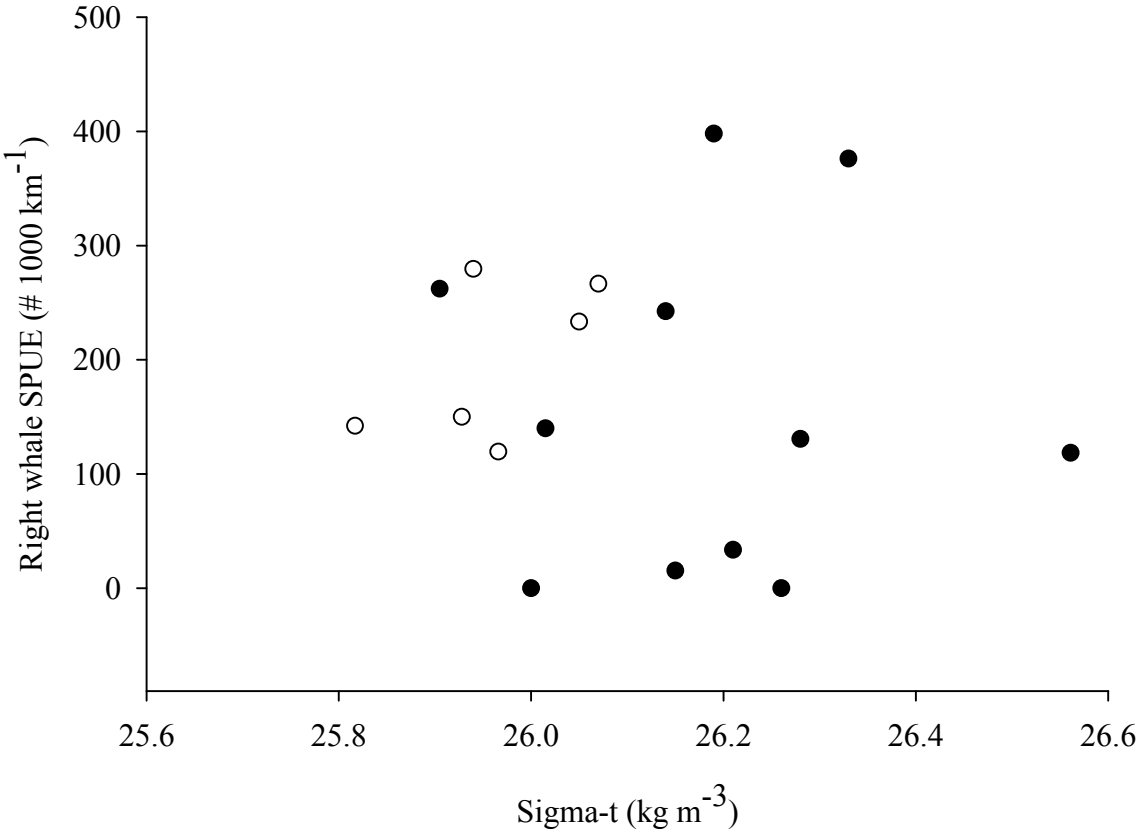

Figure 6.12 Scattergram of the relation between annual late-summer right whale sightings per unit effort (SPUE) and deep water density (sigma-t) in the Roseway (closed symbols) and Grand Manan (open symbols) basins.

6.4.6 Causes of variation in diapausing copepod abundance

All explanatory datasets were available for Roseway Basin during the periods 1999 - 2001 and 2005 - 2007 (n = 6, Table 6.6). The magnitude of the spring bloom and net annual primary productivity were positively correlated (r^2=0.60) and the magnitude of the spring bloom and the proportion of slope water were strongly negatively correlated (r^2 = 0.88). The timing of the spring bloom and the duration of the spring bloom were also negatively correlated (r^2 = 0.56). If I only used the thermal integral, spring bloom magnitude and duration for multivariate analysis, and the number of factors was reduced to three, my degrees of freedom are still too small for a robust multivariate analysis.

None of the possibly explanatory variables I examined explained interannual variation in diapausing copepod concentration in Roseway Basin (P >0.5 in each case). Although no one factor played a primary role, there were indications that interaction among the variables may be relevant, but the series is much too short to say anything definitive. For example, the year 2007 saw the highest copepod concentration, the highest magnitude in spring bloom and the highest net primary productivity. This suggests that bloom dynamics are relevant. Also in 2007, the thermal integral and the proportion of slope water were both the lowest observed. The two years that contained the lowest copepod concentrations were 1999 and 2005. In 1999, the spring bloom and net primary productivity magnitude were the lowest of the series, further indicating that phytoplankton dynamics are relevant. However, in 2005, primary productivity was about average. The duration of the spring bloom was also only 9 days, and there was very little slope water on the Shelf, indicating a limited off-Shelf copepod supply in 2005. These two factors may modulate the influence of primary production, for example, if there was a mismatch in time between the short spring bloom and the copepods on the Shelf emerging from diapause. In summary, it is likely that several of these factors interact with each other to create optimal population growth conditions for copepods on the Shelf, but my series was too short for the number of factors that could be involved, and this limitation precludes any ability to draw conclusions.

Since the Roseway Basin dataset was too short for multivariate analysis, then the Grand Manan dataset (n = 4) was also too short (Table 6.7). No single factor explained any significant variation in the diapausing copepod abundance in Grand Manan Basin (P

>0.1 in each case). When the net primary productivity from the Scotian Shelf and Gulf of Maine were added together, the linear regression between total annual productivity for the Scotia - Fundy region explained 95% of the variation in diapausing copepod abundance in Grand Manan Basin ([copepod] = 22649 – 81.69NPP, df = 3, F-*ratio* = 34.8, P = 0.027). However, the sample size is small and the negative correlation is difficult to explain from an ecological perspective. This illustrates that interpretive caution is required when there are few degrees of freedom in the analysis.

Table 6.6 Summary of annual diapausing copepod concentration (m^{-3}) in Roseway Basin is compared with a number of explanatory variables measured on the Scotian Shelf, including sea surface temperature (Jan - Aug thermal integral, ^{o}C), net phytoplankton productivity (NPP, gC m^{-2} yr^{-1}), spring bloom magnitude (mg Chl m^{-2}), onset timing (day of year) and duration (number of days), and proportion of slope water (%).

Year	[Copepod] (m^{-3})	NPP (gC m^{-2} yr^{-1})	Thermal Integral (^{O}C)	Slope Water Prop. (%)	sp. blm. Magnitude (mg Chl m^{-2})	sp. blm. Onset (DOY)	sp. blm. Duration (# days)
1999	180	122	1827	19	160	40	67
2000	588	128	1827	19	240	97	43
2001	417	123	1632	23	278	72	53
2005	163	125	1611	13	633	90	9
2006	1784	124	1868	20	254	89	12
2007	2124	132	1512	7	939	76	35

Table 6.7 Summary of annual diapausing copepod concentration (m^{-3}) in Grand Manan Basin is compared with a number of explanatory variables measured on the Scotian Shelf (SS) and Gulf of Maine (GoM), including sea surface temperature (Jan - Aug thermal integral, ^{o}C), net phytoplankton productivity (NPP, gC m^{-2} yr^{-1}), and proportion of slope water (Scotian Shelf only).

Year	[Copepod] (m^{-3})	GoM - NPP (gC m^{-2} yr^{-1})	GoM - Thermal Integral (^{O}C)	SS - NPP (gC m^{-2} yr^{-1})	SS - Thermal Integral (^{O}C)	SS - Slope Water Prop. (%)	SS + GoM net 1^{0} productivity (gC m^{-2} yr^{-1})
1999	2057	131	2250	122	1827	19	253
2000	528	141	2316	128	1827	19	269
2001	777	147	1956	123	1632	23	270
2002	1295	135	2148	125	1764	30	260

6.5 Summary and Discussion

In summary, right whale habitat occupancy as indexed using available SPUE estimates varied from year to year in each of the Roseway and Grand Manan Basin, and this variation was explained by habitat-averaged diapausing copepod concentrations in Roseway Basin only. There was no such correlation for the Grand Manan Basin. During the two years of the Roseway abandonment when SPUE was measured in both habitats (1994 and 1997), right whale SPUE was high in Grand Manan Basin. I found no relationship between right whale SPUE and water mass density, indicating that neither of my proposed copepod aggregation scenarios influenced SPUE in either habitat. Finally, I could not test for a temperature-phytoplankton dependent model for diapausing copepods in either Basin due to the limited extent of the time series.

6.5.1 Limitations of opportunistic data

Nearly all data presented in this chapter were collected by other research programs for purposes unrelated to the objectives of this chapter. I capitalized on the data availability because, as is often the case, my objectives required a longer time series than I was able to collect. Unfortunately, the opportunistic data were mostly inadequate for the task; the greatest limitation to the analysis being the low and biased survey effort among all variables. The only way that this limitation can be overcome in the future is through further dedicated sampling in each basin over multiple years. Seasonal AZMP / groundfish monitoring surveys completed by DFO do not regularly sample either of the basins for copepods or hydrography at depths exceeding 100 m, and this limits the availability of opportunistic archival oceanographic data. The NARWC does not survey Roseway Basin each year due to limited ship time and funding, which limits the ability to conduct regular right whale surveys in the habitat. Spatial biases in right whale survey effort are due to the fact that the NARWC's primary mandate is to collect photo-identification data and biopsies to assess whale health, fishing gear entanglements, and scarring from ship strikes etc. (Brown *et al.* 2007). To do this, surveys typically break from the trackline, and rarely is the entire grid surveyed in any one year. If the question of interannual variation in right whale habitat occupancy becomes a conservation priority

in the future, then adequate survey effort will be required. In Chapter 7, I will offer some suggestions on how this kind of research might be adequately achieved to address the unanswered questions.

6.5.2 Factors influencing interannual variation in right whale occupancy

Despite the low degrees of freedom, **t**he strong positive relationship between right whales and their prey in Roseway Basin suggests that the absence of right whales in the habitat during 1993 - 1999 was due to low prey availability. During the two years of the abandonment when SPUE was measured in both habitats (1994 and 1997), right whale SPUE was high in Grand Manan Basin, suggesting that when the whales abandoned Roseway they foraged in Grand Manan. Very low calving rates in the population were measured in 1998, 1999 and 2000 (Kraus *et al.* 2007) and these rates could be linked to low food availability in Roseway Basin, and higher 'competition' for food in Grand Manan as speculated by Patrician and Kenney (2001). Interestingly, though, the calving rates of females that consistently bring their calves to Grand Manan Basin and those that do not are highly correlated, and calving rates in both of these sub-groups declined in the 1990s, indicating that reproductive decline in the 1990s was not related to the use of the Grand Manan Basin (Kraus *et al.* 2007).

The correlation between habitat-average diapausing copepod abundance and right whale SPUE in Roseway Basin was higher than any correlation between prey and whale population dynamics in Grand Manan Basin (this study) or in the spring-early summer Critical Habitats, Cape Cod Bay or Great South Channel (e.g., Pendleton *et al.* 2009). There are two possible explanations for why the correlation between whales and their average prey concentrations in Roseway Basin was strong, whereas the correlation in all other northern Critical Habitats in weak or non-existent.

First, this pattern may occur because average prey concentrations are an adequate indicator of the total amount of food available to right whales in Roseway Basin, while average prey concentrations are not adequate indicators in the other Critical Habitats. This may be because copepod aggregation processes are more important indicators of the food available to right whales in other habitats. I tested whether water mass density acted as an important vertical aggregation mechanism in Grand Manan Basin but found no

relationship between right whale abundance and water mass density. I also identified other copepod aggregation mechanisms such as fronts, vertical migration, and accumulation on slopes at tidal frequencies acting in Roseway Basin, though I was not able to quantify their interannual variation in either late-summer Critical Habitat. In Cape Cod Bay and Great South Channel, the food resource for right whales is not limited to diapausing *C. finmarchicus*, but includes several calanoid copepod species that differ in their seasonal abundance, energy and vertical distribution patterns (Costa *et al.* 2006). Thus a model of food availability in Cape Cod Bay may need to be more complex and variable in time than simple average *C. finmarchicus* concentrations. An integral of the amount of food energy available and the integral of the number of whales in the habitat both measured over the feeding season may be better correlated.

Second, this pattern may occur because food is the only factor attracting whales into Roseway Basin, while the other habitats have other qualities unrelated to food that make them important. The number of whales in Grand Manan Basin is, by one measure (photo-IDs), inversely related to the number of whales in Roseway Basin (r^2 = -0.64, Hamilton *et al.* 2007). I did not find a similar relationship when I examined effort-corrected SPUE between the two habitats, however during the two years of the Roseway abandonment when SPUE was measured in both habitats right whale SPUE was high in Grand Manan Basin. This suggests that there are times when the number of right whales in the Grand Manan Basin can be explained by the quality of other habitats. Further, Grand Manan Basin is a well established nursery ground for 2/3 of all mother-calf pairs, and cows bringing calves into Grand Manan had first been brought there by their own mothers (Kraus et al. 2007). Perhaps the number of whales sighted in Grand Manan Basin is also a function of right whale reproduction variables, such as how many mother-calf pairs are in the population in a given year.

6.5.3 Conclusions

Interannual right whale occupancy in the late-summer Critical Habitats is variable and can be explained by prey field variation only in Roseway Basin, where the decline in right whale occupancy during the 1990s can be linked to a decline in food in the habitat during that period. Factors other than local prey field affect the number of whales that

occupy Grand Manan Basin. Variation in the right whale prey field could not be linked to temperature and food dependent growth in the Scotia - Fundy - GoM region because a number of variables are involved and the time series was too short.

Chapter 7

Conclusions

Roseway Basin is a late-summer feeding habitat for North Atlantic right whales. The Basin is also a target area for conservation initiatives because right whales are dispersed during migration, and aggregated in feeding or breeding areas between migrations. The whales aggregate in Roseway Basin because their prey, diapausing calanoid copepods, accumulate within the habitat in discrete patches that are maintained for weeks to months. This food source is important for energy accumulation by the whales because they are thought to fast throughout the winter migration and calving season. To determine how much energy is potentially available to right whales in Roseway Basin, the total amount of prey energy and the distribution of the energy were characterized in the habitat. Right whales foraging within the Basin do not use the entire potential habitat, but rather seek very high concentration patches of food to maximize their net energy gain. Using the distributions of prey energy and the whales, I focused on the energetically valuable area along the southern Basin slope. The southern slope has oceanographic characteristics that facilitate a predictable accumulation of highly concentrated prey patches, thus explaining why right whales are often aggregated there. The number of right whales that are observed in the Roseway Basin habitat each year is more variable than any other critical feeding habitat, a phenomenon that is primarily a function of the habitat-average prey concentrations in the Basin. Thus, spatial and temporal variation in right whale habitat occupancy in Roseway Basin is primary driven by the dynamics of their food base, which is itself driven by the oceanography of the Scotian Shelf and adjacent continental slope.

The overall goal of this thesis was to quantify space and time variation in the copepod prey field of North Atlantic right whales in the Roseway Basin, to use this information to identify the location and extent of right whale Critical Habitat in that area. To accomplish this, I estimated individual copepod energy (Chapter 2) and mapped the

spatial distribution of prey energy density along and across the Roseway Basin habitat (Chapter 3). Critical Habitat in Roseway Basin can now be defined as the area that contains high energy density aggregations of co-located diapausing *Calanus finmarchicus* stage-C5 and *Calanus hyperboreus* stage-C4. Oceanographic and bathymetric conditions that promote these aggregations include a bathymetric depth > 100 m containing waters that are influenced by continental slope water. This work has contributed to the federal designation and protection of the Roseway Basin Critical Habitat in Canada, one of the first Critical Habitats designated for a marine species. The provisional Critical Habitat boundaries of the area are adequate to encompass the entire potential prey field, however ephemeral slope water intrusions also make the channel separating Baccaro and Roseway Banks a corridor for right whale prey entering the Basin from the continental slope, and should be investigated further. Legal protection of Critical Habitat under the Fisheries Act, at the time of this writing, protects the Basin from habitat destruction (e.g., future oil and gas exploration) for the purpose of preserving it for North Atlantic right whale use. Proposed legislative changes to the Fisheries Act are cause for concern because they may weaken or eliminate this protection in the near future.

The second goal of this thesis was to quantify variation in the right whale prey field at locations where whales often aggregate within the Basin, to resolve mechanisms responsible for prey accumulation at scales relevant to a foraging whale. The most prominent aggregation mechanism in the Basin is the vertical accumulation of diapausing copepods at depth in water of the highest possible density. Thus the copepods are most often found in intermediate Bottom Water, which is influenced by higher density water from the continental slope (Chapter 3). The vertical distribution of diapausing copepods is restricted from below by the seafloor, and from above by the density of the local water mass during diapause. The 1026 kg m^{-3} isopycnal appears to be a vertical density barrier below which the animals are not able to maintain neutral buoyancy (Chapters 4 and 5). This may be related to the specific gravity of the animals' body tissue which, when they are full of lipid, is approximately 1026 kg m^{-3}. It may be energetically too costly for diapausers to maintain their vertical position in water that is lighter than their body tissue. At times and locations where water mass density is higher (i.e., when the 1026 kg m^{-3} isopycnal shoals), diapausing copepods are less restricted and form vertically thicker

layers than when and where water mass density is lower (i.e., the 1026 kg m^{-3} isopycnal deepens).

When the copepods enter diapause and sink to a depth of neutral buoyancy, they do not remain geographically stationary. Rather, they are constantly advected by a gyre-like circulation pattern in the Basin (Chapter 3). Constant advection facilitates the accumulation and dispersal of high concentration patches on which the whales prefer to forage at shorter (e.g., tidal) time scales. Advection near fronts and tidal advection on a sloped boundary with a semi-vertical density gradient are two advective processes that facilitate accumulation of high concentration patches in Roseway Basin (Chapters 3 and 4). Accumulation is likely to occur at fronts because of the interaction between vertical and horizontal gradients in the current velocities and the vertical position maintenance at a depth of neutral buoyancy by the animals. The lack of information concerning the vertical current structure, and the copepods' buoyancy characteristics in relation to water mass density, are knowledge gaps that needs to be addressed to advance research in this area.

The third objective of this thesis was to investigate interannual variation in the Roseway Basin Critical Habitat quality among the years 2007 – 2009 (Chapter 5). I determined that there was substantial variation in all habitat characteristics among all three years, indicating that the habitat is very dynamic from year to year. In 2007, the average copepod concentration in the habitat was very high, containing patches exceeding 12 000 m^{-3}. Water mass density was also very high, and the 1026 kg m^{-3} isoycnal was quite shallow. This expanded the wide and shallow western Basin margin to the diapausing population. In 2008, the average copepod concentration was low, however there were discrete, high density patches associated with a slope water intrusion and fronts throughout the Basin. Water mass density was generally low in 2008, which restricted the copepods near-bottom and excluded diapausers from the western Basin margin. During the 2009 survey, approximately one-half the copepod population was diapausing, while the other half was in an earlier phase of development and aggregated at the surface. Each year, the copepod aggregation mechanisms differed, and in the absence of data on the right whale distribution among years, it is not possible to know which of the identified mechanisms, if any, were important to right whale foraging. Opportunistic

sightings of 42 right whales in 2007 and one right whale in 2008 suggest that 2007 was a better year for right whale foraging in the Basin. Forty-four whales were sighted in 2009 during a formal right whale survey, and, consistent with the findings of this thesis, these animals were primarily located along the 140 m isobath at the southern and southwestern Basin margins (NARWC 2009).

Interannual variation in Critical Habitat quality was expected since the cycles of biological production and advection are fundamentally annual on the Scotian Shelf. Of primary importance to right whales are interannual changes the average abundance of diapausing copepods in the Basin (Chapters 5 and 6). These changes are driven by temperature- and food-dependent copepod population growth on the Scotian Shelf, as well as supplements to the on-Shelf population from the continental slope at various times of the year (Chapter 6). Average copepod abundance also depends on the circulation patterns on the Shelf that cause variation in copepod fluxes to the Basin. For example, volume transport from the Gulf of St. Lawrence and Eastern Scotian Shelf toward Roseway Basin in relation to the timing of biological production will affect the number of *C. hyperboreus* and *C. finmarchicus* found in Roseway. While these factors are surely important, a robust multivariate model that described interannual changes in diapausing calanoid copepods in the Basin could not be developed. This is because the available time series were short, and an accurate model would require sampling over the entire growing season (January – September) to estimate copepod fluxes to the deep Basin in relation to biological production and advection (Chapter 5). This would be a very interesting topic for another doctoral thesis.

Finally, the contemporary analyses were used to calibrate a time series of prey and hydrographic data that was spatially limited in each of the late-summer Critical Habitats, with an emphasis on the right whale abandonment of Roseway Basin during 1993 - 1999 (Chapter 6). Right whale habitat occupancy varied from year to year in both Roseway and Grand Manan Basin, but this variation was explained by habitat-average prey concentrations only in Roseway Basin. The two habitats do not consistently co-vary with respect to either right whale occupancy or prey field variation, as has been hypothesized in the past. Conclusions drawn from this analysis were limited due to the short duration of the time series and effort bias among years and habitats. To address

these issues in the future, I propose a new collaborative study be undertaken in which the four major Critical Habitats are treated as a single dynamic habitat and surveyed concurrently over multiple years.

7.1 Future Research

Directed research on right whales began in 1980 and continues to this day because of the effort by a collaboration of researchers belonging to the North Atlantic Right Whale Consortium. Their primary mandates are management driven; untangle whales from fishing gear, alert ships of right whale locations, and conduct annual surveys to collect photo-IDs, genetic samples and assess the health and demographics of the population on or near the continental Shelf from Florida to the Scotian Shelf. The amount of survey effort has been inconsistent in some areas because of variable funding (e.g., Roseway Basin in the 1990s). These mandates and funding restrictions are very likely to remain the main drivers of field programs undertaken by the Consortium into the future. Therefore if new research questions are proposed that require different or refined right whale sampling methodologies, then collaborative field programs must be initiated.

Studies of right whales and their prey in the four northern Critical Habitats tend to treat each habitat as isolated, assuming no migration among habitats and that the characteristics within a habitat are the main driver of the right whale dynamics in that habitat. However it is well established that (1) right whales do not exhibit a mass seasonal migration of the entire population but rather migrate individually or in small groups, and (2) right whales are highly migratory during the feeding season among all four northern Critical Habitats at daily to monthly frequencies (e.g., Baumgartner and Mate 2005, Vanderlaan 2010). Yet there has not been a coordinated effort among research programs to measure right whale and prey distributions in all habitats over the feeding season in the same year. The migratory corridors between habitats have also been largely ignored. I believe we have reached a limit to what can be learned by treating each Critical Habitat as a singular entity. To move forward with right whale habitat research, a more collaborative approach that treats the Scotia-Fundy-Gulf of Maine region as one large, dynamic habitat would be a logical and worthwhile step.

Consider for a moment each right whale Critical Habitat as a resource patch within a single large habitat. A legitimate null hypothesis could be that right whales exhibit an ideal free distribution (IDF). IDF predicts that the number of individuals that are aggregated in various patches at any given time will be proportional to the amount of resources available in each patch; this will minimize resource limitation among individuals. Right whales in the Scotia – Fundy - GoM region meet the necessary assumptions of IDF in that they are free to move among patches to find the best quality ones, the animals seem to be aware of patch quality since, within the Critical Habitats, they tend to aggregate in areas with high prey abundance (Baumgartner and Mate 2003), and we can assume individuals are more-or-less equal when it comes to foraging since they rely on the environment to aggregate their prey for them. This is a nice null hypothesis because the food resource is a primary motivator for right whale occupancy in the region, and if deviations from an IDF are found, these can provide insights into other drivers of right whale distribution within and among the four Critical Habitats.

The novel result of my thesis work was in using real data to diagnose the oceanographic processes that aggregated right whale prey in the Roseway Basin habitat. Focusing on the food base allowed me to elucidate processes that might be important to right whale foraging. However, as I concluded in Chapter 5, one drawback of my study was my inability to link the aggregation processes with right whale foraging behavior to assess whether right whales exploit those aggregations or not. Other studies have had the opposite approach; they focused on the prey field near whales, but their oceanographic sampling was insufficient to clearly elucidate the processes that aggregated those prey (Baumgartner and Mate 2003, Baumgartner *et al.* 2003). Thus a useful future study would assess two components simultaneously; one component that measures the habitat-scale variation in the prey field, hydrography and right whale abundance, and another that focuses on the prey field and hydrography near feeding right whales, with a focus on what individual whales are doing (e.g., by tagging whales). This would link the potential niche (the prey available) with the realized niche (what portion of the potential niche is actually used).

Future Research Objectives

I propose a new collaborative research project that has the following objectives:

1) Investigate variation in right whale occupancy and prey energy density in all four habitats in the same year to answer the following questions: do right whales exhibit an ideal free distribution with respect to the total prey field in the Scotia-Fundy-GoM region? How does this distribution vary seasonally with the seasonal changes in prey energy density among Critical Habitats?
2) Link the potential niche of right whales to the realized niche within each habitat by simultaneously performing a habitat-scale and an individual-scale right whale/prey survey.
3) At the habitat-scale, survey right whales specifically to estimate real whale densities (i.e., not following the NARWC protocol).
4) If a single year survey was successful and funding available, repeat it over multiple years to assess interannual variation among habitats

Field Program

The field program I propose is an idealized program subject to funding and ship time constraints. However, the basic survey is logistically quite feasible based on funding and ship time that the relevant collaborators are generally able to acquire.

This project would require two vessels surveying each habitat at the same time; one to collect the habitat-scale data, and one to collect the individual-scale data. There are baseline data on right whale and prey ecology in all 4 major Critical Habitats that can serve as a guideline for survey development. The equipment needed to collect the data is not highly specialized and can be operated from relatively small vessels. To collect the habitat-scale data for this thesis, we used a 90' Salvage Tug with an A-frame and two winches on deck; a smaller vessel could be used for the individual-scale survey.

I envision a habitat-scale survey conducted at a constant speed during daylight hours along transect lines that span the entire habitat. The habitat-scale right whale survey would require trained observers and adequate sighting conditions (Brown *et al.* 2007). The observers would record all right whale sightings, the time and place they occurred. The vessel would not break track to follow whales. At the same time the right

whale survey is taking place, the prey field can be surveyed using TUBSS (OPC + CTD on a batfish), tow-yoed over the appropriate depth interval behind the vessel. This requires at least two people, one to operate the winch and one to monitor the computer. At some time before, during, or after the survey, BIONESS collections should be made to calibrate the OPC and collect samples for prey energy estimation (use size as a proxy, Chapter 2). If the ship was equipped with an ADCP to measure current speed and direction at the same time, that would be even more informative and would allow some direct collaboration with a physical oceanographer, which would be beneficial. Vessel speed during TUBSS deployment is about 5 km hr^{-1}, while right whale survey vessels normally move at 20 km hr^{-1} while surveying, so this is a logistical issue that would need to be addressed. At 5 km hr^{-1}, it took 44 survey hours to complete the ~250 km transect survey of Roseway Basin in 2008 (Figure 3.1a, Table 3.2). From April - September, there are 12-15 daylight hours, so at maximum it would take 4 survey days to survey Roseway. Roseway Basin is approximately twice as large in area as Grand Manan Basin, the same size as Cape Cod Bay, and one quarter the area of Great South Channel (Kraus and Rolland 2007, Hamilton *et al.* 2007).

I envision the individual-scale survey to follow the NARWC protocol; performing the standard survey design and breaking track to collect photo-IDs and biopsies as necessary. Aboard this vessel would be one or two oceanographers who operate a vertical profiling OPC, a vertical profiling CTD, and a BONGO net, all of which could be operated by a single small winch. Deploying these instruments near feeding whales will collect data on the 'realized niche'. At the end of the survey, the individual-scale and habitat-scale data will be geo-referenced to one another to examine the portion of the larger habitat that the whales are actually using.

Ideally, monthly surveys would be conducted in all habitats from spring to autumn, but logistically this is unfeasible. It is well established that right whales tend to use Cape Cod Bay and Great South Channel more often in spring and early summer, then generally migrate to Roseway and Grand Manan Basins in late-summer. Vanderlaan (2010) has developed monthly transition probabilities for right whales among the four Critical Habitats, and the seasonal variation in the prey fields in each habitat is fairly well

defined, so these data could be used to guide the timing of the surveys in a way that most effectively addresses the project objectives within the ship time and funding constraints.

I believe that performing this kind of survey over multiple years is the best way to answer the major question of this chapter: what causes interannual variation in right whale Critical Habitat occupancy? It is debatable whether this question will ever become high priority is terms of right whale recovery and conservation. Currently, most funding is dedicated to the immediate threats to right whale survival: reducing entanglements, untangling whales, reducing ship strikes and developing new technologies to be more effective in those areas. Right now right whales are enjoying a period of recovery; the calving rates have increased over the past few years and there is reason for optimism. But how much of this variation is natural, and how much is due to conservation efforts? We do not know, nor will we ever know because of the lack of survey effort, why the right whale calving rates plummeted in the 1990s. If it was due to reduced food availability, this phenomenon could also make adults less healthy and more vulnerable to mortality once they become entangled or are struck. I wonder, if the population falters again in the future, will conservation biologists be held responsible, and the efficacy of their management strategies questioned, if they cannot say with confidence that the decline is due to natural variation in the environment?

This thesis was broad in scope, incorporating aspects of right whale conservation, zooplankton ecology and physical oceanography. Thus, the results should be of interest to a wide range of researchers and environmental policy makers. The applications to right whale conservation have been highlighted several times throughout the thesis. This is the first time that Roseway Basin has been oceanographically characterized; hence the results will also be of interest to numerous oceanographers concerned with the Scotian Shelf dynamics. It is also the first detailed characterization of diapausing copepods and their habitat in a Shelf Basin, and can be used to advance the understanding of the relationship between copepod buoyancy and water mass characteristics; something that has previously only been studied in continental slope and open ocean populations. In the future, I hope this information will be used to guide further research into the mechanisms that explain right whale foraging behaviors and distributions.

Literature Cited

Albers, C.S., Kattner, G. and Hagen, W. 1996. The compositions of wax esters, triacylglycerols and phospholipids in Arctic and Antarctic copepods: evidence of energetic adaptations. Mar. Chem. 55 347-358.

Anderson, J. T., and Warren, W.G. 1991. Comparison of catch rates among small and large bongo samplers for *Calanus finmarchicus* copepodite stages. Can. J. Fish. Aquat. Sci. 48 303−308.

Aretxabaleta, A.L., McGillicuddy Jr., D.J., Smith, K.W., and Lynch, D.R. 2008. Model simulations of the Bay of Fundy gyre: 1. Climatological results. J. Geophys. Res. 113: C10027

Aretxabaleta, A.L., McGillicuddy Jr., D.J., Smith, K.W., and Lynch, D.R. 2009. Model simulations of the Bay of Fundy gyre: 2. Hindcasts for 2005-2007 reveal interannual variability in retentiveness. J. Geophys. Res. 114 C09005

Arts, M.T., and Evans, M.S. 1991. Optical-digital measurements of energy reserves in calanoid copepods: intersegmental distributions and seasonal patterns. Limnol. Oceanogr. 36 289-298.

AZMP Monitoring Group. 2008. Physical, chemical and biological status of the environment. In Atlantic Zone Monitoring Program Annual Bulletin. Fisheries and Oceans Canada ISSN 1916-6362. Available online at: *http://www.meds-sdmm.dfo-mpo.gc.ca/zmp/main_zmp_e.html*

AZMP Monitoring Group. 2009. Physical, chemical and biological status of the environment. In Atlantic Zone Monitoring Program Annual Bulletin. Fisheries and Oceans Canada ISSN 1916-6362. Available online at: *http://www.meds-sdmm.dfo-mpo.gc.ca/zmp/main_zmp_e.html*

AZMP Monitoring Group. 2010. Physical, chemical and biological status of the environment. In Atlantic Zone Monitoring Program Annual Bulletin. Fisheries and Oceans Canada ISSN 1916-6362. Available online at: *http://www.meds-sdmm.dfo-mpo.gc.ca/zmp/main_zmp_e.html*

Båmstedt, U. 1986. Chemical composition and energy content. In: Corner, E.D.S. and O'Hara, S.C.M. (eds). The biological chemistry of marine copepods. Clarendon, Oxford, pp.1-58.

Båmstedt, U. 1988. Ecological significance of individual variability in copepod bioenergetics. Hydrobiologia, 167/168: 43-59.

Baumgartner, M.F. 2003. Comparisons of *Calanus finmarchicus* fifth copepodite abundance estimates from nets and an optical plankton counter. J. Plankton Res. 25: 855-868.

Baumgartner, M.F., and Mate, B.R. 2003. Summertime foraging ecology of North Atlantic right whales. Mar. Ecol. Prog. Ser., 264: 123-135.

Baumgartner, M.F., Cole, T.V.N., Clapham, P.J., and Mate, B.R. 2003a. North Atlantic right whale habitat in the lower Bay of Fundy and on the southwest Scotian Shelf during 1999-2001. Mar. Ecol. Prog. Ser. 264: 137-154.

Baumgartner, M.F., Cole, T.V.N., Campbell, R.G., Teegarden, G.J., and Durbin, E.G. 2003b. Associations between North Atlantic right whales and their prey, *Calanus finmarchicus*, over diel and tidal time scales. Mar. Ecol. Prog. Ser. 264: 155-166.

Baumgartner, M.F., and Mate, B. R. 2005. Summer and fall habitat of North Atlantic right whales (*Eubalaena glacialis*) inferred from satellite telemetry. Can. J. Fish. Aq. Sci. 62: 527-543.

Baumgartner, M.F., Mayo, C.A. and Kenney, R.D. 2007. Enormous carnivores, microscopic food and a restaurant that's hard to find. In S.D. Krauss and R. Rolland [eds.], The urban whale: North Atlantic right whales at a crossroads. Harvard University Press.

Beardsley, R.C., Epstein, A.W., Changsheng, C., Wishner, K.F., Macaulay, M.C., and Kenney, R.D. 1996. Spatial variability in zooplankton abundance near feeding right whales in the Great South Channel. Deep-Sea Res. II 43: 1601-1625.

Bottger, R. and Schnack, D. 1986 On the Effect of formaldehyde fixation on the dry-weight of copepods. Meeresforschung-Rep. Mar. Res. 31 141-152.

Brown, M.W., Brault, S., Hamilton, P.K., Kenney, R.D., Knowlton, A.R., Marx, M.K., Mayo, C.A., Slay, C.K. and Kraus, S.D. 2001. Sighting heterogeneity of right whales in the western north atlantic 1980-1992. J. Cetacean Res. Manage., Spec. Issue 2: 245-250.

Brown, M.W., Kraus, S.D., Slay, C.K. and Garrison, L.P. 2007. Surveying for discovery, science and management. In S.D. Krauss and R. Rolland [eds.], The urban whale: North Atlantic right whales at a crossroads. Harvard University Press.

Brown, M.W., Fenton, D., Smedbol, K., Merriman, C., Robichaud-Leblanc, K., and Conway, J.D. 2009. Recovery Strategy for the North Atlantic Right Whale (*Eubalaena glacialis*) in Atlantic Canadian Waters [Final]. Species at Risk Act Recovery Strategy Series. Fisheries and Oceans Canada. vi + 66p.

Bumpus, D.F. 1960. Sources of water contributed to the Bay of Fundy by surface circulation. J. Fish. Res. Bd. Can. 17: 181-197.

Campbell, R.W. 2008. Overwintering habitat of Calanus finmarchicus in the north atlantic inferred from autonomous profiling floats. Deep-Sea Res. I 55: 630-645.

Campbell, R.W. and Dower, J.F. 2003. Role of lipids in the maintenance of neutral buoyancy by zooplankton. Mar. Ecol. Prog. Ser.263: 93-99.

Caswell, H., Fujiwara, M., and Brault, S. 1999. Declining survival probability threatens the North Atlantic right whale. Proc. Natl. Acad. Sci. USA 96: 3308 – 3313.

Comita, G.W., Marshall, S.M. and Orr, A.P. 1966. On the biology of *Calanus finmarchicus* XIII. Seasonal change in weight, calorific value and organic matter. J. Mar. Biol. Assoc. U.K. 46: 1-17.

Costa, A.D., Durbin, E.G. and Mayo, C.A. 2006. Variability in the nutritional value of the major copepods in Cape Cod Bay (Massachusetts, USA) with implications for right whales. Marine Ecology 27: 109-123.

Darimont, C.T., Paquet, P.C. and Reimchen, T.E. 2008. Spawning salmon disrupt trophic coupling between wolves and ungulate prey in coastal British Columbia. BMC Ecology 8:14.

David Suzuki Foundation media release on December 7, 2010. http://www.davidsuzuki.org/media/news/2010/12/decisive-killer-whale-court-win-offers-hope-for-at-risk-species/

Deines, K.L. 1999. Backscatter estimation using broadband acoustic Doppler current profilers. Proc. IEEE working conference on current measurement: 249-253.

Falk-Petersen, S., Mayzaud, P., Kattner, G. and Sargent, J.R. 2009. Lipids and life strategy of Arctic *Calanus*. Mar. Biol. Res. 5: 18-39.

Federal Court Docket T-541-09, citation: 2010 FC 1233 obtained online on 28 March 2011 via http://www.davidsuzuki.org/media/news/downloads/2010/Killer_Whale_Judgement.pdf

Fisheries and Oceans Canada. 2008. Recovery strategy for the Northern and Southern Resident killer whales (*Orcinus orca*) in Canada. Species at Risk Act Recovery Strategy Series, Fisheries and Oceans Canada, Ottawa, ix+81pp.

Fisheries and Oceans Canada. 2010. Recovery strategy for Northern Bottlenose whales in Canada. Species at Risk Act Recovery Strategy Series, Fisheries and Oceans Canada, Ottawa, ix+81pp.

Franks, P.J.S. 1992. Sink or swim: accumulation of biomass at fronts. Mar. Ecol. Prog. Ser. 82: 1-12

Galbraith, P.S., Pettipas, R.G., Chassé, J., Gilbert, D., Larouche, P., Pettigrew, B., Gosselin, A., Devine, L., and Lafleur, C. 2010. Physical oceanographic conditions in the Gulf of St. Lawrence in 2009. DFO CSAS Res. Doc. 2009/014, 73 pp.

Gatien, M.G. 1976. A study in the slope water region south of Halifax. J. Fish. Res. Bd. Can. 33: 2213-2217.

Giguere, L.A., St-Pierre, J.F., Bernier, B., Vezina, A. and Rondeau, J.G. 1989. Can we estimate the true weight of zooplankton samples after chemical preservation. Can. J. Fish Aquat. Sci. 46: 522-527.

Goodyear, J.D. 1996. Significance of feeding habitats of North Atlantic right whales based on studies of diel behavior, diving, food ingestion rates, and prey. PhD thesis University of Guelf 1-268.

Greene, C.H. and Pershing, A.J. 2004. Climate and the conservation biology of North Atlantic right whales: the right whale at the wrong time? Frontiers in Ecology and the Environment 2: 29-34.

Greenberg, D.A. 1983. Modeling the mean barotropic circulation in the Bay of Fundy and Gulf of Maine. J. Phys. Oceanogr. 13: 886-904

Hamilton, P.K., Knowlton, A.R., and Marx, M.K. 2007. Right whales tell their own stories: the photo-identification catalog. In S.D. Krauss and R. Rolland [eds.], The urban whale: North Atlantic right whales at a crossroads. Harvard University Press.

Hannah, C.G., Shore, J.A., Loder, J.W., and Naimie, C.E. 2001. Seasonal circulation on the western and central Scotian Shelf. J. Phys. Oceanogr. 31: 591-615.

Harrison, G., Johnson, C., Head, E., Spry, J., Pauley, K., Maass, H., Kennedy, M., Porter, C., and V. Soukhovtsev. 2009. Optical, chemical, and biological oceanographic conditions in the Maritimes Region in 2008. DFO CSAS Res. Doc. 2009/054, 61 pp.

Harrison G., C. Johnson, E. Head, K. Pauley, H. Maass, M. Kennedy, C. Porter and V. Soukhovtsev. 2008. Optical, chemical and biological oceanographic conditions in the Maritimes region in 2007. DFO Can. Sci. Adv. Sec. Res. Doc. 2008/044, 66 p.

Hasset, R.P. 2006. Physiological characteristics of lipid-rich “fat” and lipid-poor “thin” morphotypes of individual *Calanus finmarchicus* C5 copepodites in nearshore Gulf of Maine. Limnol. Oceanogr. 51: 997-1003.

Head, E.J.H., Harris, L.R. and Petrie, B. 1999. Distribution of *Calanus* spp. on and around the Nova Scotia shelf in April: evidence for an offshore source of *Calanus finmarchicus* to the central and western regions. Can. J. Fish Aquat. Sci. 56: 2463-2476.

Herman, A.W. 1988. Simultaneous measurement of zooplankton and light attenuance with a new optical plankton counter. Cont. Shelf. Res. 8: 205-221.

Herman, A.W. 1992. Design and calibration of a new optical plankton counter capable of sizing small zooplankton. Deep-Sea Res. 39:395–415

Herman, A.W., Sameoto, D.D., Shunian, C., Mitchell, M.R., Petrie, B, and Cochrane, N. 1991 Sources of zooplankton on the Nova Scotia shelf and their aggregation within deep basins. Cont. Shelf Res. 11: 211-238

Hinch, P.R., and de Santo, E.M. 2011. Factors to consider when evaluating the management and conservation effectiveness of a whale sanctuary to protect and conserve the North Atlantic right whale (*Eubalaena glacialis*). Marine Policy 35: 163-180

Hirche, H.J. 1996. Diapause in the marine copepod *Calanus finmarchicus* – a review. Ophelia 44: 129-143.

Hirche, H.J. 1997. Life cycle of the copepod *Calanus hyperboreus* in the Greenland Sea. Mar. Biol. 128: 607-618.

Hlista, B.L., Sosik, H.M., Traykovski, L.V.N., Kenney, R.D. and Moore, M.J. 2009. Seasonal and interannual correlations between right-whale distribution and calving success and chlorophyll concentrations in the Gulf of Maine, USA. Mar. Ecol. Prog. Ser. 394: 289-302.

Houghton, R.W., and Fairbanks, R.G. 2001. Water sources for Georges Bank. Deep-Sea Res. II 48: 95-114.

Houghton, R.W., Smith, P.C. and Fournier, R.O. 1978. A simple model for cross-shelf mixing on the Scotian Shelf. J. Fish. Res. Bd. Can. 35: 414-421

Johnson, C., Harrison, G., Head, E., Spry, J., Pauley, K.,Maass, H., Kennedy, M., Porter, C., Yashayaeva, I. and Casault, B. 2012. Optical, chemical and biological oceanographic conditions in the maritimes in 2009 and 2010. Can. Sci. Advis. Secret. 2012/012

Kattner, G. 1989. Lipid composition of *Calanus finmarchicus* from the North Sea and the Arctic. A comparative study. Comp. Biochem. Physiol. 94B: 185-188.

Kenney, R.D., Hyman, M.A.M., Owen, R.E., Scott, G.P., and Winn, H.E. 1986. Estimation of prey densities required by North Atlantic right whales. Mar. Mamm. Sci. 2: 1-13.

Klanjscek, T., Nisbet, R. M., Caswell, H., and Neubert, M.G. 2007. A model for energetic and bioaccumulation in marine mammals with applications to the right whale. Ecol. Applic. 17: 2233-2250.

Knowlton, A. R., Kraus, S. D., and Kenney R. D. 1994. Reproduction in North Atlantic right whales (*Eubalaena glacialis*). Can. J. Zool. /Rev. Can. Zool. 72: 1297-1305.

Kogeler, J.W., Falk-Petersen, S., Kristensen, A., Petterson, F. and Dalen, J. 1987. Density and sound speed contrasts in sub-Arctic zooplankton. Polar Biol. 7: 231-235.

Kraus, S. D., and R. M. Rolland. 2007. Right whales in the urban ocean, p. 1-38. In S.D. Kraus and R. Rolland [eds.], The urban whale: North Atlantic right whales at the crossroads. Harvard University Press.

Kraus, S. D., Hamilton, P. K., Kenney, R. D., Knowlton, A. R., and Slay, C. K. 2001. Reproductive parameters of the North Atlantic right whale. J. Cetacean Res. Manage., Spec. Issue 2: 231-236.

Kraus, S.D., Pace, R.M., and Frasier, T.R. 2007. High investment, low return: the strange case of reproduction in *Eubalaena glacialis*. In S.D. Krauss and R. Rolland [eds.], The urban whale: North Atlantic right whales at a crossroads. Harvard University Press.

Lamprecht, I. 1999. Combustion calorimetry. In: Kemp, R.B. (ed). Handbook of thermal analysis and calorimetry Vol. 4: From macromolecules to man. Elsevier Science, Amsterdam, pp. 175-187.

Laurinolli, M.H. 2002. Localization of North Atlantic right whale (*Eubalaena glacialis*) sounds using hydrophone arrays in the Bay of Fundy. MSc Thesis, Dalhousie University, Halifax, NS.

Lavery, A., Wiebe, P.H., Stanton, T.K., Lawson, G.L., Benfield, M.C., and Copley, N.J. 2007. Determining dominant scatterers of sound in mixed zooplankton populations. J. Acoust. Soc. Amer. 122: 3304–3326.

Lee, R.F. 1974. Lipid composition of the copepod *Calanus hyperboreus* from the Arctic Ocean. Changes with depth and season. Mar. Biol. 26: 313-318.

Lee, R.F., Hagen, W., and Kattner, G. 2006. Lipid storage in marine zooplankton. Mar. Ecol. Prog. Ser. 307: 273-306.

Loder, J.W. 1980. Topographic rectification of tidal currents on the sides of Georges Bank. J. Phys. Oceanogr. 10: 1399-1416

Loder, J.W., Han, G., Hannah, C.G., Greenberg, D.A., and Smith, P.C. 1997 Hydrography and baroclinic circulation in the Scotian Shelf region: winter versus summer. Can. J. Fish. Aquat. Sci. 54: 40-56.

Madsen, S. J., Neilson, T.G., Tervo, O.M. and Soderkvist, J. 2008. Importance of feeding for egg production in Calanus finmarchicus and C. glacialis during the Arctic spring. Mar. Ecol. Prog. Ser. 353: 177-190.

McLaren, I.A., Head, E. and Sameoto, D.D. 2001. Life cycles and seasonal distributions of *Calanus finmarchicus* on the central Scotian Shelf. Can. J. Fish. Aq. Sci. 58: 659-670.

McLaren, I.A., Tremblay, M.J., Corkett, C.J., and Roff, J.C. 1989. Copepod production on the Scotian Shelf based on life-history analyses and laboratory rearings. Can. J. Fish. Aquat. Sci. 46: 560–583.

Melle, W. and Skjoldal, H.R. 1998. Reproduction and development of *Calanus finmarchicus, C. glacialis* and *C. hyperboreus* in the Barents Sea. Mar. Ecol. Prog. Ser. 169: 211-228.

Mellinger, D.K., Nieukirk, S.L., Matsumoto, H., Heimlich, S.L., Dziak, R.P., Haxel, J., Fowler, M., Meinig, C., and Miller, H.V. 2007. Seasonal occurrence of North Atlantic right whale (*Eubalaena glacialis*) vocalizations at two sites on the Scotian Shelf. Mar. Mamm. Sci. 23: 856-867.

Michaud, J., Taggart, C.T. 2007. Lipid and gross energy content of North Atlantic right whale food, *Calanus finmarchicus*, in the Bay of Fundy. Endang. Species Res. 3: 77-94

Michaud, J., Taggart, C.T. 2011. Spatial variation in right whale food, *Calanus finmarchicus*, in the Bay of Fundy. Endang. Species. Res. 15: 179-194

Michaud, J. 2005. The prey field of the North Atlantic right whale in the Bay of Fundy: spatial and temporal variation. PhD Thesis. Dalhousie University, Halifax, NS, pp. 64-137.

Michaud, J. And Taggart, C.T. *in prep.* Does the food energy available in the Bay of Fundy meet the North Atlantic right whale energy demand?

Miller, C.A., Reeb, D., Best, P.B., Knowlton, A.R., Brown, M.W. and Moore, M.J. 2011. Blubber thickness in right whales *Eubalaena glacialis* and *Eubalaena australis* related with reproduction, life history status and prey abundance. Mar. Ecol. Prog. Ser. 438: 267-283.

Miller, C.B., Crain, J.A. and Morgan, C.A. 2000. Oil storage variability in *Calanus finmarchicus*. ICES J. Mar. Sci. 57: 1786-1799.

Miller, C.B., Morgan, C.A., Prahl, F.G. and Sparrow, M.A. 1998. Storage lipids of the copepod *Calanus finmarchicus* from Georges Bank and the Gulf of Maine. Limnol. Oceanogr. 43: 488-497.

Moller, E.F., Maar, M., Jonasdottir, S.H., Neilson, T.G., and Tonnesson, K. 2012. Effects of changes in temperature and food on the development of *Calanus finmarchicus* and *Calanus helgolandicus* populations. Limnol. Oceanogr. 57: 211-220.

Moore, M.J., McLellan, W.A., Daoust, P.Y., Bonde, R.K. and Knowlton, A.R. 2007. Right whale mortality a message from the dead to the living. In: Kraus, S.D. and Rolland, R.M. (eds) The urban whale: North Atlantic right whales at the crossroads. Harvard University Press, Cambridge, MA. p 358-379.

Morris, R.J. 1972. Preservation of some oceanic animals for lipid analysis. J. Fish Res. Board Can. 29: 1303 -1307.

Murison, L.D., and Gaskin, D.E. 1989. The distribution of right whales and zooplankton in the Bay of Fundy, Canada. Can. J. Zool. 67: 1411-1420.

NARWC. 2008. North Atlantic Right Whale Consortium sightings database, 22 July 2008. New England Aquarium, Boston, MA.

NARWC. 2009. NARWC Annual Meeting Abstracts and Sighting Summaries. New Bedford, MA.

Omori, M. 1978. Some factors affecting dry weight, organic weight and concentrations of carbon and nitrogen in freshly prepared and in preserved zooplankton. Int. Rev. Hydrobiol. 63: 261-269

Ou, H.W., and Maas, L. 1986. Tidal-induced buoyancy flux and mean transverse circulation. Contin. Shelf Res. 5: 611-628.

Pasternak, A., Arashkevich, E., Tande, K. And Falkenhaug, T. 2001. Seasonal changes in feeding, gonad development and lipid stores in *Calanus finmarchicus* and *C. hyperboreus* from Malangen, northern Norway. Mar. Biol. 138: 1141-1152

Patrician, M.R. and Kenney, R.D. 2010. Using the continuous plankton recorder to investigate the absence of North Atlantic right whales (*Eubalaena glacialis*) from the Roseway Basin. J. Plankt. Res. 32: 1685-1695.

Pawlowicz, R., Beardsley, B., and Lentz, S. 2002. Classical tidal harmonic analysis including error estimates in MATLAB using T_TIDE. Comp. Geosci. 28: 929-937.

Payne, P.M., Wiley, D.N., Young, S.B., Pittman, S., Clapham, P.J. and Jossi, J.W. 1990. Recent fluctuations in the abundance of baleen whales in the southern Gulf of Maine in relation to changes in selected prey. Fish. Bull. 88: 687-696

Pendleton, D.E., Pershing, A.J., Brown, M.W., Mayo, C.A., Kenney, R.D., Record, N.R., and Cole, T.V.N. 2009. Regional-scale mean copepod concentration indicates relative abundance of North Atlantic right whales. Mar. Ecol. Prog. Ser. 378: 211-225.

Pepin, P. and Head, E. 2009. Seasonal and depth-dependent variations in the size and lipid contents of stage 5 copepodites of *Calanus finmarchicus* in the waters of the Newfoundland Shelf and the Labrador Sea. Deep-sea Res. Part 1 56: 989-1002.

Pepin, P. and Shears, T.H. 1997. Variability and capture efficiency of bongo and Tucker trawl samplers in the collection of ichthyoplankton and other macrozooplankton. Can. J. Fish. Aquat. Sci. 54: 765-773.

Peters, R.H. 1983. The ecological implications of body size. Cambridge University Press, New York, N.Y.

Petrie, B. and Drinkwater, K. 1993. Temperature and salinity variability on the Scotian Shelf and in the Gulf of Maine 1945-1990. J. Geophys. Res. 98: 20079-20089.

Petrie, B., Pettipas, R.G., Petrie, W.M. and Soukhovtsev, V. 2008. Physical oceanographic conditions on the Scotian Shelf and in the Gulf of Maine during 2007. DFO Can. Sci. Adv. Sec. Res. Doc. 2008/017, 47 p.

Petrie, B., Pettipas, R.G., Petrie, W.M. and Soukhovtsev, V. 2009. Physical oceanographic conditions on the Scotian Shelf and in the Gulf of Maine during 2008. DFO CSAS Res. Doc. 2009/039, 17 pp.

Petrie, B. and Pettipas, R.G. 2010. Physical oceanographic conditions on the Scotian Shelf and in the eastern Gulf of Maine (NAFO areas 4V, W, X) during 2009. NAFO SCR Doc. 10/12

Plourde, S. And Runge, J. 1993. Reproduction of the planktonic copepod *Calanus finmarchicus* in the lower St. Lawrence estuary: relation to the cycle of phytoplankton production and evidence for a Calanus pump. Mar. Ecol. Prog. Ser. 102: 217-227.

Pringle, J.M. and P.J.S. Franks. 2001. Asymmetric mixing transport: A horizontal transport mechanism for sinking plankton sediment in tidal flows. Limn. Oceanogr. 46: 381-391.

Reiss, C.S., McLaren, I.A., and Avendaño, P.A. 1999. Utility of storage lipid volumes in inferring recent trophic history of copepods. Can. J. Fish Aquat. Sci. 56: 2444-2449.

Rissik, D., Suthers, I.M., and Taggart, C.T. 1997. Enhanced zooplankton abundance in the lee of an isolated reef in the south Coral Sea: the role of flow disturbance. J. Plankton Res. 19: 1347-1368.

Rosenfeld, J.S. and Hatfield, T. 2005. Information needs for assessing critical habitat of freshwater fish. Can. J. Fish. Aquat. Sci. 63: 683-698

Salonen, K. and Sarvala, J. 1985. Combination of freezing and aldehyde fixation: a superior preservation method for biomass determination of aquatic invertebrates. Arch. Hydrobiol. 103: 217-230.

Sameoto, D.D., Jaroszynski, L.O., and Fraser, W.B. 1980. BIONESS, a new design in multiple net zooplankton samplers. Can. J. Fish. Aquat. Sci. 37: 722-724.

Sameoto, D.D., and Herman, A.W. 1990. Life cycle and distribution of *Calanus finmarchicus* in deep basins on the Nova Scotia shelf and seasonal changes in *Calanus* spp. Mar. Ecol. Prog. Ser. 66: 225-237.

Sameoto, D.D., and Herman, A.W. 1992. Effect of the outflow from the Gulf of St. Lawrence on Nova Scotia shelf zooplankton. Can. J. Fish Aquat. Sci. 49: 857-869.

Sartoris, F.J., Thomas, D.N., Cornils, A., and Schnack-Schiel, S.B. 2010. Buoyancy and diapause in Antarctic copepods: The role of ammonium accumulation. Limnol. Oceanogr. 55 1860-1864.

Schaeff, C.M., Kraus, S.D., Brown, M.W., and White, B.N. 1993. Assessment of the population structure of western North Atlantic right whales (*Eubalaena glacialis*) based on sighting and mtDNA. Can. J. Zool. 71: 339-345

Scott C.L., Kwasniewski, S., Falk-Petersen, S., and Sargent, J.R. 2000. Lipids and life strategies of *Calanus finmarchicus, Calanus glacialis* and *Calanus hyperboreus* in late autumn, Kongsfjorden, Svalbard. Polar Biol. 23:510-516.

Smith, P. 1989. Circulation and dispersion on Browns Bank. Can. J. Fish. Aquat. Sci. 46: 539-559.

Song, H., Ji, R., Stock, C., Kearney, K. and Wang, Z. 2011. Interannual variability in hytoplankton blooms and plankton productivity over the Nova Scotian Shelf and in the Gulf of Maine. Mar. Ecol. Prog. Ser. 426: 105-118.

Sprules, W.G., Jin, E.H., Herman, A.W., and Stockwell, J.D. 1998. Calibration of an optical plankton counter for use in fresh water. Limnol. Oceanogr. 43: 726-733

Stanton, T.K., and Chu, D. 2000. Review and recommendations for the modeling of acoustic scattering by fluid-like elongated zooplankton: euphausiids and copepods. ICES J. Mar. Sci. 57: 793-807

Steedman, H.F. 1976. General and applied data on formaldehyde fixation and preservation of marine zooplankton. In: Steedman, H.F. (ed). Zooplankton fixation and preservation. UNESCO Press, Paris, pp. 103-154.

Taggart, C.T., Thompson, K., Maillet, G., Lochmann, S., and Griffin, D. 1996. Abundance distribution of larval cod (*Gadus morhua*) and zooplankton in a gyre-like water mass on the Scotian Shelf. A.A. Balkema Publishers, Brookfield, VT (USA).

Tremblay, M.J., and Roff, J.C. 1983. Community gradients in the Scotian Shelf zooplankton. Can. J. Fish. Aquat. Sci. 40: 598-611.

Vanderlaan, A.S.M. 2009. Estimating the Risk to the North Atlantic Right Whale (*Eubalaena glacialis*) from Ocean-Going Vessels and Fishing Gear. PhD dissertation, Dalhousie University, Halifax, NS

Vanderlaan, A.S.M., and Taggart, C.T. 2009. Efficacy of a voluntary area to be avoided to reduce risk of lethal vessel strikes to endangered whales. Conserv. Biol. 23: 1467-1474

Vanderlaan, A.S.M., Taggart, C.T., Serdynska, A.R., Kenney, R.D., and Brown, M.W. 2008. Reducing the risk of lethal encounters: vessels and right whales in the Bay of Fundy and on the Scotian Shelf. Endang. Species Res. 4: 283-297

Vanderlaan, A.S.M., Taggart, C.T., and Smedbol, R.K. 2011. Fishing-gear threat to right whales (*Eubalaena glacialis*) in Canadian waters and the risk of lethal entanglement. Can. J. Fish. Aquat. Sci. 68: 2174-2193

Vanderzwaag, D.L. and Hutchings, J.A. 2005. Canada's marine species at risk: Science and law at the helm, but a sea of uncertainties. Ocean Dev. Int. Law. 36: 219-259.

Visser, A.W. and Jonasdottir, S. H. 1999. Lipids, buoyancy and the seasonal vertical migration of Calanus finmarchicus. Fish. Oceanogr. 8: 100-106.

Vogedes, D., Varpe, O., Soreide, J.E., Graeve, M., Berge, J. and Falk-Petersen, S. 2010. Lipid sac area as a proxy for individual lipid content of arctic calanoid copepods. J. Plankton Res. 32: 1471-1477.

Waldick, R. C., Kraus, S.D., Brown, M. and White, B. N. 2002. Evaluating the effects of historic bottleneck events: an assessment of microsatellite variability in the endangered, North Atlantic right whale. Mol. Ecol. 11: 2241-2249.

Winn, H., Price, C., and Sorenson, P. 1986. The distributional biology of the right whales (*Eubalaena glacialis*) in the western North Atlantic. In Brownell, R.J. Jr; Best, P.B.; Prescott, J.H. (eds). Workshop on the Status of Right Whales, Boston, M.A. (USA).

Wishner, K.F., Outram, D.M., and Ullman, D.S. 2006. Zooplankton distributions and transport across the northeastern tidal front of Georges Bank. Deep-Sea Res. II 53: 2570-2596.

Woodley, T.H., and Gaskin, D.E. 1996. Environmental characteristics of North Atlantic right and fin whale habitat in the lower Bay of Fundy, Canada. Can. J. Zool. 74: 75-84

Yayanos, A.A., Benson, A.A., and Nevenzel, J.C. 1978. The pressure-volume-temperature (PVT) properties of a lipid mixture from a marine copepod, *Calanus plumchrus*: implications for buoyancy and sound scattering. Deep-Sea Res. 25: 257-268.

Zakardjian, B.A., Sheng, J., Runge, J.A., McLaren, I.A., Plourde, S., Thompson, K.R., and Gratton, Y. 2003. Effects of temperature and circulation on the population dynamics of *Calanus finmarchicus* in the Gulf of St. Lawrence and Scotian Shelf: Study with a coupled three-dimensional hydrodynamic, stage-based life history model. J. Geophys. Res. 108: C11, 8016.

Zhou, M., Tande, K.S., Zhu, Y. and Sunnje, B. 2009 Productivity, trophic level and size spectra of zooplankton in northern Norwegian shelf regions. Deep-sea Res. Part 2 56: 1934-1944.